RADIATIVE DECAY AND LEVEL SHIFT OF AN ATOM IN AN OPTICAL RESONATOR

by

DANIEL JOSEPH HEINZEN

S. B., Massachusetts Institute of Technology
(1981)

SUBMITTED TO THE DEPARTMENT OF PHYSICS
IN PARTIAL FULFILLMENT
OF THE REQUIREMENTS FOR THE
DEGREE OF

DOCTOR OF PHILOSOPHY

at the

MASSACHUSETTS INSTITUTE OF TECHNOLOGY

May 1988

Signature of Author _____
Department of Physics
May 16, 1988

Certified by _____
Michael S. Feld
Professor of Physics
Thesis Supervisor

Accepted by _____
Chairman, Departmental Committee

RADIATIVE DECAY AND LEVEL SHIFT

OF AN ATOM IN AN OPTICAL RESONATOR

by

DANIEL JOSEPH HEINZEN

Submitted to the Department of Physics on May 18, 1988
in partial fulfillment of the requirements for the
Degree of Doctor of Philosophy in Physics

ABSTRACT

This thesis describes a theoretical and experimental investigation of the intensities, linewidths, and frequencies of radiation by an atom in an optical resonator. It is found that the atom's spontaneous emission rate may be enhanced or inhibited, depending on the tuning of the resonator, and its transition frequencies shifted. A simple classical description of these effects is given in which the atom is modelled as a dipole oscillator whose radiated field is reflected back onto itself by the resonator's mirrors. A more rigorous and detailed quantum mechanical description is also given, and it is found that for the case of a weakly excited two-level atom, the quantum and classical calculations agree.

Two separate experiments are carried out. In the first, an atomic beam of ytterbium passes between the mirrors of a confocal resonator and is excited by a single mode cw dye laser on the $^1S_0$ - $^3P_1$ transition, and the intensity of radiation by the atoms into the cavity modes is recorded as a function of cavity tuning. The spontaneous emission rate of the atoms into the cavity modes is enhanced or inhibited by a factor of the order of the resonator's finesse when the resonator is tuned or detuned from the atomic resonance, respectively. This is the first observation of cavity-modified spontaneous emission by atoms in a resonator at visible wavelengths. The total spontaneous emission rate is modified by only about 2%, because the solid angle subtended by the cavity mirrors is small. This change in total spontaneous emission rate is indirectly verified by a measurement of the intensity of fluorescence out the sides of the resonator.

In the second experiment, barium atoms are excited near the center of a concentric optical resonator, and the center frequency and linewidth of the $^1S_0$ - $^1P_1$ transition is studied as a function of resonator tuning. Shifts in the transition center frequency, due to radiative level shifts, and changes in linewidth, due to enhanced and suppressed spontaneous emission, are observed. The total spontaneous emission linewidth is increased by 20% and decreased by 8%. This is the first demonstration of both line narrowing and broadening and frequency shifts arising from vacuum radiative effects in a spectroscopic experiment.

The experimental conditions are very precise: two-level atoms are excited by a single cw dye laser, and competing decay channels and nonradiative effects are absent. Therefore a direct comparison between theory and experiment can be made, and it is found that good agreement is obtained.

Thesis Supervisor: Michael S. Feld

Title: Professor of Physics

ACKNOWLEDGEMENTS

It is a pleasure to acknowledge the many contributions and support of my friends and coworkers who have helped in one way or another to complete this work. First and foremost I thank Professor Michael Feld who has given continual guidance and support since I first joined the lab as an undergraduate in 1980. He has always been ready to help whenever help is called for, and his ideas, energy, and optimism were a major factor in whatever progress I have made. He has certainly influenced my development as a scientist and I hope that I will be able to adopt some of his many positive qualities. I also thank the other members of the thesis committee, Prof. Kleppner, Prof. Litster, and Prof. Glauber, for reading this thesis and for their useful and constructive comments.

Also deserving a great deal of credit as role models and teachers are John Thomas and Carter Kittrell. Probably I have learned more about working in the laboratory from these two than all others put together. John also brought a great deal of enthusiasm to the lab, and during our many discussions contributed to both the ideas behind these experiments and also showed me how to do such things as lock the laser to a transition, or calculate matrix elements, and besides all this provided a reliable partner for chinese lunches. Carter also was quite a guru when it came to practical laboratory advice, and amid all of his "junk piles" always seemed to have such useful gems as 600 Amp transformers for running tube ovens, or a couple of extra photomultiplier tubes or amplifiers. I also enjoyed our many late night conversations, as he seemed to have an unorthodox but (usually) very well thought out opinion on just about any subject.

Another person who has helped a great deal along the way and deserves thanks is Dr. Ramachandra Dasari. Besides helping out with many laboratory matters such as obtaining new plasma tubes, he has frequently served as a source of useful advice. Carol Campbell also has been a friend from the earliest days of my stay here, and has given plenty of "moral support" (if she's not giving me grief instead!). Other office people who I remember as being particularly helpful are Renel Thomas and Kim Tseko.

Of course, the "old gang" of Bill Quivers, Rick Forber, Greg Shimkaveg, and Amal Ghosh cannot go without mention. I remember these days as being the most friendly time around the lab, and especially the trips out to "Leo J." Also very high on the list of friends to thank are labmates Mike Kash, George Welch, and John Iu. I especially thank Mike Kash for being a close friend and George Welch for being such an entertaining person.

They also deserve loads of credit for helping me in the lab, especially George, who not only let me use "Murdoch" to take the Yb data but spent time changing around his computer program to help make it easier. I also thank others who have helped out in the lab, including visiting scientist Igor Shumay and UROPer Chris Monroe. Also, Jim Childs, who is taking over the experiment, has made significant contributions to the work. I wish him very well and hope that there are many interesting surprises yet to be discovered in this experiment.

Over the past few years there have been a large number of other students, staff, and outside visitors who have given help and made the spec lab a nicer place to work. Among them are Rim Cothren, Gary Hayes, Joe Izatt, Rebecca Richards-Kortum, Firooz Partovi, Joe Mackin, Kyungwon An, Mike Otteson, and Tim Hutton. Numerous members of the support staff deserve thanks, including Erik Erikson, John Devir, Bob Quinn, Don Postell, Tony Willis, George Leach, and Johnny Annese. All of these guys have provided valuable help at one time or another. One other person who deserves special mention is Eugene Gath. Besides humoring me by attempting to explain the intricacies of supersymmetric string theory to a lowly experimentalist, he provided the answer to the integral worked out in Appendix 1 and also evaluated the sums of Bessel functions in chapter III. I will also fondly remember the thursday night "bughouse" crowd of Eugene, Mark Smith, John Baez, Monty McGovern, and Bob Holt.

Finally, I thank my parents Joseph and Mary Heinzen for their many years of caring and support.

RADIATIVE DECAY AND LEVEL SHIFT OF AN ATOM IN AN OPTICAL RESONATOR

Contents

CHAPTER I

INTRODUCTION AND SURVEY.

I.A. Spontaneous Emission and Level Shifts in Cavities.

The decay of an excited atom by spontaneous emission is the most fundamental consequence of the coupling of an atom to the radiation field. Spontaneous emission is intimately connected with every aspect of optical physics - blackbody radiation, optical absorption and scattering, optical pumping, and radiation pressure - involving the interaction between atoms and radiation. As first pointed out by Einstein[1], spontaneous emission must occur if thermal equilibrium between atoms and their surroundings is to be maintained. The explanation of spontaneous emission by quantum electrodynamics[2] (QED) was one of the first successes of this theory, and is one of the most important reasons why it is accepted as *the* theory of light and matter.

Because of the fundamental nature of spontaneous emission, we tend to view it as an unavoidable and unchangeable phenomenon. Generally, we think of the radiative lifetime of an atomic state as a property only of that particular state; for instance, we say that the "lifetime of the Na $^2P_{3/2}$ state" is 16 ns. But as was first pointed out by Purcell,[3] a radiative lifetime may depend not only on the atomic state, but on the surrounding environment as well. In particular, Purcell pointed out that an atom in a resonant cavity of quality factor Q and volume V has a spontaneous emission rate given by

$$\Gamma_{cav} = \frac{3Q}{4\pi^2}\frac{\lambda^3}{V}\Gamma_{free}, \tag{1.1}$$

where λ is the emission wavelength and Γ_{free} the spontaneous emission rate in free space. For the low order modes of cavities, $V \sim \lambda^3$, so the spontaneous emission rate is enhanced by a factor of order Q.

Spontaneous emission may also be inhibited by a cavity. For example, if an atom is placed in a cavity whose lowest order mode has a frequency much higher than the atomic frequency, then in the limit of infinite Q, there is no mode available at all for decay; the spontaneous emission rate is zero. Essentially, the wave emitted by the atom cannot "fit" into the cavity. For the case where the cavity Q is finite, it can be shown that the radiation is inhibited by a factor of the order of 1/Q. [4]

Experimentally, enhanced and inhibited spontaneous emission were initially somewhat difficult to observe. The first work in this area was by Drexhage.[5] He studied the fluorescence lifetime of a monomolecular layer of dye molecules deposited over a thin dielectric layer on top of a metal substrate. For dielectric layer thicknesses of much less than a wavelength, the flourescence lifetime was lengthened over that for thicker layers.

More recently, there has been a great deal of interest in this area, mainly stimulated by the development of techniques for studying the interaction of Rydberg atoms with microwave cavities. Kleppner[4] first proposed that inhibited spontaneous emission might be observed using these techniques. Shortly after this, both enhanced[6] and inhibited[7] spontaneous emission were observed, as well as a number of other related effects.[8-13]

In all of these atom-cavity experiments, the wavelength of the radiation was very long, in the millimeter or microwave range; no studies were carried out in the visible. Yet clearly such studies would be of great interest, since it is only at visible wavelengths that the rates of spontaneous emission typically become significant when compared with other processes. Working in the visible also has important experimental advantages, including the ability to detect single photons, and the absence of thermal excitation of the radiation field. It is also generally easier to obtain high signal-to-noise ratios in visible experiments, so finer details of the theory may be examined.

The reason for the absence of such experiments in the optical range appears to be that it was felt the cavity size must always be of the order of the wavelength. For instance, Filipovicz et al[14] argued using Purcell's result (1.1) that since any practical optical resonator must have $\lambda^3 << V$, the enhanced emission rate would always be small in spite of the high Q of optical cavities.

However, in this thesis we point out that it is possible to observe enhanced spontaneous emission at visible wavelengths. Of course, Purcell's result is correct, in as much as it applies to a single mode. But in certain resonator geometries, a large number of resonator modes have the same resonant frequency. In this case the combined effect of all the modes, when tuned to the atomic resonance, is sufficient to significantly enhance the spontaneous emission rate. Conversely, when all the modes are detuned the radiation may be significantly suppressed.

Eq. (1.1) is also correct only if the volume V is interpreted not as the actual volume of the resonator, but as the "effective mode volume" V_{eff}, which is weighted by the inverse of the square of the field amplitude at the atom's position. For example, it is easy to show that if the atom is located precisely in the center of a spherical resonator of radius $a >> \lambda$, the atom interacts with *only* with the lowest order transverse mode of the sphere, and that the effective volume of this mode is $V_{eff} = 3\lambda^2 a/2\pi$. This is much less than the volume $V = 4\pi a^3/3$, and takes into account a strong focussing of the field onto the atom. Since the Q of this resonator is $4\pi a/\lambda(1-R)$, where R is its reflectivity, we obtain from eq. (1.1) that $\Gamma_{cav}/\Gamma_{free} = 2/(1-R)$, which can easily be much greater than 1. Therefore, the effect of the resonator on the atom's radiation can be dramatic, even though $V >> \lambda^3$ and the interaction is with only a single mode.

An effect closely related to spontaneous emission is the radiative level shift. Here too, the subject is of great importance to optical and atomic physics. The most significant example of this is Bethe's calculation[15] of the Lamb shift, in which he demonstrated that the observed splitting between the hydrogen $2s_{1/2}$ and $2p_{1/2}$ states is essentially radiative in character. The calculation of such level shifts provides another important test of QED.

In principle radiative level shifts should also be modified in a cavity.[16-18] However, there has been much less attention focussed on this issue, since this effect is generally much more difficult to observe experimentally, at least for the Rydberg atom-microwave cavity case. The reason is that the size of the shift scales in proportion to the spontaneous emission rate of the transitions affected by the cavity, which is very small ($\sim 10^2\ s^{-1}$) for Rydberg atoms. For example, Dobiasch and Walther[17] have estimated that in a waveguide configuration, with a cutoff wavelength of 0.5 mm, the change in the Lamb shift of the 23s state of hydrogen is only about 100 Hz, or about 2×10^{-10} of the 23s-24p transition frequency. This must be detected against a linewidth of at least 26 kHz which arises from the decay of the atoms back down to lower levels. The effect can be made larger by decreasing the plate spacing of the waveguide, but this can only be carried so far before nonradiative shifts due to the Van derWaals interaction between the atoms and the cavity walls become important.[19]

As was the case for spontaneous emission, the possibility of studying radiative level shifts in the optical regime has been largely ignored. But the optical regime presents several advantages for the observation of radiative frequency shifts. First, the effect scales in proportion to the much larger decay rate ($\sim 10^8\ s^{-1}$). Also, this decay rate can be the only broadening mechanism, so that the size of the effect and the linewidth are of the same order. Finally, nonradiative effects are negligible in the large open resonator.

I.B. Physical Interpretation of Cavity Effects on Spontaneous Emission.

I.B.1. Vacuum Fluctuations and Radiation Reaction.

Physically, spontaneous emission may be interpreted as arising from the effect of "vacuum fluctuations". Since the expectation value of the dipole moment of an atom in a pure excited state is zero, it cannot radiate classically. But the quantized electromagnetic field carries a zero-point energy of $\frac{1}{2}\hbar\omega$ per mode, and associated with this energy is a randomly fluctuating electric field. This field couples to the atom, inducing a dipole moment and causing it to radiate. Thus, spontaneous emission may be viewed as "stimulated by vacuum fluctuations". Note that this interpretation is inherently quantum mechanical; there is no sensible classical explanation for a "noisy vacuum".

Alternatively, spontaneous emission may be interpreted as arising from the effect of "radiation reaction". If the atom has a dipole moment, its optically active electron is accelerating, and therefore radiates. Associated with this radiated field is a component reacting back onto the electron, producing a force on it which accounts for the energy loss. The objection that the atom in a pure excited state has no dipole moment may be overcome by our noting that the expectation value of the square of the dipole moment is nonzero; i. e. the atom does have randomly fluctuating dipole moment. Note that this interpretation of spontaneous emission can be consistent with a classical electromagnetic field.

The extent to which one or the other of these interpretations is correct has been the subject of considerable debate.[20-24] Milonni, Ackerhalt, and Smith have pointed out that the interpretation depends in some sense of the ordering of certain *commuting* operators.[22] For one choice of ordering, both spontaneous emission and the level shift can be interpreted as arising from radiation reaction alone.[21] It is also possible to choose an ordering which attributes the level shift entirely to vacuum fluctuations, but there is *no* ordering in which spontaneous emission can be interpreted in terms of vacuum fluctuations alone. More recently, Dalibard, Dupont-Roc, and Cohen-Tannoudji have presented a very compelling argument for a particular ordering of operators.[24] Assuming this choice is correct, both vacuum fluctuations and radiation reaction are essential. They find that half the downward transition rate of an excited state atom is due to vacuum fluctuations, and half due to radiation reaction. Surprisingly, they find that a ground state atom also radiates

energy into the vacuum due to the effect of radiation reaction, which is balanced by the absorption of energy from vacuum fluctuations.

Thus even for the spontaneous emission of an atom in free space, the physical interpretation is somewhat problematic. Nevertheless, it is always useful to have a simple physical picture of a process, which in this case is provided by either vacuum fluctuations or radiation reaction.

I.B.2. Effect of the Cavity.

To describe the effect of a cavity on spontaneous emission, two approaches are generally used. In the first, one solves for the normal modes of the field, and obtains a solution in terms of an expansion in these normal modes. A different set of normal modes is obtained in a cavity, due to the boundary conditions imposed by the reflecting surfaces. From this point of view, changes in spontaneous emission are attributed to "changes in mode density". For example in free space there are $\rho_{free}(\omega) = V\omega^2/\pi^2c^3$ modes per unit frequency, whereas for a single cavity mode there is essentially one mode per cavity linewidth $\Delta\omega_c$; i. e. $\rho_{cav}(\omega) \sim 1/\Delta\omega_c = Q/\omega_c$. According to Fermi's golden rule, the decay rate of an unstable state is proportional to the density of modes, so we expect that the ratio of the decay rate of the atom in the cavity to that in free space is given by $\rho_{cav}/\rho_{free} \sim Q\lambda^3/V$, in agreement with eq. (1.1).

The mode density point of view is more naturally associated with a physical interpretation in terms of vacuum fluctuations: because there is a zero point energy of $\frac{1}{2}\hbar\omega$ per mode, an increase in the mode density will be accompanied by an increase in vacuum fluctuations, and therefore the decay rate increases. This situation is illustrated in Fig. 1.1. Figure 1.1(a) shows the atom in free space. The vacuum fluctuations are uniform in frequency and in space. Figure 1.1(b) shows the atom in a parallel plate cavity, assumed to be tuned to the atomic resonance (e.g. the plate spacing is $\lambda/2$). The vacuum fluctuations are very much enhanced in the cavity, due the the increased mode density associated with the cavity resonance. Only noise at the cavity resonance frequency is illustrated; at other frequencies the noise is reduced inside the cavity.

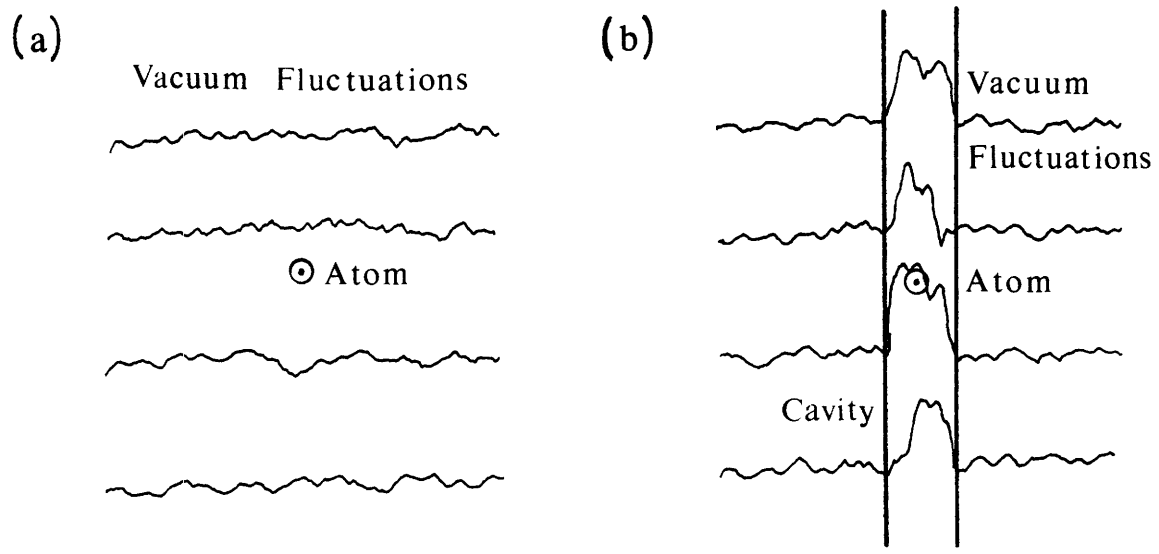

Fig. 1.1. Vacuum fluctuation interpretation of cavity-modified spontaneous emission. (a) Atom in free space. (b) Atom between parallel plates.

The second approach to the problem of cavity modified spontaneous emission is to view it as an interference phenomenon. This point of view is illustrated in Fig. 1.2, for the case of an atom between parallel plates. In free space, the atom radiates a wave E_D which escapes to infinity. But in the cavity the directly radiated wave is only partially transmitted through the mirror, and to this transmitted direct wave E_D we must coherently add the contribution of a series of waves E_{Ri} transmitted through the cavity mirrors after one or more reflections from them. This situation is illustated in Fig. 1.2(b), for a plate spacing of $\lambda/2$. The cavity is tuned to resonance, so the fields interfere constructively, and the radiation is enhanced.

This intereference point of view corresponds to a Green's function or image method solution of the problem: the mirrors produce an infinite chain of image dipoles, and the field at any give point is obtained by summing over the contributions from the dipole and all its images. Milonni and Knight[25] have pointed out that there is an interesting quantum mechanical interpretation of this. A photon arriving at a given point carries no information as to whether it came from the atom or one of the fictitious image atoms. Therefore the effect may be thought of as a Dicke superradiance or subradiance[26] of the atom together with all of its images.

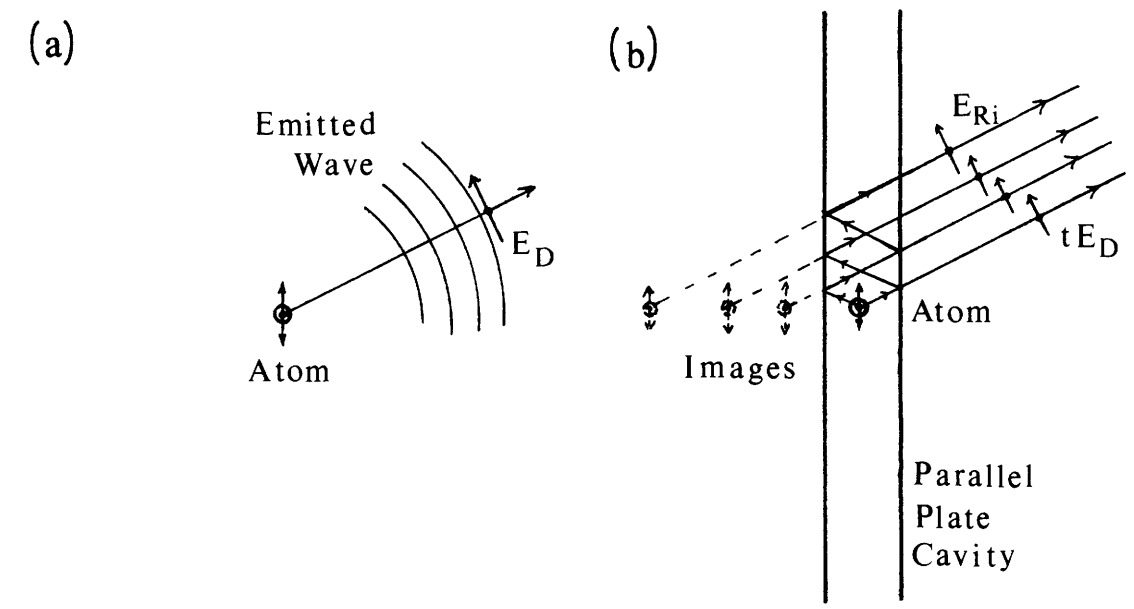

Fig. 1.2. Interference picture of cavity-modified spontaneous emission.
(a) Atom in free space. (b) Atom between parallel plates.

This interference picture is more naturally associated with a physical interpretation in terms of radiation reaction. Normally, the radiation reaction experienced by the atom is associated with its electron's acceleration at the current instant of time. But in the cavity, the field radiated at past times is reflected back onto the atom, adding to or subtracting from the radiation reaction field, and producing a net increase or decrease in the decay rate depending on the tuning of the cavity.

I.B.3. Possibility of Using Large-Sized Cavities.

The previous section discussed the case of an atom in a plane parallel cavity with a spacing less than a wavelength. Clearly, as the plate spacing becomes greater than a wavelength, the effect of the cavity will be very much diminished. This is because the phase shift associated with the round trip path difference between parallel sets of light rays varies rapidly with angle, as illustrated in Fig. 2.3(a). The interference is constructive at some angles, but destructive at others, so the radiated power averaged over all angles is unaffected. Also, note that the radiation reaction field is weak because the wave diverges greatly before it is reflected back onto the atom.

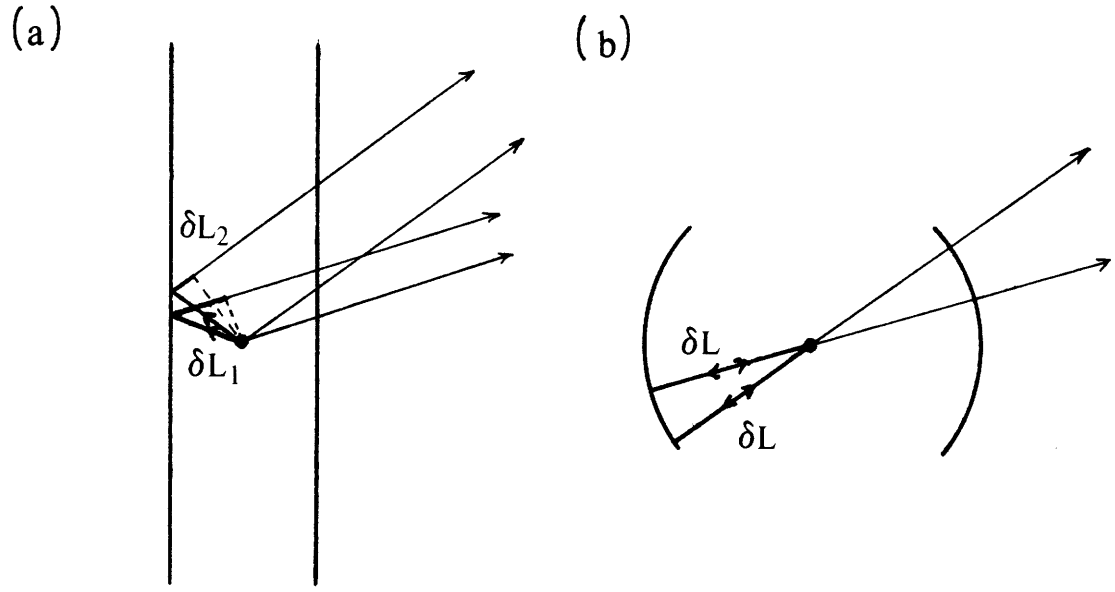

Fig. 1.3. (a) Large plane-parallel cavity. The phase shift between parallel sets of light rays is a function of the angle. (b) Large concentric cavity. The phase shift is constant.

This does not imply that large-sized resonators cannot be used. All one has to do is to "bend around" the mirror as in the concentric resonator illustrated in Fig. 1.3(b). In this case, the phase shift is a constant function of the angle. The contribution of the reflected field to radiation reaction is now very strong, due to the tight focussing of the field back onto the atom.

Actually, the illustration of Fig. 1.3(b) holds only if the atom is located precisely at the center of the resonator. However, in chapter II we will show that these same properties apply so long as the atom is displaced from the center by a distance much less than $\sqrt{\lambda L}$, where L is the spacing between the mirrors. We also discuss the confocal resonator, which has properties similar to that of the concentric.

An interesting question is how large the cavity can be. Clearly as the cavity becomes very large, retardation will play a major role. We defer a discussion of this issue until chapter VI, but for now we mention that as long as the round trip time in the cavity is less than the spontaneous emission lifetime, retardation effects do not play an important role.

I.B.4. High Q Limit.

The previous discussions have been phrased in terms of "decay rates" and "level shifts". This presupposes that the Wigner-Weisskopf approximation[2] is valid; i.e., that the spontaneous decay is to a continuum of final states. For a low Q cavity this limit applies, because the atom essentially interacts with only the center of the broad cavity lineshape. However, if the atom interacts with only a single cavity mode, then as the Q is increased the mode eventually becomes so sharp that the Wigner-Weisskopf treatment breaks down. We refer to this limit as the high Q or ideal cavity limit.

The interaction of a two level atom with a single lossless cavity mode was first treated by Jaynes and Cummings.[27] They show that if at t = 0 the atom is in its excited state and the cavity mode contains exactly n photons, then the probability for the atom to be found in the excited state at a later time t is

$$P_e(t) = \frac{4(n+1)g^2}{\Delta^2 + 4(n+1)g^2}\cos^2\left(\frac{1}{2}\sqrt{\Delta^2 + 4(n+1)g^2}\, t\right), \tag{1.2}$$

where $\Delta = \omega - \omega_c$ is the atom-cavity detuning and

$$g = \frac{\mu}{\hbar}\sqrt{\frac{2\pi\hbar\omega}{V_{eff}}} \tag{1.3}$$

is the atom-cavity mode coupling constant, with μ the atomic dipole matrix element. This formula looks very much like the usual semiclassical result for Rabi oscillations,[28] but surprisingly the Rabi cycling behavior persists down to the vacuum state n = 0.

For $\Delta = 0$ and n = 0, corresponding to a resonant cavity mode initially in the vacuum state, we find that

$$P_e(t) = \cos^2(gt)\,. \tag{1.4}$$

Rather than exhibiting exponential decay, the excitation oscillates sinusoidally between the atom and the cavity! This result makes some physical sense: the atom emits a photon into the cavity, which cannot leave the cavity due to the high Q, and is eventually reabsorbed by the atom. This behavior is referred to as the "vacuum Rabi oscillation".

The boundary between the high and low Q limits is determined by the relative values of the coupling constant g and the cavity linewidth $\Delta\omega_c = \omega_c/Q$. For $\Delta\omega_c >> g$ the cavity damping is so large that its damps out the vacuum Rabi oscillation and we are in the low Q, Wigner-Weisskopf limit. The condition $\Delta\omega_c << g$ gives the high Q limit. For $\Delta\omega_c << g$ but Q still finite, the decay rate of the energy out of the cavity actually is proportional to

1/Q. Thus there is an intermediate value of the Q at which the decay rate of the energy from the atom-cavity system is a maximum.

The behavior of a single atom interacting with an ideal cavity mode in the vacuum state has never been studied experimentally, which unfortunately remains the case in the present work as well. This situtation is commented on in chapter VI.

I.C. Survey of Recent Studies of Cavity-Modified Radiation.

As already mentioned, the first experimental observation of inhibited spontaneous emission was that of Drexhage,[5] who studied radiation by dye molecules near a conducting surface. Most of the experimental work, however, has involved Rydberg atoms in microwave cavities. Enhanced spontaneous emission of Rydberg atoms in a cavity was observed by Goy, Raimond, Gross, and Haroche,[6] and the first observation of inhibited spontaneous emission of an atom in a cavity was that of Hulet, Hilfer, and Kleppner.[7] A closely related effect, inhibited spontaneous absorption of blackbody radiation, was studied by Vaidyanathan, Spencer, and Kleppner.[8] Other interesting related Rydberg atom-cavity experiments were the observation of the "collective absorption" of blackbody radiation[9], superradiance of atoms in a cavity,[10] a "one atom maser",[11] the "quantum collapse and revival" of Rabi oscillation by atoms in a cavity,[12] and two photon maser action.[13]

Inhibited spontaneous emission has also very recently been observed on an infrared transition of Cs atoms passing between two parallel plates spaced by less then one-half of the infrared wavelength.[30] A similar experiment has been carried out with a dye solution between two mirrors.[31] Also, Gabrielse and Dehmelt[32] have observed inhibited spontaneous emission of cyclotron radiation by electrons in a Penning trap.

Theoretically, the first suggestion that spontaneous emission might be modified in a cavity appears to have been that of Purcell.[3] This effect was referred to by Townes and Schawlow in their book on microwave spectroscopy.[33] Interest in this subject was renewed in an article by Kleppner.[4] The general subject of radiation by atoms between conducting plates or near conducting boundaries has received a considerable amount of theoretical attention, including articles by Kastler,[34] Milonni and Knight,[25] Barton,[16] Agarwal,[35] Lütken and Ravndal,[18] and Arnouldus and George.[36] Other articles on spontaneous emission in cavities include those of Parker and Stroud,[37] who explicitly considered the effect of finite retardation time, and Barut and Dowling[38], who described the problem from the "self energy" formulation of QED. Various authors have speculated about the existence of other cavity effects, such as on the electron g-factor and mass.[39-41]

The interaction between an atom and a cavity in the high Q limit was first considered by Jaynes and Cummings.[27] This problem was reconsidered by Sanchez-Mondragen, Narozhny, and Eberly, who calculated the spectrum of the radiation in the cavity.[42] Recently Lewenstein, Mossberg, and Glauber,[43] and Lewenstein and Mossberg[44]

calculated the spectrum of fluorescence of a *driven* atom in a cavity. They made the point that a "dynamical" suppression of spontaneous emission may take place. The proper inclusion of cavity damping in the theory has received relatively little attention. One exception is the work of Sadchev,[45] who accounted for the damping using reservoir theory as developed by Lax,[46] and calculated the time dependent behavior of the atom in the cavity at values of Q intermediate between the high and low Q cases. This problem has recently been addressed from a mode density point of view.[47] There have as yet been no experimental observations of the time-dependent or spectral properties of a single atom in an ideal cavity in the absence of blackbody photons.

The interaction between one or more atoms in a cavity has been proposed as a means for the generation of nonclassical electromagnetic fields. For instance, the generation of squeezed states[48] or number states[49] has been discussed.

The question of cavity-induced level or frequency shifts has been discussed in many of the above articles, including those by Barton,[16] Dobiasch and Walther,[17] and Lütken and Ravndal.[18] Also, Chance, Prock, and Silbey discussed the frequency shift of a dipole oscillator near a conducting surface from a classical point of view.[50] There has as yet been no experimental observation of a cavity-modified radiative level shift other than the present work. A related effect, the frequency shift of a dipole resonance in metal island films spaced a small distance from a reflecting surface, has been observed by Holland and Hall.[51]

I.D. Contributions of the Present Work.

The purpose of this thesis is to carefully study the radiative decay and level shifts of atoms in an optical resonator. These studies are fundamentally different from previous atom-cavity experiments, in that we monitor both the natural linewidth and the center frequency of a transition and are able to detect changes in both. Also, the size of the resonator is much larger than a wavelength, and visible transitions are studied for the first time. As mentioned earlier, experiments in the optical regime are important, because spontaneous emission occurs at more significant rates than at longer wavelengths. Furthermore, since our experimental conditions are quite unique, it is possible that effects not observed in long wavelength experiments might be observed in ours.

Two separate experiments are carried out. The first experiment studies the spontaneous emission rate of excited ytterbium atoms in a confocal resonator. As is well known, the transverse modes of this resonator are degenerate, and therefore many modes are simultaneously brought into and out of resonance as the resonator is tuned. In this experiment we observe, for the first time, enhanced and inhibited spontaneous emission by atoms in a resonator at visible wavelengths. We find that the spontaneous emission rate into the resonator modes is enhanced and inhibited by a factor of $1/(1-R) \sim 40$ relative to the free space rate into the same solid angle, where R is the reflectivity of the mirrors. The changes in the total rate are small, about +1.5% and -0.6%, because the solid angle subtended by the mirrors is small. Therefore no direct observation is made of a change in the lifetime, natural linewidth, or radiative level shift. However, we are able to indirectly verify the change in total spontaneous emission rate in an experiment which measures the intensity of fluorescence emitted out the sides of the cavity.

The second experiment studies the center frequency and natural linewidth of the $^1S_0$ - $^3P_1$ transition of barium atoms in a concentric resonator. We directly observe, for the first time, changes in the natural linewidth of a transition due to enhanced and inhibited spontaneous emission. We also observe, for the first time, shifts in the frequency of a transition due to radiative level shifts. The changes are much larger than in the ytterbium experiment because the resonator subtends a much larger solid angle: the natural linewidth of 19 MHz increases by 20% and decreases by 8%, and the transition frequency shifts by about 1.5 MHz.

There has been a great deal of theoretical attention to cavity modified decay rates and shifts, but none of it is immediately applicable to the case of an open, optical resonator. We remedy this deficiency by presenting calculations of the spontaneous emission rate and level shift of atoms in confocal and concentric optical resonators. Both a classical and a quantum mechanical calculation are presented, and the results are found to agree.

Our experimental conditions are very precise: two-level atoms are excited by cw dye laser radiation, and competing decay channels and nonradiative effects are absent. The signal to noise ratio is very high, so we are able to measure each effect fairly precisely. We find that good agreement between theory and experiment is obtained. This is in contrast to most previous atom-cavity experiments, in which it was observed that the spontaneous emission rate was enhanced or inhibited, but there was no quantitative comparison with the theory.

To summarize, in this thesis the following new contributions are presented:

(i) First observation of enhanced and inhibited spontaneous emission by an atom at *visible* wavelengths.

(ii) Identification of a *new regime* of cavity modified spontaneous emission, in which the size of a resonator is much larger than a wavelength.

(iii) First direct observation of a change in the *natural linewidth* of a transition, due to enhanced and inhibited spontaneous emission.

(iv) First observation of a cavity-modified *radiative level shift.*

(v) Development of the classical theory of decay rates and frequency shifts of an atom in an *optical* resonator, and the quantitative comparison of the theory and experiment.

CHAPTER II.

CLASSICAL THEORY OF RADIATION BY A DIPOLE IN AN OPEN OPTICAL RESONATOR.

In this chapter we study the classical problem of radiation by a dipole in an open optical resonator. The treatment is essentially that illustrated in Fig. 1.2; i.e., we model the atom as a classical dipole, and find the field outside the cavity by superposition of the directly transmitted wave with a series of reflected waves. We also calculate the field reflected back onto the dipole, and this "reaction" field is found to account for both the modification of its decay rate and for a frequency shift. This picture provides a simple and physically intuitive model of spontaneous emission by an atom in a resonator.

II.A Radiation by a Dipole in Free Space.

II.A.1 Radiated Field and Intensity of the Free Dipole.

We first review the radiation by a dipole in free space. Consider a classical dipole consisting of an electron of charge e and mass m harmonically bound to a point $\mathbf{r}_d$ by a force $\mathbf{F}_b = -K\mathbf{x}$ where K is the force "spring constant" and $\mathbf{x}$ is the displacement of the electron relative to $\mathbf{r}_d$. Neglecting the effect of radiation damping, the motion of the electron is given by $\mathbf{x}(t) = \mathbf{x}_0 e^{-i\omega_0 t}$, where $\mathbf{x}_0$ is a constant vector and $\omega_0 = \sqrt{K/m}$ the oscillation frequency.

This oscillating electron has a dipole moment $\mathbf{d}(t) = e\mathbf{x}(t) = \mathbf{d}_0 e^{-i\omega_0 t}$, where $\mathbf{d}_0 = e\mathbf{x}_0$. Assuming that $|\mathbf{x}_0| << \lambda$, where $\lambda = 2\pi c/\omega_0$ is the emission wavelength, the oscillating electron can be treated as essentially a point dipole located at the position $\mathbf{r}_d$. This dipole gives rise to a radiated field[52]

$$\mathbf{E}_{free}(\mathbf{r},t) = -\frac{\omega_0^2}{c^2}((\mathbf{n}_d \times \mathbf{d}) \times \mathbf{n}_d)\frac{e^{ik|\mathbf{r}-\mathbf{r}_d|}}{|\mathbf{r}-\mathbf{r}_d|}\,, \tag{2.1}$$

where $\mathbf{n}_d$ is a unit vector in the direction of $\mathbf{r} - \mathbf{r}_d$, and it is assumed that $|\mathbf{r} - \mathbf{r}_d| >> \lambda$. (See Fig 2.1.) If also $|\mathbf{r}| >> |\mathbf{r}_d|$, the field is approximately given by,

$$\mathbf{E}_{free}(\mathbf{r},t) = -\frac{\omega_0^2}{c^2 r}((\mathbf{n} \times \mathbf{d}) \times \mathbf{n})\, e^{ik|\mathbf{r}-\mathbf{r}_d|}\,, \tag{2.2}$$

where $\mathbf{n}$ is a unit vector in the direction of $\mathbf{r}$. If we further assume that the three components of $\mathbf{d}$ are in phase, so that the dipole is linearly polarized, then the radiated power per unit solid angle is

$$\left(\frac{dP}{d\Omega}\right)_{free} = \frac{c}{8\pi} r^2\, \mathbf{E}\cdot\mathbf{E}^* = \frac{\omega^4}{8\pi c^3}|\mathbf{d}|^2 \sin^2\theta\,, \tag{2.3}$$

where θ is the angle between $\mathbf{d}$ and $\mathbf{r}$. The total power radiated by the dipole is

$$P_{free} = \int_{4\pi}\left(\frac{dP}{d\Omega}\right)_{free} d\Omega = \frac{1}{3}\frac{\omega^4}{c^3}|\mathbf{d}|^2\,. \tag{2.4}$$

This result holds true for arbitrary polarization.

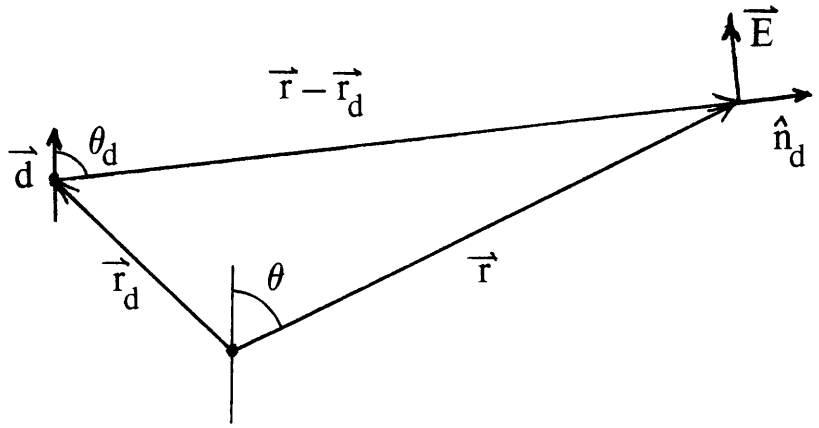

Fig. 2.1. Field radiated by a dipole in free space.

II.A.2 Radiation Reaction Field and the Abraham-Lorentz Equation.

Since energy is being carried away by the radiated field, it is evident that the electron must be doing work against some force other that the conservative force $\mathbf{F}_b$. This force is provided by the "radiation reaction field", i.e. the field produced at the position $\mathbf{r}_d$ due to the electron itself. It is interesting to note that for a truly point electron, a completely satisfactory account of radiation reaction has never been given.(53) The difficulty arises in the divergence of the Coulomb field of the electron at short distances, resulting in an infinite self-energy contribution to the electron mass. In order to circumvent such difficulties it is generally assumed that the electron has a finite size, or equivalently, that only the modes of the electromagnetic field up to some maximum frequency ω_{max} can couple to the electron.

A useful form for the self-field of the oscillating electron has been given by Stroud and Jaynes.(20) They find that the electron self-field can be written as

$$\mathbf{E}_{free}(\mathbf{r},t) = \int_{-\infty}^{t} G_{free}(\mathbf{r},t;\mathbf{r}_d,t')\ddot{\mathbf{d}}(t')dt' , \qquad (2.5)$$

where the Green's function $G_{free}(\mathbf{r},t;\mathbf{r}_d,t')$ is given at the position $\mathbf{r} = \mathbf{r}_d$ by

$$G_{free}(r_d,t;r_d,t') = -\frac{4}{3\pi c^3}\int_0^{\omega_{max}} d\omega\ \omega\sin\omega(t-t')$$

$$= \frac{4}{3\pi c^3}\frac{\partial}{\partial t}\left(\frac{\sin\omega_{max}(t-t')}{(t-t')}\right), \qquad (2.6)$$

and where the upper cutoff frequency ω_{max} is taken very large, but not so large that δm (defined below) is greater than m. Note that since ω_{max} is very large, only past times $t' \gtrsim t - (1/\omega_{max})$ which are very close to t will contribute significantly to $\mathbf{E}_{free}$. Inserting the expression for G_{free} into eq. (2.5) gives

$$\mathbf{E}_{RR,free}(t) = \mathbf{E}_{free}(r_d,t) = \frac{2}{3c^3}\dddot{\mathbf{d}}(t) - \frac{4\omega_{max}}{3\pi c^3}\ddot{\mathbf{d}}(t)\ . \qquad (2.7)$$

Using this result, we can now write down the equation for the bound electron:

$$m_{bare}\ddot{\mathbf{x}} + K\mathbf{x} = e\mathbf{E}_{RR}\ , \qquad (2.8)$$

which can be rewritten as,

$$(m_{bare} + \frac{4}{3}\delta m)\ddot{\mathbf{x}} + K\mathbf{x} = \frac{2e^2}{3c^3}\dddot{\mathbf{x}}\ . \qquad (2.9)$$

Here m_{bare} is the "bare" electron mass, i.e., the electron mass in the absence of any consideration of the electromagnetic field, and

$$\delta m\, c^2 = \frac{e^2\omega_{max}}{\pi c} = \frac{\alpha}{\pi}\hbar\,\omega_{max}\ , \qquad (2.10)$$

where $\alpha = e^2/\hbar c$ is the fine structure constant. It may easily be demonstrated that δm is nothing more than the Coulomb self-energy contribution to the electron mass, and as such it should already be regarded as having been included in the observed electron mass $m = m_{bare} + (4/3)\delta m$. This point is emphasized in the treatments given by Jackson[53] and by Dalibard, Dupont-Roc, and Cohen-Tannoudji.[24] However, in certain treatments of this problem the term δm itself is interpreted as giving rise to a radiative or "Lamb" shift.[20, 23] (The factor of 4/3 is a spurious consequence of the noncovariant cutoff procedure used in eq. (2.6); this discrepancy is removed in more rigorous treatments.[53])

Substituting for m, eq. (2.9) can be written as,

$$m(\ddot{\mathbf{x}} - \tau\dddot{\mathbf{x}}) = \mathbf{F}_b\ , \qquad (2.11)$$

or in our case as,

$$\ddot{\mathbf{x}} + \omega_0^2\,\mathbf{x} = \tau\dddot{\mathbf{x}}\ . \qquad (2.12)$$

Eq. (2.11) is known as the Abraham-Lorentz equation. Here the parameter $\tau = 2e^2/3mc^3 = 6.26 \times 10^{-24}$ s is a characteristic time, which in the classical theory of the electron is of the order of the time taken for light to travel across the finite electron radius

$r_0 = e^2/mc^2$. The motion of the electron will be strongly damped if the period of oscillation $T \gtrsim t$; otherwise, it will be weakly damped. In the optical range $\omega_0 \tau << 1$ and therefore the damping is always weak.

The solution to eq. (2.10) can be written as $x = x_0 e^{\alpha t}$, where α is given, correct to second order in $\omega_0\tau$, by

$$\alpha = \frac{\Gamma}{2} \pm i(\omega_0 + \Delta\omega) , \tag{2.13}$$

where

$$\Gamma = \omega_0^2 \tau = \frac{2e^2\omega_0^2}{3mc^3} \tag{2.14}$$

and

$$\Delta\omega = -\frac{5}{8}\omega_0^3\tau^2 = -\frac{5}{18}\frac{e^4\omega_0^3}{m^2c^6} . \tag{2.15}$$

For the sodium D-lines, $\omega_0 = 3.2 \times 10^{15}\ s^{-1}$ ($\omega_0\tau = 2.0 \times 10^{-8}$), resulting in $\Gamma = 6.4 \times 10^7\ s^{-1}$ ($\Gamma/2\pi = 10$ MHz) and $\Delta\omega = -0.8\ s^{-1}$ ($\Delta\omega/2\pi = -0.13$ Hz). It is interesting to note that this value for Γ is precisely the observed value. (This is because the oscillator strength for this transition equals 1.) The frequency shift in this model is of second order in $\omega_0\tau$ and is extremely small. It is of the same character (proportional to Γ^2/ω_0) as that observed for any damped classical oscillator.

II.B. Field Radiated by a Dipole in an Optical Resonator.

II.B.1 Effect of a Symmetrical Optical Resonator on a Radiating Dipole

Consider a dipole at the position $\mathbf{r}_d$ in a symmetrical optical resonator of length $L = 2a$, consisting of mirrors M1 and M2, each of diameter 2b, and of reflectivity R_1 and R_2, and radius of curvature $+R_c$ and $-R_c$, respectively (Fig. 2.2). We assume that the mirrors are lossless, so that the transmission coefficients of M1 and M2 are given by $T_1 = 1 - R_1$ and $T_2 = 1 - R_2$, respectively, and we also define the quantitites $r_1 = \sqrt{R_1}$, $t_1 = \sqrt{T_1}$, $r_2 = \sqrt{R_2}$, and $t_2 = \sqrt{T_2}$. We take the z-axis to coincide with the resonator's optical axis, with the origin O exactly halfway betwen the two mirrors, and we take the x-axis in the direction of the dipole's displacement from the resonator axis, so that $\mathbf{r}_d = z_d\mathbf{z} + x_d\mathbf{x}$. The focal lengths of M1 and M2 are $f_1 = +R_c/2$ and $f_2 = -R_c/2$, respectively, where the mirror radius or focal length is considered to be positive if the center of curvature lies in the - z direction. We assume throughout that $|r_d| << a$, and also that the dipole is linearly polarized in the x-y plane. We also assume that $b << a$ so that the light propagating between M1 and M2 may be treated in the paraxial approximation. (Terms of order $(b/a)^3$ may be neglected.) This also implies that the vector nature of the field may be neglected, for the part of the field propagating between M1 and M2.

In order to calculate the total power radiated by the dipole, we integrate the intensity passing through a spherical surface S centered on the origin whose radius we take for convenience to be $a + \delta a$ ($\delta a << a$), i.e., a spherical surface passing just outside M1 and M2. The spherical surface divides naturally into three parts: S_1, the part lying just outside M1, S_2, the part just outside M2, and S_{side}, the remainder of the sphere. S_1, S_2, and S_{side} subtend solid angles $\Delta\Omega_1$, $\Delta\Omega_2$, and $\Delta\Omega_{side}$, respectively, where $\Delta\Omega_1 = \Delta\Omega_2 \cong 4\pi b^2/L^2$ ($b << L$), and $\Delta\Omega_1 + \Delta\Omega_2 + \Delta\Omega_{side} = 4\pi$.

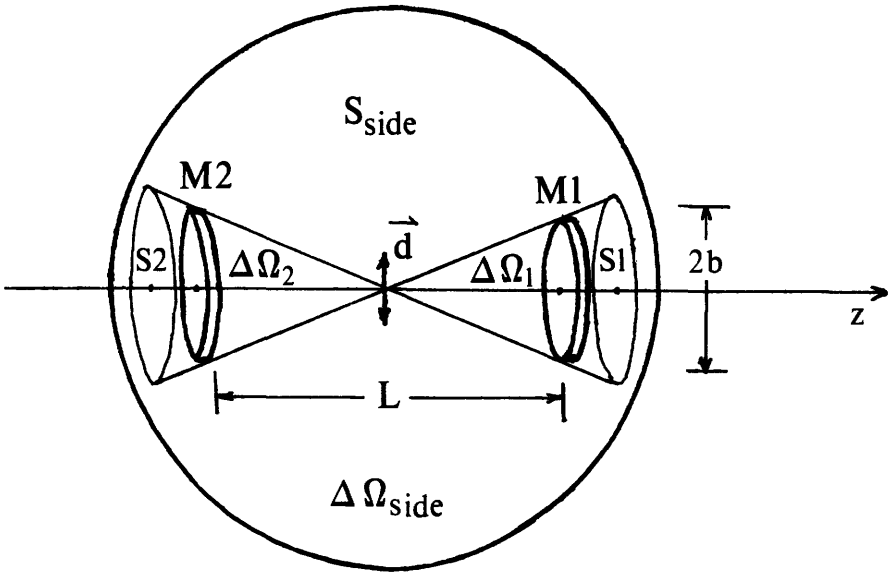

Fig. 2.2. Dipole in a symmetrical optical resonator.

Consider first the power radiated through S_{side}. Clearly, the power per unit solid angle into $\Delta\Omega_{side}$ will be unchanged from free space, provided that any radiation reflected by mirrors M1 and M2 is contained entirely in $\Delta\Omega_1$ and $\Delta\Omega_2$ and does not "spill over" into $\Delta\Omega_{side}$. A necessary condition for this to be the case is that the resonator must be *stable*. For the symmetrical two mirror resonator the stability crtierion can be written as[54]

$$0 \leq \left| 1 - \frac{2a}{R_c} \right| \leq 1 . \tag{2.16}$$

In addition, it is necessary that the Fresnel number $F = \pi b^2/\lambda L >> 1$, that $z_d << a$ and $x_d << b$, and that $R_c \leq 2a$, as discussed below. From eq. (2.16), we see that the two limits of stability are $R_c = +\infty$, which corresponds to a plane parallel resonator, and $R_c = +a$, which corresponds to a concentric resonator.

If we assume these requirements are satisfied, then the total power P_{side} passing through S_{side} is simply the total free space power P_{free} minus the power p_{free} ordinarily emitted into $\Delta\Omega_1$ and $\Delta\Omega_2$. Note that, from eqs. (2.3) and (2.4),

$$p_{free} = \left(\frac{dP}{d\Omega}\right)_{\substack{free \\ (\theta=\pi/2)}} \Delta\Omega_{cav} = \frac{3}{8\pi} \Delta\Omega_{cav} P_{free}, \tag{2.17}$$

where

$$\Delta\Omega_{cav} = \Delta\Omega_1 + \Delta\Omega_2 = 8\pi b^2/L^2. \tag{2.18}$$

Therefore,

$$P_{side} = P_{free}\left[1 - \frac{3}{8\pi}\Delta\Omega_{cav}\right]. \qquad (2.19)$$

Again, in this equation it has been assumed that the dipole is oriented at right angles to the cavity axis (so the radiated intensity is peaked in the direction of the mirrors), and that the solid angle subtended is small.

In order to calculate the power emitted through S_1 and S_2, we must take into account not only the field emitted by the dipole and transmitted through M1 or M2, but also the fields arriving at S_1 or S_2 after having first been reflected from M1 and M2 one or more times and then transmitted. If on the average, there is a net constructive or destructive interference among these waves, the power radiated by the dipole will be enhanced or inhibited.

For arbitrary mirror focal length, this effect is generally very small. This is because the phase of the interference pattern varies rapidly across the mirror aperture, resulting in many regions of constructive and destructive interference, and in the average over all these regions the effect is washed out. However, for certain mirror radii of curvature, the phase of the interference may be essentially constant over the entire mirror aperture, so that a large net enhancement occurs when the interference is constructive, and an inhibition when it is destructive. These special radii arise whenever the resonator has the property that the light emitted by the dipole is refocussed back onto itself after n round trips of the resonator (n = 1, 2, 3 . . .). This property may be understood by our noting that any ray emitted by the dipole will return to it after n round trips, and that the round trip accumulated phases of all such rays are identical. Associated with this "ray degeneracy" is a degeneracy of the corresponding Hermite-Gaussian modes[54] of the resonator.

Mirror radii of curvature having this property are tabulated in table 2.1, for n = 1 to 4. The radii at which such degeneracies occur are given by the formula

$$\frac{R_c}{L} = \frac{1 + \tan^2\left(\frac{\pi s}{2n}\right)}{2\tan^2\left(\frac{\pi s}{2n}\right)}, \qquad (2.20)$$

where s is an integer. This formula may be derived by calculating the change in resonance frequency of a Hermite-Gaussian resonator mode when the transverse mode index changes by one unit,[54] and requiring that it be equal to $s\pi c/nL$. Note that we have included the plane parallel resonator in table 2.1, since the Hermite-Gaussian modes of a nearly plane-parallel resonator do become degenerate in the limit that the mirror radius of curvature goes

to infinity. However, the "spot size" of these modes also diverges to infinity; i.e. the modes consist of essentially plane waves with an infinitely slow transverse spatial modulation. Therefore their mode volume is infinite, and the plane parallel resonator is not interesting from the point of view of enhanced and inhibited spontaneous emission. Of primary interest are the two simplest cases other than plane parallel: n =1, or the concentric resonator, and n = 2, the confocal resonator.

R_c/L	Name	s	n	Mode Spacing (Hz)	$r_0/\sqrt{\lambda L/2\pi}$
0.5000	Concentric	1	1	c/2L	0
0.5858	———	3	4	c/8L	0.644
0.6667	———	2	3	c/6L	0.760
1.000	Confocal	1	2	c/4L	1.00
2.000	———	1	3	c/6L	1.32
3.414	———	1	4	c/8L	1.55
∞	Plane-Parallel	0	1	c/2L	∞

Table 2.1. Mirror radii of curvature that give rise to degenerate mode spectra in the two mirror resonator of length L, for n = 1 to 4. Also tabulated are the mode spacings and the spot size r_0 (HW1/e of field amplitude) of the TEM_{00} mode.

Only the resonators with $1/2 \leq R_c/L \leq 1$ confine all the radiation incident upon the mirrors. This includes the concentric and confocal cases. For $R_c/L > 1$, some of this radiation is initially lost out the sides of the resonator, but the radiation remaining after n round trips remains confined. The exception is the plane parallel resonator, for which all of the radiation eventually escapes out the sides.

II.B.2. Propagation of Uniform Spherical Waves Between Curved Mirrors.

Consider a uniform spherical wave with center of curvature $\mathbf{r}_c$ incident upon one of the mirrors M, positioned at z = a. We consider the case where the center of cuvature is only slightly displaced from the z-axis by an amount $|x_c| << |a - z_c|$. The incident wave can be written as $E_i(\mathbf{r},t) = E_i(\mathbf{r})\, e^{-i\omega t}$, where

$$E_i(\mathbf{r}) = \frac{|a-z_c|}{|z-z_c|} E_0(a)\, e^{\pm ik|\mathbf{r} - \mathbf{r}_c|}, \qquad (2.21)$$

where +ik corresponds to an outgoing wave (from the center of curvature) and -ik corresponds to an ingoing one, and $E_0(a)$ gives the overall amplitude and phase of the wave. In the paraxial approximation, eq. (2.21) can be written as,

$$E_i(\mathbf{r}) = \frac{|a-z_c|}{|z-z_c|} E_0(a)\, e^{\pm ik[(1 - \frac{1}{2}\alpha^2(z))(z-z_c) + \frac{x^2+y^2}{2R_c(z)} + \alpha(z)x]} \tag{2.22}$$

where $R_c(z) = z - z_c$ is the wavefront radius of curvature and $\alpha(z) = -x_c/(z-z_c)$ is the wavefront angle of tilt at the z-axis. Here +ik corresponds to a wave propagating in the +z direction and -ik to one propagating in the -z direction, the wavefront curvature is taken as positive if the center of curvature lies in the - z direction, and $\alpha(z)$ is taken as positive if the line passing through the points (0,0,z) and $\mathbf{r}_c$ has positive slope in the x-z plane.

When the incident wave E_i impinges upon the mirror M, it gives rise to a transmitted wave $E_t = tE_i$ and a reflected wave E'. It may easily be seen this reflected wave is a new uniform spherical wave given by,

$$E'(\mathbf{r}) = \frac{|a-z_c'|}{|z-z_c'|} E_0'(a)\, e^{\pm ik[(1 - \frac{1}{2}\alpha'^2(z))(z-z_0') + \frac{x^2+y^2}{2R_c'(z)} + \alpha'(z)x]} , \tag{2.23}$$

where the parameters of the new wave are given by,

$$z_c' = a - R_c'(a) \tag{2.24a}$$

$$x_c' = \frac{x_c R_c'(a)}{a - z_c} \tag{2.24b}$$

and

$$z_0' = 2a - z_c , \tag{2.24c}$$

where

$$R_c'(a) = \frac{(a-z_c)f}{(a-z_c) - f} , \tag{2.24d}$$

and as before $R_c'(z) = z - z_c'$, $\alpha'(z) = -x_c'/(z - z_c')$, and the wave has center of curvature $\mathbf{r}_c' = z_c'\mathbf{z} + x_c'\mathbf{x}$. In addition it is implicitly understood that $E'(\mathbf{r}) = 0$ at points outside the geometrical boundary of the wave.

It is evident that this description of the field by a uniform spherical wave is only an approximate one, since it neglects the diffraction of the wave by the sharp boundary of M. For a nearly plane wave in the near field of M, these effects will be negligible. However it is necessary to be somewhat more cautious in applying this approximation to the region near the geometric focal point $\mathbf{r}_c$ of a converging spherical wave. This problem is treated by Born and Wolf,[55] and we review the main results here. We consider a spherical wave

emerging from an aperture of radius b located at z = a and converging to a focus at its center of curvature r_c, and we assume $|r_c| << |a|$. The main results can then be stated as follows:

(i) The intensity is symmetrical about the geometric focal plane $z = z_c$ (except for the slight tilt of the geometric boundary if $x_c \neq 0$). In the far field the incident wave is well approximated by the form $E_0(r)\, e^{-ik|r - r_c|}$, and the wave diverging past the focus by $E_0(r)\, e^{+ik|r - r_c|}$, except for an extra phase factor (point (iii) below).

(ii) The intensity in the focal plane can be written as,

$$I(z_c, \rho) = \left[\frac{2J_1(kb\rho/a)}{kb\rho/a}\right]^2 I_0 , \tag{2.25}$$

where $\rho = \sqrt{(x-x_c)^2 + y^2}$ and $I_0 = \frac{c}{8\pi}|E(r_c)|^2$ is the intensity at the focal point. By conservation of energy, if the field at z = a has magnitude |E(a)|, then

$$\frac{c}{8\pi}(\pi b^2)|E(a)|^2 = \int_0^\infty I(z_c,\rho)2\pi\rho d\rho . \tag{2.26}$$

Noting that [56] $\int_0^\infty dq \frac{J_1^2(q)}{q} = \frac{1}{2}$, eq. (2.26) gives,

$$|E(r_c)| = \frac{kb^2}{2a}|E(a)| . \tag{2.27}$$

(iii) The phase of the field is not related simply to the phase of the input field by $\phi = \pm k|r - r_c|$ but undergoes an additional phase shift upon propagation through the focus (the "Gouy phase shift"). In particular, if the phase of the incident wave is

$$\phi(z<z_c) = -k|r - r_c| + \phi_0 , \tag{2.28}$$

then the phase of the wave at the focal point is,

$$\phi(r_c) = \phi_0 - \frac{\pi}{2} , \tag{2.29}$$

and the phase of the wave transmitted past the focal point is,

$$\phi(z>z_c) = k|r - r_c| + \phi_0 - \pi . \tag{2.30}$$

The relations (2.21) - (2.30) summarize all the properties necessary to calculate the effect of the resonator on the radiated field.

II.C. Field Radiated by a Dipole in a Confocal Resonator.

In this section we calculate the cavity part of the fields generated by a dipole in a confocal resonator, in which the radii of curvature of M1 and M2 are +2a and -2a, respectively. It will be seen that the fields generated correspond to two nearly plane wave components, which we label as $E^{(2)}$ and $E^{(4)}$, and two stongly focussed spherical wave components, which we label as $E^{(1)}$ and $E^{(3)}$, as illustrated in Fig. 2.3.

II.C.1. Power Radiated into the Cavity.

We first consider the wave emitted by the dipole towards M1. Using eqs. (2.1), (2.21), and (2.22), we can write the wave incident upon M1 as

$$E^{(1)}_{R,1} = +E_0(r)\, e^{+ik|r - r_d|} + ik\left[\left(1 - \frac{1}{2}\left(\frac{x_d}{z}\right)^2\right)(z-z_d) + \frac{x^2+y^2}{2(z-z_d)} - \frac{x_d}{z}x\right]$$

$$= +E_0(r)\, e \qquad , \qquad (2.31)$$

where

$$E_0(r) = -\frac{\omega_0^2 d_0}{c^2 r} \, . \qquad (2.32)$$

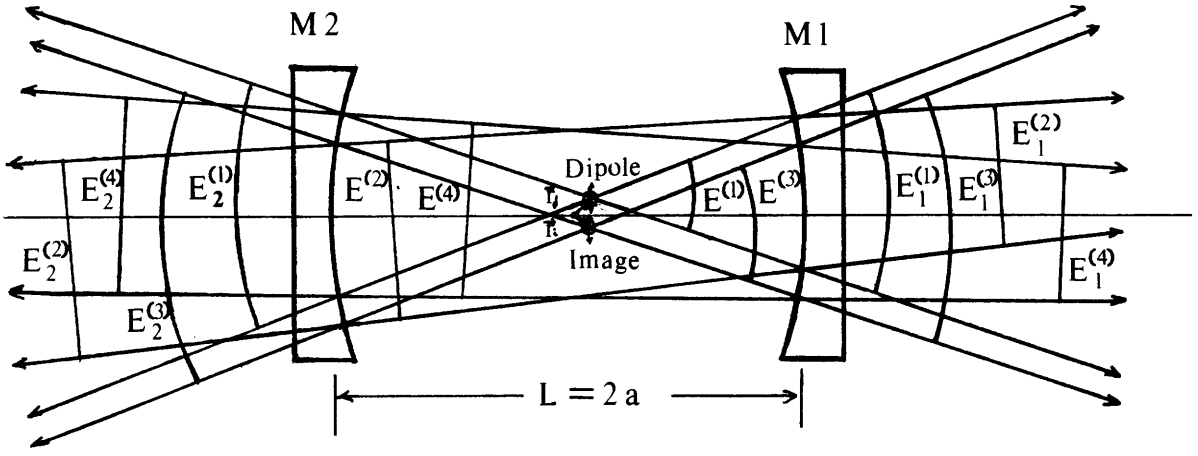

Fig. 2.3. Fields radiated by a dipole in a confocal resonator, showing the four types of emitted waves, $E^{(1)}$, $E^{(2)}$, $E^{(3)}$, and $E^{(4)}$.

Upon striking M1 this wave is divided into a transmitted component

$$E^{(1)}_{1,1} = +t_1 E_0(r)\, e^{+ik|r - r_d|}, \tag{2.33}$$

and a reflected component,

$$E^{(2)}_{L,1} = -r_1 E_0(a)\, e^{-ik\left[\left(1 - \frac{1}{2}\left(\frac{x_d}{a}\right)^2\right)(z+z_d-L) - \frac{x^2+y^2}{2a^2/z_d} + \frac{x_d}{a}x\right]}, \tag{2.34}$$

where we have used the reflection conditions of eqs. (2.23) and (2.24) together with the fact that $x_d << b << a$. This reflected wave is a nearly plane wave with a slight tilt. When it reaches M2, it will have a diameter which may be slightly larger than 2b, and it may in addition be shifted slightly off to one side of the mirror, causing a clipping effect on the wave by M2. However, the first effect will be negligible provided that $z_d << a$, and the second provided that $x_d << b$, as previously assumed. In addition, the reflected wave has a sharp edge. We can neglect the diffraction of this wave by the sharp edge upon propagation from M1 to M2 provided that the Fresnel number $F = \pi b^2/\lambda L$ of the resonator is large. This insures that M2 is in the near field of M1 and the only effect of diffraction a slight modulation of the field near the boundary of the geometric shadow. We note that this condition is compatible with the paraxial approximation; together the two conditions can be written as,

$$\sqrt{\lambda a} << b << a. \tag{2.35}$$

Upon reaching M2 the wave is again divided into a transmitted component,

$$E^{(2)}_{2,1} = -r_1 t_2 E_0(a)\, e^{-ik\left[\left(1 - \frac{1}{2}\left(\frac{x_d}{a}\right)^2\right)(z+z_d-L) - \frac{x^2+y^2}{2a^2/z_d} + \frac{x_d}{a}x\right]}, \tag{2.36}$$

and a reflected wave,

$$E^{(3)}_{R,1} = -\mathrm{Sgn}(z) R E_0(r)\, e^{+ik\left[\left(1 - \frac{1}{2}\left(\frac{x_d}{z}\right)^2\right)(z-z_d+2L) + \frac{x^2+y^2}{2(z-z_d)} + \frac{x_d}{z}x\right]}$$

$$= -\mathrm{Sgn}(z) R E_0(r)\, e^{2ikL}\, e^{+\mathrm{Sgn}(z) ik|r - r_i|}, \tag{2.37}$$

where $R = r_1 r_2$, and

$$\mathrm{Sgn}(z) = \begin{cases} +1, & z > z_d \\ -1, & z < z_d \end{cases} \tag{2.38}$$

This is a spherical wave converging to the focal point $\mathbf{r}_i = +z_d\mathbf{z} - x_d\mathbf{x}$, i.e. the light is imaged onto a point directly opposite the z-axis from the dipole. Also note the prescence of the Gouy phase shift via the factor Sgn(z).

Following along further, when $E^{(3)}_{R,1}$ impinges upon M1 it is again divided into a transmitted component,

$$E^{(3)}_{1,1} = -t_1 R E_0(r)\, e^{2ikL}\, e^{+ik|\mathbf{r} - \mathbf{r}_i|}, \tag{2.39}$$

and a reflected wave,

$$E^{(4)}_{L,1} = +r_1 R E_0(a)\, e^{-ik\left[\left(1 - \frac{1}{2}\left(\frac{x_d}{a}\right)^2\right)(z+z_d-3L) - \frac{x^2+y^2}{2a^2/z_d} - \frac{x_d}{a}x\right]}, \tag{2.40}$$

which is again a nearly plane wave with a slight tilt, opposite to $E^{(2)}$. Finally, $E^{(4)}_{L,1}$ strikes M2, producing a transmitted wave,

$$E^{(4)}_{2,1} = +t_2 r_1 R E_0(a)\, e^{-ik\left[\left(1 - \frac{1}{2}\left(\frac{x_d}{a}\right)^2\right)(z+z_d-3L) - \frac{x^2+y^2}{2a^2/z_d} - \frac{x_d}{a}x\right]}, \tag{2.41}$$

and a reflected wave,

$$\begin{aligned} E^{(1)}_{R,2} &= +\mathrm{Sgn}(z) R^2 E_0(r)\, e^{+ik\left[\left(1 - \frac{1}{2}\left(\frac{x_d}{z}\right)^2\right)(z-z_d+4L) + \frac{x^2+y^2}{2(z-z_d)} - \frac{x_d}{z}x\right]} \\ &= +\mathrm{Sgn}(z) R^2 E_0(r)\, e^{4ikL}\, e^{+\mathrm{Sgn}(z)ik|\mathbf{r} - \mathbf{r}_d|}. \end{aligned} \tag{2.42}$$

We see that after two complete round trips of the resonator, the wave focuses exactly back down onto the dipole at $\mathbf{r}_d$, and that the field diverging past the dipole is identical to the first emitted wave, apart from the factor R^2e^{4ikL}, which accounts for the attenuation and phase shift of the wave upon the two round trips in the resonator.

It is now quite clear what is going to happen: as the wave continues to bounce back and forth between the two mirrors, it will produce upon every 2(n+1)th round trip a contribution to the field $E^{(j)}_{i,n+1} = R^2e^{4ikL}E^{(j)}_{i,n}$ which is identical to the contribution $E^{(j)}_{i,n}$ from the (2n)th round trip, apart from the factor R^2e^{4ikL}. Thus the total field for any one of the particular waves is,

$$E_i^{(j)} = E_{i,1}^{(j)} (1 + R^2 e^{4ikL} + R^4 e^{8ikL} + \cdots)$$

$$= E_{i,1}^{(j)} \frac{1}{1 - R^2 e^{4ikL}} \quad . \tag{2.43}$$

The same situation is true for the reverse direction of propagation around the resonator. A wave $E_{L,1}^{(1)}$ is emitted by the dipole, which divides into a transmitted component $E_{2,1}^{(1)}$ and reflected component $E_{R,1}^{(4)}$. This reflected wave is nearly plane, and upon striking M1 it is divided into a transmitted component $E_{1,1}^{(4)}$ and reflected component $E_{L,1}^{(3)}$. This reflected wave focusses onto the image point $\mathbf{r}_i$ and subsequently strikes M2, producing a transmitted wave $E_{2,1}^{(3)}$ and reflected wave $E_{L,1}^{(2)}$. As before, this wave is nearly plane, and upon striking M1 it divides into a transmitted wave $E_{1,1}^{(2)}$ and a reflected wave $E_{L,2}^{(1)}$, which again focusses back down upon the dipole and again reproduces $E_{L,1}^{(1)}$ times the phase factor $R^2 e^{4ikL}$.

Taking all these contributions into account, we may easily show that the total field to the right of M1 can be written as,

$$E_1 = E_1^{(1)} + E_1^{(2)} + E_1^{(3)} + E_1^{(4)} \ , \tag{2.44}$$

where

$$E_1^{(1)}(\mathbf{r}) = +t_1 E_0(r)\, e^{+ik|r - r_d|} \frac{1}{1 - R^2 e^{4ikL}} \tag{2.45}$$

$$E_1^{(2)}(\mathbf{r}) = +t_1 r_2 R E_0(a)\, e^{+ik[(1 - \frac{1}{2}\left(\frac{x_d}{a}\right)^2)(z+z_d+3L) - \frac{x^2+y^2}{2a^2/z_d} + \frac{x_d}{a}x]} \times \frac{1}{1 - R^2 e^{4ikL}} \tag{2.46}$$

$$E_1^{(3)}(\mathbf{r}) = -t_1 R E_0(r)\, e^{2ikL}\, e^{+ik|r - r_i|} \frac{1}{1 - R^2 e^{4ikL}} \tag{2.47}$$

and

$$+ ik[(1 - \frac{1}{2}\left(\frac{x_d}{a}\right)^2)(z+z_d+L) - \frac{x^2+y^2}{2a^2/z_d} - \frac{x_d}{a}x]$$

$$E_1^{(4)}(r) = -t_1 r_2 E_0(a)\, e$$

$$x \frac{1}{1 - R^2 e^{4ikL}} \cdot \quad (2.48)$$

A very similar expression is obtained for the field to the left of M2.

The power passing through S_1 is simply given by,

$$p_1 = \int_{S_1} dA\ I_1 \ , \quad (2.49)$$

where

$$I_1 = \frac{c}{8\pi}\left(|E_1^{(1)}|2 + |E_1^{(2)}|2 + |E_1^{(3)}|2 + |E_1^{(4)}|2 \right)$$

$$+ \frac{c}{8\pi} \sum_{i \neq j} |E_1^{(i)}||E_1^{(j)}|\, e^{i(\phi_i - \phi_j)} \ , \quad (2.50)$$

and where $E_1^{(i)} = |E_1^{(i)}|\, e^{i\phi_i}$. The contribution from the cross terms will be nonzero only if the integral of the phase factors over S_1 is nonzero:

$$\int_{S_1} dA\ e^{i(\phi_i(r) - \phi_j(r))} \neq 0 \ , \quad (i \neq j) \ . \quad (2.51)$$

In particular, we need to be concerned about possible interference between the spherical waves $E_1^{(1)}$ and $E_1^{(3)}$, and also between the plane waves $E_1^{(2)}$ and $E_1^{(4)}$. In both of these cases $e^{i(\phi_i - \phi_j)} = e^{\pm(2ikL + ik(2x_d/a)x)}$. Since x varies in the integral (2.49) over a range of order [-b,b], the phase difference $\phi = \phi_i - \phi_j$ varies over the range $[-4\pi x_d b/\lambda a, +4\pi x_d b/\lambda a]$, i.e. over a total range $\Delta\phi \sim 8\pi x_d b/\lambda a$. If the range of this phase difference $\Delta\phi >> 2\pi$, i.e. if

$$x_d >> \frac{\lambda a}{4b} \ , \quad (2.52)$$

then the integral of eq. (2.49) oscillates rapidly over many cycles and therefore averages to zero. Obviously such terms as $\int_{S_1} dA\ E_1^{(2)} E_1^{(3)*}$ then also average to zero.

Therefore, provided that $x_d >> \lambda a/4b$, the cross terms of eq. (2.49) can be ignored, giving simply,

$$I_1 = I^{(1)}_1 + I^{(2)}_1 + I^{(3)}_1 + I^{(4)}_1 \tag{2.53}$$

where

$$I^{(1)}_1 = \frac{c}{8\pi}|E^{(1)}_1|^2 = \frac{c}{8\pi}T_1\,|E_0(a)|^2\,\frac{1}{(1-R^2)^2 + 4R^2\sin^2 2kL}\,, \tag{2.54}$$

and similarly for $I^{(2)}_1$, $I^{(3)}_1$, and $I^{(4)}_1$. Thus we obtain for the power emitted through S_1,

$$p_1 = \frac{c}{8\pi}(\pi b^2)\;|E(a)|^2\,\frac{T_1(1 + R^2 + R_2 + R_2 R^2)}{(1-R^2)^2 + 4R^2\sin^2 2kL}\,. \tag{2.55}$$

Similarly, the power transmitted through S_2 can be shown to be,

$$p_2 = \frac{c}{8\pi}(\pi b^2)\;|E(a)|^2\,\frac{T_2(1 + R^2 + R_1 + R_1 R^2)}{(1-R^2)^2 + 4R^2\sin^2 2kL}\,. \tag{2.56}$$

Writing the total power emitted through S_1 and S_2 as $p_{cav} = p_1 + p_2$, we find finally,

$$p_{cav} = p_{free}\frac{1 + R^2}{1 - R^2}\,\frac{1}{1 + \dfrac{4R^2}{(1-R^2)^2}\sin^2(2kL)}\,, \tag{2.57}$$

which can also be written as,

$$p_{cav} = p_{free}\,\frac{\sqrt{1 + F_{cf}}}{1 + F_{cf}\sin^2(2kL)}\,, \tag{2.58}$$

where p_{free} was defined in eq. (2.17) and the parameter F_{cf} is given by

$$F_{cf} = 4R^2/(1 - R^2)^2. \tag{2.59}$$

We see that the power radiated by the dipole just follows the Airy function lineshape of the cavity. For the case where $1/(1-R) \gg 1$, the maximum radiation rate is given by

$$p_{cav}^{(max)} = \frac{1}{1 - R}\,p_{free}\,, \tag{2.60}$$

and the minimum radiation rate is given by

$$p_{cav}^{(min)} = (1 - R)\,p_{free}\,. \tag{2.61}$$

Thus the cavity enhances and inhibits the radiation rate by a factor of $1/(1-R)$, relative to the radiation rate by the free dipole into the same solid angle.

II.C.2 Special Case: Dipole on the Cavity Axis.

In the foregoing discussion, we assumed that $\lambda(a/4b) \ll x_d \ll b$. However it may be that $x_d \lesssim \lambda(a/4b)$; in this case the interference terms in eq. (2.50) must be taken into account. In particular suppose $x_d = 0$. Then in this case,

$$E_1^{(1)} + E_1^{(3)} = +t_1 E_0(r)\, e^{+ik|r - r_d|} \frac{1 - Re^{2ikL}}{1 - R^2 e^{4ikL}} , \tag{2.62}$$

and

$$E_1^{(2)} + E_1^{(4)} = -t_1 r_2 E_0(a)\, e^{+ ik[(z+z_d+L) - \frac{x^2+y^2}{2a^2/z_d}]} \frac{1 - Re^{2ikL}}{1 - R^2 e^{4ikL}} , \tag{2.63}$$

and

$$I_1 = \frac{c}{8\pi}(|E_1^{(1)} + E_1^{(3)}|^2 + |E_1^{(2)} + E_1^{(4)}|^2) + \frac{c}{8\pi}((E_1^{(1)} + E_1^{(3)})(E_1^{(2)} + E_1^{(4)})^* + (E_1^{(1)} + E_1^{(3)})^*(E_1^{(2)} + E_1^{(4)})) . \tag{2.64}$$

It is easy to show that the cross terms in eq. (2.64) do not contribute to the integral of eq. (2.49) provided that $b^2 >> \lambda L$, as has been already assumed. Therefore,

$$p_1 = \frac{c}{8\pi}(\pi b^2)\, |E_0(a)|^2 (T_1 + T_1 R_2) \frac{|1 - Re^{2ikL}|^2}{|1 - R^2 e^{4ikL}|^2} , \tag{2.65}$$

and similarly

$$p_2 = \frac{c}{8\pi}(\pi b^2)\, |E_0(a)|^2 (T_2 + T_2 R_1) \frac{|1 - Re^{2ikL}|^2}{|1 - R^2 e^{4ikL}|^2} , \tag{2.66}$$

which gives,

$$p_{cav} = p_{free} \frac{1 + R}{1 - R} \frac{1}{1 + \frac{4R}{(1-R)^2} \cos^2 kL} . \tag{2.67}$$

This result should be compared with that of eq. (2.57) for the case $x_d >> \lambda(a/4b)$. It is seen that the effective length of the resonator is L rather than 2L, corresponding to a free spectral range that is twice as great, and that the effective round trip loss is R rather than R^2, corresponding to peaks that are twice as high. These effects can both be understood by our noting that the field is now reproduced after every one round trip, rather than every two. Note that the condition $x_d \lesssim \lambda(a/4b)$ is essentially the requirement the the focussed spots at $\mathbf{r}_d$ and $\mathbf{r}_i$ coincide.

Points lying along the axis of the confocal resonator are therefore special points, in that dipoles located there radiate according to eq. (2.67) rather than (2.57). Note that in general $\lambda(a/4b)$ is a very small distance, and that the dipole is allowed to be located in a much larger region satisfying only $x_d << b$. If in an experiment many dipoles are randomly distributed in this much larger volume, then the overwhelming majority of them will behave according

to the off-axis conditions, and we can neglect the type of behavior given by eq. (2.67). We will assume this is the case from here on.

II.C.3 Total Radiated Power.

The total power emitted by the dipole is simply the sum of the power radiated out the side, given by eq. (2.19), and the power emitted out the ends. Assuming the on-axis behavior can be neglected, the power emitted into S_1 and S_2 is given by eq. (2.58), so that we obtain for the total power

$$P_{cav} = P_{free}\left[1 + \left[\frac{\sqrt{1 + F_{cf}}}{1 + F_{cf}\sin^2(2kL)} - 1 \right] \frac{3}{8\pi}\Delta\Omega_{cav} \right] . \qquad (2.68)$$

For $1/(1-R) >> 1$, the maximum total radiation rate is given by

$$P_{cav}^{(max)} = P_{free}\left[1 + \left(\frac{1}{1 - R}\right) \frac{3}{8\pi}\Delta\Omega_{cav} \right] , \qquad (2.69)$$

whereas the minimum total rate is given by

$$P_{cav}^{(min)} = P_{free}\left[1 - \frac{3}{8\pi}\Delta\Omega_{cav} \right] . \qquad (2.70)$$

From these results, we see that to significantly suppress the total radiation rate, it is necessary for the resonator to subtend a large solid angle. However, to significantly enhance the radiation rate, it is only the product of $1/(1-R)$ and the solid angle that must be large. Thus, a small solid angle cavity can have a significant effect on the total rate if its finesse is sufficiently high.

II.D. Fields Radiated by a Dipole in a Concentric Resonator.

In this section we calculate the fields generated by a dipole in a concentric resonator, for which the radii of curvature of M1 and M2 are given by +a and -a, respectively. In this case the generated fields are somewhat simpler than in the confocal case, consisting of two strongly focussed standing spherical waves, which we label as $E^{(1)}$ and $E^{(2)}$, as illustrated in Fig. 2.4.

II.D.1.Power radiated into the cavity.

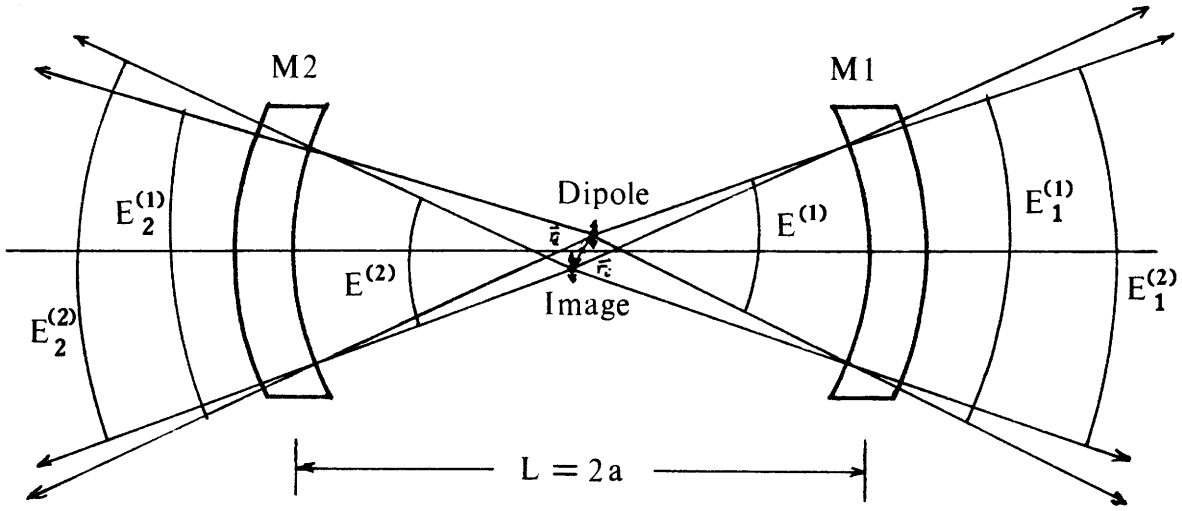

Fig. 2.4. Dipole in a concentric resonator.

The calculation of the power $p_{cav} = p_1 + p_2$ is very similar to the preceeding section. The dipole illuminates M1 with a field $E^{(1)}_{R,1}$, producing a transmitted wave $E^{(1)}_{1,1}$ and a reflected wave $E^{(2)}_{L,1}$. This reflected wave is a converging spherical wave focussed onto an image point $\mathbf{r}_i = -\mathbf{r}_d$ which is now directly opposite the origin from $\mathbf{r}_d$. Upon striking M2, the wave is again divided into a transmitted component $E^{(2)}_{2,1}$ and a reflected component $E^{(1)}_{R,2}$ which now refocusses down upon the dipole at $\mathbf{r}_d$. Thus in the concentric cavity the field reproduces itself after every one round trip, rather than every two, and it can easily be shown that the field $E^{(1)}_{R,2}$ diverging past the dipole is given by

$E^{(1)}_{R,2} = Re^{2ikL} E^{(1)}_{R,1}$. This corresponds to a round trip attenuation by the factor R and a round trip phase shift of 2kL. Therefore in a manner similar to the confocal case, each type of wave is given by a sum over the contributions of many round trips as,

$$E^{(j)}_i = E^{(j)}_{i,1} (1 + Re^{2ikL} + R^2e^{4ikL} + \cdots)$$

$$= E^{(j)}_{i,1} \frac{1}{1 - Re^{2ikL}} \quad . \tag{2.71}$$

Similarly in the reverse direction, the wave emitted by the dipole towards M2 is $E^{(1)}_{L,1}$, which divides into a transmitted wave $E^{(1)}_{2,1}$ and a reflected wave $E^{(2)}_{R,1}$. This reflected wave reaches M1 and divides into an additional transmitted wave $E^{(1)}_{1,1}$ and reflected wave $E^{(1)}_{L,2}$, and so on.

With the above considerations in mind, we can show that the field to the right of M1 is given by,

$$E_1 = E^{(1)}_1 + E^{(2)}_1 \ , \tag{2.72}$$

where

$$E^{(1)}_1 = t_1E_0(r)\, e^{ik|r-r_d|} \frac{1}{1 - Re^{2ikL}} \ , \tag{2.73}$$

$$E^{(2)}_1 = t_1r_2E_0(r)\, e^{ikL}\, e^{ik|r+r_d|} \frac{1}{1 - Re^{2ikL}} \ , \tag{2.74}$$

and $E_0(r)$ is defined in eq. (2.32).

The field to the left of M2 is given by,

$$E_2 = E^{(1)}_2 + E^{(2)}_2 \ , \tag{2.75}$$

where

$$E^{(1)}_2 = t_2E_0(r)\, e^{ik|r-r_d|} \frac{1}{1 - Re^{2ikL}} \ , \tag{2.76}$$

and

$$E^{(2)}_2 = t_2r_1E_0(r)\, e^{ikL}\, e^{ik|r+r_d|} \frac{1}{1 - Re^{2ikL}} \ . \tag{2.77}$$

The power emitted through S_1 is again given by eq. (2.49), where now

$$I_1 = \frac{c}{8\pi}\left(|E^{(1)}_1|2 + |E^{(2)}_1|2 + E^{(1)*}_1E^{(2)}_1 + E^{(1)}_1E^{(2)*}_1 \right). \tag{2.78}$$

In a manner similar to the previous section, the cross terms will contribute to the integral of eq. (2.49) only if

$$\int_{S_1} dA\, e^{i(\phi_1(r) - \phi_2(r))} \neq 0 \ , \tag{2.79}$$

where again $E_1^{(i)} = |E_1^{(i)}| e^{i\phi_i}$. This phase difference

$(\phi_1 - \phi_2) = k\left(\frac{x^2 + y^2}{z^2}\right) z_d + \frac{2x_d}{z} x$ + constant. The maximum value of

$(x^2 + y^2)/z^2$ on S_1 is b^2/a^2 and the maximum value of (x/z) is (b/a) . Thus in the integral (2.49) the contribution of the cross terms vanishes if

$$z_d >> \lambda\left(\frac{a}{b}\right)^2 \tag{2.80a}$$

or

$$x_d >> \lambda\left(\frac{a}{4b}\right) . \tag{2.80b}$$

If we assume that one or the other of the conditions (2.80) is satisfied, then we can neglect the cross terms in eq. (2.78), giving,

$$p_1 = \frac{c}{8\pi}(\pi b^2)\, |E(a)|^2 \frac{T_1 + R_1 T_2}{(1-R)^2 + 4R\sin^2 kL} \ , \tag{2.81}$$

and similarly,

$$p_2 = \frac{c}{8\pi}(\pi b^2)\, |E(a)|^2 \frac{T_2 + R_2 T_1}{(1-R)^2 + 4R\sin^2 kL} \ . \tag{2.82}$$

We thus obtain the result,

$$p_{cav} = p_{free} \frac{1 + R}{1 - R} \frac{1}{1 + \frac{4R}{(1-R)^2}\sin^2 kL} \ , \tag{2.83}$$

which can also be written as,

$$p_{cav} = p_{free} \frac{\sqrt{1 + F}}{1 + F\sin^2 kL} \ , \tag{2.84}$$

where the parameter F is given by

$$F = \frac{4R}{(1 - R)^2} \tag{2.85}$$

These results should be compared with eqs. (2.57) - (2.59) for the confocal resonator; it is seen that the results are essentially the same, except that 2L is replaced by L, and R^2 is replaced by R. In the case that $1/(1-R) << 1$, the maximum and minimum powers emitted into the cavity are given by

$$p_{cav}^{(max)} = \frac{2}{1 - R} p_{free} \tag{2.86}$$

and

$$p_{cav}^{(min)} = \frac{1 - R}{2} p_{free} . \tag{2.87}$$

In this case the radiation is enhanced or inhibited by a factor of 2/(1-R), depending on the tuning of the resonator.

II.C.2 Special Case: Dipole at the Exact Center.

We now consider the case where $z_d \lesssim \lambda(a/b)^2$ and $x_d \lesssim \lambda(a/4b)$. Note that these conditions correspond to the overlapping of the dipole and image focal spots. In particular we consider $x_d = 0$ and $z_d = 0$. Then it may easily be shown that the total power p_{cav} is given by,

$$p_{cav} = p_{free} \frac{(1-R^2) + [r_2(1-R_1) + r_1(1-R_2)]\cos(kL)}{(1-R)^2 + 4R\sin^2(kL)} . \tag{2.88}$$

If $R_1 = R_2$, then

$$p_{cav} = p_{free} \frac{1 + r}{1 - r} \frac{1}{1 + \frac{4r}{(1-r)^2}\sin^2(kL/2)} , \tag{2.89}$$

This result should be compared to eq. (2.83) for the case where the dipole is displaced from the exact center of the cavity. It corresponds to an effective length L/2 rather than L, so that the free spectral range is c/L, and a "round trip loss" of r rather than R. In the case $R_1 \neq R_2$ eq. (2.88) does not simplify to an equation of the form (2.89), and in fact residual peaks with a spacing of c/2L remain halfway between those given by (2.88).

Points lying very near the exact center of the concentric resonater are therefore special points, in that a dipole positioned there radiates power according to eq (2.88) rather than eq.(2.83). However, the extent of these points $z_d \lesssim \lambda(a/b)^2$ and $x_d \lesssim \lambda(a/4b)$ is generally very small. If in an experiment dipoles are distributed randomly over a much larger range, then only a small fraction will be sufficiently near the center to exhibit the behavior of eq. (2.88), so that this special case can be neglected.

II.C.3 Total radiated power.

The power radiated by the dipole into the cavity is therefore given by eq. (2.84), and combining this result with eq.(2.19), we find that,

$$P_{cav} = P_{free}\left[1 + \left[\frac{\sqrt{1+F}}{1+F\sin^2(kL)} - 1\right]\frac{3}{8\pi}\Delta\Omega_{cav}\right]. \qquad (2.90)$$

Again, this result shows that in order to obtain a large inhibition of spontaneous emission, a large solid angle is necessary, but that a large enhancement can be obtained with a moderate solid angle if the cavity finesse is sufficiently large.

II.C.4. Field Inside the Cavity.

In the next section regarding radiation reaction, the field inside the resonator will be of interest. This can be written as

$$E = E^{(1)} + E^{(2)}, \qquad (2.91)$$

where $E^{(2)} = E^{(2)}_L + E^{(2)}_R$, with

$$E^{(2)}_L = -Sgn(z)\, r_1 E_0(r)\, e^{+ikL}\, e^{-Sgn(z)ik|r+r_d|}\frac{1}{1 - Re^{2ikL}}, \qquad (2.92)$$

and

$$E^{(2)}_R = +Sgn(z)\, r_2 E_0(r)\, e^{+ikL}\, e^{+Sgn(z)ik|r+r_d|}\frac{1}{1 - Re^{2ikL}}, \qquad (2.93)$$

This corresponds to a standing spherical wave with a focus at $-r_d$. (There will be a slight leftward or rightward propagation of energy if $R_1 \neq R_2$.)

To calculate $E^{(1)}$, we have to be slightly careful , since the directly emitted wave $E^{(1)}_{R,1}$ exists only to the right of the dipole and $E^{(1)}_{L,1}$ exists only the the left. We may write $E^{(1)}$ as,

$$E^{(1)} = E^{(1)}_0 + E^{(1)}_R + E^{(1)}_L, \qquad (2.94)$$

where

$$E^{(1)}_0 = E^{(1)}_{R,1} + E^{(1)}_{L,1} = E_0(r)\, e^{ik|r-r_d|} \qquad (2.95)$$

gives the contribution of the directly emitted wave, and

$$E_R^{(1)} + E_L^{(1)} = 2iE_0(r) \frac{Re^{2ikL}}{1 - Re^{2ikL}} \sin(k|r-r_d|), \tag{2.96}$$

the contribution of all the reflected waves. $E^{(1)}$ can be written as,

$$E^{(1)} = - E_0(r) \frac{Re^{2ikL}}{1-Re^{2ikL}} e^{-ik|r-r_d|} + E_0(r) \frac{1}{1-Re^{2ikL}} e^{+ik|r-r_d|} . \tag{2.97}$$

Note that we can identify an ingoing and outgoing component of the wave inside the resonator. It is easy to verify that the difference between the intensity of the outgoing wave and that of the ingoing wave leads again to the result (2.83) for the power radiated into the cavity.

The expression (2.97) is not valid at points in the near field of the dipole, and in particular it is not valid at the position of the dipole $\mathbf{r_d}$. This point will be discussed presently in section II.E in connection with the radiation field at the dipole.

II.E. Radiation Reaction Field and the Decay Rate and Frequency Shift of a Dipole in an Optical Resonator.

In the previous sections we have calculated the fields radiated by a dipole in a confocal or concentric optical resonator, assuming that the dipole oscillates continuously according to $\mathbf{d} = \mathbf{d}_0 e^{-i\omega_0 t}$. As was the case for free space, this is a very good approximation as long as $\omega_0 t << 1$. Nevertheless it is clear the the electron must be doing work against some force $F_{RR} = eE_{RR}$, and that this force must be modified in the presence of the resonator. In this section we calculate the field E_{RR} in the cavity and show how the electron's motion is modified relative to free space. We will carry out the calculation for the concentric case; the confocal case is identical except that R should be replaced by R^2, L by 2L, and F by F_{cf}.

II.E.1. Green's function for the Dipole Self Field.

In order to see how the modified electron motion comes about, we reconsider the expression (2.5) for the field E_{RR} in terms of the Green's function $G(\mathbf{r}_d,t;\mathbf{r}_d,t')$. Physically this Green's function gives the contribution to the field $E(\mathbf{r}_d,t)$ at the position $\mathbf{r}_d$ and time t due to the oscillating dipole moment $\ddot{\mathbf{d}}(t')$ of the dipole at the position $\mathbf{r}_d$ at time t'. It is apparent that this is exactly what we have calculated in the previous sections: the field is expressed as a sum over waves which have undergone multiple reflections, which correspond to contributions from the dipole's oscillations at a discrete set of past times separated by the cavity round trip time.

To make this point more transparent, consider the field $E_R^{(1)}(\mathbf{r}_d) + E_L^{(1)}(\mathbf{r}_d)$ at the dipole's position, which gives the contribution of all the waves reflected back onto the dipole after one or more round trips. The wave imcident from the left can be written as,

$$E_R^{(1)}(r) = -E_0(r)\,\frac{Re^{2ikL}}{1 - Re^{2ikL}}\,e^{ik|r-r_d|}, \tag{2.98}$$

Hence the contribution of this wave to the field at $\mathbf{r}_d$ is given by,

$$E_R^{(1)}(\mathbf{r}_d,t) = +\frac{ib^2\omega_0^3}{2a^2c^3}\,d_0(Re^{2ikL} + R^2e^{4ikL} + R^4e^{8ikL} + \cdots)\,e^{-i\omega_0 t}, \tag{2.99}$$

where we have used eq. (2.27) to express the amplitude of the field $E_R^{(1)}(\mathbf{r}_d)$ at the dipole in terms of the the amplitude of the field $E_R^{(1)}(a)$ at the mirror, multiplied by a factor of -i to

account for the $-\pi/2$ phase shift as given by eq. (2.29), substituted for $E_0(a)$ from eq. (2.32), and re-expanded the sum over powers of Re^{2ikL}.

Equation (2.99) was derived assuming that the dipole was oscillating continuously as $d_0e^{-i\omega_0 t}$, and each term in the expanded sum $(Re^{2ikL})^n$ corresponds to a contribution from the dipole's oscillation n round trips earlier. More accurately, the term $\omega_0^3 d_0 R^n e^{2inkL} e^{-i\omega_0 t}$ should actually have been written as

$$\omega_0^3 d_0 R^n e^{2inkL} e^{-i\omega_0 t} \Rightarrow -\omega_0 R^n \ddot{d}(t-2nL/c) . \tag{2.100}$$

This expresses the contribution of a particular term explicitly in terms of the acceleration of the electron at the retarted time $t_r = t - 2nL/c$. Thus we can write the Green's function for the contribution to the field at $\mathbf{r}_d$ as,

$$G_R^{(1)}(\mathbf{r}_d,t;\mathbf{r}_d,t') = +i\frac{b^2\omega_0}{a^2c^3}\sum_{n=1}^{\infty} R^n \delta(t'-(t-2nL/c)) \tag{2.101}$$

Note that if we assume $d(t) = d_0e^{-i\omega_0 t}$,

$$E_R^{(1)}(\mathbf{r}_d,t) = \int_{-\infty}^{t} G_R^{(1)}(\mathbf{r}_d,t;\mathbf{r}_d,t')\ddot{\mathbf{d}}(t')dt' , \tag{2.102}$$

as it should. Similarly there is a contribution $E_L^{(1)}(\mathbf{r}_d,t)$ to the field at $\mathbf{r}_d$, and it is easy to show that $E_L^{(1)}(\mathbf{r}_d,t) = E_R^{(1)}(\mathbf{r}_d,t)$, and therefore the total Green's function for the reflected waves is $G^{(1)}(\mathbf{r}_d,t;\mathbf{r}_d,t') = 2G_R^{(1)}(\mathbf{r}_d,t;\mathbf{r}_d,t')$.

It is apparent that this is not the complete contribution to the reaction field, since we have yet to take into account the first emitted wave $E_0^{(1)}$. Note, however, that we can always write the total radiation field as an integral of the form (2.5), and we choose in the present case to break the integral up into two parts as,

$$E_{RR,cav}(t) = \int_{-\infty}^{t_0} G_{cav}(\mathbf{r}_d,t;\mathbf{r}_d,t')\ddot{\mathbf{d}}(t')dt' + \int_{t_0}^{t} G_{cav}(\mathbf{r}_d,t;\mathbf{r}_d,t')\ddot{\mathbf{d}}(t')dt' , \tag{2.103}$$

where $t-c/L < t_0 < t$ and also $t-t_0 >> 1/\omega_{max}$. The function $G^{(1)}(\mathbf{r}_d,t;\mathbf{r}_d,t')$ contributes only for times $t' < t_0$. In the integral over times $t' > t_0$, the Green's function cannot involve the cavity since the time difference $t - t'$ is too short for the dipole to "know" about the cavity. Therefore it must be that the Green's function for times $t' > t_0$ is given by the free space Green's function of eq. (2.6), and since this function does not contribute for times $t < t_0$, we can write the total Green's function as,

$$G_{cav}(r_d,t;r_d,t') = G_{free}(r_d,t;r_d,t') + 2G_R^{(1)}(r_d,t;r_d,t') \ . \qquad (2.104)$$

This means that the effect of the cavity is simply to add a contribution to the free space radiation reaction field. This contribution is nothing more than the field which is reflected back onto the dipole by the mirrors.

II.E.2, Modified Abraham-Lorentz Equation.

Using eq. (2.104), the radiation reaction field can be written as,

$$E_{RR,cav}(t) = \frac{2}{3c^3}\dddot{d}(t) - \frac{4\omega_{max}}{3\pi c^3}\ddot{d}(t) - 2i\frac{b^2\omega_0}{a^2c^3}\sum_{n=1}^{\infty} R^n \ddot{d}(t-2nL/c) \ . \qquad (2.105)$$

The modified Abraham-Lorentz equation is obtained by substituting this form of E_{RR} into eq. (2.8). We can show that a solution to this equation, correct only to first order in $\omega_0\tau$, is obtained by substituting for $\dddot{d}(t)$ the approximate form $-\omega_0^2\dot{d}(t)$ and for $\ddot{d}(t-2nL/c)$ the approximate form $-\omega_0^2 d_0 e^{2inkL}\, e^{-i\omega_0 t}$. The resulting equation is

$$\ddot{x} + \omega_0^2\tau\,\dot{x} + \omega_0^2\left(1 - i\frac{b^2e^2\omega_0}{a^2mc^3}\frac{Re^{2ikL}}{1 - Re^{2ikL}}\right)x = 0 \ . \qquad (2.106)$$

We solve this equation by substituting $x = x_0 e^{\alpha t}$, where α is approximately $-i\omega_0$, obtaining,

$$\alpha^2 + \omega_0^2\tau\,\alpha + \omega_0^2(1 - \Delta) = 0, \qquad (2.107)$$

where,

$$\Delta = i\frac{b^2e^2\omega_0}{a^2mc^3}\frac{Re^{2ikL}}{1 - Re^{2ikL}} \ . \qquad (2.108)$$

Thus, correct to first order in $w_0\tau$,

$$\alpha = -\frac{\omega_0^2\tau}{2} - i\omega_0\left(1 + \frac{1}{2}\Delta\right) \ . \qquad (2.109)$$

Note that Δ can be rewritten as

$$\Delta = 2\omega_0\tau\left(\frac{3}{8\pi}\Delta\Omega_{cav}\right)\frac{i(R\cos 2kL - R^2) - R\sin 2kL}{(1-R)^2 + 4R\sin^2 kL} \ . \qquad (2.110)$$

Substituting this expression in (2.109) then gives,

$$\alpha = -\frac{\Gamma}{2} - i(\omega_0 + \Delta\omega) \ , \qquad (2.111)$$

where

$$\Gamma = \Gamma_{free}\left[1 + \left[\frac{\sqrt{1 + F}}{1 + F\sin^2(kL)} - 1 \right] \frac{3}{8\pi}\Delta\Omega_{cav} \right], \tag{2.112}$$

and

$$\Delta\omega = \frac{\Gamma_{free}}{4}\left(\frac{3}{8\pi}\Delta\Omega_{cav}\right)\frac{F\sin 2kL}{1 + F\sin^2 kL}, \tag{2.113}$$

and

$$\Gamma_{free} = \omega_0^2\tau = \frac{2e^2\omega_0^2}{3mc^3}. \tag{2.114}$$

Equations (2.112) and (2.113) give the classical prediction for the decay rate and frequency shift of the dipole oscillator. We see from eq. (2.112) that the extra contribution to the radiation reaction force from the reflected field exactly accounts for the modified energy radiation rate (2.83). Note that the frequency shift is now of *first* order in the damping parameter $\omega_0\tau$. This frequency shift is therefore distinct from the usual type of shift associated with damping. Also note that, in order to obtain these results, it is essential to take into account the effect of the free space part of the radiation reaction field, and also that of the "Gouy phase shift". These results are plotted in Fig. 2.5. The decay rate essentially follows the lineshape of the cavity, whereas the frequency shift displays a repeating odd resonance behavior as the cavity is tuned. Both the modification to the decay rate and the shift scale in proportion to the solid angle and to the free space decay rate. The interpretation of these results is fairly simple. The field radiated by the dipole is reflected back onto it by the cavity mirrors. This field has an absorptive or out of phase component which accounts for the modified decay rate, and an in phase or dispersive component which accounts for the frequency shift. As the cavity length is tuned, the phase of this reflected field is tuned, oscillating between absorptive and dispersive and producing the behavior illustrated in Fig. 2.5.

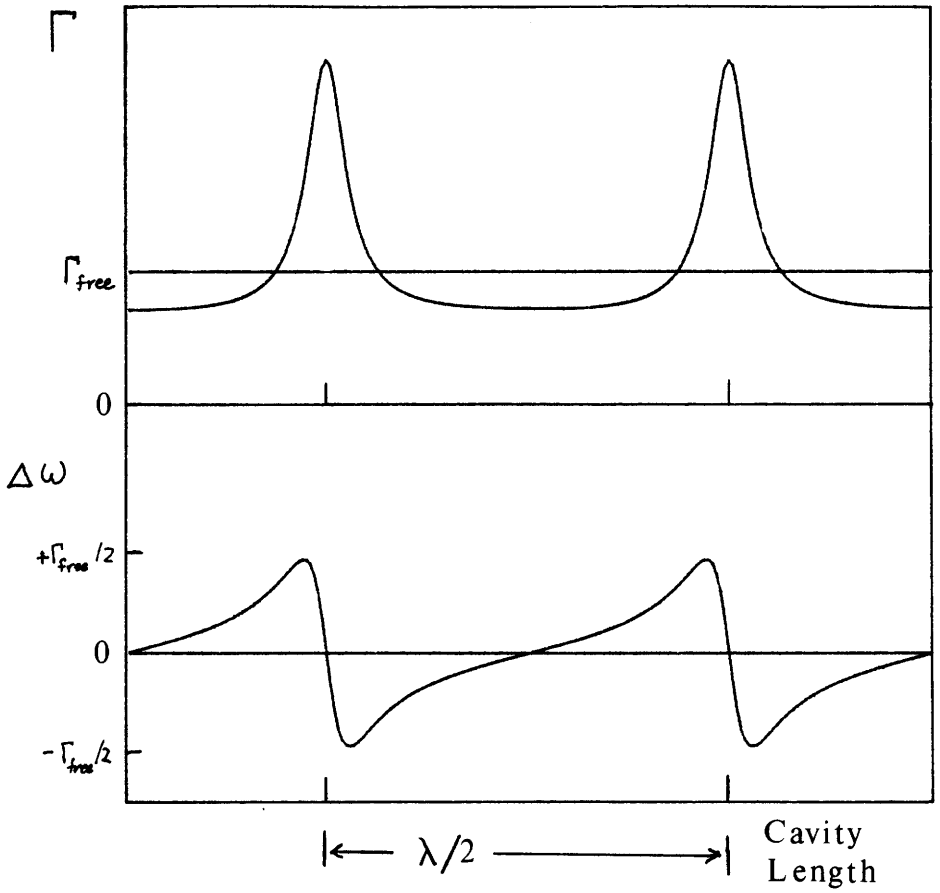

Fig. 2.5. Decay rate Γ and frequency shift $\Delta\omega$ of a dipole oscillator in a concentric resonator, as a function of resonator tuning. The cavity length decreases from left to right.

II.F. Radiation by a Dipole in a Resonator of Large Solid Angle.

In the previous sections it has been assumed that the resonator subtends a small solid angle. This insured the validity of the paraxial approximation and allowed us to neglect the vector nature of the field. In this section we explore the case where the solid angle may be large.

II.F.1. Dipole in a Spherical Confocal Resonator.

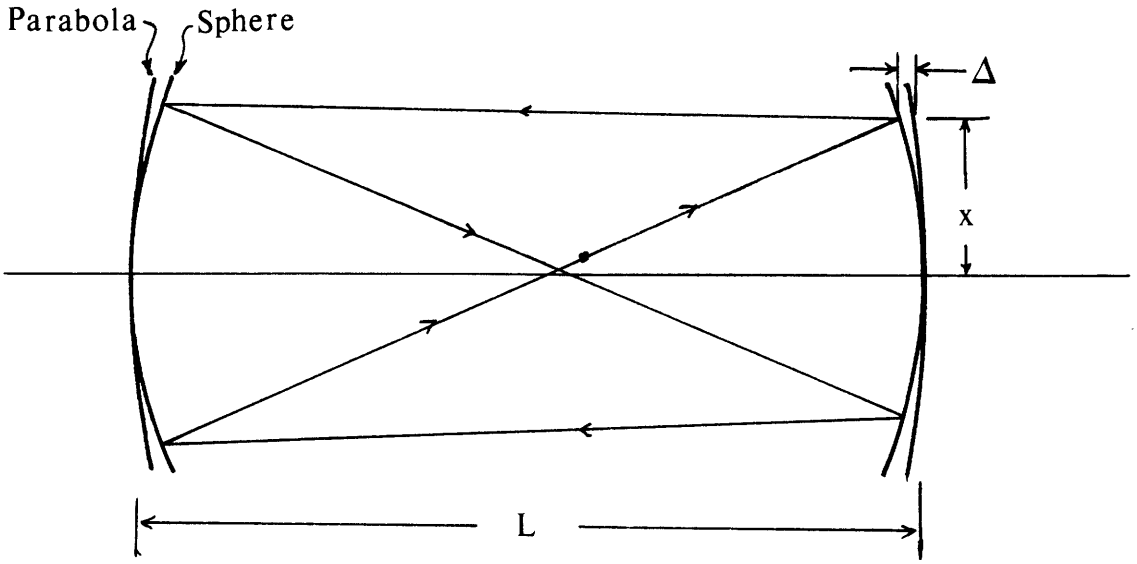

Fig. 2.6. Illustration of the breakdown of the "ray degeneracy" in the confocal resonator.

We first consider the case of a dipole in a spherical mirror confocal resonator. For simplicity we assume the dipole is located at the exact center of the resonator, as illustrated in Fig. 2.6. As mentioned earlier, the "mode degeneracy" of the confocal resonator may be understood from the ray optical point of view by our noting that every ray emitted by the dipole returns to it after one round trip, and that the round trip path of all such rays is identical. Each of these self-reproducing ray paths corresponds roughly to a "mode", and the frequency of each of these "modes" is determined by requiring that the round trip path be an integral number of wavelengths. The fact that the ray path lengths are equal insures that all of these "modes" have the same frequency. For this property to hold out to a large angle, it may be seen by elementary geometry that the ideal mirror shape is parabolic. However, in general, the mirror surfaces are spherical. The deviation of the spherical

surface from the ideal parabolic one gives rise to a breakdown of the mode degeneracy at large angles.

The ray optics of a spherical mirror confocal resonator have been reviewed by Hercher;[56] we give the main results here. Consider a ray striking the mirror at a distance x from the resonator axis. The deviation of the spherical surface from the parabolic one is given by $\Delta = \frac{1}{8}\frac{x^4}{L^3}$. Thus the total round round trip path in the spherical confocal resonator is shorter than that of the parabolic by an amount 8Δ. This gives rise to a resonant wavelength according to the relation $n\lambda = 4(L - 2\Delta)$, which implies that the resonator is characterized by a radially dependent resonance frequency,

$$\nu(x) = \nu_0\left(1 + \frac{1}{4}\left(\frac{x}{L}\right)^4\right), \tag{2.115}$$

where $\nu_0 = nc/4L$ is the resonant frequency for the paraxial rays, and n is the order of interference. This radial dependence limits the useful mirror radius in a manner that depends on the resonator finesse: the mirror will only be useful out to a radius x_0 such that the frequency shift $\Delta\nu_0 = \nu(x_0) - \nu_0$ is less than or equal to one half the fringe width $\Delta\nu_{cav} = \Delta\nu_{fsr}/F_{cf}$, where $\Delta\nu_{fsr} = c/4L$ is the free spectral range of the cavity and $F_{cf} = \pi\sqrt{R}\,/\,2(1 - R)$ the confocal resonator finesse. This gives

$$x_0 = (L^3\lambda/2F)^{1/4} \tag{2.116}$$

as the maximum useful radius of the mirror. If the resonator is tuned to a resonance with the paraxial rays, x_0 is the radius at which the intensity falls to one-half of its value on the axis. Note that $x_0/L = (\lambda/2LF)^{1/4} << 1$.

If we are only concerned with inhibiting radiation by the dipole a slightly larger radius $x_1 = (L^3\lambda/2)^{1/4}$ is useful, since the condition for the ray path to be nonresonant is less critical than the condition for resonance. If the resonator is tuned so that the paraxial rays are exactly halfway between two resonances, then x_1 is the radius of the first fringe of constructive interference.

The limitation imposed on solid angle by this "spherical aberration" effect is of course not fundamental. By use of parabolic confocal mirrors the ray degeneracy continues to hold to as large an angle as desired, at least for some small region of source points near the center of the resonator. The concentric resonator also does not suffer from this deficiency, since in this case the spherical surface is exactly the correct one to maintain the ray

degeneracy. Since, in practice, spherical mirrors are much easier to produce than parabolic, the concentric resonator will be preferable if a large solid angle is desired.

II.F.2.Ray Optics of the Concentric Resonator.

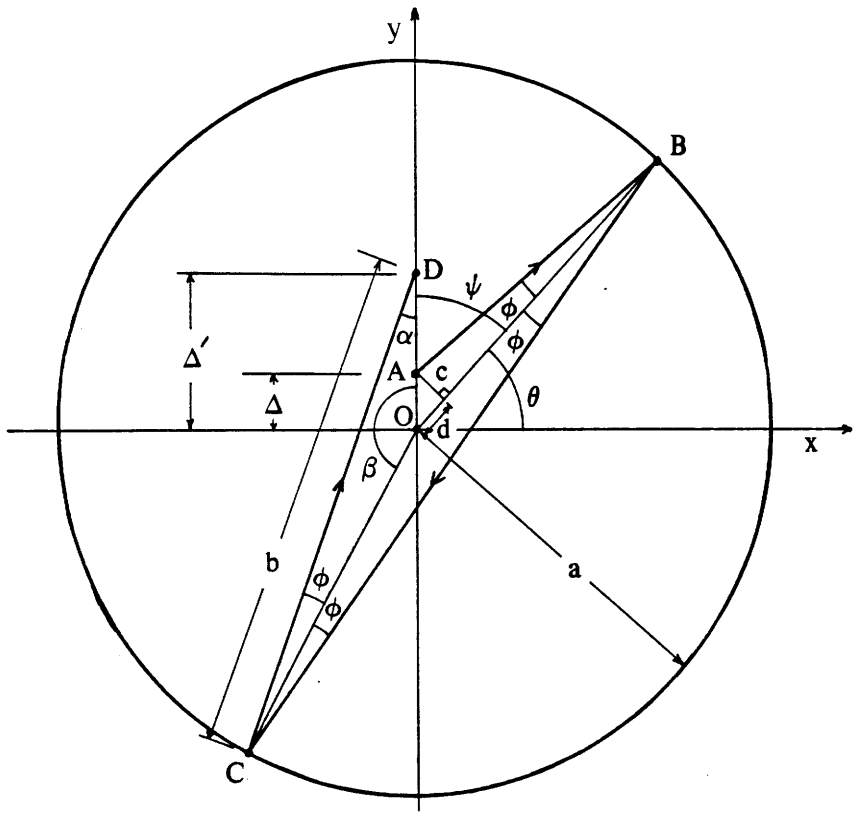

Fig 2.7. Ray propagation in a concentric resonator.

In this section we examine the ray propagation in a concentric resonator, which is nothing more than a section of a sphere. Suppose the dipole is located at a point A at a distance Δ from the center, O, of a spherical resonator of radius a, and emits a light ray which strikes the surface of the sphere at a point B (Fig. 2.7). Let the x-y plane be defined by the points OAB, and let the y-axis lie along the line OA and the x-axis perpendicular to OA and passing through O. Now the light ray reflects from B to a point C almost directly across the sphere, and is subsequently reflected back towards the center of the sphere, crossing the y-axis at a point D. We wish to calculate the distance Δ', of D from O. Let θ denote the angle between OB and the x-axis.

Now (see Fig. 2.7) $c = \Delta\cos\theta$ and $d = \Delta\sin\theta$ so that

$$\tan\phi = \frac{c}{a-d} = \frac{\Delta\cos\theta}{a-\Delta\sin\theta} . \tag{2.117}$$

It is a simple exercise in geometry to show that

$$\beta = \angle COD = \frac{\pi}{2} + \theta + 2\phi \tag{2.118a}$$

and

$$\alpha = \angle ODC = \frac{\pi}{2} - \theta - 3\phi . \tag{2.118b}$$

The law of sines applied to ΔCOD gives

$$b = \frac{\cos(\theta+2\phi)}{\cos(\theta+3\phi)} a , \tag{2.119}$$

so that by applying the law of cosines to ΔCOD we obtain,

$$\Delta'^2 = a^2 + b^2 - 2ab\cos\phi , \tag{2.120}$$

which, using eq. (2.119) may be simplified to give,

$$\begin{aligned} \Delta' &= \frac{a\sin\phi}{\cos(\theta+3\phi)} \\ &= \frac{\Delta(1 + \tan^2\phi)}{(1 - 3\tan^2\phi) - \frac{4\Delta}{a}(1 - \tan^2\phi)\sin\theta} . \end{aligned} \tag{2.121}$$

This expression may be expanded in powers of (Δ/a) to give,

$$\Delta' = \Delta\left(1 + 4\left(\frac{\Delta}{a}\right)\sin\theta + 4\left(\frac{\Delta}{a}\right)^2(1 + 3\sin^2\theta) + \cdots\right) . \tag{2.122}$$

There are two requirements for the ray degeneracy to hold:

(i) The point D should coincide with the point A, to within a distance of $\lambda/2F$ ($\lambda/2$ if we are only concerned with the off-resonance condition).

(ii) Provided that condition (i) is satisfied, the path length of all possible paths ABCA should be the same to within $\lambda/2F$ ($\lambda/2$ for the off-resonance case), regardless of the initial angle θ.

We consider first point (i). Now $\sin\theta \le 1$, so that $\Delta' - \Delta \le 4\Delta^2/a$. The condition (i) can thus be written as,

$$\Delta \le \sqrt{\frac{\lambda a}{8F}} . \tag{2.123}$$

Next consider point (ii). Assuming that condition (i) is satisfied, D coincides with A, and the round trip path length $L_{rt} = \overline{AB} + \overline{BC} + \overline{CA}$. Now A = (0,Δ), B = (a cosθ, a sinθ), and C = (-a cos(θ+2φ), -a sin(θ+2φ)). Thus

$$\overline{AB} = a\left(1 - \left(\frac{\Delta}{a}\right)\sin\theta + \frac{1}{2}\left(\frac{\Delta}{a}\right)^2\cos^2\theta\right) \tag{2.124a}$$

$$\overline{BC} = 2a\left(1 - \frac{1}{2}\left(\frac{\Delta}{a}\right)^2\cos^2\theta\right) \tag{2.124b}$$

$$\overline{CA} = a\left(1 + \left(\frac{\Delta}{a}\right)\sin\theta + \frac{5}{2}\left(\frac{\Delta}{a}\right)^2\cos^2\theta\right) \tag{2.124c}$$

accurate to second order in (Δ/a), so that

$$L_{rt} = 4a + 2a\left(\frac{\Delta}{a}\right)^2\cos^2\theta = 4a + 2a\left(\frac{\Delta}{a}\right)^2\sin^2\psi, \tag{2.125}$$

where ψ = (π/2) - θ is the approximate angle between the atomic displacement along the x-axis and the light ray propagation direction. The maximum difference between path lengths is $2a\left(\frac{\Delta}{a}\right)^2$, so that condition (ii) becomes simply,

$$\Delta \le \sqrt{\frac{\lambda a}{4F}}\ , \tag{2.126}$$

which is essentially the same as condition (i).

II.F.3. Radiation by a Dipole in a Concentric Resonator of Large Solid Angle.

According to the results of the previous section, the light rays emitted by a dipole in a concentric resonator will always return to it after one round trip, and the ray degeneracy will hold out to a large solid angle, provided that the dipole is displaced from the center of the resonator by an amount $\Delta \le \sqrt{\lambda a/4F}$. This suggests that the results of sections II.D and II.E may be generalized to the large solid angle case. A similar result also applies to the parabolic confocal resonator; however, we concentrate here on the concentric resonator since it is the one easier to realize in practice.

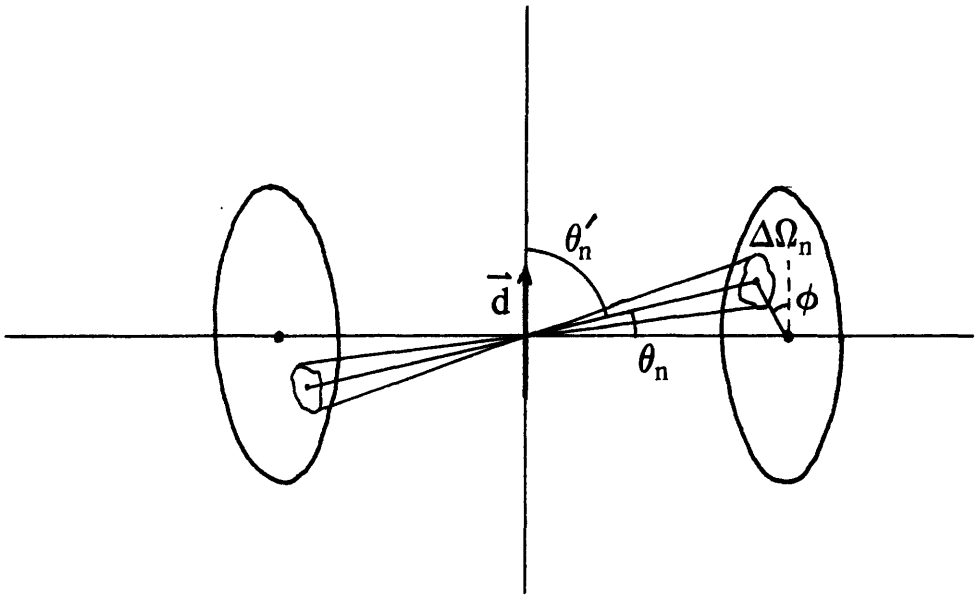

Fig. 2.8. Concentric Resonator of Large Solid Angle.

Consider a concentric resonator composed of two circular mirrors subtending a total solid angle $\Delta\Omega_{cav}$, as ilustrated in Fig. 2.8. In order to analyze this large solid angle case, we may view the reson ator as being divided in some arbitrary into a number of "elementary resonators" R_n, each subtending some solid angle $\Delta\Omega_n$, where each of these "elementary resonators" is taken to have a size sufficiently small that the paraxial approximation holds, and sufficiently large that its Fresnel number is large. In this case the resonators R_n are effectively decoupled from each other, and the analysis of sections II.D and II.E may be applied separately to each, except that it must be kept in mind that the direction of the field generated in each section is perpendicular to the ray direction, and that its magnitude is reduced by the factor $\sin\theta_n'$ (c.f. eq (2.2)), where θ_n' is the angle between the dipole and the "axis" of the n_{th} elementary resonator. The total radiated intensity is therefore reduced by the factor $\sin^2\theta_n'$. Therefore, since the power ordinarily emitted by the dipole into free space is scaled by the same factor, the power p_{cav} radiated by the dipole continues to be given by eq. (2.84) even in the large solid angle case, where p_{free} is simply the power ordinarily emitted into the solid angle $\Delta\Omega_{cav}$ in the absence of a resonator. The result for the total power can be written as,

$$P_{cav} = P_{free}\left[1 + \left[\frac{\sqrt{1+F}}{1+F\sin^2(kL)} - 1\right] f(\Delta\Omega_{cav})\right], \qquad (2.127)$$

where $f(\Delta\Omega_{cav})$ is the fraction of the power ordinarily emitted by the free dipole into the solid angle $\Delta\Omega_{cav}$.

The quantity $f(\Delta\Omega_{cav})$ may easily be calculated for the case of a concentric resonator composed of circular mirrors of subtending a half anlge θ_M, and a dipole linealry polarized perpendicularly to the cavity axis. Note that $\cos\theta' = \sin\theta \sin\phi$ (Fig. 2.8), so that $\sin\theta' = \sqrt{1 - \sin^2\theta \sin^2\phi}$. Thus the power ordinarily emitted by the dipole into the solid angle $\Delta\Omega_{cav}$ is given by

$$P_{free}(\theta_M) = \frac{\omega^4}{8\pi c^3}|d|^2 \, 2\cdot \int_0^{2\pi} d\phi \int_0^{\theta_M} \sin\theta \, d\theta \, (1 - \sin^2\theta \sin^2\phi)$$

$$= \frac{\omega^4}{3c^3}|d|^2 \left(1 - \frac{3}{4}\cos\theta_M - \frac{1}{4}\cos^3\theta_M\right), \qquad (2.128)$$

and therefore,

$$f(\Delta\Omega_{cav}) = \frac{P_{free}(\theta_M)}{P_{free}} = \left(1 - \frac{3}{4}\cos\theta_M - \frac{1}{4}\cos^3\theta_M\right). \qquad (2.129)$$

Similar considerations hold for the calculation of the radiation reaction force experienced by the dipole. Again the field generated in each of the "elementary resonators" may be treated in the same manner as in section II.D and II.E, except that the direction of the field is normal to the light rays and the magnitude of the field is reduced by the factor $\sin\theta_n'$. The resultant field experienced by the dipole is obtained by superposition over the contributions of each of the "elementary resonators". Since only the component of the field parallel to the dipole contributes to the radiation reaction force, each of these contributions is again weighted by the factor $\sin\theta'_n$; i.e. the magnitude of the reaction force contributed by each element of the resonator scales as $\sin^2\theta_n'$.

The net result is that eqs. (2.112) and (2.113) can be rewritten in the large solid angle case as,

$$\Gamma = \Gamma_{free}\left[1 + \left[\frac{\sqrt{1 + F}}{1 + F\sin^2(kL)} - 1\right] f(\Delta\Omega_{cav})\right], \qquad (2.130)$$

and

$$\Delta\omega = \Gamma_{free}\frac{f(\Delta\Omega_{cav})}{4}\frac{F\sin 2kL}{1 + F\sin^2 kL}. \qquad (2.131)$$

These results are essentially the same as those obtained earlier, in eqs. (2.112) and (2.113), and plotted in Fig. 2.5, where for small solid angle $f(\Delta\Omega_{cav}) = (3/8\pi)\Delta\Omega_{cav}$. We note that there is no reason, in principle, that we cannot obtain $f(\Delta\Omega_{cav}) = 1$. Therefore, the *total* radiation rate could be enhanced or inhibited by a factor of $\sqrt{1 + F} \cong 2/(1 - R)$.

CHAPTER III

QUANTUM THEORY OF RADIATIVE DECAY AND LEVEL SHIFTS OF AN ATOM IN AN OPTICAL RESONATOR.

In this chapter we develop the theory necessary to describe the decay rate and frequency shift of radiation by an atom in a cavity from a quantum mechanical point of view. The description is given in terms of the Wigner-Weisskopf approximation, which is appropriate whenever the atom decays into a continuum of modes. Quantum mechanically, the atom decays by spontaneous emission of a photon, and the frequency shift of the emitted radiation is due to a radiative level shift. This level shift is associated with the emission of virtual photons by the excited atom, and is closely related to the Lamb shift.

One problem which we encounter in the treatment of an open optical resonator is that it is difficult to identify a complete set of normal modes in which to quantize the field. In this chapter we present an approximate treatment, based on the idea of an "effective mode density", and find that the results agree with the classical theory and with experiment. For the case of a complete spherical resonator a complete set of modes can be easily identified; an exact theoretical treatment for this case is given in section III.C.

III.A. General Theory of Radiative Decay in the Wigner-Weisskopf Approximation.

In this section we review the general theory of radiative decay and level shifts in the Wigner-Weisskopf approximation. We then apply this theory to the decay of an atom into free space, and into a single damped cavity mode. In connection with the free space level shifts, we also briefly discuss the effect of mass renormalization and the free-space Lamb shift.

III.A.1. Field Quantization.

We begin by reviewing the quantization of the electromagnetic field. The classical vector potential **A** must obey the wave equation

$$\nabla \times (\nabla \times \mathbf{A}) + \frac{1}{c^2}\frac{\partial^2 \mathbf{A}}{\partial t^2} = 0 . \tag{3.1}$$

and in addition must satisfy any boundary condition which may be imposed by reflecting surfaces. We can write the solution to eq. (3.1) as

$$\mathbf{A}(\mathbf{r},t) = \sum_{\lambda} \mathbf{A}_\lambda(\mathbf{r},t) = \sum_{\lambda} (A_\lambda \Phi_\lambda(\mathbf{r}) e^{-i\omega_\lambda t} + A_\lambda^* \Phi_\lambda^*(\mathbf{r}) e^{+i\omega_\lambda t}) , \tag{3.2}$$

where $\Phi_\lambda(\mathbf{r})$ satisfies the equation

$$\nabla \times (\nabla \times \Phi_\lambda(\mathbf{r})) + k_\lambda^2 \Phi_\lambda(\mathbf{r}) = 0 , \tag{3.3}$$

along with any boundary conditions that may be imposed, where $k_\lambda = \omega_\lambda/c$, and where λ symbolizes a set of indices which uniquely specify the corresponding solution $\Phi_\lambda(\mathbf{r})$. In general it is possible to construct a complete, orthogonal set of solutions to eq. (3.3) such that

$$\int \Phi_{\lambda_1}(\mathbf{r}) \cdot \Phi_{\lambda_2}^*(\mathbf{r})\, d^3r = \delta_{\lambda_1 \lambda_2} \Lambda_{\lambda_1} , \tag{3.4}$$

and such that eq. (3.2) represents the most general possible solution for $\mathbf{A}(\mathbf{r},t)$. The quantity Λ_λ gives the overall normalization (volume integral of $|\Phi_\lambda|^2$) of the mode λ.

In the Coulomb gauge, for which $\nabla \cdot \mathbf{A} = 0$, the fields are given by,

$$\mathbf{E}(\mathbf{r},t) = -\frac{1}{c}\frac{\partial \mathbf{A}}{\partial t} = \sum_{\lambda} ik_\lambda (A_\lambda \Phi_\lambda(\mathbf{r}) e^{-i\omega_\lambda t} - A_\lambda^* \Phi_\lambda^*(\mathbf{r}) e^{+i\omega_\lambda t}) \tag{3.5}$$

$$\mathbf{B}(\mathbf{r},t) = \nabla \times \mathbf{A} = \sum_{\lambda} (A_\lambda (\nabla \times \Phi_\lambda(\mathbf{r})) e^{-i\omega_\lambda t} + A_\lambda^* (\nabla \times \Phi_\lambda^*(\mathbf{r})) e^{+i\omega_\lambda t}) . \tag{3.6}$$

The energy in the field is simply,

$$H_F = \frac{1}{8\pi}\int(\overline{|E|^2} + \overline{|B|^2})d^3r = \sum_\lambda \frac{k_\lambda^2}{4\pi}\int\overline{|A_\lambda|^2}d^3r = \sum_\lambda \frac{k_\lambda^2}{2\pi}|A_\lambda|^2\Lambda_\lambda , \tag{3.7}$$

where $\overline{|E|^2}$ denotes a time average of $|E|^2$, and similarly for $\overline{|B|^2}$ and $\overline{|A_\lambda|^2}$. If we make the substitution

$$A_\lambda = \left(\frac{\pi}{k_\lambda\Lambda_\lambda}\right)^{1/2}(\omega_\lambda Q_\lambda + iP_\lambda) , \tag{3.8}$$

the field energy may be rewritten as,

$$H_F = \sum_\lambda \frac{1}{2}(P_\lambda^2 + \omega_\lambda^2 Q_\lambda^2) . \tag{3.9}$$

This expression is identical with the Hamiltonian of a harmonic oscillator of unit mass. In order to quantize the field, we assume that according to eq. (3.9) each field mode may be treated as equivalent to a quantum mechanical harmonic oscillator; i.e. we assume that P_λ and Q_λ may be replaced by their corresponding quantum mechanical momentum and position operators $\hat{p}_\lambda$ and $\hat{q}_\lambda$:

$$P_\lambda \rightarrow \hat{p}_\lambda \tag{3.10a}$$

$$Q_\lambda \rightarrow \hat{q}_\lambda . \tag{3.10b}$$

We may also define the new operators $\hat{a}_\lambda$ and $\hat{a}_\lambda^\dagger$ as

$$\hat{a}_\lambda = \left(\frac{1}{2\hbar\omega_\lambda}\right)^{1/2}(\omega_\lambda\hat{q}_\lambda + i\,\hat{p}_\lambda) \tag{3.11a}$$

$$\hat{a}_\lambda^\dagger = \left(\frac{1}{2\hbar\omega_\lambda}\right)^{1/2}(\omega_\lambda\hat{q}_\lambda - i\,\hat{p}_\lambda) \tag{3.11b}$$

This implies that the quantities A_λ and A_λ^* should be replaced by the corresponding operators

$$A_\lambda \rightarrow \left(\frac{2\pi\hbar\omega_\lambda}{k_\lambda^2\Lambda_\lambda}\right)^{1/2}\hat{a}_\lambda \tag{3.12a}$$

$$A_\lambda^* \rightarrow \left(\frac{2\pi\hbar\omega_\lambda}{k_\lambda^2\Lambda_\lambda}\right)^{1/2}\hat{a}_\lambda^\dagger . \tag{3.12b}$$

Substituting for A_λ and A_λ^*, we may write the expressions for the field operators,

$$A(r) = \sum_\lambda \left(\frac{2\pi\hbar c^2}{\Lambda_\lambda\omega_\lambda}\right)^{1/2}(\hat{a}_\lambda\Phi_\lambda(r) + \hat{a}_\lambda^\dagger\Phi_\lambda^*(r)) \tag{3.13}$$

$$E(r) = \sum_\lambda i\left(\frac{2\pi\hbar\omega_\lambda}{\Lambda_\lambda}\right)^{1/2}(\hat{a}_\lambda\Phi_\lambda(r) - \hat{a}_\lambda^\dagger\Phi_\lambda^*(r)) \tag{3.14}$$

$$\mathbf{B}(\mathbf{r}) = \sum_{\lambda} \left(\frac{2\pi\hbar c^2}{\Lambda_\lambda \omega_\lambda}\right)^{1/2} (\hat{a}_\lambda \nabla x \Phi_\lambda(\mathbf{r}) + \hat{a}_\lambda^\dagger \nabla x \Phi_\lambda^*(\mathbf{r})) \,. \tag{3.15}$$

These operators have been expressed in the Schroedinger representation, in which the operators are time-independent, and all time dependence is carried by the state vectors. The details concerning the transformation of the operators and the state vectors between various representations is reviewed by Loudon[29].

Finally, we note that the Hamiltonian can be written as

$$H_F = \sum_{\lambda} \hbar\omega_\lambda (\hat{n}_\lambda + \frac{1}{2}) \,, \tag{3.16}$$

where $\hat{n}_\lambda = \hat{a}_\lambda^\dagger \hat{a}_\lambda$ is the number operator. The eigenstates of the electromagnetic field satisfy the eigenvalue equation

$$H_F |n_{\lambda_1}, n_{\lambda_2}, \ldots\rangle = ((n_{\lambda_1}+\tfrac{1}{2})\hbar\omega_{\lambda_1} + (n_{\lambda_2}+\tfrac{1}{2})\hbar\omega_{\lambda_2} + \cdots) |n_{\lambda_1}, n_{\lambda_2}, \ldots\rangle. \tag{3.17}$$

We let $|\{n_\lambda\}\rangle \equiv |n_{\lambda_1}, n_{\lambda_2}, \ldots\rangle$ denotes the state in which there are n_{λ_1} photons in mode λ_1, n_{λ_2} photons in mode λ_2, and so on. The operators $\hat{a}_\lambda$ and $\hat{a}_\lambda^\dagger$ operate on the field eigenstates as follows:

$$\hat{a}_{\lambda_i} |n_{\lambda_1}, n_{\lambda_2},\ldots,n_{\lambda_i},\ldots\rangle = \sqrt{n_{\lambda_i}}\, |n_{\lambda_1}, n_{\lambda_2},\ldots,n_{\lambda_i}-1,\ldots\rangle \tag{3.18a}$$

$$\hat{a}_{\lambda_i}^\dagger |n_{\lambda_1}, n_{\lambda_2},\ldots,n_{\lambda_i},\ldots\rangle = \sqrt{n_{\lambda_i}+1}\, |n_{\lambda_1}, n_{\lambda_2},\ldots,n_{\lambda_i}+1,\ldots\rangle \,; \tag{3.18b}$$

i.e., their effect is to "destroy" or "create" one quantum of energy in the mode λ_i, respectively.

III.A.2 Atom-Field Interaction.

The atomic eigenstates are determined from the atomic Hamiltonian H_A by the eigenvalue equation

$$H_A|I\rangle = E_I|I\rangle \,. \tag{3.19}$$

In this equation, I is a set of quantum numbers that uniquely specifies the state $|I\rangle$; the set of all such states may be assumed to form a complete orthonormal basis set of atomic states. The general atom-field state may be written in terms of the basis states $|I;\{n_\lambda\}\rangle$, where $|I;\{n_\lambda\}\rangle$ denotes a state in which the atom is in the state $|I\rangle$ and the field in the state $|\{n_\lambda\}\rangle$.

The total Hamiltonian of the atom-field sytem is given by

$$H = H_A + H_F + H_I , \tag{3.20}$$

where H_A and H_F are the atom and field Hamiltoninans, respectively, and where H_I gives the interaction energy between the atom and the field, and may be written as[58]

$$H_I = \frac{e}{mc}\mathbf{p}\cdot\mathbf{A}(\mathbf{r_a}) \tag{3.21}$$

where $\mathbf{p}$ is the momentum operator of the optically active electron and operates only on the atomic part of the wavefunction, and where $\mathbf{A}(\mathbf{r_a})$ is the vector potential operator given by eq. (3.13), evaluated at the position of the atom $\mathbf{r_a}$. Of particular interest are the matrix elements of H_I between the state $|E;0\rangle$ and the state $|I;\lambda\rangle$, where $|E,0\rangle$ denotes that the atom is in the state $|E\rangle$ and the field is in the vacuum state (no photons present), and $|I;\lambda\rangle$ denotes that the atom is in the state $|I\rangle$ and that the field has one photon in the mode λ. This matrix element is given by,

$$H_{I\lambda E} = \langle I;\lambda|\, H \,|\, E;0\rangle = \langle I;\lambda|\, H_I \,|E;0\rangle = \frac{e}{mc}\langle I|\, \mathbf{p}\, |E\rangle \cdot \langle\lambda|\, \mathbf{A}(\mathbf{r_a})\, |0\rangle. \tag{3.22}$$

Using eqs. (3.13), (3.18a), and (3.18b), we find that

$$H_{I\lambda E} = -i\left(\frac{2\pi\hbar\omega_\lambda}{\Lambda_\lambda}\right)^{1/2}\left(\frac{\omega_{IE}}{\omega_\lambda}\right)\mu_{IE}\cdot\Phi_\lambda^*(\mathbf{r_a}) = -i\hbar g_\lambda^* , \tag{3.23}$$

where

$$g_\lambda = \frac{1}{\hbar}\left(\frac{2\pi\hbar\omega_\lambda}{\Lambda_\lambda}\right)^{1/2}\left(\frac{\omega_{EI}}{\omega_\lambda}\right)\mu_{EI}\cdot\Phi_\lambda(\mathbf{r_a}) , \tag{3.24}$$

and we have used the relationship that[58]

$$\mathbf{p}_{IE} = \frac{-im\omega_{IE}}{e}\mu_{IE} , \tag{3.25}$$

where $\mathbf{p}_{IE} = \langle I|\mathbf{p}|E\rangle$ and $\mu_{IE} = \langle I|\mu|E\rangle$ are the matrix elements of $\mathbf{p}$ and the electric dipole operator μ between the state $|I\rangle$ and $|E\rangle$.

The quantity g_λ has a simple physical interpretation. If a classical field contains "one quantum" of energy $\hbar\omega_\lambda$ in the mode λ, then the amplitude of the electric field at the atom is $E_0 = (8\pi\hbar\omega_\lambda/\Lambda_\lambda)^{1/2}\Phi_\lambda(\mathbf{r_a})$. Thus, for $\omega_\lambda \cong \omega_{IE}$, eq. (3.24) can be rewritten as $2g_\lambda = \mu_{IE}\cdot E_0/\hbar$, so we see that $2g_\lambda$ may be interpreted as the Rabi frequency of the atom in the "field of one photon". For the case of a single mode, this is the same quantity g referred to in section I.B.4.

III.A.3 Decay Rate and Energy Level Shift of an Atom in the Wigner-Weisskopf Approximation.

In the absence of the interaction H_I, a state $|E; 0\rangle$ is an exact eigenstate of the Hamiltonian. This means that if an atom is initially in an excited state $|E\rangle$, it will never spontaneously jump down to some lower state $|I\rangle$, or vice versa, as illustrated in Fig. 3.1(a). However, in the presence of the interaction H_I, the state $|E; 0\rangle$ is no longer a true eigenstate, and this accounts for two distinct effects. First, the state $|E; 0\rangle$ becomes unstable and can decay to the state $|I; \lambda\rangle$ by the emission of a photon into the mode λ at a rate Γ. Second, the state $|E, 0\rangle$, which is still approximately an eigenstate, appears to be slightly shifted in energy by an amount $\hbar\delta\omega$ (and similarly for the other atomic states). Fig. 3.1(b) shows the atomic level structure in the presence of the atom-field interaction.

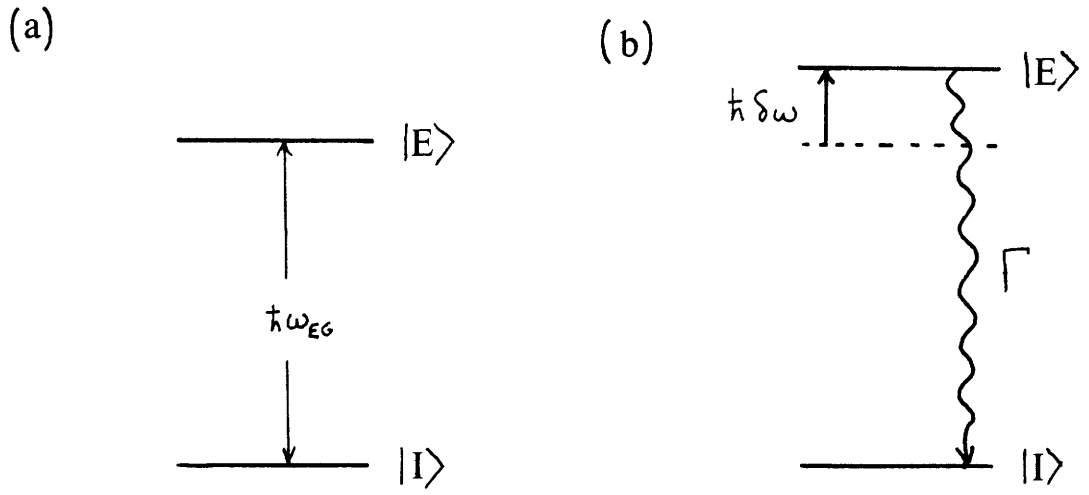

Fig. 3.1. Atomic energy level structure. (a) Atomic levels in the absence of the atom-field interaction. (b) Atomic levels including the effect of the atom-field interaction. For simplicity only the state $|E\rangle$ and one of the states $|I\rangle$, and only the decay and shift of $|E\rangle$, are shown.

The mechanisms responsible for the decay and shift of an atomic level are illustrated in Figs. 3.2(a) and 3.2(b), respectively. For the case of spontaneous emission, the atom is initially in the state $|E\rangle$ and emits a photon into the mode $|\lambda\rangle$, simultaneously making a transition to some lower state $|I\rangle$ and remaining there for an extended period of time. This photon is a "real" photon, so the overall process must conserve energy. For the case of the radiative level shift, the atom is initially in the state $|E\rangle$, emits a photon into the mode λ and simultaneously jumps into some other state $|I\rangle$, but then quickly reabsorbs the photon,

returning to the state $|E\rangle$ and remaining there for an extended period of time. This "virtual" photon emission, since it occurs over a very short time, need not rigorously conserve energy. Note that according to this picture, the "state" $|E\rangle$ is a "dressed" atom-field state, in which the atom is most of the time in the state $|E\rangle$, but is part of the time separated into an "atom + virtual photon" state. To be more precise, when we refer to the atom in the "state" $|E\rangle$, including the effect of the atom-field interaction, we actually mean the eigenstate of the total Hamiltonian of eq. (3.20) which is most nearly $|E;0\rangle$ in character, and becomes identical to $|E;0\rangle$ in the limit of vanishingly small interaction.

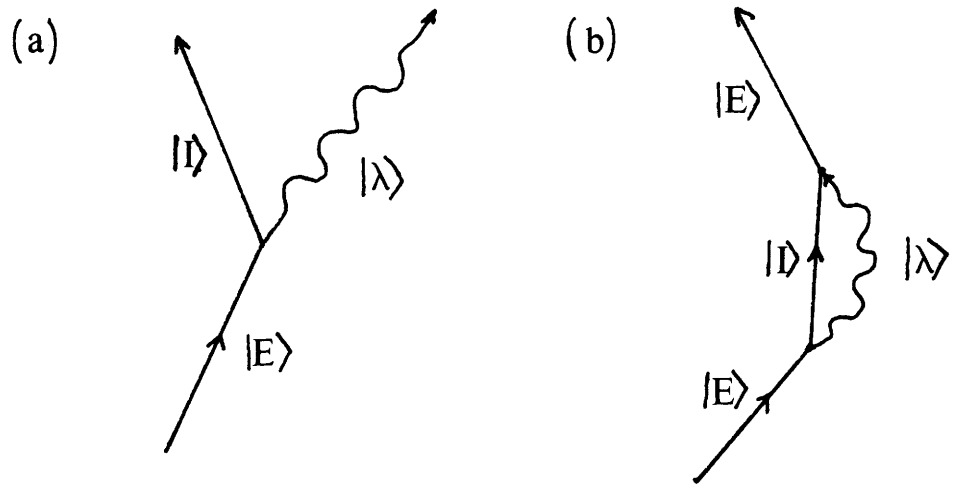

Fig. 3.2. Diagramatic representation of radiative processes. (a) Spontaneous emission of a real photon. (b) Virtual photon emission, associated with the radiative level shift.

Ideally, we would like to find the exact eigenstates $|\Psi_n\rangle$ of the total Hamiltonian H. These eigenstates could then be used as a convenient basis set to solve any interesting problem. For example, we could suppose the system is initially in the state $|E; 0\rangle$ and expand this initial state as a superposition of the eigenstates $|\Psi_n\rangle$. The time evolution of the wavefunction $|\Psi(t)\rangle$ could then be simply obtained in term of the eigenstates times their corresponding phase factors. The quantity $|\langle E;0|\Psi(t)\rangle|^2$ would then give the probability for the atom to remain in the state $|E\rangle$, and the energy of the eigenstate $|\Psi_n\rangle$ which is most nearly $|E;0\rangle$ in character would give the apparent energy of the "state" $|E\rangle$.

For simple problems involving an atom and a single cavity mode (e.g., in the ideal cavity case treated in section 1.B.4), this is in fact a reasonable procedure. However, in general the atom interacts with an infinite number of modes with a continuous spectrum of eigenfrequencies, and the exact diagonalization of the total Hamiltonian is impossible. In such cases one usually resorts to the approximate method first used by Weisskopf and Wigner[2]. An excellent discussion of the calculation of decay rates and level shifts in the Wigner-Weisskopf approximation is given by Sakurai[58], and we review the main results here.

We supose that at the time t = 0 the system is in the state $|E; 0\rangle$, and that its state at a later time t can be written as

$$|\Psi(t)\rangle = c_E(t)e^{-i\omega_E t}|E; 0\rangle + \sum_I \sum_\lambda c_{I\lambda}(t)e^{-i(\omega_I + \omega_\lambda)t}|I; \lambda\rangle , \tag{3.26}$$

where $\omega_E = E_E/\hbar$ and $\omega_I = E_I/\hbar$. More general field states in which more than one photon is excited are neglected because they are of higher order in the atom field coupling strength, which is small. This implies that our calculation will be valid only to lowest order in e^2 (e = charge of the electron). The time evolution of $|\Psi(t)\rangle$ is given by the Schroedinger equation,

$$H|\Psi(t)\rangle = i\hbar\frac{\partial}{\partial t}|\Psi(t)\rangle . \tag{3.27}$$

Substituting the form (3.25) for $|\Psi(t)\rangle$ into eq. (3.27), and taking the projection from the left with $\langle E; 0|$ and with $\langle I; \lambda|$, we obtain the amplitude equations

$$i\hbar\frac{dc_{I\lambda}}{dt} = c_E H_{I\lambda E}\, e^{-i(\omega_{EI} - \omega_I)t} \tag{3.28}$$

$$i\hbar\frac{dc_E}{dt} = \sum_I \sum_\lambda c_{I\lambda} H_{I\lambda E}^*\, e^{+i(\omega_{EI} - \omega_\lambda)t} , \tag{3.29}$$

where $\omega_{EI} = \omega_E - \omega_I$.

At this point, we make the following heuristic guess for the form of $c_E(t)$:

$$c_E(t) \cong e^{-i\Delta\omega_E t}. \tag{3.30}$$

This is motivated by the fact that, since the coupling is weak, the state $|E; 0\rangle$ should still be at least approximately an eigenstate of the Hamiltonian, with a perturbed energy $E_E' = \hbar(\omega_E + \Delta\omega_E)$. This implies that $|\Psi(t)\rangle \cong e^{-i(\omega_E + \Delta\omega_E)t}|E; 0\rangle$, and thus the form (3.30) for $c_E(t)$. Note that in general $\Delta\omega_E$ will have both a real and an imaginary part. Thus

$$|\Psi(t)\rangle \cong e^{-i(\omega_E + \mathrm{Re}(\Delta\omega_E))t}\, e^{+\mathrm{Im}(\Delta\omega_E)t}|E; 0\rangle . \tag{3.31}$$

The probability for the atom to remain in the state $|E\rangle$ is simply

$$P_E(t) = |\langle E; 0|\Psi(t)\rangle|^2 = e^{+2\mathrm{Im}(\Delta\omega_E)t} = e^{-\Gamma t} . \tag{3.32}$$

Thus, the apparent energy shift $\delta\omega$ and the decay rate Γ of the atom in the state $|E\rangle$ are given by

$$\delta\omega = \mathrm{Re}(\Delta\omega_E) \tag{3.33}$$

$$\Gamma = -2\mathrm{Im}(\Delta\omega_E) \tag{3.34}$$

Substituting the form (3.30) for $c_E(t)$ into eq. (3.28) leads to

$$c_{I\lambda}(t) = \frac{1}{\hbar} H_{I\lambda E} \frac{e^{-i(\omega_{EI} + \Delta\omega_E - \omega_\lambda)t} - 1}{(\omega_{EI} + \Delta\omega_E - \omega_\lambda)} . \tag{3.35}$$

Substitution of this form of $c_{I\lambda}$ into eq. (3.31) leads to the following self-consistent equation for $\Delta\omega_E$:

$$\Delta\omega_E = \sum_I \sum_\lambda \frac{|H_{I\lambda E}|^2}{\hbar^2} \frac{1 - e^{+i(\omega_{EI} + \Delta\omega_E - \omega_\lambda)t}}{(\omega_{EI} + \Delta\omega_E - \omega_\lambda)} . \tag{3.36}$$

Since we are calculating $\Delta\omega_E$ only to first order in e^2, we may drop the $\Delta\omega_E$ from the right hand side of eq. (3.36) and taking the limit $\omega t >> 1$, and making use of the identity

$$\lim_{t \to \infty} \frac{1 - e^{ixt}}{x} = \frac{1}{x} - i\pi\delta(x), \tag{3.37}$$

we obtain finally,

$$\Gamma = 2\pi \sum_I \sum_\lambda |g_\lambda|^2 \delta(\omega_{EI} - \omega_\lambda)) \tag{3.38}$$

$$\delta\omega = \sum_I \sum_\lambda |g_\lambda|^2 \frac{1}{(\omega_{EI} - \omega_\lambda)} . \tag{3.39}$$

These two equations (3.38) and (3.39) are the essential results of the Wigner-Weisskopf theory. Note that eq. (3.38) is equivalent to Fermi's "Golden Rule". Also note that, as expected, the delta function in the expression for Γ insures that the spontaneously emitted photons conserve energy, whereas for the shift $\delta\omega$ a range of photon energies can contribute.

III.A.3 Free Space Spontaneous Emission Rate and Level Shift.

In this section we apply the results of the previous section to the case of free space. Since there are no boundary conditions to satisfy, it is most convenient to take plane wave normal mode functions which satisfy periodic boundary conditions on a cube of edge L and

volume $V = L^3$. The free space limit is obtained as $V \to \infty$. The normal mode functions are given by

$$\Phi_{ik}(\mathbf{r}) = \varepsilon_{ik}\, e^{i\mathbf{k}\cdot\mathbf{r}}\,, \tag{3.40}$$

where the values of $\mathbf{k}$ allowed by the boundary conditions are

$$\mathbf{k} = \frac{2\pi}{L}(n_x x + n_y y + n_z z)\,;\;\; n_x, n_y, n_z = 0, \pm 1, \pm 2, \ldots\,, \tag{3.41}$$

and where ε_{ik} is a unit vector giving the polarization of the mode. The vector ε_{ik} must satisfy $\varepsilon_{ik}\cdot\mathbf{k} = 0$, so the are two independent polarizations ($i = 1,2$) for each allowed value of $\mathbf{k}$. We see that in this case $\lambda = \{i, n_x, n_y, n_z\}$ is the set of indices necessary to uniquely specify a mode. The normalization constant Λ_{ik} is given by

$$\Lambda_{ik} = \int |\Phi_{ik}(\mathbf{r})|^2\, d^3r \;=\; V, \tag{3.42}$$

and the coupling constant g_{ik} is given by

$$g_{ik} = \frac{1}{\hbar}\left(\frac{2\pi\hbar\omega_k}{V}\right)^{1/2}\left(\frac{\omega_{EI}}{\omega_k}\right)\mu_{EI}\cdot\varepsilon_{ik}\, e^{i\mathbf{k}\cdot\mathbf{r}_a}\,. \tag{3.43}$$

The sum over allowed photon modes λ involves a sum over the allowed values of $\mathbf{k}$. In the limit as $V \to \infty$, the sum over a discrete set of modes goes over to a continuous limit according to the usual prescription

$$\sum_{\mathbf{k}} \to \int d\Omega_k \int d\omega_k\, \rho(\mathbf{k})\,, \tag{3.44}$$

where $\rho(\mathbf{k})$, the number of modes per unit frequency per unit solid angle, is given for our free-space modes by

$$\rho_{free}(\mathbf{k}) = \rho_{free}(\omega_k) = \frac{V\omega_k^2}{(2\pi)^3 c^3}\,. \tag{3.45}$$

Thus, using eqs. (3.38), (3.39), (3.42), and (3.43), the decay rate and shift of the atom in the level $|E\rangle$ may be written as

$$\Gamma = 2\pi \sum_I \sum_i \int d\Omega_k \int d\omega_k \frac{|\mu_{EI}\cdot\varepsilon_{ik}|^2}{\hbar^2}\left(\frac{2\pi\hbar\omega_{EI}^2}{V\omega_k}\right)\rho(\mathbf{k})\delta(\omega_{EI} - \omega_k) \tag{3.46}$$

$$\delta\omega = \sum_I \sum_i \int d\Omega_k \int d\omega_k \frac{|\mu_{EI}\cdot\varepsilon_{ik}|^2}{\hbar^2}\left(\frac{2\pi\hbar\omega_{EI}^2}{V\omega_k}\right)\rho(\mathbf{k})\frac{1}{\omega_{EI} - \omega_k}\,. \tag{3.47}$$

Substituting for $\rho(\mathbf{k}) = \rho_{free}(\mathbf{k})$, and using the result that[58]

$$\sum_i \int d\Omega_k\, |\mu_{EI}\cdot\varepsilon_{ik}|^2 = \frac{8\pi}{3}|\mu_{EI}|^2\,, \tag{3.48}$$

we find the familiar result that

$$\Gamma_{free} = \sum_I \frac{4|\mu_{EI}|^2 \omega_{EI}^3}{3\hbar c^3} \ , \tag{3.49}$$

where the sum over I is restricted to values such that $\omega_I < \omega_E$. Also, performing the integration over solid angle, and substituting for $\rho_{free}(\mathbf{k})$ in eq. (3.47) we find that

$$\delta\omega_{free} = \frac{1}{\hbar} \sum_I \frac{2}{3\pi c^3} |\mu_{EI}|^2 \int_0^{\omega_k^{(max)}} d\omega_k \frac{\omega_{EI}^2 \omega_k}{\omega_{EI} - \omega_k} \ , \tag{3.50}$$

where $\omega_k^{(max)}$ is some upper limit of integration, and the sum over I runs over all the atomic states.

It is apparent that the result (3.50) for the frequency shift diverges in proportion to the upper limit $\omega_k^{(max)}$ of the integration and therefore does not produce a well-defined answer. Nevertheless eq. (3.50) will serve as a completely adequate expression for the calculation of the frequency shift of an atom in a cavity. This point will be discussed presently in connection with the free-space Lamb shift, and in the following sections.

III.A.4 Mass Renormalization and the Free Space Lamb Shift.

The result (3.50) for the shift for the free space level shift of an atom clearly diverges. This difficulty was resolved by Bethe[15], who applied the idea of mass renormalization to the calculation of the Lamb shift of atomic hydrogen. Basically, mass renormalization consists of subtracting from the result (3.50) a contribution which should be regarded as having already been included in the free electron mass. To see how this works, note that a free electron also interacts with the electromagnetic field according to diagrams which are strictly analogous to Figs. 3.2(a) and 3.2(b). In this case the states of the electron are normalized plane wave states $|\mathbf{p}\rangle$, where $\langle \mathbf{r}|\mathbf{p}\rangle = e^{i\mathbf{p}\cdot\mathbf{r}/\hbar}/\sqrt{V}$. The diagram analogous to Fig. 3.2(a) describes the radiative damping of the electron's kinetic energy, and the diagram analagous to Fig 3.2(b) describes the shift in energy of the free electron. This shift is also given by eq. (3.39), where now $g_\lambda = -iH_{\mathbf{p}\lambda\mathbf{p}'}/\hbar$, where the matrix element is now given by[58]

$$H_{\mathbf{p}\lambda\mathbf{p}'} = \frac{e}{m}\sqrt{\frac{2\pi\hbar}{V\omega_k}}\ \mathbf{p}\cdot\boldsymbol{\varepsilon}_{ik}^*\ \delta_{\mathbf{p}'+\hbar\mathbf{k},\,\mathbf{p}} \ , \tag{3.51}$$

where we have assumed the plane wave states $|\lambda\rangle = |i,\mathbf{k}\rangle$ for the field. Thus using eq. (3.51) to substitute for g_λ in eq. (3.39) we find that the energy of the free electron is shifted by an amount

$$\delta\omega^{(elec)} = \frac{2\pi e^2}{\hbar m^2 V} \sum_i \int d\Omega_k \, |\mathbf{p}\cdot\boldsymbol{\epsilon}_{i\mathbf{k}}^*|^2 \int d\omega_k \, \rho(\mathbf{k}) \frac{-1}{\omega_k^2} \,, \tag{3.52}$$

where we have used eq. (3.44), together with the fact that for nonrelativistic energies the energy denominator is given by $\omega_E - \omega_I - \omega_k \cong -\omega_k$. Substituting for the free-space density of modes from eq. (3.45), this can be rewritten as

$$\delta\omega_{free}^{(elec)} = -\frac{2}{3\pi} \frac{e^2 \omega_k^{(max)}}{\hbar m^2 c^3} p^2 = Cp^2 \,, \tag{3.53}$$

where

$$C = -\frac{2}{3\pi} \frac{e^2 \omega_k^{(max)}}{\hbar m^2 c^3} \,. \tag{3.54}$$

This shift in energy causes a shift in the apparent mass of the electron from m_{bare} to m_{obs}, where m_{bare} is the electron mass in the absence of any interaction with the electromagnetic field. However, this effect should be regarded as having already contributed to the atomic Hamiltonian, because the kinetic energy of the electron was written as $\mathbf{p}^2/2m_{obs}$, using the observed electron mass. In order to avoid counting this effect twice, it is necessary to subtract it off from the value of the shift already calculated. Thus the "observed" atomic level shift is given by

$$\delta\omega_{obs} = \delta\omega - \frac{1}{\hbar}\langle E| \frac{\mathbf{p}^2}{2m_{obs}} - \frac{\mathbf{p}^2}{2m_{bare}} |E\rangle = \delta\omega - C\langle E|\, \mathbf{p}^2 \,|E\rangle \,. \tag{3.55}$$

Using the completeness relation for the atomic states, together with eq. (3.25) the "mass renormalization term" can be rewritten as

$$\frac{1}{\hbar}\langle E| \frac{\mathbf{p}^2}{2m_{obs}} - \frac{\mathbf{p}^2}{2m_{bare}} |E\rangle = -\frac{1}{\hbar} \sum_I \frac{2}{3\pi c^3} |\mu_{EI}|^2 \int_0^{\omega_k^{(max)}} d\omega_k \, \omega_{EI}^2 \,. \tag{3.56}$$

Thus, substituting this expression and eq. (3.50) into eq. (3.55), we find that

$$\delta\omega_{obs} = \frac{1}{\hbar} \sum_I \frac{2}{3\pi c^3} |\mu_{EI}|^2 \int_0^{\omega_k^{(max)}} d\omega_k \frac{\omega_{EI}^3}{\omega_{EI} - \omega_k} \,, \tag{3.57}$$

where the sum over I runs over all atomic states.

This expression is much more well-behaved than (3.50), diverging only logarithmically. It is therefore very insensitive to the exact value of $\omega_k^{(max)}$. Without going into any further details, we merely remark that Bethe, arguing that $\omega_k^{(max)}$ should be taken as mc^2,

evaluted the result (3.57) for the s-states of hydrogen.[15] For the 2s state, he calculated a shift of $\delta\omega_{obs}(2s)/2\pi = +1040$ MHz, whereas the experimentally observed value is[59] +1057 MHz. This was a very important result, as it showed that the Lamb shift is a radiative effect, that it is basically a low-frequency non-relativistic effect, and that it can be calculated quite accurately using the Wigner-Weisskopf formalism, together with the idea of mass renormalization.

It should be noted that the mass renormalization term does not display any resonant behavior for $\omega_k \equiv \omega_{EI}$. In all of the freqeuncy shifts to be discussed in this thesis, what we are interested in is not the absolute frequency shift $\delta\omega_{cav}$ of the atom in the cavity, but the difference $\Delta\omega_{cav} = \delta\omega_{cav} - \delta\omega_{free}$ between the shift with the atom in the cavity and the shift with the atom in free space, since that is the quantity we can measure. In every case to be discussed here, the only effect of the cavity is to modify the atom-cavity mode coupling in the vicinity of an atomic resonance. Because of this, mass renormalization has no effect on the relative frequency shift $\Delta\omega_{cav}$.

III.A.5 Spontaneous Emission by an Atom into a Single, Damped Cavity Mode.

In this section we present a simple, heuristic calculation which allows us to obtain the spontaneous emission rate and frequency shift of a two-level atom interacting with a single, damped cavity mode. This model has been previously discussed by Filpovicz et al[14], and is a very good approximation to a Rydberg atom interacting with a single mode of a microwave cavity[6], and may also be a good approximation to the spontaneous emission of an atom in an optical resonator, if a large number of degenerate modes can be treated as an "effective single mode". Our starting point is eqs. (3.38) and (3.39). The upper level of the atom is $|E\rangle$, and the single lower level we denote by $|G\rangle$. We also make the heuristic assumption that the damped single mode may be described as having an "effective mode density" $\rho_{cav}(\omega)$ (modes per unit frequency) of "one mode" distributed in frequency according a Lorentzian lineshape of width $\omega_c/2Q$, where Q is the quality factor of the resonator mode, and ω_c its resonant frequency. Thus

$$\rho_{cav}(\omega) = 1 \times \frac{1}{\pi} \frac{(\omega_c/2Q)}{(\omega - \omega_c)^2 + (\omega_c/2Q)^2} \tag{3.58}$$

Eqs. (3.38) and (3.39) may thus be rewritten as

$$\Gamma_{cav} = 2\pi |g_\lambda|^2 \rho_{cav}(\omega_{EG}) \tag{3.59}$$

$$\delta\omega_{cav} = |g_\lambda|^2 \int \frac{\rho_{cav}(\omega)}{\omega_{EG} - \omega} \, . \tag{3.60}$$

Substituting for g_λ from eq. (3.24), and for $\rho_{cav}(\omega)$ from eq. (3.58), we find

$$\Gamma_{cav} = \frac{8\pi Q|\mu_{EG}|^2}{\hbar V_{eff}} \left(\frac{\omega_{EG}}{\omega_c}\right)^2 \frac{(\omega_c/2Q)^2}{(\omega_{EG} - \omega_c)^2 + (\omega_c/2Q)^2} \tag{3.61}$$

$$\delta\omega_{cav} = \frac{4\pi Q|\mu_{EG}|^2}{\hbar V_{eff}} \left(\frac{\omega_{EG}}{\omega_c}\right)^2 \frac{(\omega_{EG} - \omega_c)(\omega_c/2Q)}{(\omega_{EG} - \omega_c)^2 + (\omega_c/2Q)^2} \, , \tag{3.62}$$

where, for simplicity we have assumed that the dipole moment μ_{EG} is parallel to the field $\mathbf{E}(\mathbf{r}_a)$. Also we have defined a new quantity, the "effective mode volume", by

$$V_{eff} = \frac{\Lambda_\lambda}{|\Phi_\lambda(\mathbf{r}_a)|^2} \, . \tag{3.63}$$

Note that

$$\int |\Phi_\lambda(\mathbf{r})|^2 \, d^3r = |\Phi_\lambda(\mathbf{r}_a)|^2 \, V_{eff} \, . \tag{3.64}$$

Thus if the magnitude of the normal mode function $\Phi_\lambda(\mathbf{r})$ is uniform, as it is in the plane wave case, then the effective mode volume is equal to the actual volume of the resonator. If however, the magnitude squared of the normal mode function is greater at the atomic position $\mathbf{r}_a$ than its average magnitude squared, the effective mode volume V_{eff} is smaller than V, expressing the fact that the field energy is more concentrated on the atom than if the mode were uniform in intensity.

For the case of the resonator exactly on resonance, $\omega_c = \omega_{EG}$, the result for Γ_{cav} may be written in terms of Γ_{free}:

$$\Gamma_{cav} = \left(\frac{3Q}{4\pi^2}\right)\left(\frac{\lambda^3}{V_{eff}}\right)\Gamma_{free} \, . \tag{3.65}$$

This is just the result that was pointed out by Purcell[3]: if a cavity is operated in a low order mode, then $V_{eff} \sim V \sim \lambda^3$, and therefore the spontaneous emission rate is enhanced by a factor of the order of the cavity Q when the cavity is tuned to the atomic resonance. Similarly it may be shown that if the cavity is tuned such that $\omega_{EG} << \omega_c$, so that the cavity mode is far above the atomic resonance, the spontaneous emission rate of the atom is inhibited by a factor of the order of 1/Q.

The results (3.61) and (3.62) are plotted in Fig. 3.3. The essential features to notice are that the spontaneous emission rate follows the Lorentzian lineshape of the cavity, being very much enhanced on resonance, and inhibited off resonance. The frequency shift has a dispersive lineshape, with the level shifting to the red when the cavity mode is tuned to the

blue, and vice versa. This feature may be understood by noting that the atom-cavity system behaves very much like two coupled oscillators: the atom-cavity mode coupling pushes their eigenfreqencies apart.

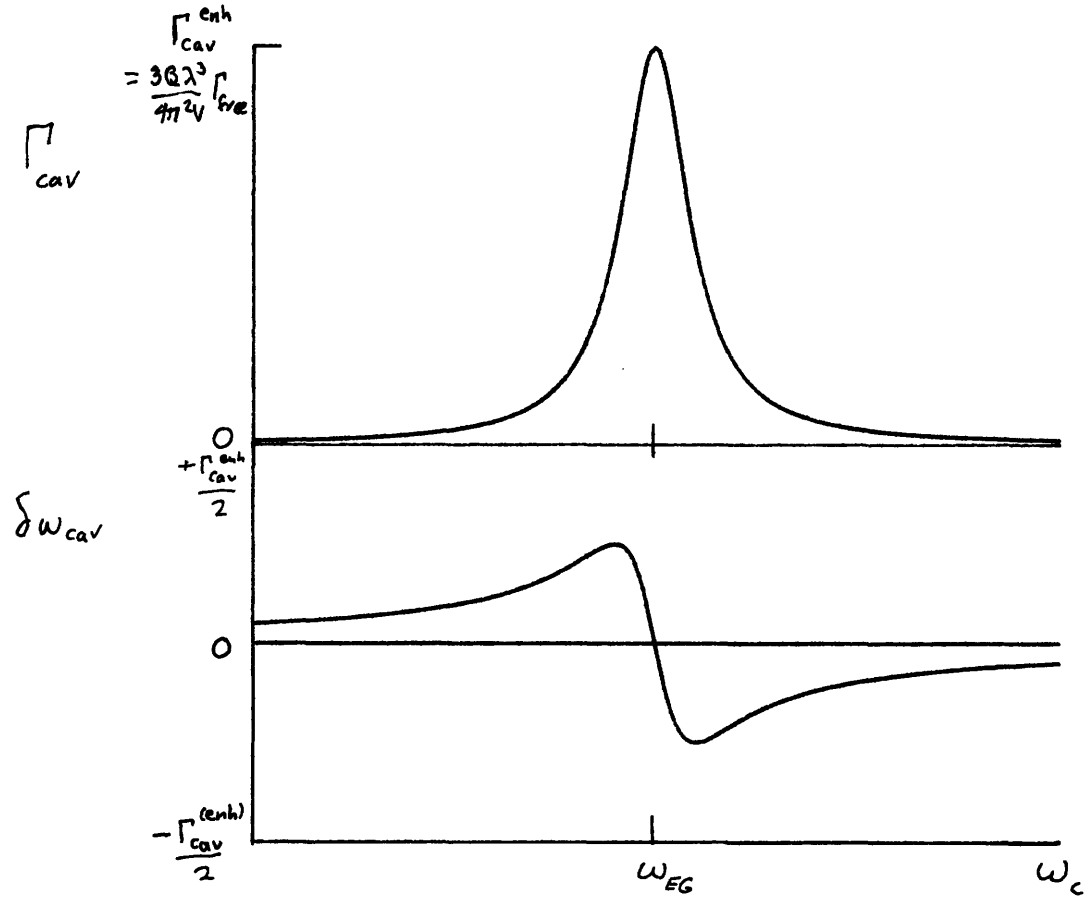

Fig. 3.3. Spontaneous emission rate and level shift of a two level atom interacting with a single damped mode. The cavity length decreases from left to right.

There are a number of issues which we have not fully addressed - the shift of the state $|G\rangle$, the shift of $|E\rangle$ and $|G\rangle$ relative to their free-space values, and the possible effect of the mass renormalization. These issues will be addressed more fully in the following section III.B, in which the frequency shift of an atom in a concentric resonator is calculated. However, the net result is that this model of an atom interacting with a single cavity mode contains all the essential physics of the problem and also gives quantitatively correct results, provided that the field can be interpreted as effectively a single damped mode.

III.B. Spontaneous Emission by an Atom in a Concentric Optical Cavity.

In this section we present a calculation of the spontaneous emission rate and level shift of an atom in an open concentric optical resonator. The approach is similar to that of section III.A.5, in that we model the damped optical cavity by means of an "effective mode density". Results obtained for the decay rate and frequency shift of a two-level atom agree with the classical model of chapter II.

III.B.1. Heuristic Model for the Cavity Mode Density.

In this section we discuss the "mode density" of a concentric optical resonator. Just as in chapter II, the resonator is composed of two spherical mirrors of radius of curvature a, separation L = 2a, reflectivity R, and a circular cross section of diameter 2b, as illustrated in Fig. 3.4. We denote the solid angle subtended by the mirrors as $\Delta\Omega_{cav}$ and the remaining solid angle as $\Delta\Omega_{side}$.

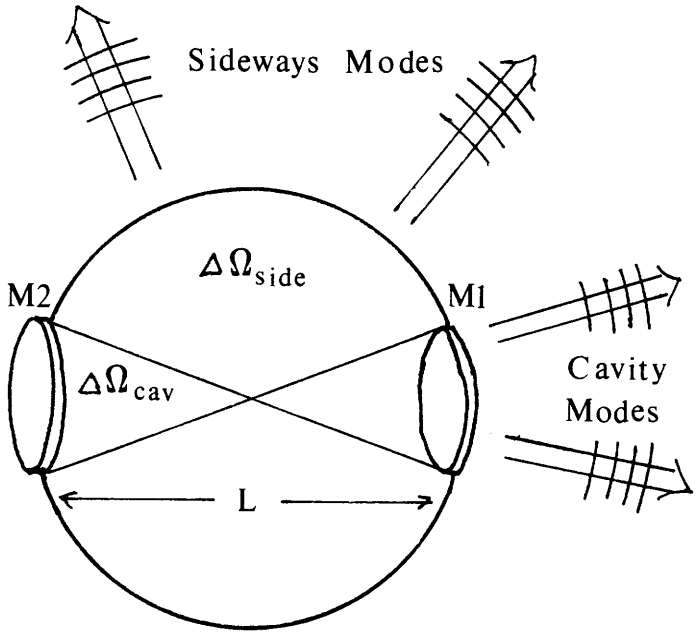

Fig 3.4. Concentric optical resonator, showing the division of the complete set of modes into "sideways modes" and "cavity modes".

Ideally, we would like to find normal mode functions of the type $\Phi_\lambda(\mathbf{r})$, which satisfy the wave equation (3.3), satisfy the boundary conditions on the mirror surface, and form a complete, orthogonal set. The solution for the decay rate and level shift could then be obtained in terms of these functions by use of eqs. (3.38) and (3.39). Unfortunately, for the case of an open resonator, the important problem of defining such a complete set of orthogonal modes has not been solved.[60] Even the rigorous solution for one mode can be a difficult problem,[61, 62] and once found, the modes of open resonators may not even be orthogonal.[60] For radiation propagating at small angles to the resonator axis in stable resonators, Hermite-Gaussian beam modes can be defined[54, 62-64], which have the property that they satisfy the wave equation and that their phasefront matches the mirror boundary. However, the Gaussian beam solutions are not valid for light propagating at large angles, are not valid when the "mode" spills over the edge of the mirror, and also do not include the sideways going modes. Worse yet, they diverge in the limit of a concentric resonator (the waist size goes to zero and the spot size on the mirror goes to infinity). The most comprehensive study of open resonator modes appears to be that of Vaynshteyn[62], but even in this work a complete, orthogonal set of mode functions, which includes both modes confined by the cavity, and sideways-going modes, is never defined.

In order to describe the open concentric resonator it is therefore necessary to resort to some approximate method. In this section we argue that the open concentric resonator may be modeled in a heuristic manner by defining an "effective mode density" $\rho_{cav}(\mathbf{k})$ to account for the effect of the cavity in eqs. (3.46) and (3.47). In order to do so, we note that if the Fresnel number $F = \pi b^2/\lambda L$ of the resonator is large, it should be possible to divide the complete set of modes into "sideways modes" and "cavity modes", as illustrated in Fig. 3.4. Clearly, the spontaneous emission out the sides of the resonator must be largely unaffected by it; we can account for this by defining $\rho_{cav}(\mathbf{k}) = \rho_{free}(\omega_{\mathbf{k}})$, if $\mathbf{k}$ points into the sideways part of the solid angle $\Delta\Omega_{side}$.

The "cavity modes" describe the spontaneous emission of the atom into the cavity part of the solid angle. Now if the cavity had perfectly reflecting mirrors, the concentric cavity would be described by almost perfectly sharp modes having a discrete set of eigenfrequencies $\omega_n = n\pi c/L$. This conclusion may be reached from either the ray optics point of view presented in chapter II, associating a "mode" with each ray direction, or from a Hermite Gaussian mode point of view. Therefore the "mode density" of such a resonator would consist of a series of evenly spaced δ-function spikes. In the presence of resonator damping, we can think of each of these modes being "spread out" according to the cavity

lineshape function $L(\omega)$. We can account for this by defining the effective mode density to be $\rho_{cav}(\mathbf{k}) = \rho_{free}(\omega_k)L(\omega_k)$, if $\mathbf{k}$ points into the resonator part of the solid angle. Now for the atom displaced from the center by a distance much less than $\sqrt{\lambda L/F}$, we know from chapter II that the cavity lineshape function is given by $L(\omega) = C/(1 + F\sin^2(\omega L/c))$, independent of the direction $\mathbf{k}$ of the "mode" in the resonator, where C is some normalization constant. This constant may be determined by demanding that the spontaneous emission rate of the atom agree with the free space rate in the limit as $L \to \infty$. This implies that

$$\overline{L(\omega)} = \frac{L}{n\pi c} \int_{\omega_0}^{\omega_0 + n\pi c} L(\omega)d\omega = 1 ; \tag{3.66}$$

and, using the relation[56]

$$\int_0^{\pi} \frac{dx}{1 + F\sin^2 x} = \frac{\pi}{\sqrt{1 + F}} , \tag{3.67}$$

that $C = \sqrt{1 + F}$.

Thus, we find that the resonator can be modeled by the effective mode density

$$\rho_{cav}(\mathbf{k}) = \begin{cases} \rho_{free}(\omega_k) , & \mathbf{k} \text{ in } \Delta\Omega_{side} \\ \rho_{free}(\omega_k)\, L(\omega_k) , & \mathbf{k} \text{ in } \Delta\Omega_{cav} \end{cases} \tag{3.68}$$

where

$$L(\omega) = \frac{\sqrt{1 + F}}{1 + F\sin^2(\omega L/c)} . \tag{3.69}$$

III.B.2. Concentric Cavity Spontaneous Emission Rate and Level Shift.

We can use our model for the "effective mode density" of the concentric cavity to calculate the spontaneous emission rate and level shift of an atom in a concentric resonator, by substituting the form (3.68) for $\rho_{cav}(\mathbf{k})$ into the expression (3.46) and (3.47) for Γ and $\delta\omega$. In this section we make the futher simplifying assumption that only one of the states $|I_1\rangle \equiv |G\rangle$ lies lower in energy than the state $|E\rangle$, but we allow for the possibility that there may exist other higher lying states $|I_n\rangle$, as illustrated in Fig. 3.5.

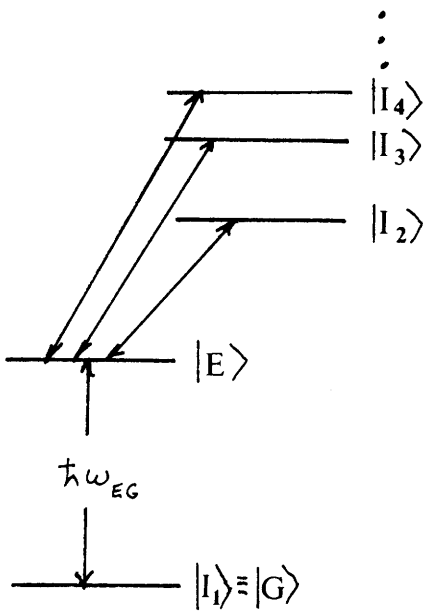

Fig. 3.5. Atomic Level Structure.

Thus

$$\Gamma_{cav} = 2\pi \sum_I \sum_i \int_{\Delta\Omega_{side}} d\Omega_k \int d\omega_k \, |g_{ik}|^2 \rho_{free}(\omega_k) \delta(\omega_{EI} - \omega_k)$$
$$+ 2\pi \sum_I \sum_i \int_{\Delta\Omega_{cav}} d\Omega_k \int d\omega_k \, |g_{ik}|^2 \rho_{free}(\omega_k) L(\omega_k) \delta(\omega_{EI} - \omega_k)$$
$$= 2\pi \sum_I \sum_i \int_{4\pi} d\Omega_k \int d\omega_k \, |g_{ik}|^2 \rho_{free}(\omega_k) \delta(\omega_{EI} - \omega_k)$$
$$+ 2\pi \sum_I \sum_i \int_{\Delta\Omega_{cav}} d\Omega_k \int d\omega_k \, |g_{ik}|^2 \rho_{free}(\omega_k) (L(\omega_k) - 1) \delta(w_{EI} - w_k) , \qquad (3.70)$$

where $\int_{4\pi}$ denotes an integration over the full solid angle $\Delta\Omega_{side} + \Delta\Omega_{cav}$. Substituting from eq. (3.43) for g_{ik}, and from eq. (3.45) for ρ_{free}, eq. (3.70) may be rewritten as,

$$\Gamma_{cav} = \Gamma_{free}[1 + (L(\omega_{EG}) - 1) f(\Delta\Omega_{cav})] , \qquad (3.71)$$

where

$$\Gamma_{free} = \frac{4|\mu_{EG}|^2 \omega_{EG}^3}{3\hbar c^3} \qquad (3.72)$$

is the free space result for the spontaneous decay rate from $|E\rangle$ to $|G\rangle$, and

$$f(\Delta\Omega_{cav}) = \frac{\sum_i \int_{\Delta\Omega_{cav}} d\Omega_k \, |\mu_{EG} \cdot \varepsilon_{ik}|^2}{\sum_i \int_{4\pi} d\Omega_k \, |\mu_{EG} \cdot \varepsilon_{ik}|^2} \qquad (3.73)$$

is the fraction of the free-space spontaneous emission rate ordinarily emitted into the solid angle $\Delta\Omega_{cav}$. Note that with the definition (3.73) for $f(\Delta\Omega_{cav})$, the result (3.71) applies regardless of the polarization of μ_{EG}.

For the case that the dipole is linearly polarized perpendicular to the resonator axis, eq. (3.73) becomes,

$$f(\Delta\Omega_{cav}) = \frac{\int_{\Delta\Omega_{cav}} d\Omega_k \, |\mu_{EG}|^2 \sin^2\theta'}{\int_{4\pi} d\Omega_k \, |\mu_{EG}|^2 \sin^2\theta'} = 1 - \frac{3}{4}\cos\theta_M - \frac{1}{4}\cos^3\theta_M , \tag{3.74}$$

where as in section II.F.3, θ' is the angle between μ_{EG} and $\mathbf{k}$, and θ_M is the half angle subtended by the mirror.

We see that the result (3.71) for the decay rate of the excited atom is identical with the classical result (2.130). This correspondence will be discused further in chapter VI.

The result for the level shift $\delta\omega_{cav}$ may be written as

$$\delta\omega_{cav} = \sum_I \sum_i \int_{\Delta\Omega_{side}} d\Omega_k \int_0^{\omega_k^{(max)}} d\omega_k \, |g_{ik}|^2 \rho_{free}(\omega_k) \frac{1}{\omega_{EI} - \omega_k}$$
$$+ \sum_I \sum_i \int_{\Delta\Omega_{cav}} d\Omega_k \int_0^{\omega_k^{(max)}} d\omega_k \, |g_{ik}|^2 \rho_{free}(\omega_k) L(\omega_k) \frac{1}{\omega_{EI} - \omega_k} , \tag{3.75}$$

where as before $\omega_k^{(max)}$ is some upper limit of integration. It is apparent that this expression for the level shift diverges in proportion to $\omega_k^{(max)}$, just as was the case in eq. (3.50) for free space. However, in the experiments what we will be able to measure is not the absolute level shift $\delta\omega_{cav}$, but only the difference $\Delta\omega_{cav} = \delta\omega_{cav} - \delta\omega_{free}$ between the shift of the atom in the cavity and the shift of the atom in free space. Substituting from eq. (3.43) for g_{ik} and from eq. (3.45) for ρ_{free}, this quantity may be written as

$$\Delta\omega_{cav} = \frac{1}{4\pi^2\hbar c^3} \sum_I \sum_i \int_{\Delta\Omega_{cav}} d\Omega_k |\mu_{EI}\cdot\epsilon_{ik}|^2 \int_0^{\omega_k^{(max)}} \delta\omega_k \frac{\omega_{EI}^2 \omega_k}{\omega_{EI} - \omega_k} (L(\omega_k) - 1). \tag{3.76}$$

Note that only the "cavity modes" contribute to the difference in frequency shifts, because the sideways modes contribute equally to the free-space shift and the cavity shift. Also note that the factor $(L(\omega_k) - 1)$ takes into account the difference between the density of modes in the cavity and free space, the former being proportional to $L(\omega_k)$ and the latter to 1. In order to further evaluate eq. (3.76) note that the fractional change of the function

$f(\omega_k) = \dfrac{\omega_k}{\omega_{EI} - \omega_k}$ in an interval $\Delta\omega_k{}^f$ is given by

$$\frac{\Delta f}{f} = \left(\frac{\omega_{EI} - \omega_k}{\omega_k} \frac{d}{d\omega_k} \frac{\omega_k}{\omega_{EI} - \omega_k} \right) \Delta\omega_k{}^f = \left(\frac{1}{\omega_k} + \frac{1}{\omega_{EI} - \omega_k} \right) \Delta\omega_k{}^f . \tag{3.77}$$

Thus a fractional change in f of order unity occurs for $\Delta f/f \sim 1$, or

$$\Delta\omega_k{}^f \sim \frac{\omega_k(\omega_k - \omega_{EI})}{\omega_{EI}} . \tag{3.78}$$

The function $g(\omega_k) = (L(\omega_k) - 1)$ changes periodically with a period $\Delta\omega_k{}^g = \pi c/L$. Thus if $\Delta\omega_k{}^f >> \Delta\omega_k{}^g$, or

$$\frac{\omega_k(\omega_k - \omega_{EI})}{\omega_{EI}} >> \frac{\pi c}{L} , \tag{3.79}$$

the factor $f(\omega_k)$ in the integrand of eq. (3.76) varies very little over many periods of the function $g(\omega_k)$ in the integrand. We may therefore approximate $f(\omega_k)$ as constant over some interval $\Delta\omega_k$, so that

$$\int_{\omega_0}^{\omega_0+\Delta\omega_k} d\omega_k \frac{\omega_{EI}{}^2\omega_k}{\omega_{EI} - \omega_k} (L(\omega_k) - 1) \cong \frac{\omega_{EI}{}^2\omega_0}{\omega_{EI} - \omega_0} \int_{\omega_0}^{\omega_0+\Delta\omega_k} d\omega_k \, (L(\omega_k) - 1)$$

$$\cong \frac{\omega_{EI}{}^2\omega_0}{\omega_{EI} - \omega_0} \Delta\omega_k \, (\overline{L(\omega_k)} - 1)) = 0, \tag{3.80}$$

where the region of integration must satisfy $\pi c/L << \Delta\omega_k << \omega_0$, and $\overline{L(\omega_k)} = 1$ is the cycle average value of $L(\omega_k)$, as in eq. (3.66). From eq. (3.80) it is evident that there is no contribution to the difference in frequency shifts $\Delta\omega_{cav}$ from any interval of frequency $[\omega_0, \omega_0 + \Delta\omega_k]$ for which the magnitude of the detuning $\omega_{EI} - \omega_k$ is much greater then a free spectral range $\pi c/L$. In particular consider the higher lying states $|I\rangle \neq |G\rangle$. Then ω_{EI} is negative, and the magnitude of the detuning $|\omega_{EI} - \omega_k|$ is <u>always</u> much greater then $\pi c/L$. Therefore there is no contribution to the difference in frequency shifts from terms in eq. (3.76) such that $I \neq G$.

Next consider the remaining contribution from the term I = G. We can write eq. (3.76) as:

$$\Delta\omega_{cav} = \frac{1}{4\pi^2\hbar c^3}\sum_i \int_{\Delta\Omega_{cav}} d\Omega_k |\mu_{EG}\cdot\epsilon_{ik}|^2 \Bigg\{ \int_0^{\omega_{EG}-\Delta\omega_k} d\omega_k \frac{\omega_{EG}^2\omega_k}{\omega_{EG}-\omega_k}(L(\omega_k)-1)$$

$$+ \int_{\omega_{EG}-\Delta\omega_k}^{\omega_{EG}+\Delta\omega_k} d\omega_k \frac{\omega_{EG}^2\omega_k}{\omega_{EG}-\omega_k}(L(\omega_k)-1) + \int_{\omega_{EG}+\Delta\omega_k}^{\omega_k(max)} d\omega_k \frac{\omega_{EG}^2\omega_k}{\omega_{EG}-\omega_k}(L(\omega_k)-1) \Bigg\}, \qquad (3.81)$$

where again $\pi c/L << \Delta\omega_k << \omega_{EG}$. By the same argument that led up to eq. (3.80), the first and third integrals on the right are equal to zero. Also note that,

$$\int_{\omega_{EG}-\Delta\omega_k}^{\omega_{EG}+\Delta\omega_k} d\omega_k \frac{\omega_{EG}^2\omega_k}{\omega_{EG}-\omega_k} \cong \omega_{EG}^3 \int_{\omega_{EG}-\Delta\omega_k}^{\omega_{EG}+\Delta\omega_k} d\omega_k \frac{1}{\omega_{EG}-\omega_k} = 0. \qquad (3.82)$$

by the antisymmetry of the integrand about the point $\omega_k = \omega_{EG}$. Therefore, the difference in frequency shifts is given by

$$\Delta\omega_{cav} = \frac{1}{2\pi} f(\Delta\Omega_{cav})\Gamma_{free} \int_{\omega_{EG}-\Delta\omega_k}^{\omega_{EG}+\Delta\omega_k} d\omega_k \frac{1}{\omega_{EG}-\omega_k} L(\omega_k), \qquad (3.83)$$

where we have used the relations (3.72) and (3.73), together with the fact that $\omega_k \cong \omega_{EG}$, $x = \Delta\omega L/c$, and $\phi = \omega_{EG}L/c$, we can rewrite the frequency integral as,

$$\int_{\omega_{EG}-\Delta\omega_k}^{\omega_{EG}+\Delta\omega_k} d\omega_k \frac{1}{\omega_{EG}-\omega_k} L(\omega_k) \cong -\int_{-\infty}^{\infty} \frac{dx}{x} \frac{\sqrt{1+F}}{1+F\sin^2(x+\phi)} = -I_1, \qquad (3.84)$$

where the limits of the integral may be extended to $\pm\infty$, since $\Delta\omega_k >> \pi c/L$, and since only values of $|x| \sim 1$ contribute significantly to the integral. The integral I_1 is evaluated in appendix 1, with the result that

$$I_1 = \frac{-\pi F\sin(2\phi)}{2(1+F\sin^2\phi)}. \qquad (3.85)$$

Therefore, combining eqs. (3.83), (3.84), and (3.85), we find that

$$\Delta\omega_{cav} = \Gamma_{free}\frac{f(\Delta\Omega_{cav})}{4}\frac{F\sin(2\omega_{EG}L/c)}{1+F\sin^2(\omega_{EG}L/c)}. \qquad (3.86)$$

Again, we find exact agreement with the classical result (2.131). However, our physical interpretation of the effect is now very different. In the classical model, we thought of the atom as being much like a classical dipole oscillator, and when we put the oscillator in the cavity, some of its emitted radiation was reflected back onto it, causing an additional contribution to its radiation reaction force which shifted its natural frequency. In the present

model, we think of the atom and the field as a combined quantum mechanical system, whose energy levels are shifted slightly as the resonator enhances the interaction between certain cavity modes and the atom, and inhibits others. When we probe the transition with a laser, the level shift of the excited state shows up as a frequency shift. This question of interpretation will be discussed further in chapter VI.

The results (3.71) and (3.86) for Γ_{cav} and $\delta\omega_{cav}$ have been illustrated in Fig. 2.5. Again, note that for $F >> 1$, the spontaneous emission rate is enhanced by a factor of approximately $\sqrt{F}\cdot f(\Delta\Omega_{cav})$ when the cavity is on resonance, and inhibited by a factor of $1/(1 - f(\Delta\Omega_{cav}))$ when the cavity is off-resonance. The shift displays a repeating dispersive-shaped behavior, vanishing when a cavity resonance is tuned exactly to the atomic resonance, and when the atomic resonance is exactly halfway between two cavity resonances. Also, the level shifts to the blue when the nearest cavity mode is tuned to the red, and vice-versa.

The result (3.86) may be understood from the form (3.76) of the integral for $\Delta\omega_{cav}$. In free space, the mode density is essentially constant over a small range of frequency near resonance, so the integrand $\rho(\omega_k)/(\omega_{EI} - \omega_k)$ is antisymmetric about resonance, resulting in no net contribution to $\Delta\omega_{cav}$ from a small region of frequency near resonance. This corresponds to equal numbers of virtual photons emitted slightly above and below resonance. In the cavity, however, the effective mode density may be enhanced by a cavity resonance slightly to one side of the atomic resonance. In this case the integrand is no longer antisymmetric, and a net contribution to $\Delta\omega_{cav}$ results. In this case the virtual photon emission is favored to the one side of resonance. Only if a cavity resonance is tuned exactly to the atomic resonance, or the atomic resonance exactly halfway between two cavity resonances, is the mode density symmetrical about resonance, and the contribution to the frequency shift equal to zero.

In applying the form (3.75) of the level shift $\delta\omega_{cav}$ to the calculation of $\Delta\omega_{cav}$ given by eq. (3.76), we have left out the mass renormalization term, which we know was important to giving us the correct value of the free-space shifts. In principle this mass renormalization term might also be modified in a resonator and therefore contribute to $\Delta\omega_{cav}$. That is, we should actually have written that

$$\Delta\omega_{cav}^{(obs)} = \left\{\delta\omega_{cav} - \left[\frac{1}{\hbar}\langle E|\frac{p^2}{2m_{obs}} - \frac{p^2}{2m_{bare}}|E\rangle\right]_{cav}\right\}$$
$$- \left\{\delta\omega_{free} - \left[\frac{1}{\hbar}\langle E|\frac{p^2}{2m_{obs}} - \frac{p^2}{2m_{bare}}|E\rangle\right]_{free}\right\} . \qquad (3.87)$$

We can calculate the energy shift of a free electron in the cavity by substituting for $\rho_{cav}(\mathbf{k})$ in eq. (3.52):

$$\delta\omega_{cav}^{(elec)} = \frac{2\pi e^2}{\hbar m^2 V}\sum_i \int_{4\pi} d\Omega_k\, |\mathbf{p}\cdot\boldsymbol{\epsilon}_{ik}^*|^2 \int_0^{\omega_k^{(max)}} d\omega_k \frac{V\omega_k^2}{(2\pi)^3c^3}\frac{-1}{\omega_k^2} ,$$
$$+ \frac{2\pi e^2}{\hbar m^2 V}\sum_i \int_{\Delta\Omega_{cav}} d\Omega_k\, |\mathbf{p}\cdot\boldsymbol{\epsilon}_{ik}^*|^2 \int_0^{\omega_k^{(max)}} d\omega_k \frac{V\omega_k^2}{(2\pi)^3c^3}\frac{-1}{\omega_k^2}(L(\omega_k) - 1)$$
$$= \delta\omega_{free}^{(elec)} , \qquad (3.88)$$

where the second term is equal to zero, by the same argument leading up to eq. (3.80). Therefore

$$\Delta\omega_{cav}^{(obs)} = \{\delta\omega_{cav} - C\langle E|\,\mathbf{p}^2\,|E\rangle\} - \{\delta\omega_{free} - C\langle E|\,\mathbf{p}^2\,|E\rangle\} = \Delta\omega_{cav} . \qquad (3.89)$$

We see that the mass renormalization term, even though it is very important for the calculation of the absolute level shift $\delta\omega_{cav}$, has essentially no effect on the difference in frequency shifts $\Delta\omega_{cav}$. As mentioned earlier, this is because the only important effect of the cavity is to modify the mode density in the vicinity of an atomic resonance, whereas the mass renormalization term exhibits no resonance behavior.

One further point is that in our experiments we will actually not measure the level shift $\Delta\omega_{cav}$ directly, but only the transition frequency from $|G\rangle$ to $|E\rangle$, which includes the level shifts of both $|G\rangle$ and $|E\rangle$. Now for the level $|G\rangle$ we can write an expression analogous to eq. (3.75) for $\Delta\omega_{cav}^{(G)}$,

$$\Delta\omega_{cav}^{(G)} = \frac{1}{4\pi^2\hbar c^3}\sum_I \sum_i \int_{\Delta\Omega_{cav}} d\Omega_k |\boldsymbol{\mu}_{GI}\cdot\boldsymbol{\epsilon}_{ik}|^2 \int_0^{\omega_k^{(max)}} d\omega_k \frac{\omega_{GI}^2\omega_k}{\omega_{GI} - \omega_k}(L(\omega_k)-1), \quad (3.90)$$

where the sum over I now denotes a sum over all the atomic states other than $|G\rangle$, including $|E\rangle$. However if $|G\rangle$ is the atomic ground state, $\omega_{GI} < 0$ for all I. Therefore, according to eq. (3.80), $\Delta\omega_{cav}^{(G)} = 0$; i.e. *there is no shift in the energy of the ground state in the cavity, relative to its energy in free space.* This means that if we probe the transition from $|G\rangle$ to $|E\rangle$, the measured shift in transition frequency will consist only of the shift $\Delta\omega_{cav}$ in the energy of the excited state $|E\rangle$.

III.C. Spontaneous Emission of an Atom into a Complete Spherical Cavity.

In this section we calculate the spontaneous emission rate and level shift of an atom in a complete spherical cavity. As mentioned earlier, the normal mode functions of the sphere are well-known and therefore this problem may be treated exactly, without any recourse to arguments based on an "effective mode density". In order to take into account the cavity damping, we follow an approach similar to that used in laser physics[65], and suppose that the partially reflecting sphere is embedded in a much larger perfectly reflecting sphere. We solve the for the eigenmodes of the combined small/large sphere system; the limit of the partially reflecting sphere in free space is then obtained as the radius of the large sphere tends to infinity. As in the previous section, we consider an atom with the level stucture illustrated in Fig. 3.5, with only a single level $|G\rangle$ lower in energy than $|E\rangle$.

III.C.1. Boundary Conditions and Normal Mode Functions.

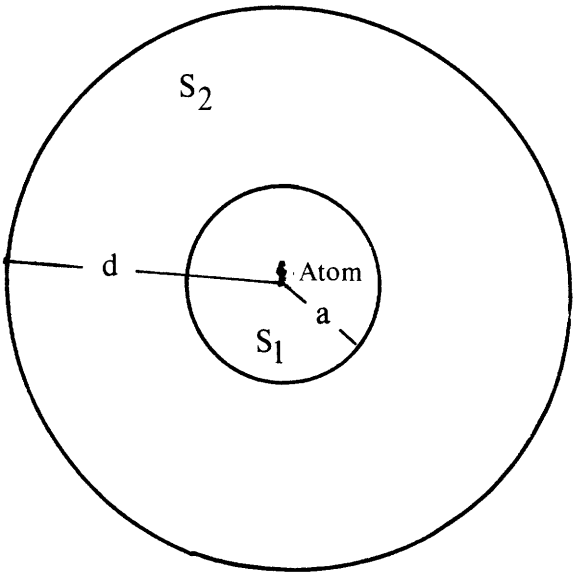

Fig. 3.6. Atom inside a partially reflecting sphere of radius a, embedded in a larger perfectly reflecting sphere of radius d.

The spherical cavity system is illustrated in Fig. 3.6. The small sphere S_1 has a radius a and a reflectivity R, and the large sphere S_2 has a radius $d >> a$, is perfectly reflecting, and is concentric with S_1. Similar to the approach of Ref. 65, we suppose that the sphere S_1 may be modeled as a spherical dielectric shell of negligible thickness t and dielectric

constant ε such that $\eta = \varepsilon t$. Thus the space inside S_2 has a spatially dependent dielectric constant

$$\varepsilon(\mathbf{r}) = 1 + \eta\,\delta(r - a). \tag{3.91}$$

Of course in reality the boundary of S_1 may be more complex, but the more complex boundary conditions resulting from a more realistic model of the reflecting surface will modify the calculation in only a trivial way, and therefore may be neglected.

Now the field inside the sphere must satisfy the wave equation

$$\nabla\times(\nabla\times\Phi_\lambda(\mathbf{r})) + (1 + \eta\,\delta(r - a))k_\lambda^2\Phi_\lambda(\mathbf{r}) = 0\,. \tag{3.92}$$

This equation follows from the macroscopic Maxwell equations, making use of the constitutive relation

$$\mathbf{D}(\mathbf{r},t) = \varepsilon(\mathbf{r})\,\mathbf{E}(\mathbf{r},t)\,, \tag{3.93}$$

and expressing the $\mathbf{E}$ as a Fourier sum according to eq. (3.5). The normal modes λ must satisfy eq. (3.94) together with the boundary condition that the tangential component of $\mathbf{E}$ vanish at the surface of the outer, perfectly reflecting sphere:

$$\Phi_\lambda(r=d)\times\hat{\mathbf{r}} = 0. \tag{3.94}$$

The solutions of eq. (3.92) may be expressed in terms of solutions in the separate regions $0 \le r \le a$ ("region I") and $a < r \le d$ ("region II") which satisfy the wave eqation in vacuum (3.3), together with auxiliary boundary conditions at $r = a$. These conditions are obtained by integrating eq. (3.94) across the boundary. Now from the Maxwell eq. $\nabla\cdot\mathbf{D} = 0$, it follows that

$$\nabla\cdot\Phi_\lambda(\mathbf{r}) = -\,\Phi_\lambda(\mathbf{r})\cdot\frac{\nabla\cdot\varepsilon(\mathbf{r})}{\varepsilon(\mathbf{r})} = -\Phi_{\lambda r}\frac{\eta\,\delta'(r-a)}{1 + \eta\delta(r-a)}\,. \tag{3.95}$$

Thus, making use of the identity

$$\nabla\times(\nabla\times\Phi_\lambda(\mathbf{r})) = \nabla(\nabla\cdot\Phi_\lambda(\mathbf{r})) - \nabla^2\Phi_\lambda(\mathbf{r}). \tag{3.96}$$

eq. (3.92) may be rewritten as

$$\nabla^2\Phi_\lambda(\mathbf{r}) + \nabla\left(\Phi_{\lambda r}(\mathbf{r})\frac{\eta\,\delta'(r-a)}{1 + \eta\delta(r-a)}\right) + (1 + \eta\,\delta(r-a))k_\lambda^2\Phi_\lambda(\mathbf{r}) = 0\,. \tag{3.97}$$

Taking the scalar product of this equation with the unit vector $\hat{\boldsymbol{\theta}}$ gives,

$$\nabla\cdot(\nabla\Phi_{\lambda\theta}) + \frac{1}{r}\frac{\partial\Phi_{\lambda r}}{\partial\theta}\frac{\eta\,\delta'(r-a)}{1 + \eta\delta(r-a)} + (1 + \eta\,\delta(r-a))k_\lambda^2\Phi_{\lambda\theta} = 0. \tag{3.98}$$

Consider a small "Gaussian pillbox" of area ΔA having faces on each side of S_1 at radii a_+ and a_-, where a_+ and a_- are infinitesimally greater than or less than a, respectively. Integrating eq. (3. 98) over this volume results in

$$\int dA\ \mathbf{n}\cdot\nabla\Phi_{\lambda\theta} + \Delta A\frac{\partial\Phi_{\lambda r}}{\partial\theta}\int_{a_-}^{a_+} dr\ \frac{\eta\ \delta'(r-a)}{1+\eta\delta(r-a)} + \Delta A\eta k_\lambda^2\Phi_{\lambda\theta}(a) = 0\,, \tag{3.99}$$

where the first integral has been evaluated using Gauss' theorem, and where **n** is an outward normal unit vector. Noting that the second integral vanishes by the antisymmetry of the integrand, this may be further evaluated to give

$$\frac{\partial\Phi_{\lambda\theta}}{\partial r}\Big|_{a_+} - \frac{\partial\Phi_{\lambda\theta}}{\partial r}\Big|_{a_-} = -\eta k_\lambda^2\Phi_{\lambda\theta}(a)\,, \tag{3.100}$$

The same result applies to the ϕ component of Φ_λ, so that the auxiliary boundary conditions may be written as,

$$\Phi_\lambda(a_+) = \Phi_\lambda(a_-) \tag{3.101}$$

$$\frac{\partial\Phi_{\lambda T}}{\partial r}\Big|_{a_+} - \frac{\partial\Phi_{\lambda T}}{\partial r}\Big|_{a_-} = -\eta k_\lambda^2\Phi_{\lambda T}(a)\,, \tag{3.102}$$

where $\Phi_{\lambda T} = \Phi_{\lambda\theta}\hat{\theta} + \Phi_{\lambda\phi}\hat{\phi}$ is the transverse part of Φ_λ, and the continuity equation (3.102) follows from an application of Stoke's theorem to the integration of the Maxwell equation $\nabla\times\mathbf{E} = -\frac{1}{c}\frac{\partial\mathbf{B}}{\partial t}$ around a small loop surrounding the boundary. There is also a slightly different boundary condition which applies to the derivative of the radial part of Φ_λ, but in our problem the fields at the boundary are entirely transverse and so we will not need to consider this condition.

The solution to the wave equation (3.3) in regions I and II may be written as[66] $\Phi(\mathbf{r}) = \mathbf{M}^\sigma_{ml}(\mathbf{r})$ or $\Phi(\mathbf{r}) = \mathbf{N}^\sigma_{ml}(\mathbf{r})$, where

$$\mathbf{M}^\sigma_{ml}(\mathbf{r}) = A\sqrt{l(l+1)}\,\mathbf{C}^\sigma_{ml}(\theta,\phi)j_l(k_\lambda r) + B\sqrt{l(l+1)}\,\mathbf{C}^\sigma_{ml}(\theta,\phi)n_l(k_\lambda r) \tag{3.103}$$

and

$$\mathbf{N}^\sigma_{ml}(\mathbf{r}) = C\Big\{l(l+1)\frac{1}{k_\lambda r}j_l(k_\lambda r)\mathbf{P}^\sigma_{ml}(\theta,\phi) + \sqrt{l(l+1)}\frac{1}{k_\lambda r}\frac{d}{dr}[rj_l(k_\lambda r)]\mathbf{B}^\sigma_{ml}(\theta,\phi)\Big\}$$
$$+ D\Big\{l(l+1)\frac{1}{k_\lambda r}n_l(k_\lambda r)\mathbf{P}^\sigma_{ml}(\theta,\phi) + \sqrt{l(l+1)}\frac{1}{k_\lambda r}\frac{d}{dr}[rn_l(k_\lambda r)]\mathbf{B}^\sigma_{ml}(\theta,\phi)\Big\}\,, \tag{3.104}$$

where, A, B, C, and D are arbitrary constants, $j_l(x)$ is the spherical Bessel function of order l, and $n_l(x)$ is the spherical Neumann function of order l. $\mathbf{C}^\sigma_{ml}$, $\mathbf{P}^\sigma_{ml}$, and $\mathbf{B}^\sigma_{ml}$ are the vector spherical harmonics of order m and l, which are given by

$$\mathbf{P}_{ml}(\theta,\phi) = \hat{\mathbf{r}}\,X^m_l(\theta,\phi) \tag{3.105a}$$

$$\mathbf{B}_{ml}(\theta,\phi) = \frac{r}{\sqrt{l(l+1)}}\nabla X^m_l(\theta,\phi) = \hat{\mathbf{r}}\times\mathbf{C}_{ml}(\theta,\phi) \tag{3.105b}$$

$$\mathbf{C}_{ml}(\theta,\phi) = \frac{1}{\sqrt{l(l+1)}}\nabla\times(rX^m_l(\theta,\phi)) = -\hat{\mathbf{r}}\times\mathbf{B}_{ml}(\theta,\phi), \tag{3.105c}$$

and where

$$X_l^m(\theta,\phi) = e^{im\phi} P_l^m(\cos\theta) \tag{3.106}$$

is the ordinary spherical harmonic of order l and m. The superscipt $\sigma = e$ or o denotes that either the even or odd part of the function is to be taken; i.e. $\mathbf{X}_{ml} = \mathbf{X}^e_{ml} + i\mathbf{X}^o_{ml}$, where $\mathbf{X}^e_{ml}$ and $\mathbf{X}^o_{ml}$ are real and where $\mathbf{X}_{ml}$ is any one of the functions $\mathbf{P}_{ml}$, $\mathbf{B}_{ml}$, or $\mathbf{C}_{ml}$. (Throughout this section, we adopt the notation of Morse and Feshbach.[66])

In order that the separate solutions in region I and II satisfy the continuity condition (3.101) it is necessary that they have the same angular dependence. Since the functions $\mathbf{C}^\sigma_{ml}$ and $\mathbf{B}^\sigma_{ml}$ form a complete orthogonal set of functions on the unit sphere,[66] this implies that the solution in region II must be of the same type (**M** or **N**) and of the same order l, m, and σ as the solution in region I. Thus each normal mode will be specified by the set of indices $\lambda = \{q, \sigma, m, l, n\}$, where $q = h$ for the **M**-type modes and $q = e$ for the **N**-type modes, and n is an integer which labels the values of $k\lambda$ allowed by the boundary conditions.

Consider first the **M**-type modes. We may write the solutions to the complete boundary value problem as

$$\Phi^{h\sigma}_{mln}(\mathbf{r}) = \begin{cases} \mathbf{M}^{\sigma I}_{mln}(\mathbf{r}) , & 0 \le r \le a \\ \mathbf{M}^{\sigma II}_{mln}(\mathbf{r}) , & a < r \le d \end{cases} \tag{3.107}$$

where

$$\mathbf{M}^{\sigma I}_{mln}(\mathbf{r}) = A^{h\sigma}_{mln}\sqrt{l(l+1)}\, \mathbf{C}^\sigma_{ml}(\theta,\phi) j_l(kr) \tag{3.108a}$$

$$\mathbf{M}^{\sigma II}_{mln}(\mathbf{r}) = C^{h\sigma}_{mln}\sqrt{l(l+1)}\, \mathbf{C}^\sigma_{ml}(\theta,\phi) j_l(k\lambda r) + D^{h\sigma}_{mln}\sqrt{l(l+1)}\, \mathbf{C}^\sigma_{ml}(\theta,\phi) n_l(k\lambda r) , \tag{3.108b}$$

and where we are neglecting the solution proportional to $n_l(\mathbf{r})$ in region I because the solution must be finite at the origon.

At this point it is convenient to make use of the fact that $k\lambda a >> 1$, for modes λ which contribute significantly to the decay rate and shift. Then the asymptotic forms for $j_l(x)$ and $n_l(x)$, valid for $x >> 1$, l^2 may be expected to hold to a high degree of accuracy for $x = k\lambda r$ and $r \sim a$:

$$j_l(x) \cong \frac{1}{x}\sin(x - \frac{l\pi}{2}) \tag{3.109a}$$

$$n_l(x) \cong -\frac{1}{x}\cos(x - \frac{l\pi}{2}) . \tag{3.109b}$$

thus the solutions for $k_\lambda r >> 1$, l^2 become

$$M^{\sigma I}_{mln}(r) = A^{h\sigma}_{mln}\sqrt{l(l+1)}\, C^{\sigma}_{ml}(\theta,\phi)\frac{1}{k_\lambda r}\sin(k_\lambda r - \frac{l\pi}{2}) \tag{3.110a}$$

$$\begin{aligned} M^{\sigma II}_{mln}(r) &= C^{h\sigma}_{mln}\sqrt{l(l+1)}\, C^{\sigma}_{ml}(\theta,\phi)\frac{1}{k_\lambda r}\sin(k_\lambda r - \frac{l\pi}{2}) \\ &\quad - D^{h\sigma}_{mln}\sqrt{l(l+1)}\, C^{\sigma}_{ml}(\theta,\phi)\frac{1}{k_\lambda r}\cos(k_\lambda r - \frac{l\pi}{2}) \\ &= E^{h\sigma}_{mln}\sqrt{l(l+1)}\, C^{\sigma}_{ml}(\theta,\phi)\frac{1}{k_\lambda r}\sin(k_\lambda r + \alpha^{h\sigma}_{mln}) , \end{aligned} \tag{3.110b}$$

Applying the boundary condition (3.94) gives $\alpha^{h\sigma}_{mln} = -k_\lambda d$, and thus

$$M^{\sigma II}_{mln}(r) = E^{h\sigma}_{mln}\sqrt{l(l+1)}\, C^{\sigma}_{ml}(\theta,\phi)\frac{1}{k_\lambda r}\sin(k_\lambda(r-d)) . \tag{3.111}$$

The continuity condition (3.101) therefore implies that

$$A^{h\sigma}_{mln}\sin(k_\lambda a - \frac{l\pi}{2}) = E^{h\sigma}_{mln}\sin(k_\lambda(a-d)) , \tag{3.112}$$

and the condition (3.105) gives

$$E^{h\sigma}_{mln}\cos(k_\lambda(a-d)) - A^{h\sigma}_{mln}\cos(k_\lambda a - \frac{l\pi}{2}) = -\eta k_\lambda A^{h\sigma}_{mln}\sin(k_\lambda a - \frac{l\pi}{2}) , \tag{3.113}$$

where, consistently with the approximation (3.109), it is legitimate to drop the terms down by a factor of $1/k_\lambda a$.

Equations (3.112) and (3.113) may be satisfied only if k_λ satisfies the eigenvalue equation

$$\tan(k_\lambda(d-a)) = \frac{\tan(k_\lambda a - \frac{l\pi}{2})}{\eta k_\lambda \tan(k_\lambda a - \frac{l\pi}{2}) - 1} . \tag{3.114}$$

We label the n^{th} root of the equation by k_{hln}; note that the values of the roots do not depend on σ or m. Provided eq. (3.114) is satisfied, we find that $A^{h\sigma}_{mln}$ is related to $E^{h\sigma}_{mln}$ by

$$\left(\frac{A^{h\sigma}_{mln}}{E^{h\sigma}_{mln}}\right)^2 = \frac{\tan^2(k_{hln}a - \frac{l\pi}{2}) + 1}{\tan^2(k_{hln}a - \frac{l\pi}{2}) + (\eta k_{hln}\tan(k_{hln}a - \frac{l\pi}{2}) - 1)^2} . \tag{3.115}$$

After some algebraic manipulation, we find that is possible to write the right hand side of this equation in a somewhat more convenient form: letting

$x = k_{hln}a - \frac{l\pi}{2}$ and $\Lambda = \eta k_{hln}$, we find that

$$\left(\frac{A^{h\sigma}_{mln}}{E^{h\sigma}_{mln}}\right)^2 = \frac{\sqrt{1+F}}{1+F\sin^2(x+\phi)}, \tag{3.116}$$

where

$$\tan(2\phi) = -\frac{2}{\Lambda} \tag{3.117}$$

and

$$F = \frac{2\Lambda\sqrt{\Lambda^2+4}}{(\sqrt{\Lambda^2+4}-\Lambda)^2}. \tag{3.118}$$

We next examine the solution to the eigenvalue equation (3.114). Let the function $f(k) = \frac{\tan(ka-(l\pi/2))}{\Lambda\tan(ka-(l\pi/2))-1}$ and the function $g(k) = \tan(k(d-a))$. The allowed eigenvalues of k occur at the intersection points $f(k) = g(k)$. Now f(k) and g(k) are both periodic, f(k) with period π/a and g(k) with period $\pi/(d-a)$. Since $d >> a$, there are many periods of g(k) for each period of f(k). The function f(k) is mostly nearly equal to 1/L, except near the points $k_q = (n+\frac{1}{2})\frac{\pi}{2} + \frac{1}{a}\tan^{-1}\frac{1}{\Lambda}$, where it diverges to $\pm\infty$. In each period of g(k), g(k) assumes all values monotonically from $-\infty$ to $+\infty$. Thus there will in general be one eigenvalue $g(k) = f(k)$ in each period of g(k), except for once in each period of f(k) at the point k_q, where there are two eigenvalues in a period of g(k). Thus there will be a nearly uniform discrete spectrum of eigenvalues separated by $\Delta k \cong \pi/(d-a) \cong \pi/d$; i.e., for each value of *m*, *l*, and σ, there will be a density of

$$\rho(\omega) = \frac{d}{\pi c} \tag{3.119}$$

eigenvalues per unit frequency. In the limit $d\to\infty$, the eigenvalue spectrum becomes continuous, so that expressions involving a sum over *n* go over to a continuous limit according to the prescription

$$\sum_n f(\omega_{hln}) \to \frac{d}{\pi c}\int d\omega\, f(\omega)\,. \tag{3.120}$$

The coupling constant for the mode $\Phi^{h\sigma}_{mln}$ is given according to eq. (3.26) by

$$g^{h\sigma}_{mln} = \mu_{EI}\cdot\Phi^{h\sigma}_{mln}(r_a)\left(\frac{2\pi\omega_{EI}^2}{\hbar\omega_{hln}\Lambda^h_{mln}}\right)^{1/2}. \tag{3.121}$$

Since the resonator is spherically symmetric, we may without loss of generality define the z-axis to lie along the atom's displacement vector $\mathbf{r_a}$; the x- and y-axes may be chosen arbitrarily. Thus $\mathbf{r_a} = r_a\mathbf{z}$ and $\theta_a = 0$. For $\theta = 0$ it is easy to show that

$$C^{e}_{ml}(0,\phi) = -\frac{\sqrt{l(l+1)}}{2}\delta_{m1}\,\mathbf{y} \tag{3.122a}$$

$$C^{o}_{ml}(0,\phi) = \frac{\sqrt{l(l+1)}}{2}\delta_{m1}\,\mathbf{x}\,. \tag{3.122b}$$

Thus

$$\Phi^{he}_{mln}(r_a) = A^{he}_{mln}(-\delta_{m1}\frac{\sqrt{l(l+1)}}{2}j_l(k_{hln}r_a))\,\mathbf{y} \tag{3.123a}$$

$$\Phi^{ho}_{mln}(r_a) = A^{ho}_{mln}(+\delta_{m1}\frac{\sqrt{l(l+1)}}{2}j_l(k_{hln}r_a))\,\mathbf{x}\,, \tag{3.123b}$$

where we must use the exact form of $j_l(k_{hln}r_a)$, since it is not necessarily true that $k_{hln}r_a >> 1, l^2$. The normalization constant is given by

$$\Lambda^{h\sigma}_{mln} = |A^{h\sigma}_{mln}|^2\int d\Omega\,|C^{\sigma}_{ml}|^2\int_0^a r^2dr\; l(l+1)j_l^2(k_{hln}r)$$

$$+\,|E^{h\sigma}_{mln}|^2\int d\Omega|C^{\sigma}_{ml}|^2\int_a^d r^2dr\; l(l+1)\frac{1}{(k_{hln}r)^2}\sin^2(k_{hln}(r-d))\,. \tag{3.124}$$

In the limit $d\to\infty$, the first integral may be neglected, since it remains finite whereas the second integral increases without limit. Noting that

$$\int_a^d dr\,\sin^2(k_{hln}(r-d)) \cong \frac{d-a}{2} \cong \frac{d}{2} \tag{3.125}$$

and that[66]

$$\int d\Omega|C^{\sigma}_{ml}|^2 = \int d\Omega|B^{\sigma}_{ml}|^2 = \frac{4\pi}{\varepsilon_m}\frac{1}{2l+1}\frac{(l+m)!}{(l-m)!}\,, \tag{3.126}$$

where

$$\varepsilon_m = \begin{cases} 1, & m = 0 \\ 2, & m > 0 \end{cases} \tag{3.127}$$

we find that

$$\Lambda^{h\sigma}_{1ln} = \frac{\pi d}{k_{hln}^2}\frac{(l(l+1))^2}{(2l+1)}|E^{h\sigma}_{mln}|^2\,, \tag{3.128}$$

and thus

$$|g^{he}_{mln}|^2 = \delta_{m1}\mu_{EIy}^2\left(\frac{\omega_{hln}\omega_{EI}^2}{2\hbar c^2 d}\right)(2l+1)\,j_l^2(k_{hln}r_a)\frac{\sqrt{1+F}}{1+F\sin^2(k_{hln}a-\frac{l\pi}{2}+\phi)} \tag{3.129a}$$

$$|g^{ho}_{mln}|^2 = \delta_{m1}\mu_{EIx}^2\left(\frac{\omega_{hln}\omega_{EI}^2}{2\hbar c^2 d}\right)(2l+1)\,j_l^2(k_{hln}r_a)\frac{\sqrt{1+F}}{1+F\sin^2(k_{hln}a-\frac{l\pi}{2}+\phi)}\,, \tag{3.129b}$$

where eqs. (3.116) has been used.

The quantity $|g^{h\sigma}_{mln}|^2$ is plotted vs. n in Fig. 3.7. It is seen that there is essentially a continuum of modes of constant density ρ, and that the magnitude squared of the coupling constant is modulated by the cavity lineshape. This modulation in the coupling constant is due to the buildup of the field inside the small cavity for modes that resonate with it. Thus from this point of view, the change in spontaneous emission rate is not due to a "change in mode density", but to an enhancement of the interaction of the atom with certain modes.

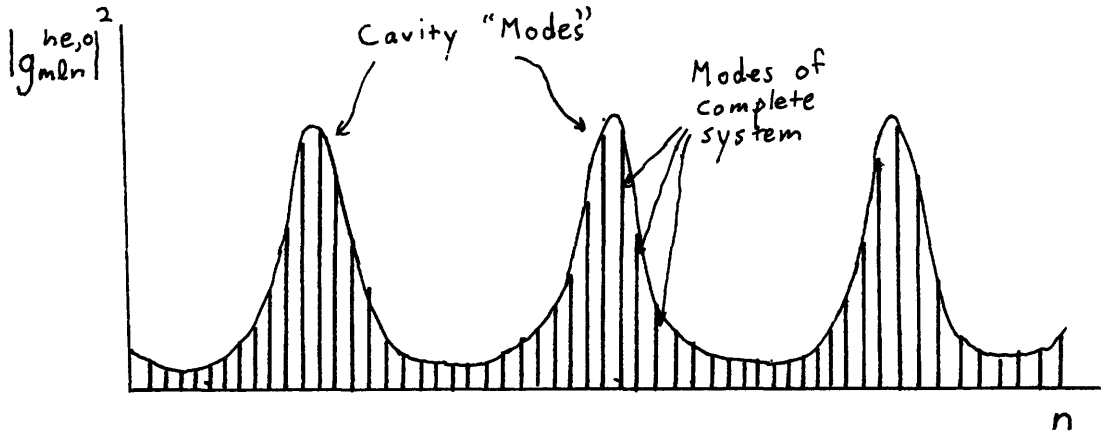

Fig. 3.7. Magnitude of the coupling constant squared vs. n.

It should be emphasized that the form (3.129) of the coupling constant is valid only for modes with $l^2 << k_\lambda a$, due to our use of the approximate forms (3.113) for $j_l(x)$ and $n_l(x)$. For $l^2 \gtrsim k_\lambda a$, a more exact expression for j_l and n_l must be used. The primary effect of this is to introduce a phase shift which causes the peaks of the Airy functions in eqs. (3.129) to be shifted. However, it is easy to show that for $r_a << \sqrt{\lambda_\lambda a}$, the coupling coefficients for $l^2 \gtrsim k_\lambda a$ are vanishingly small. This may be confirmed by directly examining the function $j_l(k_\lambda r_a)$ for $k_\lambda r_a << 2\pi\sqrt{a/\lambda_\lambda} \lesssim l$. Also, it may be understood as a consequence of angular momentum conservation. The angular momentum of one photon in the mode l is $l\hbar$. Since the intrinsic angular momentum of the photon is $\hbar$, the only way for the atom to excite the mode l is through the orbital angular momentum of the emitted photon. For a displacement of r_a, the maximum available orbital angular momentum is $l_{max}\hbar = r_a\hbar\, k_\lambda$. Thus for $r_a << \sqrt{\lambda_\lambda a}$, the maximum angular momentum which can be excited satisfies

$l_{max}^2 << k_\lambda a$, as required. This means that the theory being developed in this section is valid only if $r_a << \sqrt{\lambda_\lambda a}$.

We next explore the boundary value problem for the **N**-type modes. We can write the normal mode function as

$$\Phi^{e\sigma}_{mln}(\mathbf{r}) = \begin{cases} \mathbf{N}^{\sigma I}_{mln}(\mathbf{r}) \ , & 0 \le r \le a \\ \\ \mathbf{N}^{\sigma II}_{mln}(\mathbf{r}) \ , & a < r \le d \end{cases} \tag{3.130}$$

where

$$\mathbf{N}^{\sigma I}_{mln}(\mathbf{r}) = -A^{e\sigma}_{mln}\Big[l(l+1)\frac{1}{k_\lambda r} j_l(k_\lambda r)\mathbf{P}^{\sigma}_{ml}(\theta,\phi) + \sqrt{l(l+1)}\frac{1}{k_\lambda r}\frac{d}{dr}[r j_l(k_\lambda r)]\mathbf{B}^{\sigma}_{ml}(\theta,\phi)\Big] \tag{3.131a}$$

$$\begin{aligned}\mathbf{N}^{\sigma II}_{mln}(\mathbf{r}) &= C^{e\sigma}_{mln}\Big[l(l+1)\frac{1}{k_\lambda r} j_l(k_\lambda r)\mathbf{P}^{\sigma}_{ml}(\theta,\phi) + \sqrt{l(l+1)}\frac{1}{k_\lambda r}\frac{d}{dr}[r j_l(k_\lambda r)]\mathbf{B}^{\sigma}_{ml}(\theta,\phi)\Big] \\ &+ D^{e\sigma}_{mln}\Big[l(l+1)\frac{1}{k_\lambda r} n_l(k_\lambda r)\mathbf{P}^{\sigma}_{ml}(\theta,\phi) + \sqrt{l(l+1)}\frac{1}{k_\lambda r}\frac{d}{dr}[r n_l(k_\lambda r)]\mathbf{B}^{\sigma}_{ml}(\theta,\phi)\Big]\end{aligned} \tag{3.131b}$$

where we can neglect the $n_l(k_\lambda r)$ part of the solution in region I because the mode amplitude must be finite at the origin. As before the asymptotic forms of $j_l(x)$ and $n_l(x)$ will be valid for $x >> 1, l^2$, so that for $r \sim a, d$, we find

$$\mathbf{N}^{\sigma I}_{mln}(\mathbf{r}) = -A^{e\sigma}_{mln}\sqrt{l(l+1)}\frac{1}{k_\lambda r}\cos(k_\lambda r - \frac{l\pi}{2})\mathbf{B}^{\sigma}_{ml}(\theta,\phi) \tag{3.132a}$$

$$\begin{aligned}\mathbf{N}^{\sigma II}_{mln}(\mathbf{r}) &= C^{e\sigma}_{mln}\sqrt{l(l+1)}\frac{1}{k_\lambda r}\cos(k_\lambda r - \frac{l\pi}{2})\mathbf{B}^{\sigma}_{ml}(\theta,\phi) \\ &+ D^{e\sigma}_{mln}\sqrt{l(l+1)}\frac{1}{k_\lambda r}\sin(k_\lambda r - \frac{l\pi}{2})\mathbf{B}^{\sigma}_{ml}(\theta,\phi) \ ,\end{aligned} \tag{3.132b}$$

where terms down by a factor of $1/k_\lambda r$ may be neglected. Applying the boundary condition (3.94) at r = d, these equations may be rewritten as,

$$\mathbf{N}^{\sigma I}_{mln}(\mathbf{r}) = A^{e\sigma}_{mln}\sqrt{l(l+1)}\frac{1}{k_\lambda r}\sin(k_\lambda r - \frac{(l+1)\pi}{2})\mathbf{B}^{\sigma}_{ml}(\theta,\phi) \tag{3.133a}$$

$$\mathbf{N}^{\sigma II}_{mln}(\mathbf{r}) = E^{e\sigma}_{mln}\sqrt{l(l+1)}\frac{1}{k_\lambda r}\sin(k_\lambda(r-d))\mathbf{B}^{\sigma}_{ml}(\theta,\phi) \ . \tag{3.133b}$$

The **N**-modes are also transverse at r = a, so the solutions in region I and II are related by the auxiliary boundary conditions (3.101) and (3.102). Proceeding exactly as before, we find that k_λ must satisfy the eigenvalue equation,

$$\tan(k_\lambda(d-a)) = \frac{\tan(k_\lambda a - \frac{(l+1)\pi}{2})}{\eta k_\lambda \tan(k_\lambda a - \frac{(l+1)\pi}{2}) - 1} \ . \tag{3.134}$$

Apart from a phase shift of $\pi/2$, this is exactly the same as the earlier equation (3.114), and therefore it also gives rise to an essentially uniform discrete mode spectrum having $\rho(\omega) = d/\pi c$ solutions per unit frequency. We label the n^{th} solution of eq. (3.134) as k_{eln}. Also proceeding as before, we find that

$$\left(\frac{A^{h\sigma}_{mln}}{E^{h\sigma}_{mln}}\right)^2 = \frac{\sqrt{1+F}}{1+F\sin^2(k_{eln}a - \frac{(l+1)\pi}{2} + \phi)}, \tag{3.135}$$

where F and ϕ are as defined earlier in eqs. (3.117) and (3.118).

The coupling constant is given by

$$g^{e\sigma}_{mln} = \mu_{EI}\cdot\Phi^{e\sigma}_{mln}(r_a)\left(\frac{2\pi\omega_{EI}^2}{\hbar\omega_{eln}\Lambda^{e}_{mln}}\right)^{1/2}. \tag{3.136}$$

For $\mathbf{r}_a = r_a\mathbf{z}$, $\theta_a = 0$, it can be shown that

$$\mathbf{P}^{\sigma}_{ml}(0,\phi) = \delta_{\sigma e}\delta_{m0}\,\mathbf{z} \tag{3.137a}$$

$$\mathbf{B}^{e}_{ml}(0,\phi) = \frac{\sqrt{l(l+1)}}{2}\delta_{m1}\,\mathbf{x} \tag{3.137b}$$

$$\mathbf{B}^{o}_{ml}(0,\phi) = \frac{\sqrt{l(l+1)}}{2}\delta_{m1}\,\mathbf{y}\,. \tag{3.137c}$$

Thus

$$\Phi^{ee}_{mln}(r_a) = -A^{ee}_{mln}\Big[\delta_{m0}\,l(l+1)\frac{1}{k_{eln}r_a}j_l(k_{eln}r_a)\mathbf{z} + \delta_{m1}\frac{l(l+1)}{2}\frac{1}{k_{eln}r_a}\Big[\frac{d}{dr}[rj_l(k_{eln}r)]\Big]_{r=r_a}\mathbf{x}\Big] \tag{3.138a}$$

$$\Phi^{eo}_{mln}(r_a) = -A^{eo}_{mln}\Big[\delta_{m1}\frac{l(l+1)}{2}\frac{1}{k_{eln}r_a}\Big[\frac{d}{dr}[rj_l(k_{eln}r)]\Big]_{r=r_a}\mathbf{y}\Big]\,. \tag{3.138b}$$

Proceeding as before, we find that the normalization constant is given by

$$\Lambda^{e\sigma}_{mln} = \frac{d}{2k_{eln}^2}\frac{4\pi}{\varepsilon_m}\frac{l(l+1)}{(2l+1)}\frac{(l+m)!}{(l-m)!}|E^{e\sigma}_{mln}|^2\,, \tag{3.139}$$

Thus, combining the results of eqs. (3.135), (3.136), (3.137), and (3.138), we find that

$$|g^{ee}_{mln}|^2 = \frac{\sqrt{1+F}}{1+F\sin^2(k_{eln}a+\frac{(l+1)\pi}{2}+\phi)}\Big\{\delta_{m0}\mu_{EIz}^2\left(\frac{\omega_{eln}\omega_{EI}^2}{2\hbar c^2 d}\right)2l(l+1)(2l+1)\frac{j_l^2(k_{eln}r_a)}{(k_{eln}r_a)^2} + \delta_{m1}\mu_{EIx}^2\left(\frac{\omega_{eln}\omega_{EI}^2}{2\hbar c^2 d}\right)(2l+1)\frac{1}{(k_{eln}r_a)^2}\Big[\frac{d}{dr}[rj_l(k_{eln}r)]\Big]^2_{r=r_a}\Big\} \tag{3.140a}$$

$$|g^{eo}_{mln}|^2 = \frac{\sqrt{1+F}}{1+F\sin^2(k_{eln}a+\frac{(l+1)\pi}{2}+\phi)}\delta_{m1}\mu_{EIy}^2\left(\frac{\omega_{eln}\omega_{EI}^2}{2\hbar c^2 d}\right)$$

$$\times\,(2l+1)\frac{1}{(k_{eln}r_a)^2}\left[\frac{d}{dr}[rj_l(k_{eln}r)]\right]^2_{r=r_a}. \qquad (3.140b)$$

III.C.2. Spontaneous Emission Rate.

The spontaneous emission rate and level shift are given by eqs. (3.38) and (3.39), which in the present case may be written as

$$\Gamma_{cav} = 2\pi\sum_I\sum_l\sum_n \left(|g^{he}_{1ln}|^2 + |g^{ho}_{1ln}|^2\right)\delta(\omega_{EI} - \omega_{hln})$$
$$+ 2\pi\sum_I\sum_l\sum_n \left(|g^{ee}_{0ln}|^2 + |g^{ee}_{1ln}|^2 + |g^{eo}_{1ln}|^2\right)\delta(\omega_{EI} - \omega_{eln})$$
$$= \Gamma_h + \Gamma_e \qquad (3.141)$$

$$\delta\omega_{cav} = \sum_I\sum_l\sum_n \frac{|g^{he}_{1ln}|^2 + |g^{ho}_{1ln}|^2}{\omega_{EI} - \omega_{hln}}$$
$$+ \sum_I\sum_l\sum_n \frac{|g^{ee}_{0ln}|^2 + |g^{ee}_{1ln}|^2 + |g^{eo}_{1ln}|^2}{\omega_{EI} - \omega_{eln}}$$
$$= \delta\omega_h + \delta\omega_e\,. \qquad (3.142)$$

where Γ_h and Γ_e denote the first and second terms on the right hand side of eq. (3.141), and similarly for $\delta\omega_h$and $\delta\omega_e$.

The term Γ_h may be evaluated by substituting for $|g_{mln}^{q\sigma}|^2$, and making use of eq. (3.120):

$$\Gamma_h = 2\pi \sum_{\mathrm{I}} \sum_{l} \sum_{n} (\mu_{\mathrm{EIx}}^2+\mu_{\mathrm{EIy}}^2) \frac{\sqrt{1+F}}{1+F\sin^2(k_{hln}a-\frac{l\pi}{2}+\phi)} \left(\frac{\omega_{hln}\omega_{\mathrm{EI}}^2}{2\hbar c^2 d}\right) \xi_{1l}^2(k_{hln}r_a)\delta(\omega_{\mathrm{EI}}-\omega_{hln})$$

$$= \sum_{\mathrm{I}} \frac{\pi\omega_{\mathrm{EI}}^2}{\hbar c^2 d}(\mu_{\mathrm{EIx}}^2+\mu_{\mathrm{EIy}}^2)\Big\{ \sum_{l\ \mathrm{even}} \frac{d}{\pi c}\int d\omega \frac{\sqrt{1+F}}{1+F\sin^2(ka+\phi)} \omega\xi_{1l}^2(kr_a)\delta(\omega_{\mathrm{EI}}-\omega)$$

$$+ \sum_{l\ \mathrm{odd}} \frac{d}{\pi c}\int d\omega \frac{\sqrt{1+F}}{1+F\cos^2(ka+\phi)} \omega\xi_{1l}^2(kr_a)\delta(\omega_{\mathrm{EG}}-\omega)\Big\}$$

$$= \frac{\omega_{\mathrm{EG}}^3(\mu_{\mathrm{EGx}}^2+\mu_{\mathrm{EGy}}^2)}{\hbar c^3}\Big\{ \frac{\sqrt{1+F}}{1+F\sin^2(k_{\mathrm{EG}}a+\phi)} \sum_{l\ \mathrm{even}} \xi_{1l}^2(k_{\mathrm{EG}}r_a)$$

$$+ \frac{\sqrt{1+F}}{1+F\cos^2(k_{\mathrm{EG}}a+\phi)} \sum_{l\ \mathrm{odd}} \xi_{1l}^2(k_{\mathrm{EG}}r_a)\Big\}\,, \qquad (3.143)$$

where

$$\xi_{1l}(x) = \sqrt{2l+1}\, j_l(x)\,. \qquad (3.144)$$

Similarly, we may show that

$$\Gamma_e = \frac{\omega_{\mathrm{EG}}^3}{\hbar c^3}\Big\{ \frac{\sqrt{1+F}}{1+F\cos^2(k_{\mathrm{EG}}a+\phi)} \sum_{l\ \mathrm{even}} [\mu_{\mathrm{EGz}}^2\xi_{2l}^2(k_{\mathrm{EG}}r_a) + (\mu_{\mathrm{EGx}}^2+\mu_{\mathrm{EGy}}^2)\xi_{3l}^2(k_{\mathrm{EG}}r_a)]$$

$$+ \frac{\sqrt{1+F}}{1+F\sin^2(k_{\mathrm{EG}}a+\phi)} \sum_{l\ \mathrm{odd}} [\mu_{\mathrm{EGz}}^2\xi_{2l}^2(k_{\mathrm{EG}}r_a) + (\mu_{\mathrm{EGx}}^2+\mu_{\mathrm{EGy}}^2)\xi_{3l}^2(k_{\mathrm{EG}}r_a)]\Big\}, \qquad (3.145)$$

where

$$\xi_{2l}(x) = \sqrt{2l(l+1)(2l+1)}\,\frac{1}{x} j_l(x) \qquad (3.146)$$

and

$$\xi_{3l}(x) = \sqrt{2l+1}\,\frac{1}{x}\left[\frac{d}{d\rho}\rho j_l(\rho)\right]_{\rho=x}. \qquad (3.147)$$

Therefore, we obtain finally,

$$\Gamma_{\mathrm{cav}} = \frac{\omega_{\mathrm{EG}}^3}{\hbar c^3}\Big\{ \frac{\sqrt{1+F}}{1+F\cos^2(k_{\mathrm{EG}}a+\phi)} \Big(\mu_{\mathrm{EGz}}^2 \sum_{l\ \mathrm{even}} \xi_{2l}^2(k_{\mathrm{EG}}r_a)$$

$$+ (\mu_{\mathrm{EGx}}^2+\mu_{\mathrm{EGy}}^2)\Big[\sum_{l\ \mathrm{odd}} \xi_{1l}^2(k_{\mathrm{EG}}r_a) + \sum_{l\ \mathrm{even}} \xi_{3l}^2(k_{\mathrm{EG}}r_a)\Big]\Big)$$

$$+ \frac{\sqrt{1+F}}{1+F\sin^2(k_{\mathrm{EG}}a+\phi)} \Big(\mu_{\mathrm{EGz}}^2 \sum_{l\ \mathrm{odd}} \xi_{2l}^2(k_{\mathrm{EG}}r_a)$$

$$+ (\mu_{\mathrm{EGx}}^2+\mu_{\mathrm{EGy}}^2)\Big[\sum_{l\ \mathrm{even}} \xi_{1l}^2(k_{\mathrm{EG}}r_a) + \sum_{l\ \mathrm{odd}} \xi_{3l}^2(k_{\mathrm{EG}}r_a)\Big]\Big)\Big\}. \qquad (3.148)$$

Now Γ_{cav} depends on the atomic displacement via the factors $\sum \xi_{il}^2$. These sums have been evaluated numerically. They take on simple values at $r_a = 0$ and for $k_{EG}r_a >> 1$. For $r_a = 0$,

$$\sum_{l\,\text{even}} \xi_{1l}^2(0) = \sum_{l\,\text{even}} \xi_{2l}^2(0) = \sum_{l\,\text{even}} \xi_{3l}^2(0) = \sum_{l\,\text{odd}} \xi_{1l}^2(0) = 0 \tag{3.149a}$$

$$\sum_{l\,\text{odd}} \xi_{2l}^2(0) = \sum_{l\,\text{odd}} \xi_{3l}^2(0) = \frac{4}{3} \,. \tag{3.149b}$$

Substituting in eq. (3.148), we obtain the spontaneous emission rate for the atom at the exact center of the sphere:

$$\Gamma_{cav}(r_a=0) = \Gamma_{free} \frac{\sqrt{1 + F}}{1+F\sin^2(k_{EG}a+\phi)} \,, \tag{3.150}$$

where Γ_{free} is given by eq. (3.72). In the other simple limit $x = k_{EG}r_a >> 1$, we obtain

$$\sum_{l\,\text{even}} \xi_{2l}^2(x) = \sum_{l\,\text{odd}} \xi_{2l}^2(x) = \frac{2}{3} \tag{3.151a}$$

$$\sum_{l\,\text{even}} \xi_{3l}^2(x) = \sum_{l\,\text{odd}} \xi_{3l}^2(x) = \frac{1}{6} \tag{3.151b}$$

$$\sum_{l\,\text{even}} \xi_{1l}^2(x) = \sum_{l\,\text{odd}} \xi_{1l}^2(x) = \frac{1}{2} \,. \tag{3.151c}$$

Thus, substituting in eq. (3.148), we obtain after some algebra,

$$\Gamma_{cav}(r_a>>\lambda_{EG}) = \Gamma_{free} \frac{\sqrt{1 + F'}}{1+F'\sin^2(2k_{EG}a+2\phi)} \,, \tag{3.152}$$

where

$$F' = \frac{F^2}{4(1 + F)} \,. \tag{3.153}$$

This is in good correspondence with the result (3.86) derived earlier, with $f(\Delta\Omega_{cav}) = 1$. The phase shift 2ϕ arises from a phase shift on reflection from the thin dielectric film, which was neglected earlier. Also note that, as in section II.C.2, the exact center of the sphere is a special point at which the spontaneous emission rate vs. cavity tuning exhibits a lineshape with a free spectral range that is twice as great, and a finesse half as great, as a point slightly displaced from the center.

III.C.3. Level Shift.

We next turn to the calculation of the expression for the level shift $\delta\omega_{cav}$. The contribution of the M-type modes may be written as

$$\delta\omega_h = \sum_I \sum_l \sum_n (\mu_{EIx}^2+\mu_{EIy}^2) \frac{\sqrt{1+F}}{1+F\sin^2(k_{hln}a-\frac{l\pi}{2}+\phi)} \left(\frac{\omega_{hln}\omega_{EI}^2}{2\hbar c^2 d}\right) \xi_{1l}^2(k_{hln}r_a) \frac{1}{\omega_{EI}-\omega_{hln}}$$

$$= \sum_I \sum_{l\,\text{even}} \frac{d}{\pi c} \int \frac{d\omega}{\omega_{EI}-\omega} \frac{\sqrt{1+F}}{1+F\sin^2(ka+\phi)} \left(\frac{\omega_{EI}^2\omega}{2\hbar dc^2}\right) (\mu_{EIx}^2+\mu_{EIy}^2)\xi_{1l}^2(kr_a)$$

$$+ \sum_I \sum_{l\,\text{odd}} \frac{d}{\pi c} \int \frac{d\omega}{\omega_{EI}-\omega} \frac{\sqrt{1+F}}{1+F\cos^2(ka+\phi)} \left(\frac{\omega_{EI}^2\omega}{2\hbar dc^2}\right) (\mu_{EIx}^2+\mu_{EIy}^2)\xi_{1l}^2(kr_a). \qquad (3.154)$$

Similarly, the contribution of the type N modes is,

$$\delta\omega_e = \sum_I \sum_{l\,\text{even}} \frac{d}{\pi c} \int \frac{d\omega}{\omega_{EI}-\omega} \frac{\sqrt{1+F}}{1+F\cos^2(ka+\phi)} \left(\frac{\omega_{EI}^2\omega}{2\hbar dc^2}\right) \left[\mu_{EIz}^2\xi_{2l}^2(kr_a) + (\mu_{EIx}^2+\mu_{EIy}^2)\xi_{3l}^2(kr_a)\right]$$

$$+ \sum_I \sum_{l\,\text{odd}} \frac{d}{\pi c} \int \frac{d\omega}{\omega_{EI}-\omega} \frac{\sqrt{1+F}}{1+F\sin^2(ka+\phi)} \left(\frac{\omega_{EI}^2\omega}{2\hbar dc^2}\right) \left[\mu_{EIz}^2\xi_{2l}^2(kr_a) + (\mu_{EIx}^2+\mu_{EIy}^2)\xi_{3l}^2(kr_a)\right]. \qquad (3.155)$$

The total shift $\delta\omega_{cav} = \delta\omega_h + \delta\omega_e$ clearly diverges in proportion to the upper limit of integration. However, what we are interested is not the total shift, but only the difference in level shifts $\Delta\omega_{cav} = \delta\omega_{cav} - \delta\omega_{free}$. Substituting for $\delta\omega_{free}$ from eq. (3.50), we find

$$\Delta\omega_{cav} = \sum_I \frac{\omega_{EI}^2}{2\pi\hbar c^3} \int d\omega \frac{\omega}{\omega_{EI}-\omega}$$

$$\times \Big[(\mu_{EIx}^2 + \mu_{EIy}^2) \Big\{ \sum_{l\,\text{even}} (L(ka+\phi)\xi_{1l}^2(kr_a) + L(ka+\phi+\tfrac{\pi}{2})\xi_{3l}^2(kr_a)) + \sum_{l\,\text{odd}} (L(ka+\phi+\tfrac{\pi}{2})\xi_{1l}^2(kr_a) + L(ka+\phi)\xi_{3l}^2(kr_a)) \Big\}$$

$$+ \mu_{EIz}^2 \Big\{ \sum_{l\,\text{even}} L(ka+\phi+\tfrac{\pi}{2})\xi_{2\lambda}^2(kr_a) + \sum_{l\,\text{odd}} L(ka+\phi)\xi_{2l}^2(kr_a) - \tfrac{4}{3}|\mu_{EI}|^2 \Big] , \qquad (3.156)$$

where now $L(x) = \sqrt{1+F}/(1+F\sin^2 x)$. We first examine the contribution of terms with $I \neq G$. For these terms, by the same argument leading up to eq. (3.80), it is permissible to replace L(x) by its average value $\overline{L(x)} = 1$, and thus

$$\Delta\omega_{cav,\,I\neq G} = \sum_{I\neq G} \frac{\omega_{EI}^2}{2\pi\hbar c^3} \int d\omega \frac{\omega}{\omega_{EI}-\omega} \Big\{ (\mu_{EIx}^2 + \mu_{EIy}^2) \sum_l (\xi_{1l}^2(kr_a) + \xi_{3l}^2(kr_a)) + \mu_{EIz}^2 \sum_l \xi_{3l}^2(kr_a) - \frac{4}{3}|\mu_{EI}|^2 \Big\}. \tag{3.157}$$

Using the "summation" formula for the Bessel functions,[56] it may easily be shown that

$$\sum_l (\xi_{1l}^2(x) + \xi_{3l}^2(x)) = \frac{4}{3} \tag{3.158a}$$

$$\sum_l \xi_{2l}^2(x) = \frac{4}{3}, \tag{3.158b}$$

irrespective of the value of x. Substituting into eq. (3.157), we find the that there is no contribution to the difference in level shifts $\Delta\omega_{cav}$ from terms with $I \neq G$. By the same argument, we also find that for the remaining term with $I = G$, there is no contribution to $\Delta\omega_{cav}$ from frequencies ω far from resonance.

Thus only the term $I = G$, and only a limited range of frequencies near ω_{EG} contributes significantly to $\Delta\omega_{cav}$. Also, recall that according to eq. (3.82), the contribution of this limited range of frequencies to the free-space shift is equal to zero. Therefore the quantity $\Delta\omega_{cav}$ is equal to the quantity $\delta\omega_{cav}$, where it is understood that only the term $I = G$ is included, and that the integration is to be carried out over a range of frequencies which is large compared to $\pi c/a$, but small compared to ω_{EG}. Noting that ω^3 and $\xi_{1l}(kr_a)$ are essentially constant over the range of integration and therefore may be removed from the integral, we thus obtain, for the contibution of the **M** type modes to $\Delta\omega_{cav}$

$$\begin{aligned}\Delta\omega_h &= \frac{\omega_{EG}^3(\mu_{EGx}^2+\mu_{EGy}^2)}{2\pi\hbar c^3} \Big\{ \sum_{l\ \text{even}} \xi_{1l}^2(k_{EG}r_a)\,[-I_1(ka,\phi')] + \sum_{l\ \text{odd}} \xi_{1l}^2(k_{EG}r_a)\,[-I_1(ka,\phi')] \Big\} \\ &= \frac{\omega_{EG}^3(\mu_{EGx}^2+\mu_{EGy}^2)}{2\pi\hbar c^3} \Big\{ \sum_{l\ \text{even}} \xi_{1l}^2(k_{EG}r_a) \frac{\pi F\sin(2(k_{EG}a+\phi))}{2(1+F\sin^2(k_{EG}a+\phi))} - \sum_{l\ \text{odd}} \xi_{1l}^2(k_{EG}r_a) \frac{\pi F\sin(2(k_{EG}a+\phi))}{2(1+F\cos^2(k_{EG}a+\phi))} \Big\},\end{aligned} \tag{3.159}$$

where $\phi' = k_{EG}a + \phi$, and $\phi'' = k_{EG}a + \phi + \pi/2$. Similarly we may show that the contribution of the **N**-type modes to $\Delta\omega_{cav}$ is

$$\Delta\omega_e = \frac{\omega_{EG}^3}{2\pi\hbar c^3} \Big\{ \sum_{l\ \text{even}} [\mu_z^2\xi_{2l}^2(k_{EG}r_a) + (\mu_x^2+\mu_y^2)\xi_{3l}^2(k_{EG}r_a)] \frac{-\pi F\sin(2(k_{EG}a+\phi))}{2(1+F\cos^2(k_{EG}a+\phi))} + \sum_{l\ \text{odd}} [\mu_z^2\xi_{2l}^2(k_{EG}r_a) + (\mu_x^2+\mu_y^2)\xi_{3l}^2(k_{EG}r_a)] \frac{\pi F\sin(2(k_{EG}a+\phi))}{2(1+F\sin^2(k_{EG}a+\phi))} \Big\}. \tag{3.160}$$

Thus

$$\Delta\omega_{cav} = \frac{\omega_{EG}^3}{2\hbar c^3}\{[\frac{F\sin(2(k_{EG}a+\phi))}{2(1+F\sin^2(k_{EG}a+\phi))} \times (\mu_z^2 \sum_{l\,\text{odd}}\xi_{2l}^2(k_{EG}r_a) + (\mu_x^2+\mu_y^2)\{\sum_{l\,\text{even}}\xi_{1l}^2(k_{EG}r_a) + \sum_{l\,\text{odd}}\xi_{3l}^2(k_{EG}r_a)\})] - [\frac{F\sin(2(k_{EG}a+\phi))}{2(1+F\cos^2(k_{EG}a+\phi))} \times (\mu_z^2 \sum_{l\,\text{even}}\xi_{2l}^2(k_{EG}r_a) + (\mu_x^2+\mu_y^2)\{\sum_{l\,\text{odd}}\xi_{1l}^2(k_{EG}r_a) + \sum_{l\,\text{even}}\xi_{3l}^2(k_{EG}r_a)\})]\}. \quad (3.161)$$

Again we consider the special case $r_a = 0$. Using eq. (3.150), we find

$$\Delta\omega_{cav}(r_a=0) = \frac{\Gamma_{free}}{4}\frac{F\sin(2(k_{EG}a+\phi))}{1+F\sin^2(k_{EG}a+\phi)}. \quad (3.162)$$

We also consider the limit $k_{EG}r_a >> 1$. In this case, we may obtain, after some algebraic manipulation

$$\Delta\omega_{cav}(r_a>>\lambda_{EG}) = \frac{\Gamma_{free}}{4}\frac{F'\sin(4(k_{EG}a+\phi))}{1+F'\sin^2(2(k_{EG}a+\phi))}. \quad (3.163)$$

Again, this is in exact agreement with the previous result (3.86), for $f(\Delta\Omega_{cav}) = 1$.

From these results it is seen that the spontaneous emission of an atom near the center of the sphere may be derived rigorously (within the limit of validity of the Wigner-Weisskopf approximation) without any recourse to arguments based on an "effective mode density". The results obtained are in exact correspondence with those obtained earlier, substantiating that point of view, at least in the limit as $f(\Delta\Omega_{cav}) \rightarrow 1$.This calculation clarifies why the Wigner-Weisskopf approximation may be applied in a low-Q cavity: because the cavity has loss, it is coupled to the outside world, and when the field is quantized in the modes of the "sphere plus outside world", the mode density forms essentially a smooth continuum. Therefore the Wigner-Weisskopf treatment holds provided that the interaction of the atom with these modes is not too sharply modulated by the cavity.

CHAPTER IV

EXPERIMENTAL STUDIES OF YTTERBIUM ATOMS IN A CONFOCAL RESONATOR.

In order to test the effects of an optical resonator on spontaneous emission, experiments were carried out on a sample of ytterbium atoms in a confocal optical resonator. Substantial changes in the partial spontaneous emission rate of the atoms into the cavity modes were observed. In addition, an indirect measurement confirmed the existence of a small change in the total spontaneous emission rate. These experiments confirmed the validity of the basic concepts presented in chapters II and III, and laid the groundwork for more comprehensive experimental studies to be presented in chapter V.

IV.A. Experimental Description.

IV.A.1 Ytterbium Level Structure.

The lowest lying electronic states of ytterbium are illustrated in Fig. 4.1(a).[67] Yb has a $^1S_0$ ground state, and the first resonance transition at 555.6 nm is to the $^3P_1$ excited state, which has a lifetime of τ_{sp} = 875 ns.[68] This singlet to triplet transition is electric-dipole allowed because there is a small admixture of the higher lying $^1P_1$ state in the $^3P_1$ state. Yb has seven naturally occuring isotopes, including five even isotopes all having nuclear spin zero, and two odd isotopes, ^{171}Yb with a nuclear spin of 1/2, and ^{173}Yb with a nuclear spin of 3/2. The isotopic and hyperfine structure of the $^1S_0$ - $^3P_1$ transition is shown in Fig. 4.2. Of particular interest is the ^{174}Yb isotopic component: since this isotope has zero nuclear spin and is well-resolved from the other components, it forms an ideal, two-level system, as illustrated in Fig. 4.1(b). All of the experiments described in this chapter are carried out on this component of the 555.6 nm Yb transition.

^{174}Yb is chosen for the experiments because it has a convenient wavelength for dye-laser excitation, forms an ideal, two-level system, and is relatively easy to vaporize. The unusually long lifetime of the $^3P_1$ state is actually something of a disadvantage, albeit a small one. However, this long lifetime would be a great advantage if these experiments are to be extended into the time domain. Such possible extensions are discussed in chapter VI.

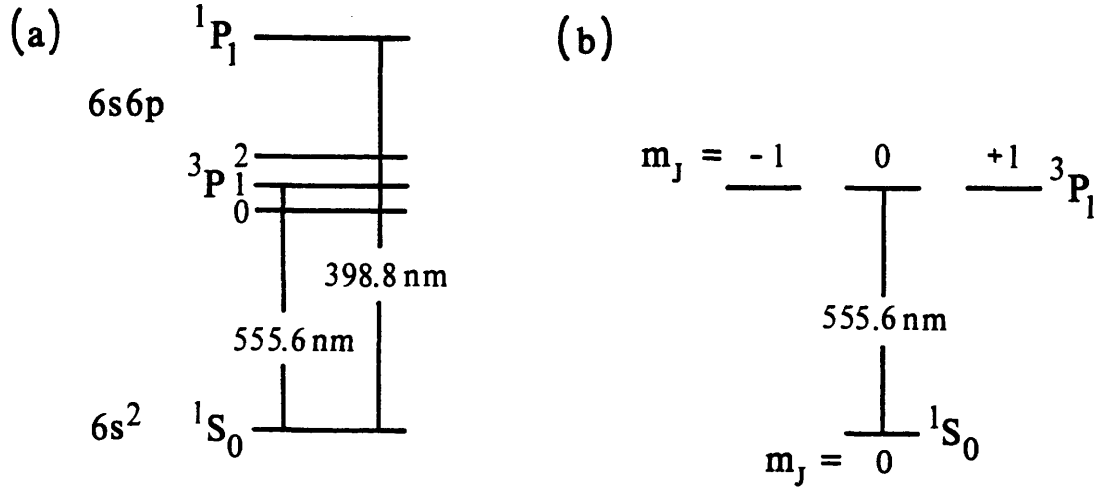

Fig 4.1. Yb level structure. (a) Lowest lying electronic states. (b) Ideal two-level system formed by the ^{174}Yb $^1S_0$ - $^3P_1$ transition.

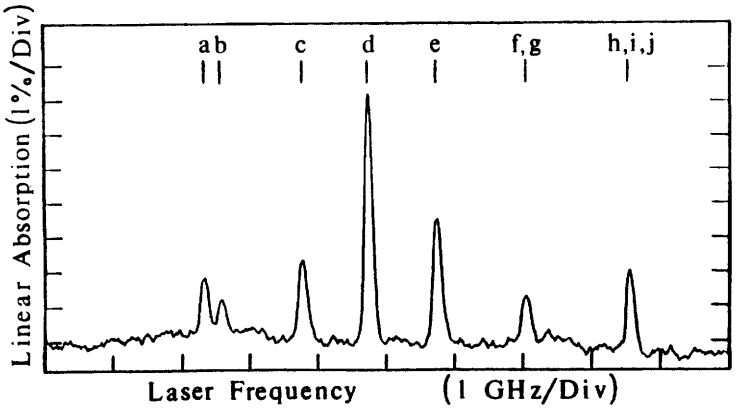

Compt.	Isotope	F_{upper}	Relative Frequency (MHz)
a	^{173}Yb	7/2	-2389
b	^{171}Yb	1/2	-2131
c	^{176}Yb	1	-955
d	^{174}Yb	1	0
e	^{172}Yb	1	1001
f	^{170}Yb	1	2288
g	^{173}Yb	5/2	2313
h	^{168}Yb	1	3656
i	^{171}Yb	3/2	3804
j	^{173}Yb	3/2	3810

Fig. 4.2. Isotopic and hyperfine structure of the $^1S_0$ - $^3P_1$ transition of atomic Yb. This data displays the absorption of a high density atomic beam of Yb; these lines are about 10 times broader than in the experiments described in this chapter. The component identifications and relative frequencies are from reference 69.

IV.A.2 Lasers and Optical Layout.

The overall experimental layout is illustrated in Fig. 4.3. The central component of the experiment is a vacuum chamber containing an Yb atomic beam source and the confocal resonator structure.

Tunable, single mode radiation at 555.6 nm is provided by a Coherent model CR699-21 ring dye laser with Rh110 dye, pumped by 6W of all lines blue-green radiation from a Coherent model 52 argon ion laser. Typical dye laser output power at 555.6 nm is 250-500 mW, with a bandwidth of approximately 1 MHz. Laser frequency diagnostics are provided by splitting part of the dye laser into the spectrum analyzer SA.

In order to line up the confocal cavity, part of the dye laser output is picked off by the beam splitter BS1, forming a "cavity probe beam". This beam is focussed into the cavity by collimator COLL1 and subsequently reflected off the movable mirror M3 into the photodiode PD. When alignment of the cavity is complete, the cavity probe beam is blocked off by beam stop BST2, and mirror M3 is flipped back out of the beam path.

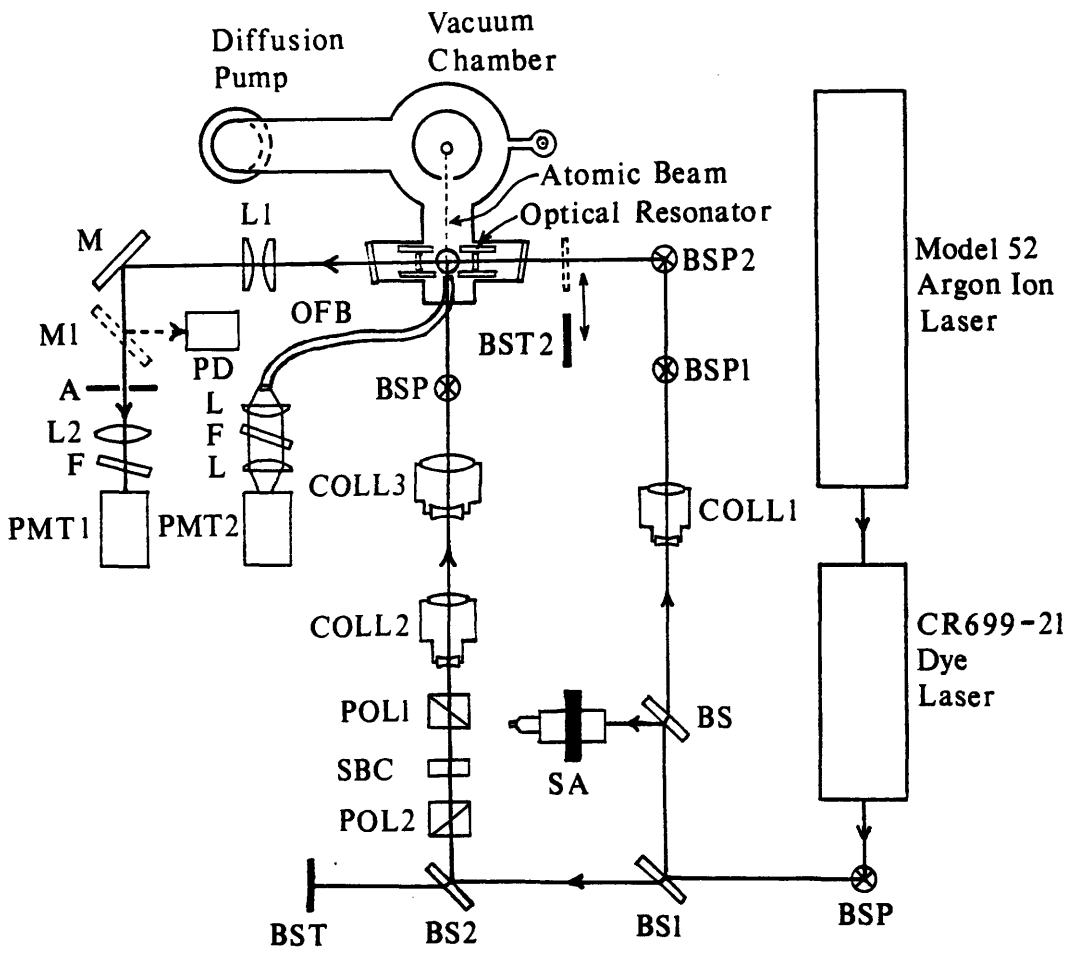

Fig. 4.3. Experimental layout. BSP: beam steering post; BS: beamsplitter; BST: beam stop; SA: spectrum analyzer; COLL: collimator; POL: polarizer; SBC: Soleil-Babinet compensator; M: mirror; OFB: optical fiber bundle; L: lens; A: aperture; F: interference filter. PMT: photomultiplier tube; PD: photodiode.

The laser beam which pumps the Yb atoms ("pump beam") is picked of by beamsplitter BS2. It then passes through the combination of the two Glan-prism polarizers POL1 and POL2 and the Soliel-Babinet compensator SBC, which functions as a variable attenuator. The pump beam is then focussed into the atomic beam by the combination of collimator COLL2, which is an ordinary collimator, and COLL3, which is a cylindrical lens collimator. The combination of COLL1 and COLL2 allows the pump beam to be focussed to a line; the beam waist sizes at the atoms were adjusted to 2.5 mm (FWHM of intensity) parallel to the resonator axis, and 180 μm (FWHM of intensity) perpendicular to the axis. The pump beam is polarized perpendicularly to the resonator axis, and taking the laser polarization direction to be the quantization axis, the laser therefore excites only a pure, two-level, $\Delta m = 0$ transition, as illustrated in Fig. 4.1(b).

Flourescence emitted by the atoms follows the two beam paths leading up to photomultiplier tubes PMT1 and PMT2. A light tight box is placed around these optics to shield the photomultiplier tubes from background light.

IV.B.3. Atomic Beam.

The atomic beam system is illustrated in Fig 4.4. The oven consists of a 304 stainless steel tube $6\frac{5}{8}$" long by $\frac{1}{2}$" outside diameter by .020" wall thickness which is filled with 8-10 g of Yb metal, and crimped flat $1\frac{3}{8}$" long at each end. The oven is heated resistively by flowing an AC current of approximately 150 A through it, delivered through two copper leads which clamp onto the crimped part of the oven. The atoms escape through a D = 0.41 mm diameter hole drilled near the center of the oven; the stainless steel wall near the hole is thinned down to .006" thick with an end mill before the hole is drilled. The oven temperature T_{oven} near the hole is measured by a chromel-alumel thermocouple spot welded directly to the oven.

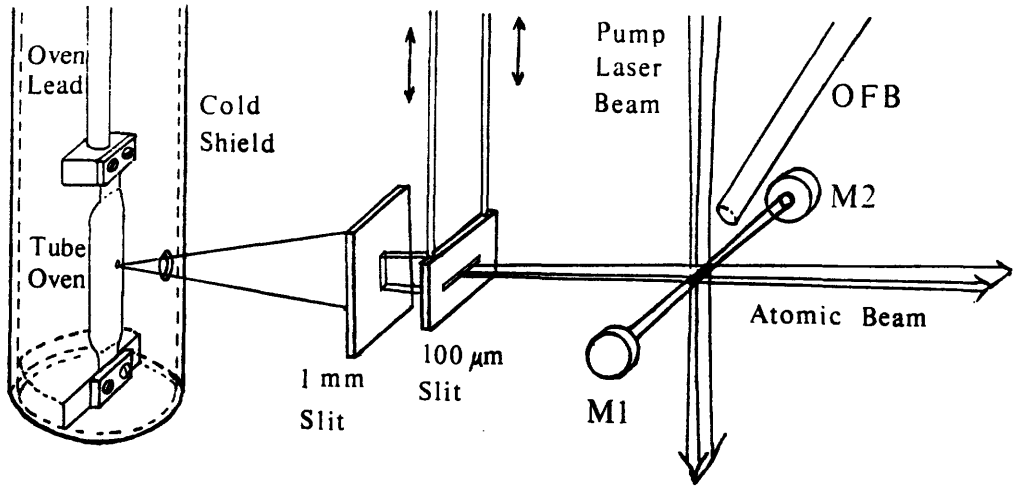

Fig. 4.4. Atomic beam system.

The oven current returns through a copper cold shield which is concentric with the oven. This results in a minimal (<< 1 Gauss) magnetic field outside the shield, as verified directly with an AC gaussmeter. The oven leads and cold shield are water cooled to prevent excessive heating of the apparatus by the oven.

The atomic beam is collimated to a width of 1 mm by an slit placed 10 cm from the oven, and to a height of 100 μm by a slit placed 11 cm from the oven. The collimated beam flows through the center of the confocal cavity at a distance of X = 15 cm from the oven. The 100 μm slit is mounted in such a way that it can be translated vertically and rotated slightly while the beam is running.

It was found that this tube oven design provided a simple, reliable way to produce an Yb atomic beam. The typical oven current of 150A produced an oven temperature as measured by the thermocouple of approximately $T_{oven} = 900$ °C. It was found that the flux of Yb from the oven corresponded to a vapor pressure that is characteristic of a temperature T_{Yb} about 300 °C lower that T_{oven}. Thus, at $T_{oven} = 900$ °C, $T_{Yb} \cong 600$ °C, corresponding to a vapor pressure of[70] $P \cong 4 \times 10^{-4}$ atm, a source density of $n_0(cm^{-3}) = 7.32 \times 10^{21} P(atm)/T_{Yb}(°K) \cong 3 \times 10^{15}$ cm^{-3}, and a mean free path of $\lambda_0 \cong 1/n_0\sigma \cong 6 \times 10^{-2}$ cm, where $\sigma \cong 50$ Å^2 is the collision cross section. Since the hole diameter is $D = 4.1 \times 10^{-2}$ cm, this corresponds to a source pressure near the effusive limit.

The mean thermal speed of the atoms is $u \cong \sqrt{2k_B T_{oven}/M} \cong 2.4 \times 10^4$ cm/s, where k_B is Boltzmann's constant and $M = 2.9 \times 10^{-22}$ g is the mass of an Yb atom. The flux is $\Phi_n \cong \frac{1}{4} n_0 u \frac{\pi D^2}{4} \cong 5 \times 10^{16}$ s^{-1}, or in terms of mass flow, about 5×10^{-3} g/hr. This corresponds to a ^{174}Yb density in the cavity of $n \cong \alpha\Phi_n/\pi u X^2 \cong 1 \times 10^9$ cm^{-3}, where $\alpha = .31$ is the natural isotopic abundance of ^{174}Yb.

The vacuum chamber was pumped out by a Varian M-2 2" diffusion pump attached to the source region via a 3" pipe. When a new oven was heated for the first time, the background pressure in the chamber soared to above 10^{-4} torr, then settled back down after about an hour. Typical operating background pressures were in the range of $1 - 4 \times 10^{-6}$ torr, as measured by a Bayard Alpert ionization gauge attached to the source region. On some occasions running the beam actually improved the vacuum to values as low as 5×10^{-7} torr, presumably due to a gettering effect.

In order to tune the laser to the proper frequency and to align the laser and atomic beams properly, the following procedure is used. First, the pump laser beam is introduced into the chamber while the atomic beam is running, and the laser is slowly scanned in frequency until fluorescence is observed. This fluorescence is easily visible by eye. The pump laser beam is then blocked off and the cavity probe beam is adjusted to a spot size of about

0.2 mm and introduced into the cavity. After verifying that the cavity probe beam is aligned to the axis of the cavity, the height and tilt of the100 μm slit are adjusted until the atomic beam is best aligned with the probe beam, as verified by the visible line of fluorescence. Next the pump beam is introduced back into the chamber, so that two separate lines of fluorescence become visible. The position and angle of the line of fluorescence induced by the pump beam is adjusted until it overlaps with the line of fluorescence induced by the cavity probe beam, and the alignment is complete.

The size of the pumped volume of atoms, determined by the intersection of the atomic and pump laser beams, is approximately $\Delta z = 1.5$ mm along the cavity axis, $\Delta y = 140$ μm in the vertical direction, and $\Delta x = 180$ μm in the along the atomic beam propagation direction. However, the atoms remain excited for a somewhat greater distance along the atomic beam propagation direction, because they drift for a distance of $u\tau_{sp} \cong 210$ μm during their lifetime. Thus the atoms are excited over a net distance of about $\Delta x = 400$ μm in this direction, so that the interaction volume is $V \cong 8 \times 10^{-5}$ cm^3, and the total number of ^{174}Yb atoms in this volume is $N = nV \cong 2 \times 10^5$.

Because the natural linewidth $\Gamma_{free}/2\pi = 180$ kHz of the Yb resonance line is so small, the atomic beam is still Doppler broadened. The Doppler width as seen by the cavity probe laser is approximately $\Delta\nu_{Dz}^{(calc)} \cong \frac{\Delta z+D}{X}\frac{ku}{2\pi} = 5.5$ MHz, while that seen by the pump laser is $\Delta\nu_{Dy}^{(calc)} \cong \frac{\Delta y+D}{X}\frac{ku}{2\pi} = 1.6$ MHz. In practice linewidths of $\Delta\nu^{(obs)} \sim 5$-10 MHz are observed for both of these, since there is a contribution of 0.4 Mhz/mrad from misalignment broadening, and of 1-2 MHz from laser frequency jitter. One further point which should be emphasized is that the interaction of the atoms with the noncentral parts of the cavity is Doppler broadened by as much as $\Delta\nu_D^{(max)} \cong \theta_M ku/2\pi = 35$ MHz, where $\theta_M = 0.080$ rad is the half-angle subtended by the cavity mirrors.

IV.A.4. Optical Resonator.

The optical resonator is very similar in construction to an ordinary spectrum analyzer. The structure consists of a $1\frac{3}{4}$" outside diameter machined brass cylinder that is designed to fit inside the $1\frac{7}{8}$" inside diameter walls of the vacuum chamber. Slots cut into the sides of

the cylinder allow the atomic and laser beams, the optical fiber bundle OFB, and a movable beam stop BST1 to pass through. One of the mirrors M1 is mounted on a large cylindrical piezo-electric transducer PZT which provides for the tuning of the cavity. The PZT requires about 25 V to generate a displacement of $\lambda/4$. The other end mirror M1 is mounted on a cylinder which slides smoothly inside the larger cylinder and can be locked into place. Mechanically the resonator was not as rigid or as finely adjustable as might be desired. However, it was very simple to construct, easily fit inside the existing vacuum system, and was sufficiently to stable to hold a good alignment for the several hours required to take data.

The confocal resonator mirrors M1 and M2 were standard Coherent spectrum analyzer mirrors model 240M-2-B. They have a radius of curvature of 5.00 cm, corresponding to a separation of L = 5.00 cm and to a free spectral range of $\Delta\nu_{fsr} = c/4L = 1500$ MHz. Apertures placed over each mirror restrict their clear diameter to 2b = 4.0 mm. The measured transmission of M1 is $T_1 = 2.8\pm0.1$ %, and that of M2 is $T_2 = 1.8\pm0.1$ %. Assuming negligible absorption and scattering loss, this gives $R = \sqrt{R_1R_2} = 0.997$, and a finesse $F_{cf}^{(calc)} = \pi\sqrt{R}/2(1-R) = 68$ and a fringe width $\Delta\nu_{cav}^{(calc)} = \Delta\nu_{fsr}/F_{cf}^{(calc)} = 24$ MHz.

The cavity is aligned using the cavity probe beam and photodiode detector. The rough alignment of the cavity is accomplished with three adjustment screws at each end of the cavity. The cavity is adjusted to confocal spacing by sliding the small cylinder holding M1 until the observed transmission of the cavity vs. cavity tuning displays a degenerate mode spectrum with a spacing c/4L. The spot size of the probe laser is set to about 0.5 -1.0 mm for this procedure, so as to excite many transverse modes and give good sensitivity to the correct confocal spacing. This part of the procedure must be carried out with the vacuum sytem open.

The fine adjustment of the cavity probe laser to the resonator axis is accomplished by translating and tilting the cavity probe beam, using the mirror mounts on the two beam steering posts BSP1 and BSP2, until a mode spectrum with a free spectral range of c/2L is observed. This occurs because the mode spectrum of spacing c/4L consists of a set of spatially symmetric modes of spacing c/2L, alternating with a set of spatially antisymmtric modes, also of spacing c/2L.[54] When the symmetrical gaussian beam is exactly aligned to the axis of the cavity, the antisymmetric modes disappear. It is also possible to "mode match" the laser beam into only antisymmetric modes, but this can be avoided by verifying

that the transmitted laser beam consists of only one spot rather than two. Note that that this procedure is in effect the same as aligning the cavity, since tilting the mirrors slightly merely has the effect of redefining the optical axis.[n]

The fringe width of the aligned cavity depends on the spot size of the probe laser. For small spot sizes (< 0.5 mm), fringe widths of 22.5-25.0 MHz are observed. This is limited entirely by the mirror transmission, and thus absorption and scattering losses are small (< 0.2% per surface). For larger spot sizes, the finesse was significantly lower, primarily due to the spherical aberration effect discussed in section II.F.1. For L = 5 cm, this aberration effect limits the "spot size" for constuctive interference to a radius $x_0 = (\lambda L^3/2F)^{1/4} = 0.85$ mm, and for destructive interference to a radius $x_1 = (\lambda L^3/2)^{1/4} = 2.4$ mm. These points are further discussed in section II.F.1 and in the article by Hercher.[57] Note that our mirror clear diameter of 4.0 mm is considerably larger than $2x_0$ but is less then $2x_1$, so as to exclude the first fringe of constructive interference when the cavity is off resonance. (We have also verified that this fringe is not present experimentally.)

IV.A.5. Fluorescence Imaging and Detection.

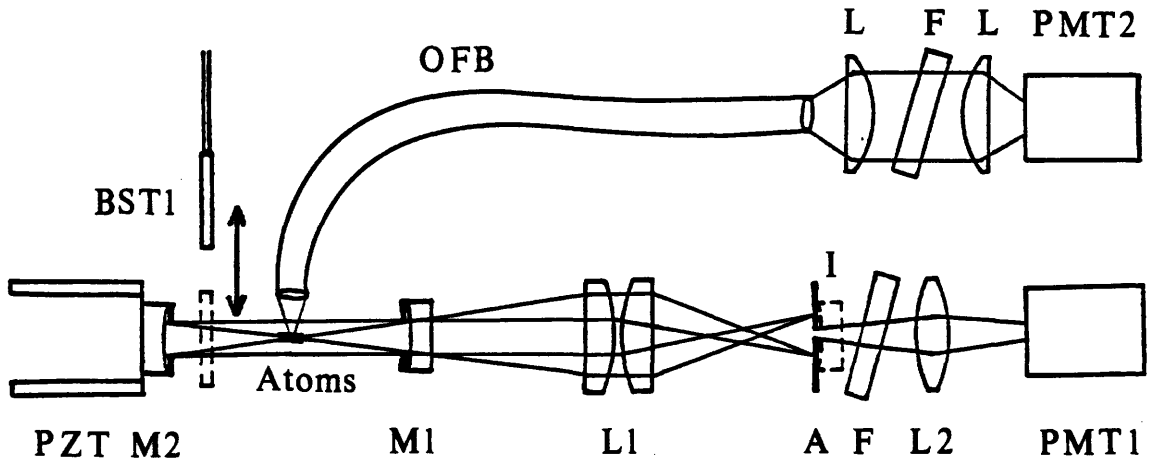

Fig. 4.5. Schematic diagram of fluorescence collection optics.

The fluorescence collection optics are shown in Fig. 4.5. Fluorescence emerging from the sides of the resonator is collected at an angle of 37° to the pump beam by the 1/4" diameter optical fiber bundle OFB at a distance of 3/4" from the atoms. Light emerging from the optical fiber bundle is collected by an *f*/0.8 aspheric lens, passes through an

interference filter, and is refocussed by a second aspheric lens onto photomultiplier tube PMT2.

Fluorescence emerging through M1 passes through a series of baffles and is focussed by lens L1 onto the aperture A. This aperture is positioned at the image I of M1, which is produced by L1 with a magnification of 1.0, and is therefore equivalent to an aperture placed at M1. Fluorescence passing through the aperture is then refocussed by a lens, through an interference filter, onto photomultiplier tube PMT1. These optical elements are aligned using the cavity probe beam.

The interference filters are 10 nm bandpass filters centered at 560 nm, tilted by 12° in order to angle tune their bandpass center to 556 nm. The pair of aspheric lenses in front of PMT2 has the important effect of reducing the angle of divergence of the light passing through the filter to within its limited acceptance angle.

PMT1 and PMT2 are Hamamatsu R1635-02 3/8" diameter bialkalai-cathode photomultiplier tubes. These are chosen for their low dark count rate, high sensitivity, and conveniently small size.

The signal from PMT1 gives a measure of the spontaneous emission rate of the atom into the cavity. In order to calibrate this against the free space rate into the same solid angle, a movable beam stop BST1 may be inserted between the atoms and M2, thus removing the effect of the cavity. This calibration may be carried out by taking into account the transmissions of the two mirrors. Since the power emitted through each mirror is proportional to its transmission, the photon counting rate $\gamma_{cav}^{(1)}$ of PMT1 with the cavity open is given by

$$\gamma_{cav}^{(1)} = \eta \frac{T_1}{T_1 + T_2} \gamma_{cav}, \tag{4.1}$$

and its counting rate $\gamma_{bl}^{(1)}$ with the cavity blocked is

$$\gamma_{bl}^{(1)} = \eta \frac{1}{2} T_1 \gamma_{free}, \tag{4.2}$$

where γ_{cav} is the spontaneous emission rate of the atom into the cavity (emitted through both mirrors), γ_{free} is the free space rate into the same solid angle, and η is the detection efficiency. If we define the quantity $\gamma_{free}^{(1)}$ by

$$\gamma_{free}^{(1)} = \frac{2}{T_1 + T_2} \gamma_{bl}^{(1)} \cong \frac{1}{1 - R} \gamma_{bl}^{(1)}, \tag{4.3}$$

it will be correctly normalized so that

$$\frac{\gamma_{cav}^{(1)}}{\gamma_{free}^{(1)}} = \frac{\gamma_{cav}}{\gamma_{free}} \quad . \tag{4.4}$$

That is, if the observed counting rate $\gamma_{cav}^{(1)}$ is taken as a measure of the spontaneous emission rate of the atom into the cavity, the quantity $\gamma_{free}^{(1)}$ is normalized correctly so as to give the equivalent free space rate into the same solid angle.

IV.A.6. Electronic Control and Data Acquisition.

The experimental control and data acquisition electronics are illustrated in Fig. 4.6. For most of the measurements, only the connections shown as solid lines were made. In this configuration, the light intensity falling on PMT1 is measured as a function of resonator tuning, while the pump laser frequency is locked to the ^{174}Yb resonance line. The additional connections shown as dashed lines were added for the sidelight modulation measurements described in section IV.C.

The light signal falling on PMT1 is detected in photon counting mode. PMT1 generates negative going pulses of 1.5 - 4 mV amplitude and 1 ns duration into a 50 Ω load. These pulses are amplified by three stages of a EG&G AN-302 quad amplifier to minus 100-300 mV in amplitude and 3 ns duration. The signal is then processed by an EG&G T105/N discriminator, which rejects pulses smaller than 70 mV, and outputs a standard NIM pulse for each input pulse greater than 70 mV. The signal is then processed by a NIM-TTL converter and recorded by a 20 MHz counter in a DEC LSI 11/23 microcomputer. In order to avoid pulse pile-up error, the count rate is always kept below about 10^6 counts/s.

The cavity is scanned in frequency by applying a voltage ramp to the PZT, generated by the computer via an A/D converter and high voltage amplifier. The voltage ramp proceeds in 1024 steps; at each voltage output value the computer records the number of photocounts from PMT1 for a prescribed period of time (usually about 50-400 ms). The data is then processed by the computer to show the number of photocounts per second vs. cavity tuning.

The laser has a short term frequency stability of 1 MHz, but can drift by an amount comparable to the residual Doppler width of the beam during the time taken to complete a scan. In order to avoid this difficulty, the laser frequency is locked to the ^{174}Yb transition

by a slow servo loop. This is accomplished by leaving the 699-21 dye laser locked to its own internal reference cavity and controlling its frequency by applying a signal to its external scan input. This signal contains a voltage dither generated by a PAR 121 lock-in amplifier operating in the internal reference mode. The laser scan range is set to 1 GHz, with the ^{174}Yb resonance somewhere near the center, and the dither is adjusted so as to produce a 2 MHz peak-to-peak oscillation in the laser frequency at a 400 Hz rate. This frequency oscillation will induce an oscillation in the intensity of fluorescence detected by PMT2 if the laser center frequency is off to one side of the Yb transition center frequency. This oscillation is detected by the lock in amplifier, producing at its output a dispersive error signal which is fed into an integrator in the "lock box". The output of this integrator is summed with the voltage dither and applied to the laser external scan input. The lock-in and "lock box" controls are adjusted so that the integrator accumulates additional voltage as necessary to drive the error signal to zero, producing a stable lock.

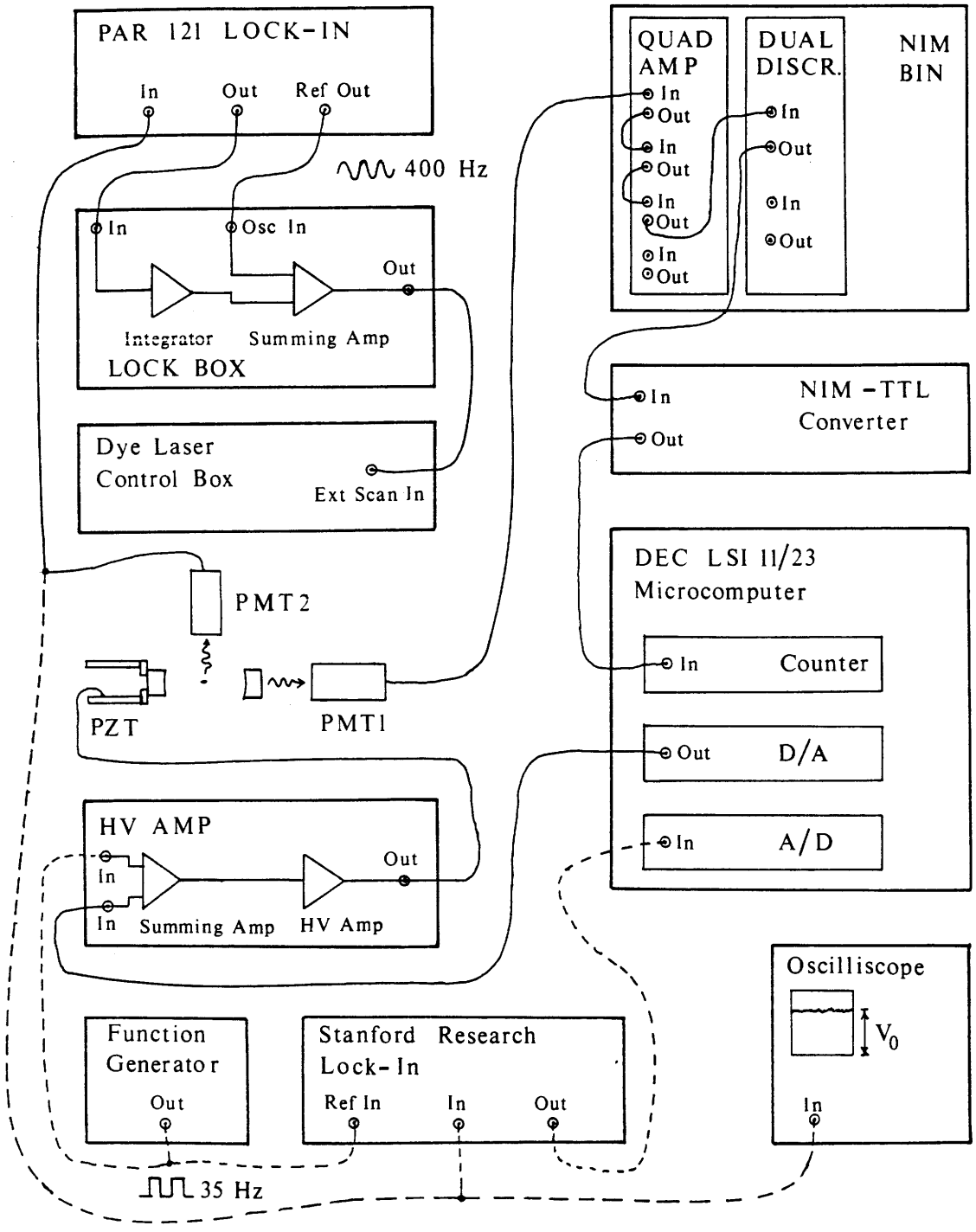

Fig. 4.6. Experimental control and data acquisition electronics. For most of the experiments, only the connections shown as solid lines were made; the additional connections shown as dashed lines were made only for the sidelight modulation measurement.

IV.B. Experimental Results for the Cavity Spontaneous Emission Rate.

IV.B.1. Results for the Spontaneous Emission Rate vs. Cavity Tuning.

The experimental results are presented in Fig. 4.7. Traces (a) - (c) show the observed counting rate vs. cavity tuning, with an aperture diameter of 1.0 mm and a laser pump power of 60 μW. Trace (a) shows the observed count rate $\gamma_{cav}^{(1)}$ with the cavity open, and trace (b) shows the calibration of the free space rate $\gamma_{free}^{(1)}$ obtained by multiplying the count rate with the cavity blocked $\gamma_{bl}^{(1)}$ by the factor $2/(T_1+T_2)$. Trace (c) shows the count rate with the cavity open and the laser detuned from resonance; this data is just the background counting rate and demonstrates the absence of scattered laser light from the system.

In plotting the data of Fig. 4.7, two corrections have been applied to the data. First, the background counting rate of 30 counts/s has been subtracted from $\gamma_{cav}^{(1)}$ and $\gamma_{bl}^{(1)}$. Second, the data with the cavity blocked has been corrected for a small error in the focus of lens L1. This focus had initially been adjusted by measuring the distances with a ruler. But by directly observing the image of M1, it was later discovered the aperture A was approximately x = 0.6 cm behind the image of M1. As illustrated in Fig. 2.3, there are two contributions to the field outside M1: a collimated plane wave and a diverging spherical wave. In deriving eq. (4.4), it was implicitly assumed that the two waves have the same diameter. But this is only true at the surface of M1. It is easy to show that at a distance x behind M1, $\gamma_{cav}^{(1)}/\gamma_{bl}^{(1)}$ is further increased by a factor of

$$\xi = \frac{1}{2}\left[\left(1 + \frac{x}{a}\right)^2 + 1\right], \tag{4.5}$$

where a = L/2 = 2.5 cm is the distance from the atoms to the mirror. Substituting for a and x, we find that $\xi = 1.29$. Thus the data $\gamma_{free}^{(1)}$ of Fig. 4.7b were futher multiplied by $\xi = 1.29$ to compensate for this effect.

In a subsequent run of the experiment, the focus of L1 was carefully set by directly observing the image of M1. In this case, good agreement between theory and experiment was obtained without any correction factor ξ.

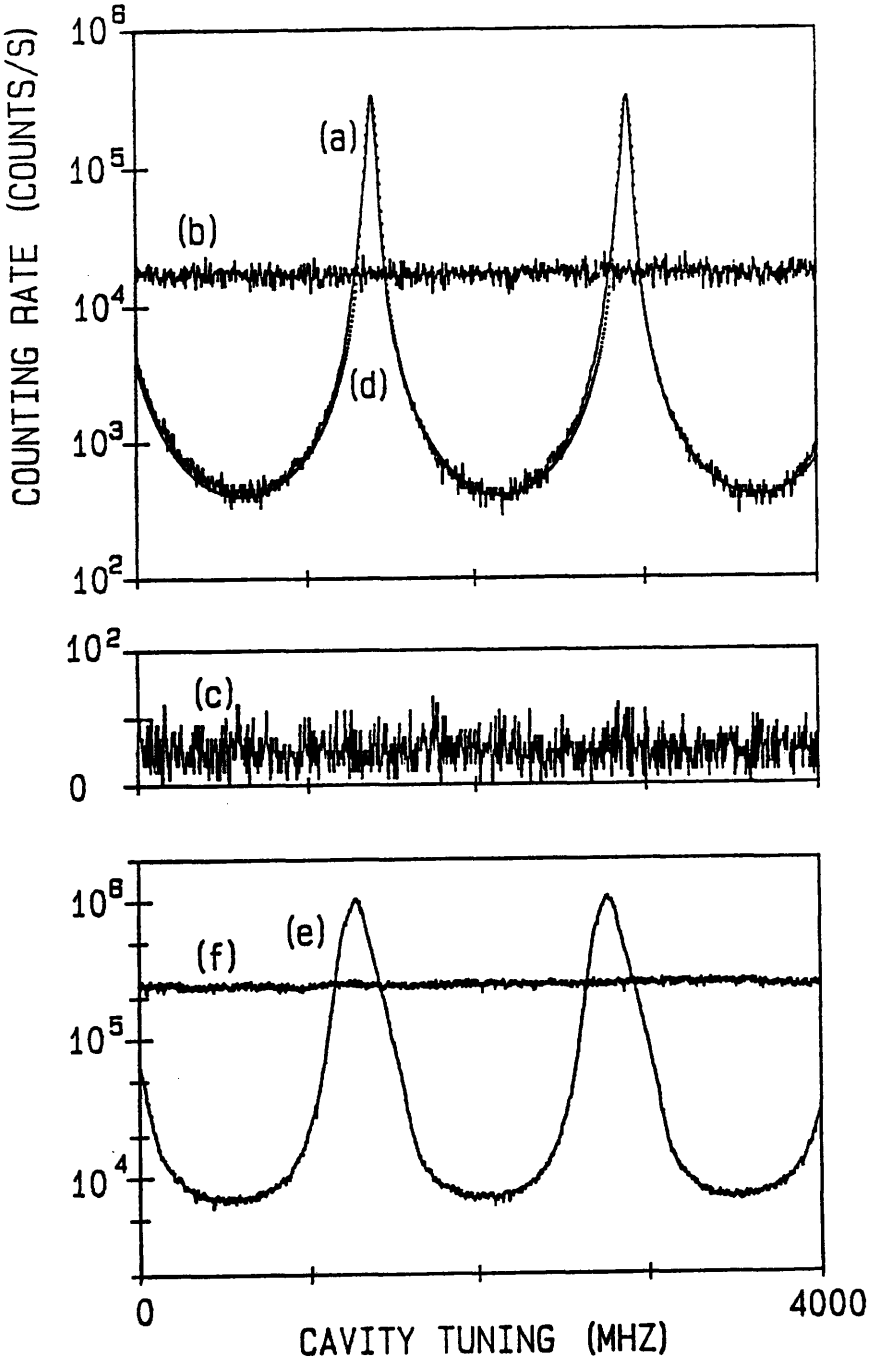

Fig 4.7. **Observed counting rate as a function of cavity tuning. For traces (a) through (c) the aperture size was 1.0 mm; for (e) and (f) it was 4.0 mm. (a) Cavity open. (b) Normalized count rate with the cavity blocked, showing the equivalent free space rate into the same aperture as (a). (c) Cavity open but laser detuned from resonance. (d) Theoretical fit (dotted line). (e) Cavity open. (f) Normalized count rate with the cavity blocked, showing the free space rate into the same aperture as (e).**

As expected, the spontaneous emission rate into the cavity is dramatically changed by the resonator tuning. Note that the data is plotted on a logarithmic scale and spans nealy three orders of magnitude. The maximum enhancement factor $\gamma_{cav}^{(enh)}/\gamma_{free} = 19$, and the maximum inhibition factor $\gamma_{free}/\gamma_{cav}^{(inh)} = 42$. The enhancement factor is smaller than the expected value of $1/(1-R) = 43.5$, because of broadening of the resonance due to Doppler shifts and mirror surface aberrations. Off resonance, the radiation is inhibited by a factor of $1/(1-R)$, as expected.

The data of Fig. 4.7 show the sharpest peaks that were observed. Reducing the aperture size further to 0.4 mm produced almost identical results. Presumably this is due to the fact that the atoms themselves are distributed over a finite size region of about 0.4 mm, and therefore unavoidably interact with the central 0.5 - 1.0 mm of the mirror.

Traces (e) and (f) of Fig 4.7. show the results obtained with an aperture size equal to the clear mirror diameter of 4.0 mm. Trace (e) shows the counting rate with the cavity open, and trace (f) shows the counting rate with the cavity blocked, multiplied by $2/(T_1+T_2) = 43.5$, thus showing the free space rate into the same aperture as (e). In this case the enhancement factor is only equal to 4.3, which is much less then that observed for only the central part of the mirror. This is due to the much worse mirror aberration over the larger aperture. However, the inhibition factor is 34.6, which is still nearly equal to $1/(1-R)$. Again, this is because the condition for resonance is much more critical than the condition to be off resonance.

IV.B.2. Analysis and Discussion.

Ideally, according to eq. (2.57), the data should be fit by the function

$$\gamma_{cav}^{(1)} = \gamma_{free}^{(1)}\left(\frac{1}{1-R}\right)\frac{1}{1 + \left(\frac{1}{1-R}\right)^2 \sin^2(2kL)}\ , \tag{4.6}$$

where we have used the fact that $1-R << 1$, and have assumed the correspondence $\gamma = p/\hbar\omega$. However, this formula was derived assuming no Doppler broadening or mirror surface aberrations are present. In the presence of such aberrations we may think of the

cavity as having a "distribution of resonance frequencies", corresponding to the different parts of the mirror. A simplified model of the actual lineshape can be given as a convolution of the ideal lineshape (4.6) over this distribution:

$$\gamma_{cav}^{(1)} = \gamma_{free}^{(1)}\left(\frac{1}{1-R}\right)\int \frac{f(\delta)d\delta}{1 + \left(\frac{1}{1-R}\right)^2 \sin^2(2k(L+\delta))} \quad , \tag{4.7}$$

where δ is a parameter coresponding to the deviation of the mirror surface from the ideal shape, and $f(\delta)$ is a normalized distribution function for the values of δ.

Trace (d) of Fig 4.7 shows a fit to the data by eq. (4.7), using the measured values of $1/(1-R) = 43.5$ and of $\gamma_{free}^{(1)} = 1.73 \times 10^4$ counts/s, where $f(\delta)$ was taken as a normalized gaussian distribution of width δ_0

$$f(\delta) = \frac{1}{\delta_0\sqrt{\pi}} e^{-(\delta/\delta_0)^2} , \tag{4.8}$$

and where δ_0 was adjusted to produce a good fit to the data at $\delta_0 = 2.9 \times 10^{-7}$ cm $= \lambda/192$. In terms of the cavity resonance frequency $\nu_n = nc/4(L+\delta)$, this corresponds to a width of $\delta\nu_n = \nu_n(\delta_0/L) = 32$ MHz, for $\nu_n \cong c/\lambda$. A good fit to the data is obtained, and the value of $\delta\nu_n = 32$ MHz is quite reasonable, given a spot size on the mirror of 1 mm.

IV.D. Indirect Measurement of the Change in the Total Spontaneous Emission Rate.

Acording to eq. (2.68), we expect that the total spontaneous emission rate of the atom in the cavity should be given by

$$\Gamma_{cav} = \Gamma_{free}\left[1 + \left(\frac{\gamma_{cav}}{\gamma_{free}} - 1\right)\frac{3}{8\pi}\Delta\Omega_{cav}\right], \tag{4.9}$$

where we have assumed the correspondence $\Gamma = P/\hbar\omega$, and that $(1-R) << 1$, and again $\Delta\Omega_{cav} = 8\pi b^2/L^2$ is the solid angle subtended by both cavity mirrors. Also, γ_{cav} and γ_{free} refer to the spontaneous emission rates into the full cavity aperture. Γ_{cav} has a maximum value of

$$\Gamma_{cav}^{(enh)} = \Gamma_{free}\left[1 + \left(\frac{\gamma_{cav}^{(enh)}}{\gamma_{free}} - 1\right)\frac{3}{8\pi}\Delta\Omega_{cav}\right], \tag{4.10}$$

and a minimum value

$$\Gamma_{cav}^{(inh)} = \Gamma_{free}\left[1 + \left(\frac{\gamma_{cav}^{(inh)}}{\gamma_{free}} - 1\right)\frac{3}{8\pi}\Delta\Omega_{cav}\right]. \tag{4.11}$$

In our case, $\frac{3}{8\pi}\Delta\Omega_{cav} = 0.0048$, and from the data of Fig.4.7 (e) and (f), $\gamma_{cav}^{(enh)}/\gamma_{free} = 4.3$, and $\gamma_{cav}^{(inh)}/\gamma_{free} = .025$. We thus expect that the total rate will increase by the fractional amount $\frac{\Delta\Gamma^{(enh)}}{\Gamma_{free}} = \frac{\Gamma^{(enh)} - \Gamma_{free}}{\Gamma_{free}} = +1.6\%$ when the resonator is on resonance, and decrease by the fractional amount $\frac{\Delta\Gamma^{(inh)}}{\Gamma_{free}} = \frac{\Gamma^{(inh)} - \Gamma_{free}}{\Gamma_{free}} = -0.5\%$ when the resonator is detuned from resonance. This corresponds to changes in the natural linewidth of +2.8 kHz and -0.8 kHz, or to changes in lifetime from 875 ns to 889 ns and to 871 ns, when the resonator is tuned on or off resonance, respectively. Unfortunately, these changes are too small to be detected easily.

We can, however, indirectly verify these changes in the total rate by measuring the intensity of spontaneous emission out the sides of the resonator. This intensity I_{side}, measured by PMT2, is simply proportional to the number of excited atoms n_e. Under conditions of weak excitation, $n_e = R_{12}n_0/\Gamma_{cav}$, where n_0 is the total atomic population, and $R_{12} = \sigma_D I/\hbar\omega$ is the average rate of induced transitions, with σ_D the absorption cross-section and I the average laser intensity. Therefore, a fractional change $\Delta\Gamma_{cav}/\Gamma_{cav}$ in the total spontaneous emission rate should be accompanied by a fractional change in the sideways intensity of

$$\frac{\Delta I_{side}}{I_{side}} = \frac{\Delta n_e}{n_e} = -\frac{\Delta \Gamma_{cav}}{\Gamma_{cav}} \quad . \tag{4.12}$$

A phase-sensitive detection technique may be used to detect this small change in sideways intensity. For this measurement, the additional connections shown as dashed lines in Fig. 4.6 are added. As before, the laser is locked to the ^{174}Yb transition via the 400 Hz oscillation frequency servo-loop, and and the computer records the data vs. a cavity scan voltage output by its D/A converter. In addition, a 35 Hz, 12.5 V pk-pk square wave modulation is superimposed on the PZT scan voltage, and the signal from PMT2 is monitored for a change in fluorescence intensity at 35 Hz by a second lock-in amplifier (Stanford Research SR510). Clearly if I_{side} is independent of cavity tuning, no signal will be detected. However, suppose that, as expected, I_{side} depends on the cavity tuning ω_c, as illustrated in Fig 4.8(a). Then, at a particular value of the cavity scan voltage, ω_c oscillates between two values $\omega_c^{(l)}$ and $\omega_c^{(u)}$, as illustrated in Fig. 4.8(b). This in turn produces the signal I_{side} vs. time t shown in Fig. 4.8(c). As a function of cavity scan voltage, $\omega_c^{(l)}$ and $\omega_c^{(u)}$ tune smoothly together past the peaks in I_{side} vs. ω_c. This will produce the lock-in output voltage illustrated in Fig. 4.8(d).

Any change signal detected by the lock-in is read into the computer via an A/D converter. The peak amplitude of this signal referred to the lock-in input is $\Delta V/\sqrt{2}$, where ΔV is the amplitude of the square wave input signal corresponding to ΔI. The value of $\Delta I_{side}/I_{side} = \Delta V/V_0$ can be determined by measuring the signal ampitude V_0 corresponding to I_0 on a calibrated oscilliscope plug-in. Note that this technique will not be separately sensitive to the values of $\Delta I_{side}^{(enh)}$ and $\Delta I_{side}^{(inh)}$, but only to the total difference $\Delta I_{side} = \Delta Iside^{(enh)} - \Delta I_{side}^{(inh)}$ between the intensities with the cavity on resonance and off resonance.

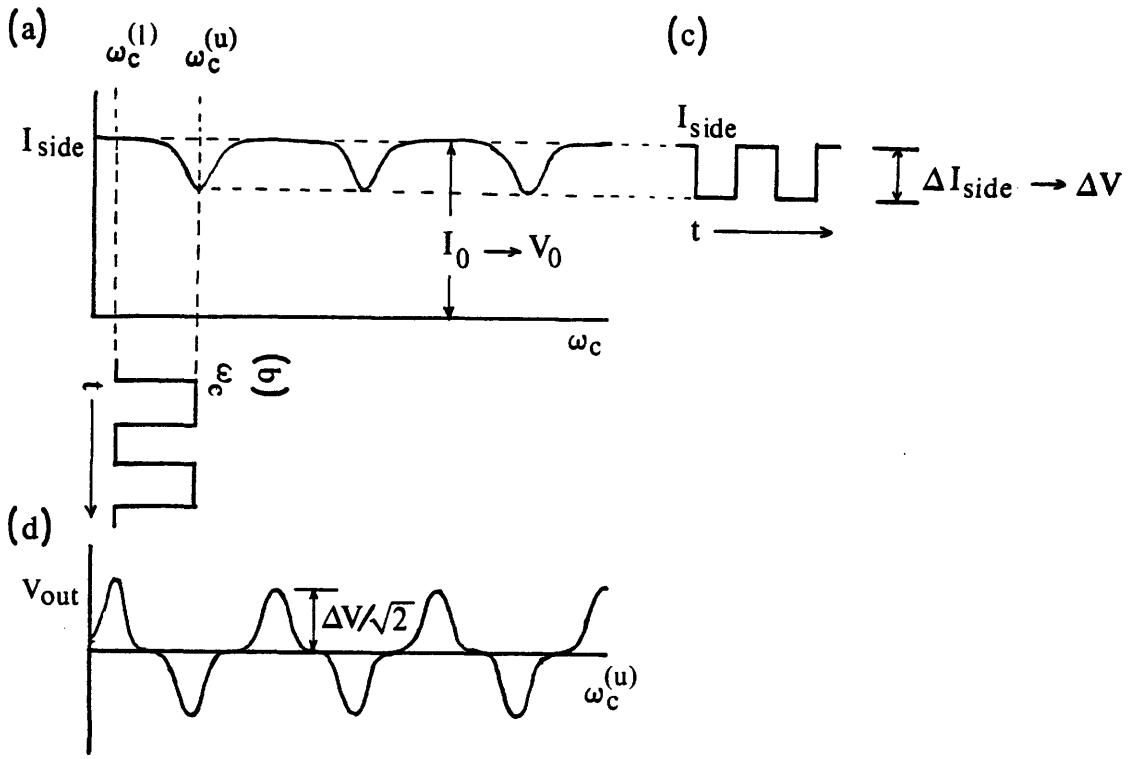

Fig. 4.8. Modulation of the sideways intensity I_{side} induced by modulation of the cavity tuning. (a) Anticipated form of I_{side} vs. the cavity tuning ω_c. (b) ω_c vs. time t. (c) I_{side} vs. t corresponding to (b). (d) Lock in output voltage vs. $\omega_c^{(u)}$.

The results of the experiment are illustrated in Fig. 4.9, for a pump power of 10μW. As expected, the change signal vs. cavity tuning displays the behavior predicted by Fig. 4.8(d). The peak amplitude of the signal is $\Delta I_{side}/I_{side} = -2.2 \pm 0.2$ %. That the sign of the change was correct was verified by applying a much smaller sinusoidal modulation to the cavity and observing the sign of the resulting dispersive-shaped output signal. The observed value is in excellent agreement with the value of $(\Delta I_{side}^{(enh)} - \Delta I_{side}^{(inh)})/I_{side} = -2.1$ % predicted on the basis of the on-axis data. We may therefore claim to have verified, indirectly, that the total spontaneous emission rate is changing as expected.

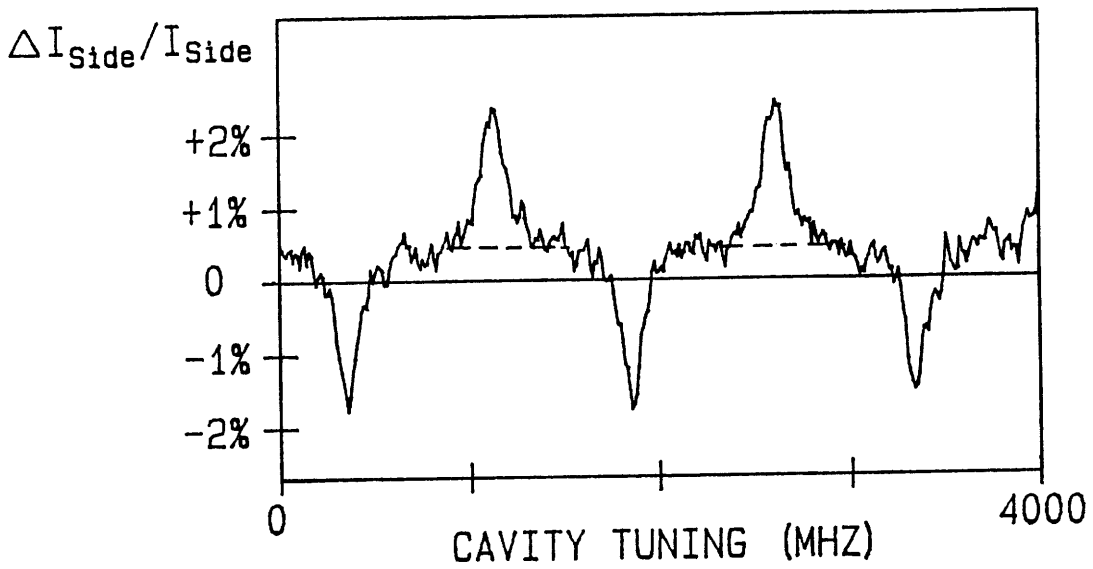

Fig. 4.9. Observed modulation in the sideways intensity vs. cavity tuning. The positive going peaks (above dashed lines) are an artifact of the modulation technique used to record the data. The level of zero change is not measured but is inferred from the on-axis data of Fig. 4.7.

CHAPTER V

MEASUREMENT OF THE RADIATIVE LEVEL SHIFT AND SPONTANEOUS EMISSION LINEWIDTH OF BARIUM ATOMS IN A CONCENTRIC RESONATOR.

In the previous experiment, the changes in the total spontaneous emission rate were very small, and could only be detected in an indirect manner. Clearly, it would be desirable to directly measure the change in the total spontaneous emission rate, either by a direct measurement of the lifetime, or by a measurement of the natural linewidth. It would also be desirable to measure the radiative level shift, which was presumably too small to measure in the Yb experiment.

In the Yb experiment, these effects were small for two reasons. First, both of them scale in proportion to the natural linewidth, which was only 180 kHz for Yb. Secondly, these effects scale in proportion to the fraction of spontaneous emission intercepted by the cavity mirrors, which was limited in the previous experiment to $f(\Delta\Omega_{cav}) \cong .005$ by the spherical aberration effect.

In order to circumvent these difficulties, new experiments studying the linewidth and transition frequency of the $^1S_0$ - $^3P_1$ transition of atomic barium in a concentric resonator were carried out. This transition was chosen for its relatively large natural linewidth of $\Gamma_{free}/2\pi = 19$ MHz, and because a two level system may be obtained. Also, as emphasized in section II.F, the concentric resonator geometry allows for a much large solid angle with spherical mirrors. In most of the experiments discussed in this chapter, $f(\Delta\Omega_{cav}) = 0.106$ was obtained. Thus the product $\Gamma_{free} f(\Delta\Omega_{cav})$ was increased by a factor of more than 2,000.

In the experiment, both the shift in transition frequency associated with the radiative level shift, and the changes in linewidth were directly observed. The results were found to be in good agreement with the theory presented in chapters II and III.

V.A. Experimental Description.

Although the experiment was similar in principle to the previous one, in practice the experiment required extensive modification and was more difficult to carry out. This included the enlargement of the vacuum system to accomodate an improved resonator structure, and the addition of a second interaction region outside the cavity. In this section the experimental apparatus is described, with particular attention paid to the modifications from the Yb experiment.

V.A.1. Barium Level Structure.

The lowest lying energy levels of atomic barium are illustrated in Fig. 5.1(a). The ground state is $^1S_0$, and the first allowed transition is to the $^1P_1$ excited state, with a wavelength of 553.5 nm.[71] The level structure is slightly complicated by the presence of a branching transition from the $^1P_1$ state to the metastable $^1D_2$ state, but the transition probability to this state is about 400 times less than the transition probability back to the ground state,[72] so it can be neglected for our purposes. The $^1P_1$ - $^1S_0$ decay rate is[73] $\Gamma_{free}/2\pi$ = 19 MHz.

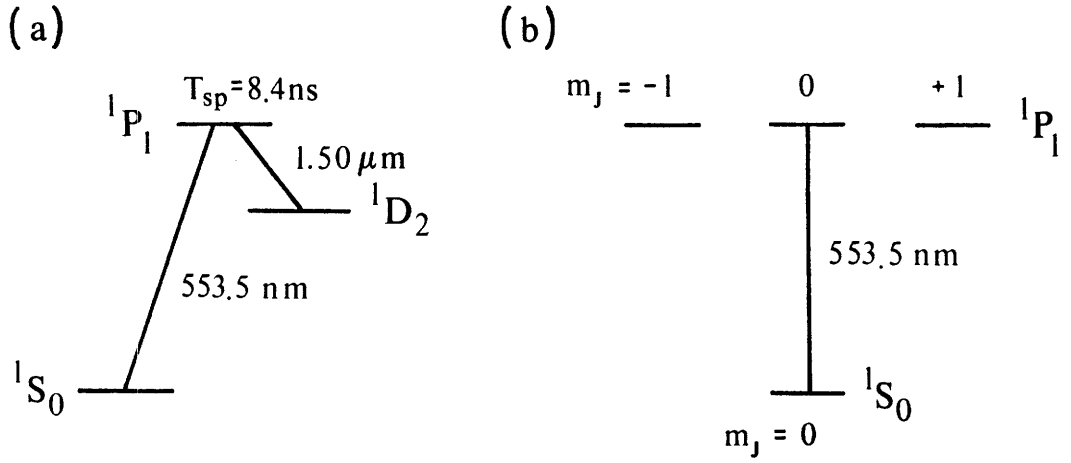

Fig. 5.1 Barium level structure. (a) Lowest lying electronic states. (b) Ideal two-level system formed by the ^{138}Ba component of the $^1S_0$ - $^3P_1$ transition.

The isotopic and hyperfine structure of the $^1S_0$ - $^3P_1$ transition is shown in Fig. 5.2. Barium has five naturally occuring isotopes, the most common of which is ^{138}Ba, with an

abundance of 72%. The three even isotopes have nuclear spin I = 0. The two odd isotopes each have nuclear spin I = 3/2, so that their $^1P_1$ states are split into three hyperfine levels having F_{upper} = 5/2, 3/2, and 1/2. Of particular interest for our purposes is the ^{138}Ba component of the line, labelled "a" in Fig. 5.2. Since its nuclear spin is I = 0, it has a nondegenerate level structure. Also, this component is resolved from the ^{137}Ba $^1S_0(F=3/2) \rightarrow {}^1P_1(F=5/2)$ component (labelled "b") by 65 MHz; less than 1% of the intensity of the ^{138}Ba component is due to the contribution of this ^{137}Ba component. Therefore, the ^{138}Ba $^1S_0$ - $^3P_1$ transition effectively forms and ideal, two-level system, as illustrated in Fig. 5.1(b).

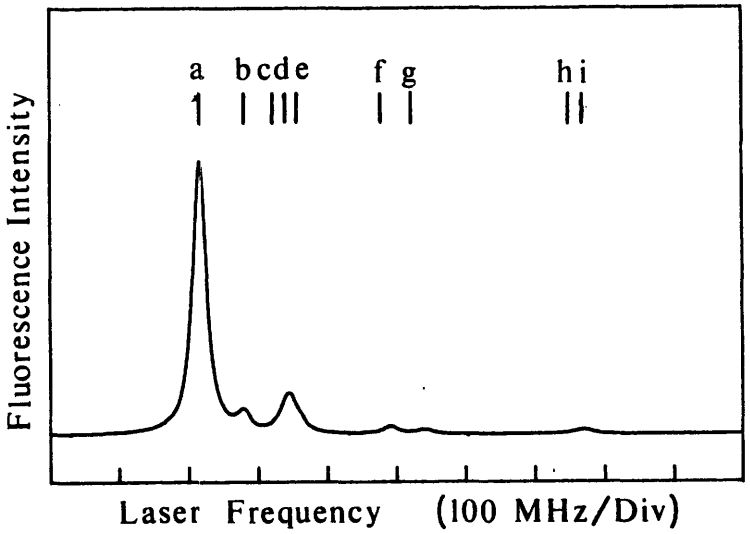

Compt.	Isotope	F_{upper}	Relative Frequency (MHz)
a	^{138}Ba	1	0
b	^{137}Ba	5/2	65
c	^{135}Ba	5/2	105
d	^{136}Ba	1	125
e	^{134}Ba	1	140
f	^{137}Ba	3/2	260
g	^{135}Ba	3/2	305
h	^{135}Ba	1/2	535
i	^{137}Ba	1/2	555

Fig. 5.2. Isotopic and hyperfine structure of the $^1S_0$ - $^3P_1$ transition of atomic barium. The component identifications and relative frequencies are from references 74 and 75.

V.A.2. Concentric Optical Resonator.

The most important modification to the experiment was the substitution of the concentric resonator for the confocal. As emphasized in section II.F, this geometry has the advantage that, with readily available spherical mirrors, the cavity can subtend a large solid angle and still maintain the "mode degeneracy" over its full aperture. However, one problem with the concentric resonator configuration is that the usual types of resonator construction employed for confocal or plane parallel cavities are completely unsuitable for use as a concentric cavity. Therefore it was neccessary to design and build a new type of resonator

explicitly for use as a concentric resonator. This new type of cavity proved to be a key to the success of the experiment.

One difficulty with the concentric cavity is that the requirements on resonator stability and adjustability are much more stringent than for the confocal or plane parallel resonator. This is because the centers of curvature of the two mirrors must coincide to within tolerances of the order of a wavelength in all three dimensions: there is no "redefining of the optical axis", and the spacing has to be exactly right. The difficulty of meeting these alignment tolerances was studied with a pair of spherical mirrors mounted near concentric spacing in Aerotech mounts. Even with these high quality mounts, it was very difficult to obtain a good concentric alignment. The concentric cavity geometry is very sensitive not only to mirror tilt, but also to the sideways translation of the mirrors. Therefore, the usual structures employed for flat plate interferometers are not suitable for this purpose, since they are typically rather sloppy with respect to sideways translation of the mirrors.

A second difficulty with the concentric cavity configuration is the need to focus the light into and out of the cavity with low f-number lenses. This implies that the resonator aperture should be clear out to the solid angle subtended by the mirrors, and also that the input and output lenses should be mounted very near the cavity mirrors so that they are not inordinately large. In practice this means that the input and output lenses should be mounted as an integral part of the resonator structure. Again, this is a requirement which the usual types of resonator strucures are not able to meet.

In order to circumvent these difficulties, a structure designed specifically for use as a concentric resonator was constructed, as shown in Fig. 5.3. A four rod structure is chosen for its rigidity, and consists of two 1" thick by 6 1/2" wide by 6 3/4" high aluminum endplates clamped onto four 1" diameter invar rods. Attached to one of the endplates is an aluminum ring, via a .010" thick by 5 1/4" outside diameter by 4 3/4 " inside diameter phosphor bronze "washer". This washer is secured to the endplate at three points 120 ° apart, and to the aluminum ring at another three points 120 ° apart and offset by 60 ° from the first. The separation between the aluminum ring and the end plate is controlled by three differential screws with submicron resolution (Klinger model BD17-04), which lift the ring from the plate until it feels a restoring force from the phosphor bronze washer.

Attached to the opposite endplate is a second aluminum ring via three PZT stacks, each consisting of six 3/4" diameter by .076" thick disk PZTs (Vernitron PZT-5A). The PZT stacks provide a net displacement of $\lambda/2$ for 120 V.

The two resonator mirrors M1 and M2 are actually mounted onto aluminum cylinders of 3" I.D. which project back into a hole cut into each endplate. Inside of these cylinders are mounted $f/1.2$ camera lenses L1 and L2 (Canon FD50 1.2) which are used to focus light into and out of the cavity. In order to line up the cavity, it is very important that lens L1 focus the light so that the rays cross within $\sim$ 10 μm of the center of the cavity. Lenses L1 and L2 have a resolution of 100 lines/mm, which is sufficient to insure this is the case.

This resonator design proved to be very sucessful. The three differential screws provided for a "coarse" adjustment of the cavity, while the three PZT stacks provided for a very sensitive fine adjustment of the three degrees of freedom of the resonator. The flexure type mounting allowed for both tilt and a net translation of M2 along the resonator axis, but was very rigid with respects to sideways translation. Using this resonator it was found that a good concentric alignment could easily be achieved and maintained.

The cavity mirrors had a radius of curvature of a = 2.5 cm, and were coated with a thin aluminum film of reflectivity R = 0.65. This corresponds to a separation of L = 5.00 cm, a free spectral range $\Delta\nu_{fsr}$ = 3000 MHz, a finesse $F^{(calc)} = \pi\sqrt{R}/(1-R) = 7.2$, and a fringe width $\Delta\nu_{cav}^{(calc)} = \Delta\nu_{fsr}/F$ = 420 MHz. The mirror substrate was 0.8 cm thick, and the back surface had a radius of curvature of 3.3 cm, which is concentric with the reflecting surface. This is very important, since otherwise the mirror substrate would act as a lens, and the resulting aberrations would in effect ruin the resolution of the input lens L1, making alignment of the cavity impossible.

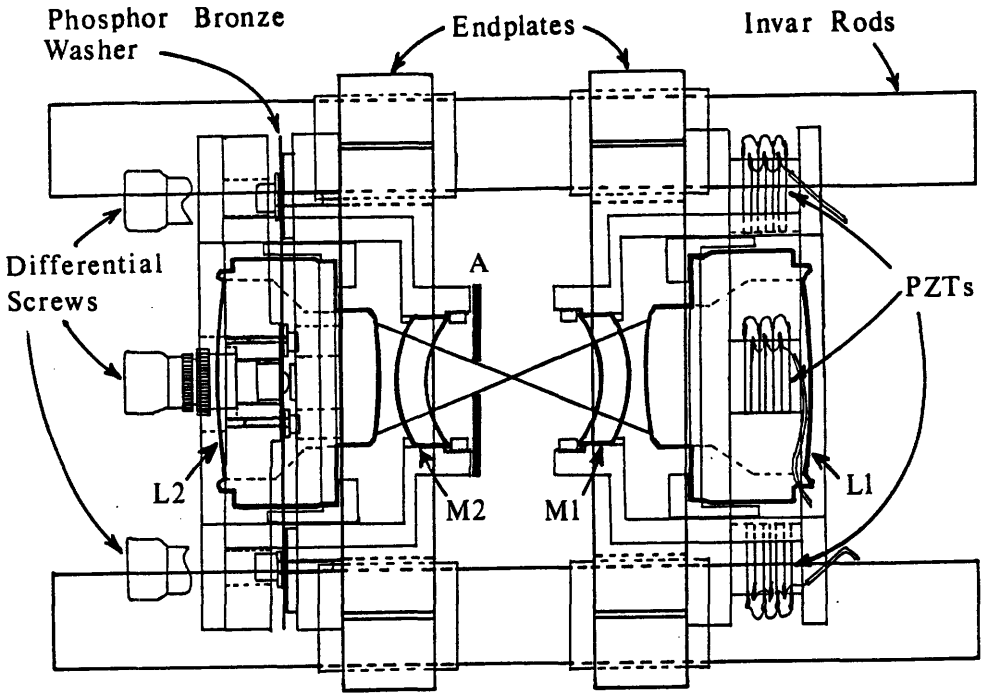

Fig. 5.3. Concentric Optical Resonator. The drawing is to scale, and shows the placement of the cavity mirrors M1 and M2, camera lenses L1 and L2, piezoelectric transducers PZTs, and the intracavity aperture A.

The clear diameter of the mirrors is 3.3 cm, which corresponds to a half angle subtended by the mirrors of $\theta_M = 42°$, and to a solid angle of $\Delta\Omega_{cav}/4\pi = 1 - \cos\theta_M = 0.257$. Assuming that the atomic dipole is oriented perpendicular to the cavity axis, so that eq. (3.74) applies, this implies that the mirrors intercept a fraction $f(\Delta\Omega_{cav}) = 0.340$ of the total spontaneous emission. The f/1.2 camera lens subtends a half angle of $\theta_L = 22.6°$, which corresponds to $\Delta\Omega_L/4\pi = .078$. Thus the lens illuminates only the central 30% of the solid angle subtended by the mirror.

For most of the measurements carried out in this chapter, an aperture A was placed in the cavity which subtended a half angle of $\theta = 22°$, so that the effective clear diameter of the mirror was 1.88 cm, and the fraction of spontaneous emission intercepted by the mirrors was $f(\Delta\Omega_{cav}) = .106$, where again we assume eq. (3.74) applies. This insured that the lenses L1 and L2 were able to view the entire solid angle subtended by the cavity.

The cavity is aligned by illuminating it with a laser through the input lens L1, and adjusting it and the focus of the incoming laser while simultaneously viewing the

transmitted beam. When the cavity and the cavity probe beam are perfectly aligned, the entire aperture becomes uniformly bright when the cavity is tuned to resonance, and uniformly dark off resonance. Concentric rings indicate a cavity spacing which is slightly too long or too short; straight or curved bands indicate a mirror tilt.

Once the cavity is aligned to concentricity, it is tuned by a small linear displacement of M1. A typical scan of the total transmitted intensity vs. cavity tuning is shown in Fig. 5.4. The linewidth of the central fringe is about 500 MHz, which is broader than $\Delta\nu_{cav}^{(calc)}$ because of surface aberrations. Also note that the finesse degrades significantly with a displacement of only a few fringes. This occurs because we are tuning the cavity by controlling the mirror separation only, when actually what is desired is to tune the mirror radii; i.e. the rays at the edge of the mirror "tune" differently than rays between the center of the mirrors. The behavior illustrated in Fig. 5.4 is characteristic of the resonator when it is very well aligned: it is actually possible to identify *which fringe* is the closest to concentric spacing. In general an effort is made to stay within one fringe of this spacing during the experiment, although in practice the spacing may have been off by two or three fringes.

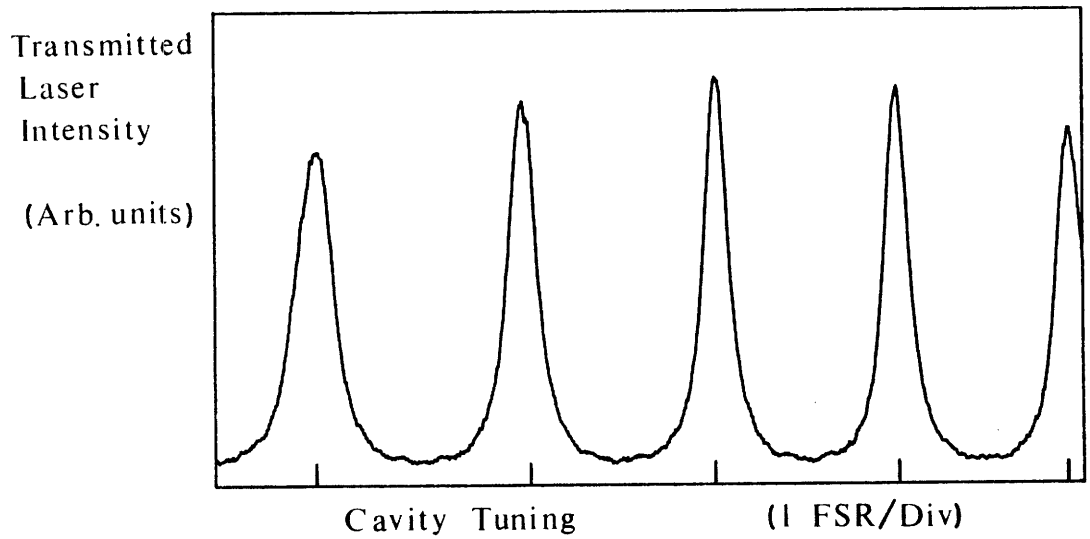

Fig. 5.4. Probe laser transmission vs. cavity tuning.

Another difficulty with the concentric resonator geometry is that it places a very tight restriction on the displacement of the atoms from the center of the resonator. Recall from eq. (2.125) that the round trip path length of a ray initiating at a displacement of Δ is given by

$$L_{rt} = 4a + \frac{2\Delta^2}{a} \sin^2 \psi \,, \tag{5.1}$$

where ψ is the angle between the atomic displacement vector and the light ray direction, as illustrated in Fig. 2.7. Noting that the resonance frequency associated with a particular ray is $\nu_n = nc/L_{rt}$, we find that the ray starting from a displacement of Δ is shifted in frequency with respect to the concentric rays by

$$\delta\nu = -\frac{c\Delta^2}{2\lambda a^2} \sin^2\psi \,. \tag{5.2}$$

This frequency shift is plotted in Fig. 5.5 for λ = 554 nm, a = 2.5 cm, and $\psi = 90°$ and $\psi = 22°$. For atomic displacements perpendicular to the resonator axis, the shift in resonance frequency is closely described by the $\psi = 90°$ curve. For displacements along the cavity axis, ψ lies between 0 ° and 22 °.

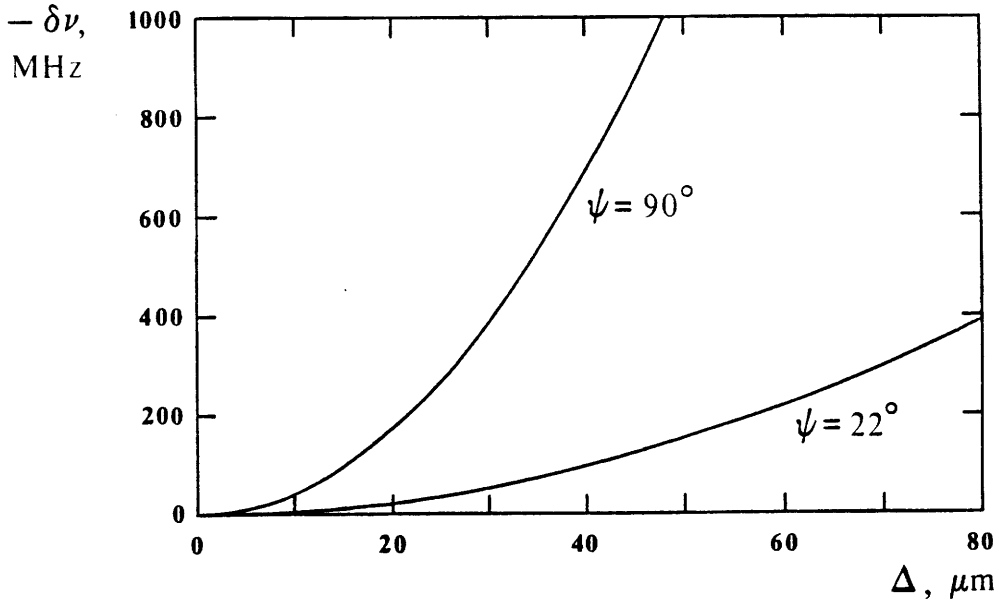

Fig. 5.5. Frequency shift vs. atomic displacement Δ, for λ = 553.5 nm, a = 2.5 cm, and $\psi = 90°$ and $\psi = 22°$.

In order that these frequency shifts not significantly affect the results of the experiment, they should not exceed the linewidth of the cavity. If we take as a criterion that the largest shift not exceed the cavity half width, this implies that the atoms should be confined to a displacement of less than 22 μm perpendicular to the cavity axis, and less than 60 μm parallel to it. This small interaction volume implies that only a small number of atoms can be excited at any one time, resulting in a small signal. This is partly compensated for by the rapid decay rate of barium. Also note that the distance by which the atoms drift during their

lifetime may be important. Again, the short lifetime of barium is an advantage, since the atoms only drift a distance of $u\tau_{sp} \cong 2\ \mu m$.

V.A.3. Atomic beam and interaction regions.

For the concentric cavity experiments the atomic beam apparatus was modified as illustrated in Fig. 5.6. A much larger vacuum vessel consisting of a 12" diameter by 12" high stainless steel cylinder was added to house the resonator structure. Also, a modification of the source region allows the atomic beam source position to be adjusted while the beam is running.

The atomic beam is collimated by a 1 mm diameter aperture A1 at a distance of 19.3 cm from the source, and intercepted by a beam ("reference beam") from the cw dye laser, and then recollimated by a second aperture A2 of 25 μm diameter at a distance of 28.1 cm from the source. The atomic beam propagates an additional 0.2 cm from A2, where it is intercepted by a second beam ("pump beam") from the same laser. Two regions of excited atoms are thus created, one ("region 1") outside the cavity near A1, and a second ("region 2") inside the cavity near A2. The aperture A2 is mounted in such a way that it can be translated while the beam is running.

For convenience, throughout this chapter we shall adopt the following coordinate system. The origin of coordinates is taken at the precise center of the resonator, with the x-axis lying along the atomic beam propagation direction, the y-axis in the vertical direction (parallel to the pump beam propagation direction), and the z-axis along the cavity axis.

The pump beam is focussed to a diameter of approximately 20 μm. The atoms in region 2 are therefore confined to a volume of approximately $V = \pi \times (12.5\ \mu m)^2 \times 20\ \mu m = 1.0 \times 10^{-8}\ cm^3$. This is sufficiently small that the frequency shifts associated with the atomic displacement are small.

The tube oven source is filled with about 6 g of barium and is heated typically to about $T_{oven} = 930$ °C with an oven current of 165 A. In this case the atoms escape through a $D = 1.0$ mm diameter hole. For the barium tube ovens, it appeared that the effective temperature T_{Ba} of the barium was about 250 °C colder than T_{oven}. Thus $T_{Ba} \cong 680$ °C, which was sufficient to produce a vapor pressure of[70] $P_0 \cong 5 \times 10^{-6}$ atm, corresponding

to a source density of $n_0 \cong 4 \times 10^{13}$ cm^{-3}, and to a flux of atoms of $\Phi_n \cong 2 \times 10^{15}$ s^{-1}. The mass flow is about 2×10^{-3} g/hr, and the mean thermal velocity $u \cong 2.4 \times 10^4$ cm/s. The source flow is purely effusive.

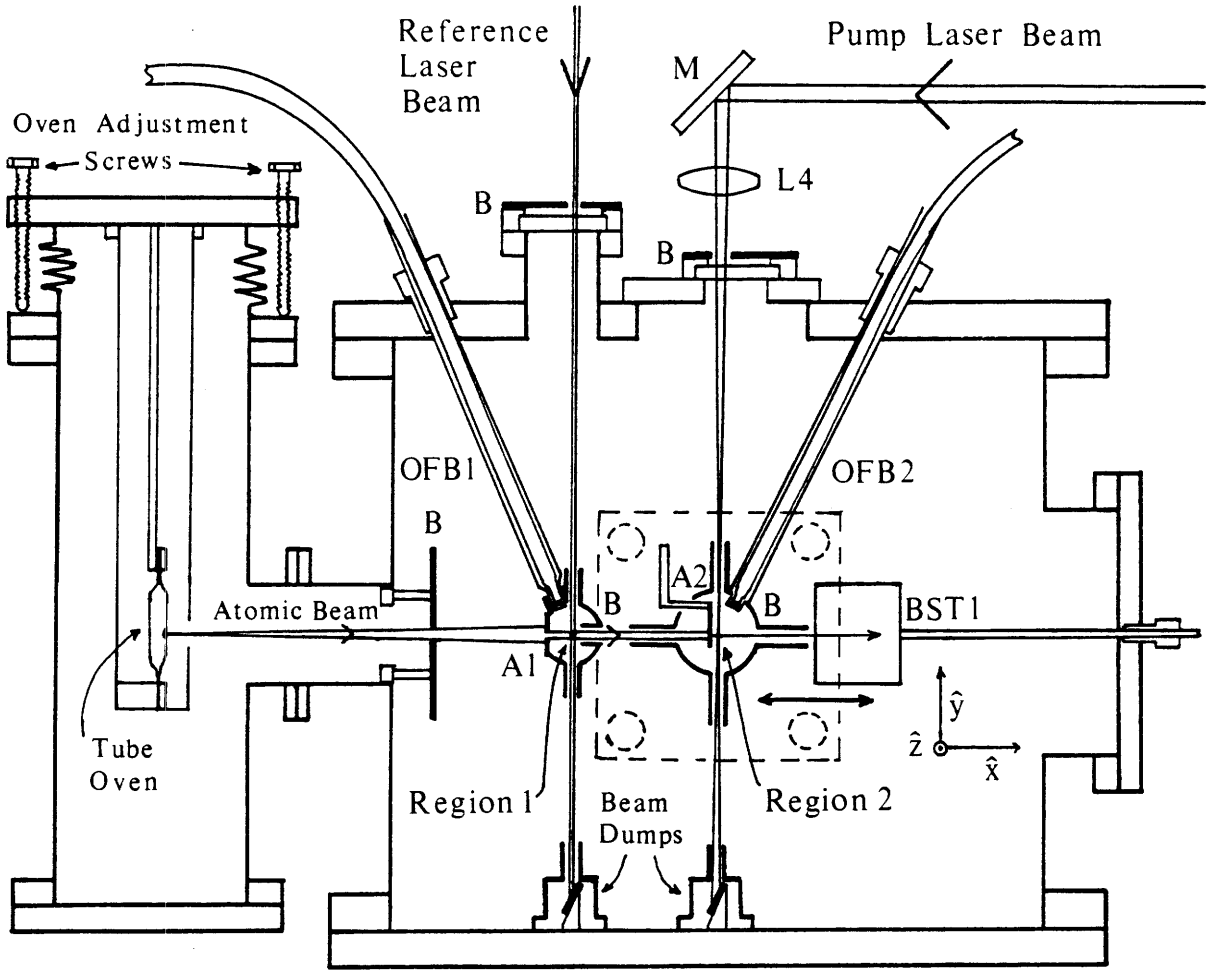

Fig 5.6. Atomic beam apparatus. M: mirror; L: lens; B: baffle; OFB: optical fiber bundle; A1 and A2: atomic beam collimation apertures, BST1: movable beam stop. Region 2 lies in the center of the concentric resonator; the dashed lines indicate the position of its rods and endplates. Also illustrated are the x, y, and z directions referred to in the text.

The ^{138}Ba density in region 2 is approximately $n = \alpha\Phi_n/\pi u X^2 \cong 2 \times 10^7$ cm^{-3}, where $\alpha = .72$ is the isotopic abundance of ^{138}Ba and X = 28.3 cm the distance from the source, so that the average number of atoms in region 2 is $N = nV \cong 0.2$. Therefore a maximum of about $N\Gamma_{free}/2 = 1 \times 10^7$ photons/s will be scattered by the atoms, implying that with our detection efficiency of $\eta \cong 2 \times 10^{-4}$, only about 2000 counts/s will be detected.

This means that an extremely high sensivity is required. To detect these small signal levels a small background light level is necessary. This is accomplished by means of a set a blackened light baffles at the windows to the chamber, at the entrance to the (glowing) source chamber, and surrounding the interaction regions. Also, in order to avoid scattered laser light, both beams are absorbed by a piece of black glass tilted at Brewster's angle inside of a "beam dump". These measures were sufficient to reduce the background counting rate of PMT2 and PMT3 to several hundred counts/s.

The larger volume and greater number of components in the chamber were a significant load on the vacuum pump. In particular, the two camera lenses could not be used as purchased inside of the vacuum system. These were dissasembled, as many extraneous parts as possible were discarded, and all grease removed from the focussing mechanisms and replaced with vacuum grease. With this modification, the entire system could be pumped down to about 6×10^{-6} torr after 24 h of pumping.

Several problems were encountered in the operation of the barium beam. First, at oven temperatures T_{oven} around 1000 °C, significant beam density variations were observed, which seemed to be associated with melting and freezing of the barium. (The barium melting point is 725 °C.) Also, at background pressures above 5×10^{-6} torr, significant beam density variations were observed that seemed to be associated with background pressure fluctuations. It was found that these variations could be eliminated by running the experiment at lower background pressures of about 2×10^{-6} torr, which could be achieved by first pumping on the chamber for several days, then running the beam at an oven temperature of 1000 °C for several hours, and then turning the oven back down to 930 °C for the experiment. It did not seem to be possible to obtain a steady beam at very much higher temperatures.

V.A.4. Lasers and Optical Layout.

The overall experimental layout is illustrated in Fig. 5.7. In this case the CR699-21 dye laser with Rh110 dye was pumped by 6W of 514.5 nm radiation from a Coherent CR18 argon ion laser. The dye laser output is split off by beamsplitters to form three separate beams: the "reference beam", the "cavity probe beam", and the "pump beam".

The reference beam is used to pump the atoms in region 1, and is adjusted to a diameter at the atoms of 1 mm by the collimator COLL1, and to a power of about 2 μW. This gives a peak intensity of $I \cong 0.2\ mW/cm^2 << I_S$.

The cavity probe beam is expanded 60x by the combination of lenses L5 and L6, and after passing through an aperture A forms a beam about 5 cm in diameter of uniform intensity. This beam is used to align the cavity; the cavity lineshape may also be measured by reflecting the transmitted beam from the movable mirror M3 into the photodiode PD. During the experiment this beam is blocked off by the beamstop BST2 and the mirror M3 is flipped back out of the way.

The pump beam is used to pump the atoms in region 2. This beam must be attenuated by seven orders of magnitude. The two beamsplitters BS1 and BS2 provide for some initial attenuation of the intensity. This beam then passes through the combination of the two polarizers POL2 and POL3 and the Soliel-Babinet Compensator SBC, which provide a further adjustable atteuation. The collimator COLL2 adjusts the spot size of the beam to at a lens L4 of f = 25 cm focal length which is mounted above the interaction region; this lens in turn focusses the beam onto the atoms. The spot size at L4 was carefully studied using a 0.15 mm pinhole and a power meter; it was found to have a radius (half width of the intensity at 1/e point) of $\Delta x = 0.205$ cm in the x-direction, and of $\Delta z = .275$ cm in the z-direction. The lens will therefore focus the pump beam to spot sizes (HW1/e of intensity) of $\Delta x' = \lambda f/2\pi\Delta x = 8.5\ \mu m$ and $\Delta z' = \lambda f/2\pi\Delta z = 11\ \mu m$ in the x and z directions, respectively. The power of the pump beam was set to P = 0.02 μW, which corresponds to a peak intensity of $I = P/\pi\Delta x\Delta z = 6.8\ mW/cm^2$.

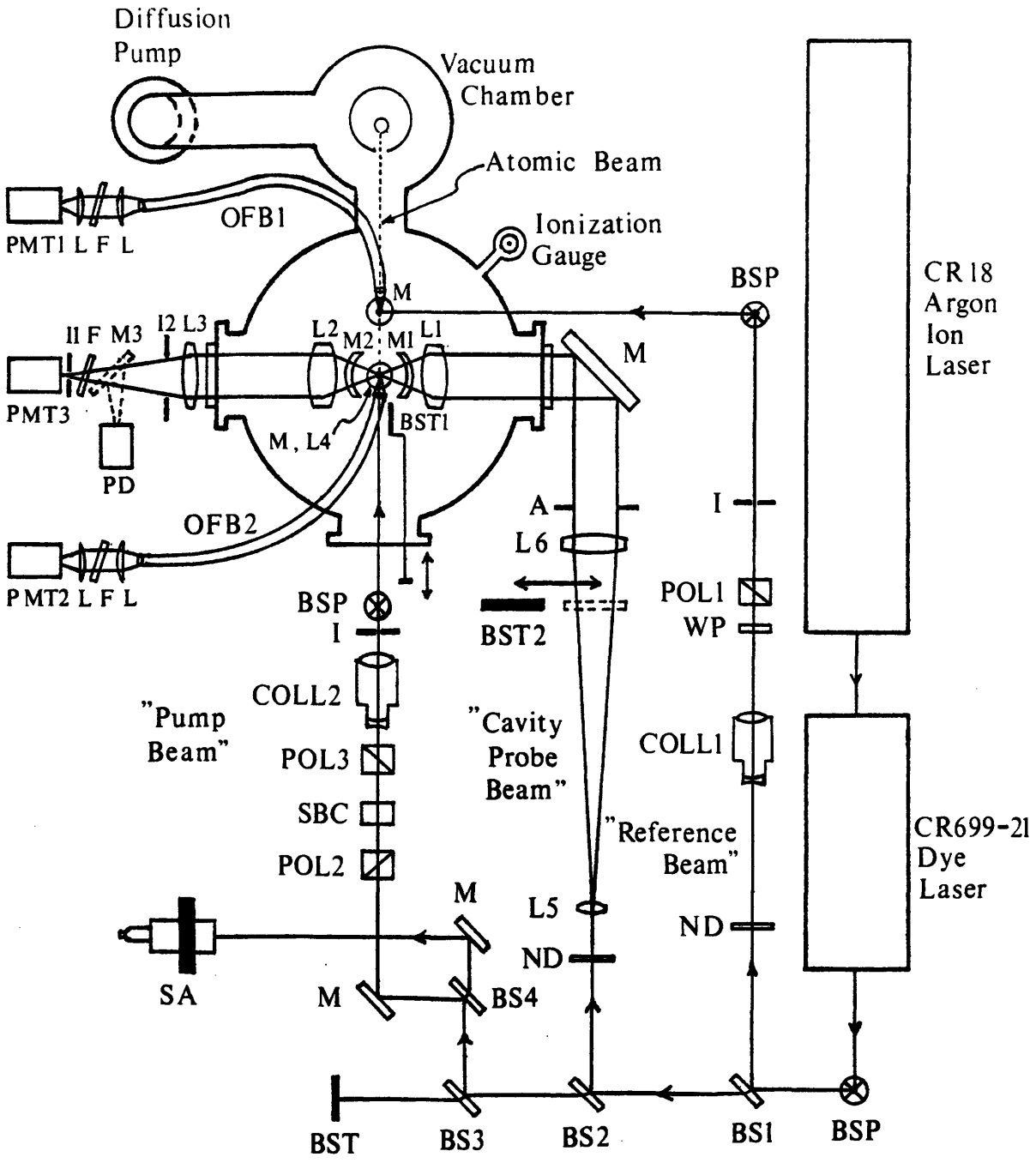

Fig. 5.7. Optical layout for concentric cavity experiments. BSP: beam steering post; BS: beamsplitter; ND: neutral density filter; COLL: collimator; WP: waveplate; POL: polarizer; I: iris; BST: beamstop; A: aperture; L: lens; F: interference filter; PMT: photomultiplier tube; PD: photodiode; SA: spectrum analyzer; SBC: Soliel-Babinet compensator; OFB: optical fiber bundle.

As an independent test of the width $\Delta z'$ of the focussed pump beam, the width of the of the scattered flourescence intensity vs. the displacement of the lens L4 in the z-direction was recorded at various heights (y position) of this lens. The observed widths were consistent with a Gaussian beam of waist size (HW1/e of intensity) of 11 μm, and the observed minimum width of 30 μm (FWHM) was consistent with the convolution of the pump beam and atomic beam widths. This procedure was also used to carefully position the focus of the lens L4.

Both the reference beam and the pump beam are linearly polarized in the x-direction. This implies that only a single $\Delta m = 0$ transition is excited, as in Fig 5.1(b). Also, the atomic dipole is oriented perpedicularly to the atomic beam, so that the formula (3.74) for the fraction of spontaneous emission intercepted by the cavity mirrors applies.

The fluorescence from the atoms in region 1 is collected by the optical fiber bundle OFB1, and is detected by PMT1 in the same manner as described in section IV.A.6. Similarly, the fluorescence emitted from the sides of the cavity in region 2 is collected by optical fiber bundle OFB2 and detected by PMT2. A third photomultiplier PMT3 detects the light emitted through the end mirror M2 of the cavity. This light is collected by the camera lens L2, then passes through a second lens L3, an iris I2, another interference filter F, and finally another iris I1 mounted in front of PMT3.

As before, a movable beam stop BST1 may be inserted between the atoms and the cavity mirror M1, thus removing the effect of the cavity. This enables the signal with the cavity blocked to be used as a calibration of the free space spontaneous emission rate. The transmission coefficient of each mirror is T = 0.09, so there is a loss coefficient of L = 1 - R - T = 0.26, which must be taken into account. The spontaneous emission rate of the atom into the cavity includes not only the part $\gamma_{cav}^{(T)}$ transmitted through the mirrors but the part $\gamma_{cav}^{(L)}$ absorbed by the mirror:

$$\gamma_{cav} = \gamma_{cav}^{(T)} + \gamma_{cav}^{(L)}, \tag{5.3}$$

where

$$\gamma_{cav}^{(T)} = \frac{T}{T+L}\gamma_{cav}; \qquad \gamma_{cav}^{(L)} = \frac{L}{L+T}\gamma_{cav}\,. \tag{5.4}$$

The actual counting rate detected by PMT3 with the cavity open is

$$\gamma_{cav}^{(1)} = \frac{\eta}{2}\gamma_{cav}^{(T)} = \frac{\eta}{2}\frac{T}{T+L}\gamma_{cav}, \tag{5.5}$$

whereas the counting rate with the cavity blocked is

$$\gamma_{bl}^{(1)} = \frac{\eta}{2} T \gamma_{free}\,, \tag{5.6}$$

where η is the detection efficiency. Thus the quantity

$$\gamma_{free}^{(1)} = \frac{1}{T+L}\gamma_{bl}^{(1)} = \frac{1}{1-R}\gamma_{bl}^{(1)} \tag{5.7}$$

is correctly normalized so that

$$\frac{\gamma_{cav}^{(1)}}{\gamma_{free}^{(1)}} = \frac{\gamma_{cav}}{\gamma_{free}}\,. \tag{5.8}$$

The quantity $\gamma_{free}^{(1)}$ may therefore be taken as a measure of the equivalent free space rate into the same solid angle as $\gamma_{cav}^{(1)}$.

V.A.5 Electronics and Data Acquistition.

The experimental control and data acquisition electronics are illustrated in Fig. 5.8. The signals from both PMT2 and PMT3 are detected by photon counting electronics as described in section II.A.6, except that the NIM pulses from the discriminator are now fed into a BI RA model 2101 dual 40 MHz scaler/timer in a CAMAC crate. This crate is controlled via a GPIB interface by an IBM-XT microcomputer. Also, the pulses from PMT2 are amplified by two Avantek AWL-500M amplifiers, with a -20 dB attenuator in between to limit the total gain. The photocurrent from PMT1 is processed as an analog signal by a Keithley 150B microammeter and read into the computer via an A/D converter.

The three PZT stacks are controlled by a "PZT control box" and three HV power supplies (Kepco ABC) operated in voltage programming mode. The gain of each HV supply is adjusted to compensate for differences in the responses of the three PZT stacks. The control box allows the voltage on each PZT stack to be independently adjusted for cavity alignment, and there is also an offset control which allows for an additional voltage to be applied to all three PZT stacks, causing a net linear displacement of the mirror. This displacement voltage may also be controlled via an external scan input.

The normal configuration of the experiment is indicated by the solid lines. The cavity tuning is set to some fixed value, and the computer simultaneously records the signal from all three PMTs as a function of laser frequency. This laser tuning is controlled via its external scan input by a D/A converter.

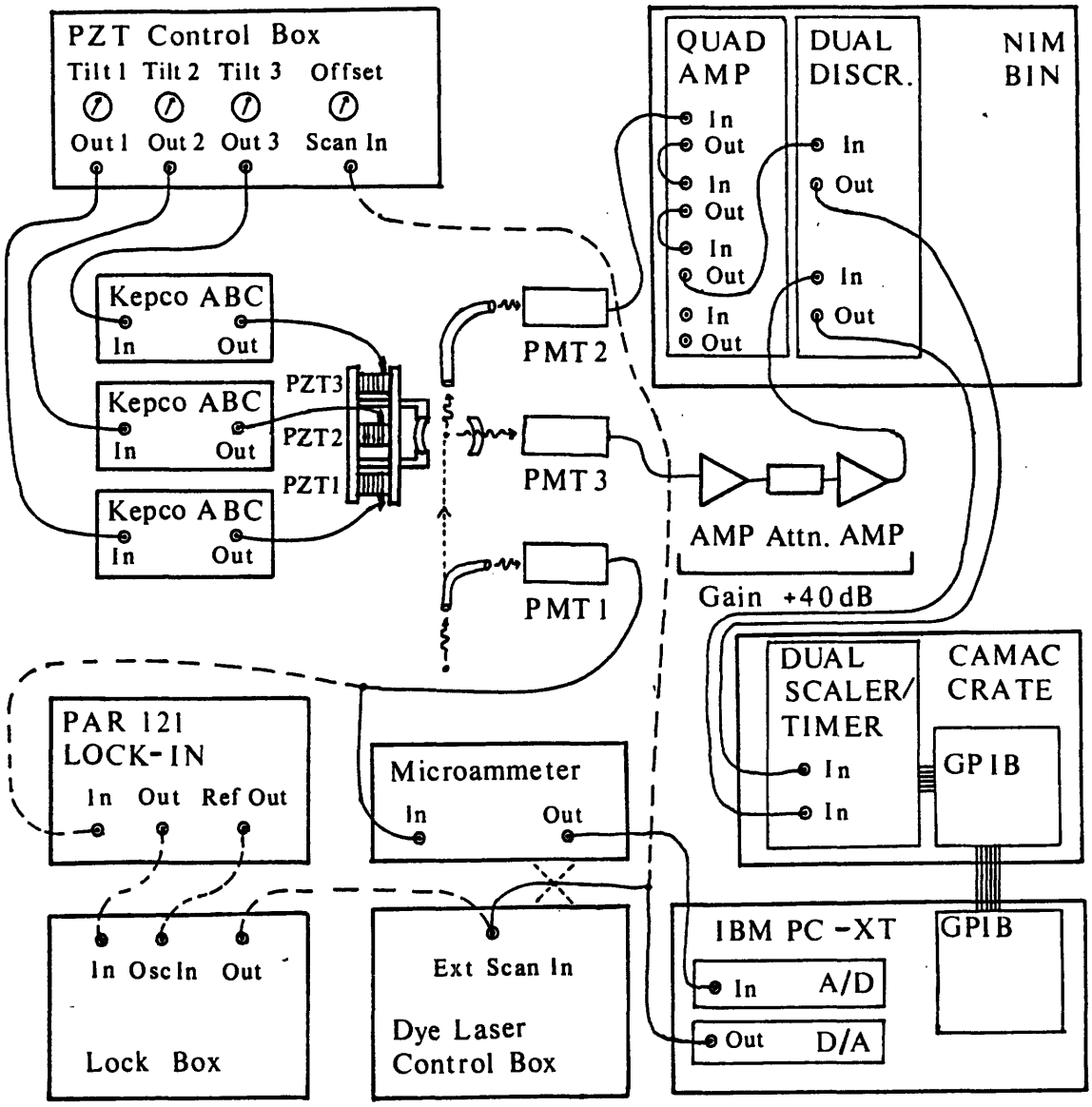

Fig. 5.8. Data acquisition system. For the linewidth and lineshift measurements, only the connections shown as solid lines are made. The fluorescence intensity as a function of cavity tuning may also be studied; in this case the D/A is disconnected from the dye laser external scan input and the additional connections shown as dashed lines are made. Also, either one of the discriminator outputs may be processed by a ratemeter and displayed on an oscilliscope (not shown).

Alternatively, the experiment can be run in a mode similar to that of the Yb experiment, as indicated by the dashed lines. In this mode the laser frequency is locked to the ^{138}Ba resonance line by the same technique described in section II.A.6, and the computer

records the signal from all three PMTs as a function of cavity tuning. The laser frequency lock loop is also very useful during system alignment.

V.A.6. Alignment procedure.

The most difficult aspect of the experiment is the alignment of the cavity, atomic beam, and laser beams. The only practical way that was found to accomplish this alignment is the following procedure, which can take many hours when starting from scratch.

First, the cavity is lined up using the cavity probe beam as described in section V.A.2. The components between the cavity and PMT3 are also lined up using this beam, with the lens L3 adjusted so that probe beam comes to a focus at the center of the iris I1 mounted on PMT3. Next, the cavity probe beam is blocked off, the atomic beam is turned on, and the laser frequency locked to the ^{138}Ba line using the fluorescence signal from region 1. Next, the lens L4 is removed or defocussed, and the much wider pump beam centered in the cavity. If no fluorescence is observed in region 2, it indicates that the oven hole and apertures A1 and A2 do not lie in a straight line. If this is the case, the oven is moved around in a two-dimensional search until fluorescence in region 2 is detected by PMT2. This fluorescence cannot be seen by eye and must be monitored using the photon counting system. Once the fluorescence is detected in region 2, the lens L4 is put back into the pump beam, and the pump beam translated in the z direction until it intersects the atomic beam, as registered by the reappearance of fluorescence.

The next step of the alignment is to position the atoms to the axis of the cavity. This is accomplished by first locating the position of PMT3 and I1 at which the fluorescence emitted by the atoms passes through I1 and is detected. By reintroducing the cavity probe beam into the system and observing the spot to which it now focusses I1, the distance and direction by which the excited atoms are displaced from the cavity axis may be determined. The atoms are repositioned by translating the aperture A2 and the pump beam. This procedure is iterated until the image of the atoms on I1 coincides with the focal spot of the cavity probe laser. It may also be necessary to move the oven occasionally during this procedure.

At this point this iris I2 is closed down to a small fraction of the full aperture, a repetitive ramp voltage is applied to the cavity, and the count rate of PMT3 displayed on an

oscilliscope vs. cavity tuning. Fine adjustments are made to the position of the excited atoms until a modulation in the count rate vs. cavity tuning is evident. Next the iris I2 is opened all the way up, and the modulation becomes very weak. This modulation is peaked up by moving the atoms along the cavity axis, by simultaneously displacing A2 and the pump laser along the cavity axis. (It may be convenient to do this by opening up the iris I2 in stages.) Again, it may be necessary to move the oven during this procedure.

Eventually, a strong modulation in the count rate of PMT3 vs. cavity tuning will be observed with the iris I2 all the way open. At this point, the cavity alignment, oven position, aperture A2 and pump beam postions are all adjusted to optimize the size of the signal and to give the deepest modulation possible, and the alignment is complete.

V.B. Experimental Results - Cavity Spontaneous Emission Rate vs. Cavity Tuning.

The experiment was first carried out in a manner similar to that of the ytterbium experiment, i.e. the laser frequency is locked to the ^{138}Ba resonance, and the flourescence intensity out the end and out the sides of the cavity is recorded as a function of cavity tuning. The results of this experiment are shown in Fig. 5.9. Trace (a) shows the count rate $\gamma_{cav}^{(1)}$ for light emitted out the end of the cavity with the cavity open, and trace (b) shows the calibration of the free space rate into the same solid angle $\gamma_{free}^{(1)}$. Trace (c) shows the counting rate for light emitted out the sides of the cavity with the cavity open, recorded simultaneously with trace (a). Finally, trace (d) shows the count rate for light emitted out the sides of the cavity, with the cavity blocked, thus showing the free space rate into the same solid angle as (c).

In plotting the data, two corrections have been applied. First, the background counting rate (observed with the laser detuned from resonance) of 150 counts/s for (a) and (b), and of 480 counts/s for (c) and (d), was subtracted from the raw data. Second, the signals are normalized by the intensity recorded by PMT1 to correct for small changes in laser intensity and atomic beam density.

Just as in the Yb case, the spontaneous emission rate of the atom into the cavity is enhanced when a cavity mode is tuned to the ^{138}Ba resonance, and inhibited when it is detuned. The observed enhancement factor is approximately 2.0, and the observed inhibition factor approximately 3.1.

The intensity of light emitted out the sides out the cavity displays a modulation with cavity tuning, as in the Yb case. In this case, however, the amplitude of the modulation is much larger, about 35%, so that the modulation may be observed directly, without the use of a lock-in technique. Also, by comparing the data (c) with the data (a), the sign of the modulation may be directly determined: the intensity out the sides of the cavity decreases when the spontaneous emission rate into the cavity incareases. Again, this is due to the fact that the excited state population decreases, due to an increase in the total decay rate. Finally, by comparing the data (c) with the corresponding free space intensity of trace (d), the absolute change in the total spontaneous emission rate may be determined. It is evident from this data that the total spontaneous emission rate is increased when the cavity is on resonance, and decreased when the resonator is off resonance.

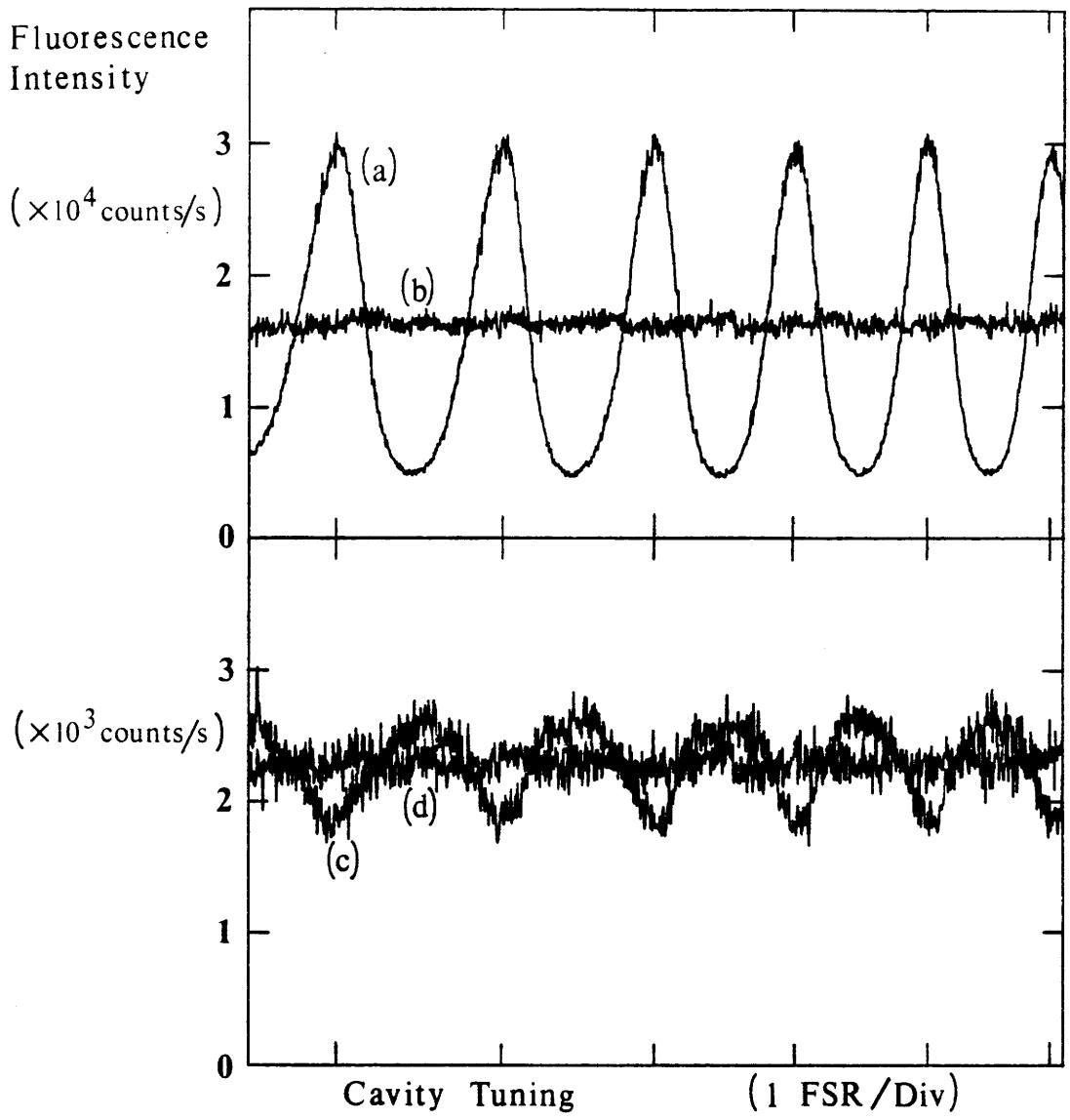

Fig. 5.9. Detected photon counting rate vs. cavity tuning. (a) Rate emitted out the end of the cavity, cavity open. (b) Calibration of the free space rate into the same solid angle as (a). (c) Intensity out the sides of the cavity, cavity open. (d). Intensity out the sides of the cavity, cavity blocked.

V.C. Experimental Results - Spontaneous Linewidth and Frequency Shift.

The results of the previous experiment, like those of the Yb experiment, give only an indirect measure of the total rate, and no measure at all of the frequency shift. In this section we present direct measurements of the linewidth and frequency shift of the $^1S_0$ - $^1P_1$ transition of the ^{138}Ba atoms in a concentric resonator.

In this experiment, the cavity tuning is held fixed and the fluorescence intensity from all three channels is simultaneously recorded as a function of laser frequency. A typical set of such data is shown in Fig. 5.10. The top trace (a) shows shows the fluorescence intensity from region 1, detected by PMT1, the second trace (b) shows the fluorescence intensity out the ends of the cavity, detected by PMT3, and the third trace (c) shows the fluorescence intensity out the sides of the cavity, detected by PMT2.

For each such set of data, the peak intensity I, width W (full width at half maximum), and center frequency ω are measured for the signal from region 1 (I_{ref}, W_{ref}, and ω_{ref}), for that out the ends of the cavity (I_{end}, W_{end}, and ω_{end}), and for that out the sides of the cavity (I_{side}, W_{side}, and ω_{side}). From these measurements we also calculate the differences $\Delta\omega_{end} = \omega_{end} - \omega_{ref}$ and $\Delta\omega_{side} = \omega_{side} - \omega_{ref}$ between the center frequency of the atoms in the cavity and those in region 1.

There may exist a shift in center frequency between region 1 and region 2 even if the cavity is blocked, due to a slight difference in the residual Doppler shift. This shift occurs because each laser beam may not be perfectly perpendicular to the atomic beam, so that a small component of the atomic velocity appears along the laser beam propagation direction. In order to correct for this effect, we first measure the shifts $\Delta\omega_{side}^0$ and $\Delta\omega_{end}^0$ obtained with the cavity blocked. These are always found to be equal to within experimental error; we denote their average as $\Delta\omega_0$. We then subtract this contribution to the shift from the shifts with the cavity open, defining the new quantities $\Delta\omega_{end}' = \Delta\omega_{end} - \Delta\omega_0$ and $\Delta\omega_{side}' = \Delta\omega_{side} - \Delta\omega_0$. These new quantities give only the part of the shift induced by the cavity, with any Doppler effect subtracted out.

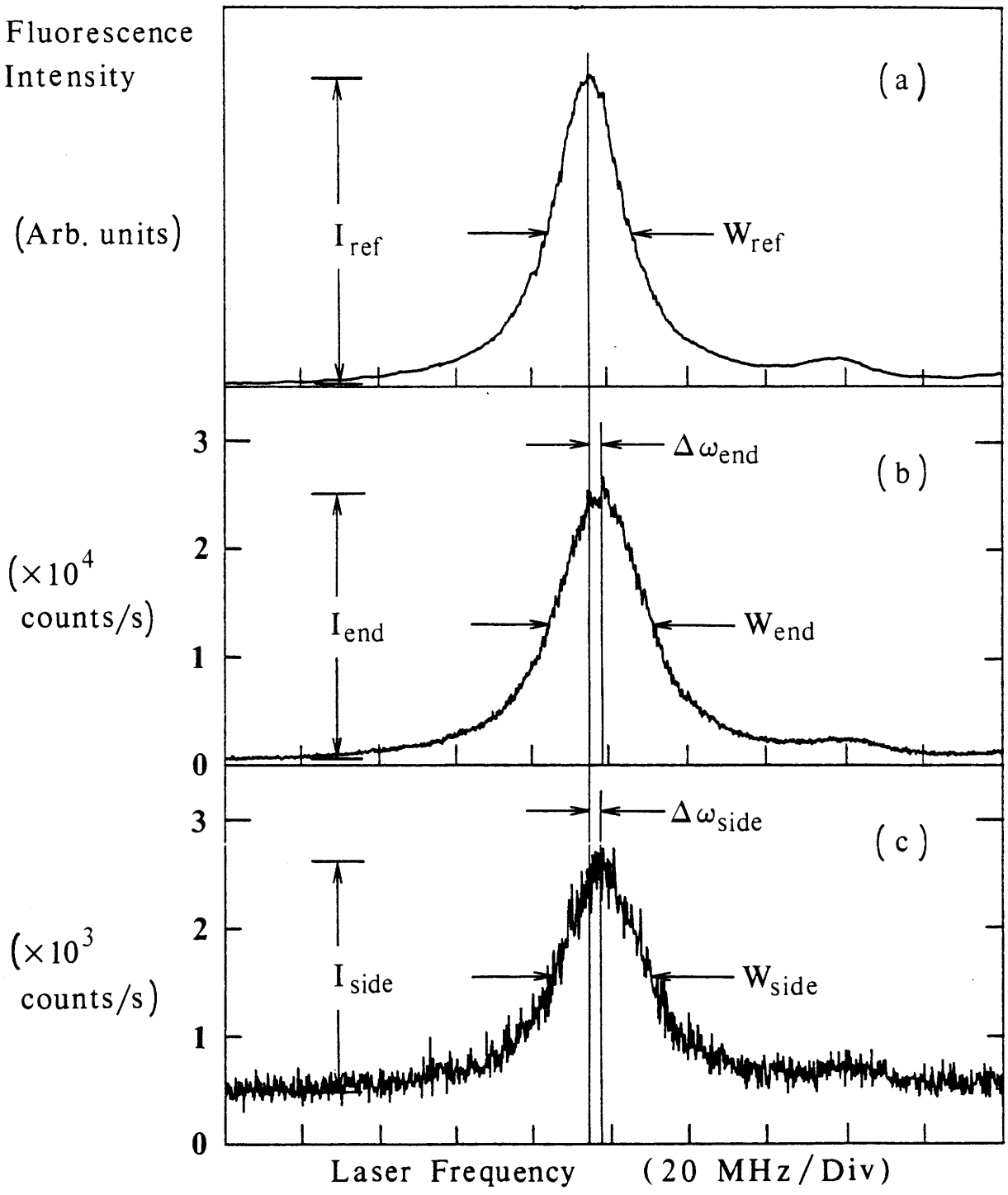

Fig. 5.10. Fluorescence intensity vs. laser tuning recorded by the three detectors, at a fixed cavity tuning.

The experiment is then repeated at a succession of equally spaced cavity tunings. Ideally, I_{ref}, W_{ref}, and ω_{ref} should be the same for all cavity tunings. Actually, ω_{ref} (i.e. the position of ω_{ref} with respect to the scan voltage input to the dye laser) drifts by several MHz from one scan to the next, due to a drift in the internal frequency reference of the dye laser. This is the primary reason for including region 1: the fluorescence from these atoms provides an accurate frequency calibration of the free space atomic resonance frequency to which the resonance frequency of the atoms in the cavity may be compared. In addition, I_{ref} varies by about 2% from one scan to the next, due to variations in dye laser power and atomic beam density, and W_{ref} varies by about 5%, due to variations in the frequency scan rate associated with drifts in the dye laser internal frequency reference. We use these values of I_{ref} and W_{ref} to obtain corrected values of $I_{side}' = I_{side}/\eta_I$, $I_{end}' = I_{end}/\eta_I$, $W_{side}' = W_{side}/\eta_W$, and W_{end}'/η_W at each cavity tuning. Here $\eta_I = I_{ref}/\overline{I_{ref}}$ and $\eta_W = W_{ref}/\overline{W_{ref}}$, where $\overline{I_{ref}}$ and $\overline{W_{ref}}$ and the values of I_{ref} are W_{ref} averaged over all cavity tunings.

The results of the experiment are shown in Fig. 5.11. In this set of data the intracavity aperture was in place, restricting the half angle of the mirrors to 22°, and the fraction of spontaneous emission intercepted by the mirrors to $f(\Delta\Omega_{cav}) = 0.106$. The top set of data (a) shows the observed peak height I_{end}', the second set (b) shows the observed peak height I_{side}', the third set (c) shows the observed linewidths W_{end}' and W_{side}', and the last set (d) shows the observed shifts $\Delta\omega_{end}'$ and $\Delta\omega_{side}'$, all as functions of cavity tuning. The Doppler shift was $\Delta\omega_0/2\pi = +1.8$ MHz in this case. The staight line in data set (a) shows the height $I_{free}^0 = I_{end}^0/(1 - R)$, where I_{end}^0 is the observed peak height with the cavity blocked; multiplying this quantity by 1/(1-R) gives the effective free space intensity into the same solid angle I_{free}^0. The straight lines in data sets (c) and (d) give the height I_{side}^0 and the width W_0 observed with the cavity blocked. (These values of I_{free}^0, I_{side}^0, and W_0 are based on an average of three scans with the cavity blocked.) The width $W_0 = \Gamma_{free} + \Gamma_0$ contains a contribution $\Gamma_0/2\pi = 5.0$ MHz to the broadening from sources other then the natural linewidth. This may be attributed to laser frequency jitter of approximately 1 MHz, a Doppler width of at least $(D/X)ku/2\pi = 1.5$ MHz, and a contribution from transit time broadening of approximately $u/2\pi\Delta x' = 4.4$ MHz.

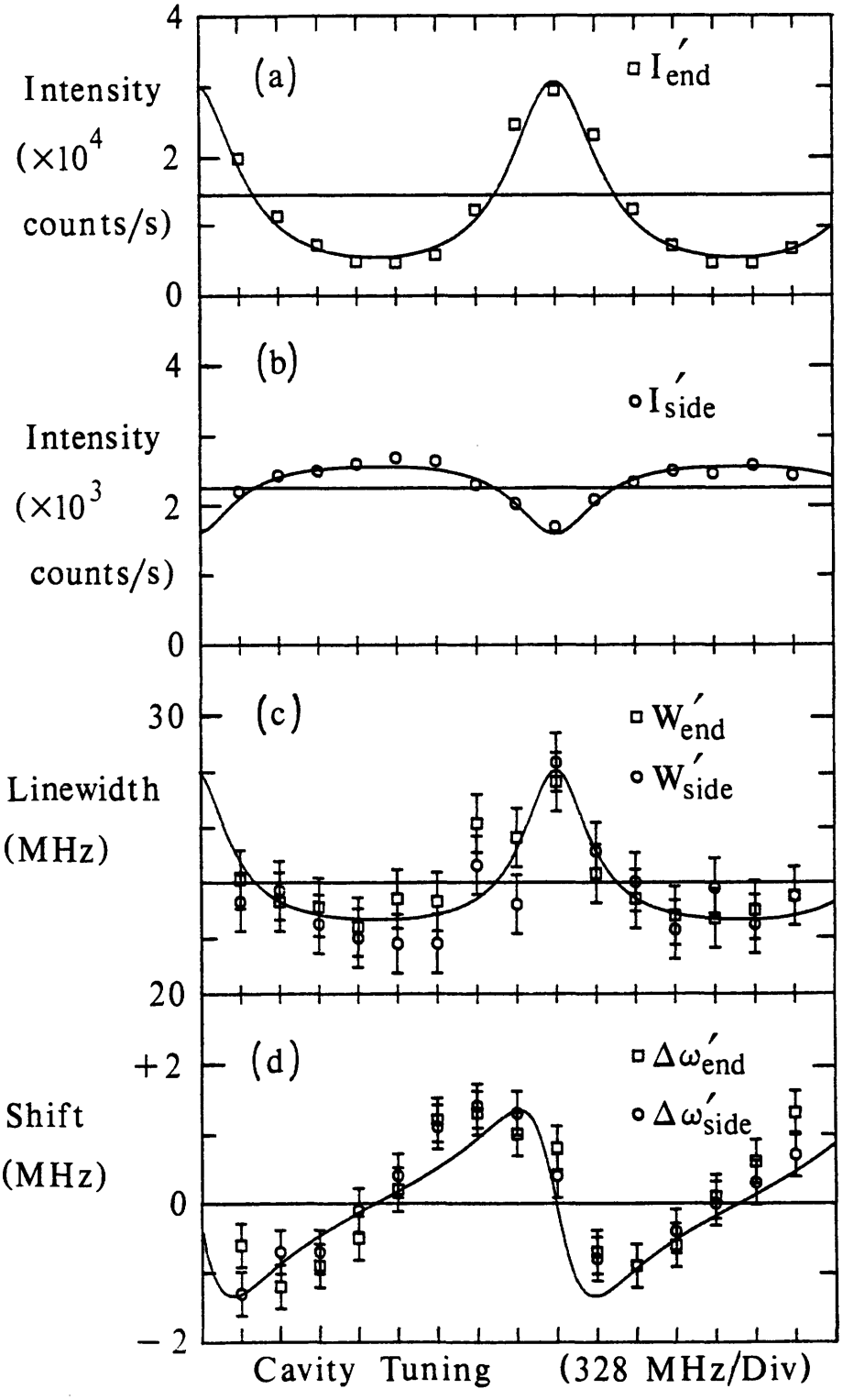

Fig. 5.11. Peak intensities, linewidths, and lineshifts of the fluorescence emitted by the atoms in the cavity, as a function of cavity tuning. The cavity length decreases from left to right.

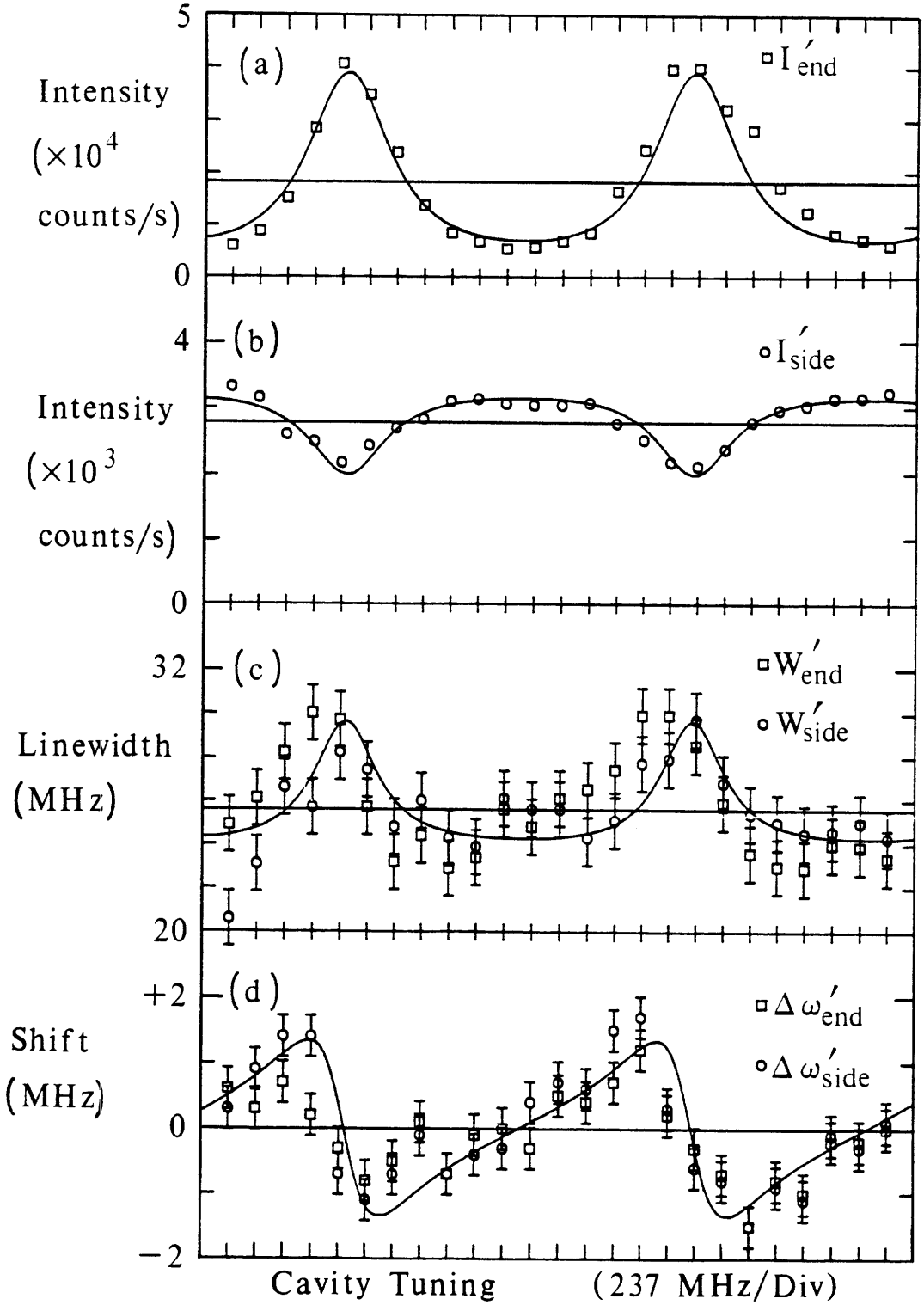

Fig. 5.12. Results of a second run of the experiment, again showing the peak intensities, linewidths, and lineshifts of the fluorescence emitted by the atoms in the cavity, as a function of cavity tuning.

A similar set of data from a different run of the experiment is shown in Fig. 5.12. In this case the intracavity aperture was also in, and the observed Doppler part of the shift was $\Delta\omega_0/2\pi = 0.0$ MHz. A greater number of cavity tunings was taken with the cavity open, and the values of I_{end}^0, I_{side}^0, and W_0 were based on an average of ten scans with the cavity blocked. In this case $W_0/2\pi = 25.6$ MHz implies a slightly larger additional broadening of $\Gamma_0/2\pi = 6.6$ MHz. The most likely explananation for the slightly greater broadening is that some extra Doppler broadening was present due to pump beam misalignment.

V.D. Analysis and Discussion.

The data presented in Figs. 5.11 and 5.12 clearly displays the behavior anticipated by the theory presented in chapter II and chapter III. When the cavity is tuned to resonance, as evidenced by the peak in the intensity I_{end}, the linewidth of the transition increases, relative to free space, and when the cavity is detuned from resonance it decreases. This measurement of a change in linewidth provides a very direct confirmation of a change in the total spontaneous emission rate. In addition, there exists a frequency shift that exhibits exactly the expected behavior: when the cavity is exactly tuned to resonance or halfway between resonances, the shift vanishes, and when the nearest cavity mode is tuned to the blue, the transition shifts to the red, and vice versa.

The data of Figs. 5.11 and 5.12, traces (a) and (b), is equivalent to that of Fig. 5.9; i.e., it displays the peak intensity out the end or side of the cavity as a function of cavity tuning. The peak intensity I_{side} out the side of the cavity is proportional to n_e, the average number of atoms in the excited state, whereas the intensity I_{end} out the ends of the cavity is proportional to $n_e\gamma_{cav}$. Again, γ_{cav} is the partial spontaneous emission rate of the atom into the cavity and according to the theory of section III.B should be given by $\gamma_{cav} = \gamma_{free}L(\omega_{EG})$. Under conditions of weak excitation, $n_e = n_0(\sigma I/\hbar\omega\Gamma)$. In contrast to the Yb case, the Ba transition is homogeneously broadened, and the cross section $\sigma = 8\pi k\mu^2/(\hbar(\Gamma+\Gamma_0))$ is no longer independent of the total spontaneous emission rate Γ. Thus $n_e \propto 1/(\Gamma(\Gamma+\Gamma_0))$, rather than simply $1/\Gamma$.

Taking these factors into account, we therefore expect that the experimentally measured quantities should be fit by the functions

$$I_{side}' = I_{side}{}^0\frac{\Gamma_{free}(\Gamma_{free} + \Gamma_0)}{\Gamma_{cav}(\Gamma_{cav} + \Gamma_0)} \tag{5.9}$$

$$I_{end}' = I_{free}{}^0\frac{\Gamma_{free}(\Gamma_{free} + \Gamma_0)}{\Gamma_{cav}(\Gamma_{cav} + \Gamma_0)}\,L(\omega_{EG}) \tag{5.10}$$

$$W_{end}' = W_{side}' = (\Gamma_{cav} + \Gamma_0) \tag{5.11}$$

$$\Delta\omega_{end}' = \Delta\omega_{side}' = \Delta\omega_{cav}\,, \tag{5.12}$$

where, according to eqs. (3.71) and (3.86)

$$\Gamma_{cav} = \Gamma_{free}(1 + (L(\omega_{EG}) - 1)f(\Delta\Omega_{cav})) \tag{5.13}$$

$$\Delta\omega_{cav} = \Gamma_{free}\frac{f(\Delta\Omega_{cav})}{4}\frac{F\sin(2\omega_{EG}L/c)}{1 + F\sin^2(\omega_{EG}L/c)}\,, \tag{5.14}$$

and where

$$L(\omega_{EG}) = \frac{\sqrt{1 + F}}{1 + F\sin^2(\omega_{EG}L/c)} \quad . \tag{5.15}$$

Note that, since the variation in the excited state population is substantial, it is important to take into account its effect on I_{end}', as well as on I_{side}'.

Equation (5.13) simply expresses the fact that the observed width should consist of the sum of the natural linewidth, plus whatever other contributions Γ_0 to the broadening may be present. (Clearly these other sources do not depend on whether the cavity is blocked or unblocked.) Also, we expect that the observed shift with Doppler effects subtracted off should be simply given by the calculated shift $\Delta\omega_{cav}$.

The curved line in each set of data of Fig. 5.11 shows the fit by the functions of eqs. (5.9) - (5.12). The known value of $\Gamma_{free}/2\pi = 19.0$ MHz, and the measured values of $f(\Delta\Omega_{cav}) = .106$, $\Gamma_0/2\pi = 5.0$ MHz, and of I_{end}^0 and I_{free}^0 were used. The parameter F was adjusted to produce a good fit to the data at F = 8.0.

Ideally, the data should be fit with the value of F = 21.0 calculated on the basis of mirror reflectivity. However, in the derivation of Eqs. (5.9) - (5.12), it was assumed that the mirrors have perfectly shaped surfaces, that the atoms are located exactly at the center of the cavity, and that Doppler shifts are negligible. If these conditions are not satisfied, the cavity lineshape function $L(\omega)$ must be modified. In general these effects will broaden the peaks in $L(\omega)$ and reduce the amplitude of its modulation. As a first approximation, these effects may be accounted for by a reduced value of F.

The ideal cavity linewidth (FWHM) is $\Delta\nu_{cav}^{(calc)} = 2\Delta\nu_{FSR}/\pi\sqrt{F} = 420$ MHz. The linewidth corresponding to the "observed" value of F = 8.0 is $\Delta\nu_{cav}^{(obs)} = 680$ MHz, which corresponds to an additional 260 MHz of broadening. This can be accounted for from the three sources of broadening mentioned previously. First, even with the cavity perfectly aligned and illuminated by a laser, the observed linewidth is 500 MHz. Thus, there is an additional 80 MHz of broadening which may be attributed to mirror surface aberrations. Second, the atoms are distributed over a region of 20 μm extent, and may not be exactly aligned to the center of the cavity. Thus there will a distribution of values of Δ of order ± 10 μm, which according to Eq. (5.2) corresponds to an additional broadening from this source of about 40 MHz. Finally, the atoms have a mean thermal velocity of $u = 2.4 \times 10^4$ cm/s. Although this results in no Doppler shift for the light rays striking the

portion of the mirror forming a stripe in the y-z plane, the remainder of the mirror does see the atomic resonance as Doppler shifted, by an amount $\pm k u \sin\theta$, where θ is the angle between the light ray and the y-z plane. The maximum value of θ is 22°, and if we take half that angle $\theta = 11°$ as "average" angle subtended of the light rays, we find that the atom-cavity interaction will experience a broadening due to this effect of $(ku/2\pi)\sin\theta = 80$ MHz. The sum of these three contributions is 200 MHz, which is close the the "observed" value of 260 MHz. Therefore, the value of F = 8.0 used to fit the data is quite reasonable, being of a proper magnitude to take into account these additional sources of broadening.

The total magnitude of the change in the spontaneous emission rate may calculated from the function (5.13), or read off directly from the linewidth data. On resonance, we observe that the total rate increases by the fractional amount of $(\sqrt{1+F} - 1)f(\Delta\Omega_{cav}) = 4.0$ MHz/19 MHz = +21%. Off resonance, it is inhibited by a factor of $(\frac{1}{\sqrt{1+F}} - 1)f(\Delta\Omega_{cav}) = -1.34$ MHz/19 MHz = -7.1%. This compares with the values of +39% and -7.9% expected on the basis of the ideal limit F = 21.

V.E. Experimental Results for Very Large Solid Angle.

Throughout most of the experiments, the intracavity aperture A was installed in the resonator, which restricted the resonator solid angle to that subtended by the lenses L1 and L2. This insured that the detector PMT3 was able to record the fluorescence from the full solid angle over which the spontaneous emission is modified. However, in principle it should be possible to observe much larger changes in the linewidth and and shift by removing the aperture. In this case, the cavity subtends a half angle $\theta_M = 42°$, corresponding to $f(\Delta\Omega_{cav}) = 0.34$, which is 3.2 times as large as the previous value. Thus all else being equal, we would expect on the basis of the previous results to see an increase of the natural linewidth of +12.8 MHz, a decrease of - 4.3 MHz, and shifts of $\pm$ 4.3 MHz.

The results of the experiment with the aperture removed are illustrated in Fig. 5.13. In this case the shift $\Delta\omega_0/2\pi = +0.4$ MHz and $\Gamma_0/2\pi = +6.0$ MHz. It is apparent that no dramatic increases in the linewidth change or shift are observed; at most these quantities increase by perhaps 30%. It also is not possible to obtain a good fit to all four sets of data simultaneously. A reasonable fit to the lower three sets only may be obtained with a very much reduced value of F. The solid curves in Fig. 5.13 show the fit obtained for F = 1.6, where again the measured values of $f(\Delta\Omega_{cav}) = 0.34$, Γ_{free}, Γ_0, I_{free}^0, and I_{side}^0 are used. It is possible to obtain a better fit if both $f(\Delta\Omega_{cav})$ and F are taken as adjustable parameters; the dotted curve shows the fit obtained for F' = 6.0. and $f'(\Delta\Omega_{cav}) = 0.15$.

The discrepancy between the theory and the experiment cannot be ascribed only to the increased Doppler broadening experience by the parts of the cavity outside the view of PMT3. Taking the "average angle" subtended by the mirror as $\overline{\theta} = \theta_M/2 = 21°$, we find that the Doppler broadening is of the order of 160 MHz, which is less than the ideal cavity linewidth of 420 MHz, and is very much less than the amount necessary to account for the broadening seen in the data of Fig. 5.13.

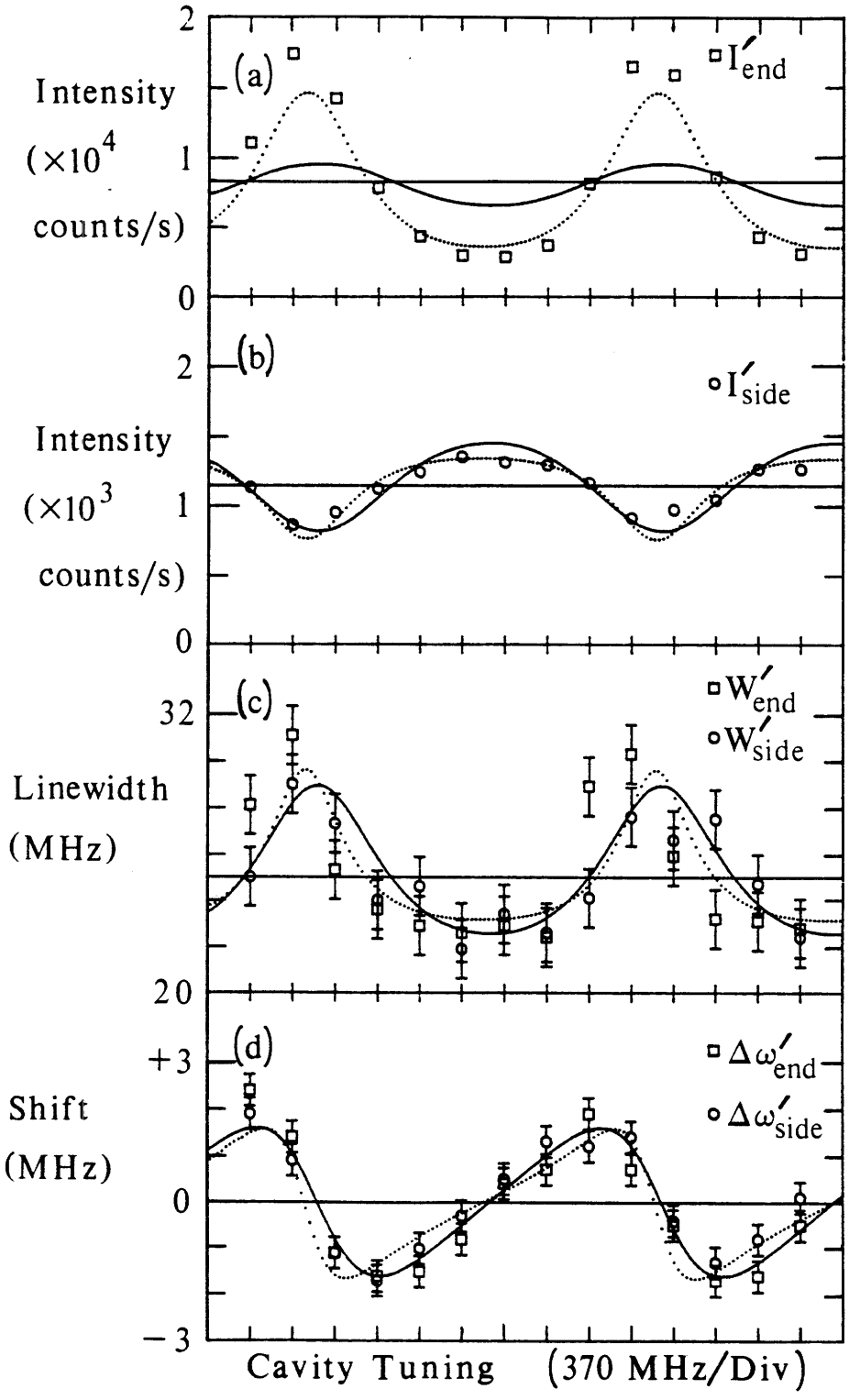

Fig. 5.13. Results the experiment with the full cavity aperture open, corresponding to $f(\Delta\Omega_{cav}) = 0.34$.

The discrepancy is also probably not due to poor alignment of the part of the cavity not viewed by the lens. The cavity was first aligned using the visible central part of the cavity; this procedure is very sensitive and should produce an alignment which is almost exactly right for the mirror as a whole. Then, the modulation of the sideways intensity vs. cavity tuning was displayed on an oscilliscope and an exhaustive search was made for cavity and atom alignments which improved the depth of the modulation. In no case was a significant improvement over the results shown in Fig. 5.13 obtained.

The most likely explanation for the discrepancy is that the outer parts of the mirror deviate from the ideal spherical shape. This would cause those parts of the mirror to exhibit alternating bands of constructive and destructive interference, the effect of which would average to zero, and essentially limit the useful solid angle of the mirror to only the central, spherical part. Note that the detector PMT3 cannot see the outer parts of the mirror, and therefore the first set of data I_{end} only records the light from the "good part", whereas the other three sets of data measure the effect of the cavity as a whole. From this point of view the quantity $f'(\Delta\Omega_{cav})$ can be viewed as the size of the "effective cavity aperture", and F' as the "effective finesse" of the cavity over this aperture.

Ideally, one would like to obtain a lens which views a much larger solid angle. Unfortunately, there is no commercially available lens which has a significantly larger aperture than the camera lenses used, and also has the required resolution and back focal length. An $f/0.78$ lens ($\theta_L = 32.5°$; $f(\Delta\Omega_{cav}) = 0.22$) which can meet these criteria has been designed[76] and may be soon added to the experiment; the design of a significantly larger aperture lens meeting these critera appears to be a formidable task.

V. F. Effect of Atomic Displacement.

According to eq. (5.2), a displacement of the atoms from the center of the cavity should have a significant effect on the experimental results. This includes both a shift in the apparent resonance frequency of the cavity and a significant increase in the broadening of the atom-cavity interaction. This broadening is due to both the effect of the distribution of atomic positions and to the variation of the angle ψ at which the light rays are striking various parts of the mirrors.

In order to test this, an experiment was carried out in which the position of the excited atoms was deliberately displaced from the center of the cavity. The experiment was carried out in a manner similar to that of the Yb experiment; i.e., the laser frequency was locked to the center of the ^{138}Ba resonance line, and the fluorescence intensity I_{end} emitted out the ends of the cavity, and the fluorescence intensity I_{side} out the sides of the cavity were recorded as a function of cavity tuning. The intracavity aperture A was in place during these measurements. Again, note that the intensity I_{end} is essentially a direct measure of the partial spontaneous emission rate of the atoms into the cavity, whereas the intensity I_{side} is a measure of the change in the total spontaneous emission rate Γ, according to the approximate relation $2\Delta\Gamma/\Gamma \cong - \Delta I_{side}/I_{side}$.

The results of the experiment are illustrated in Fig. 5.14. The atoms were first aligned to the center of the cavity as carefully as possible; the resulting modulation in the intensities I_{side} and I_{end} are shown in the top set of data. Then, the lens L4 was displaced in the x-direction by calibrated amounts, thus displacing the excited atoms by the same amount. The successive data sets in Fig. 5.14 show the results obtained for displacements of Δ = 10 μm, 20 μm, 40 μm, 60 μm, 80 μm, and 120 μm.

During these measurements, the cavity length was drifting slightly due to thermal expansion. In order to correct for this, after the last set of data the atoms were returned to the center of the cavity, and the amount by which the peaks drifted from their position in the first data set was measured. Then, assuming that the drift was a linear function of time, the amount by which the cavity length had drifted for each of the traces in Fig. 5.14 was calculated, and the data for each trace was offset from the previous ones to compensate for that drift. The staight vertical line through all the data sets indicates the the cavity length at which the central peak occured for $\Delta = 0$.

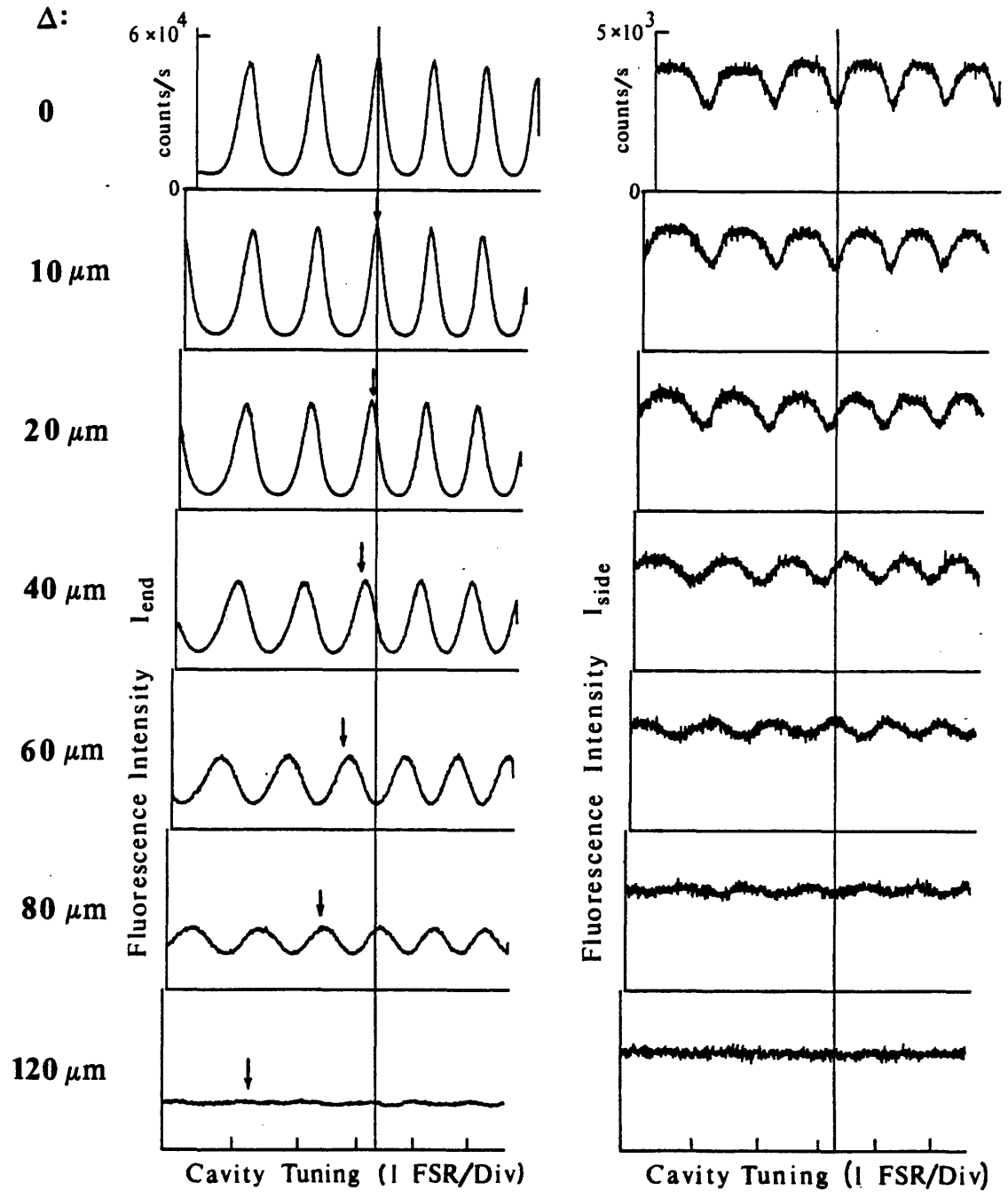

Fig. 5.14. Fluorescence intensity as a function of cavity tuning, at various diplacements Δ of the atoms from the center of the cavity. Left hand column: Intensity I_{end} out the end of the cavity. Right hand column: Intensity I_{side} out the side of the cavity. In each scan, the cavity length increases from left to right.

The displacement clearly has a dramatic impact on the modification of the spontaneous emission rate. Even for a displacement of only 10 μm, there is a discernable degradation in the depth of the modulation of the spontaneous emission rate. For a displacement of

60 μm, the modulation is the spontaneous emission rate is noticably reduced, and at a displacement of 120 μm, it has practically vanished.

The broadening which is evident in the data of Fig. 5.14 may be attributed to two sources. First, since the frequency shift $\delta\nu = - c\Delta^2/2\lambda a^2$, where $\sin^2\psi \cong 1$, a distribution in the values of Δ of width $d\Delta$ causes a distribution in the frequency shifts of width

$$d_\Delta(\delta\nu) \cong \frac{c(d\Delta)}{\lambda a^2}\Delta \tag{5.16}$$

In our case $d\Delta \cong 17$ mm is set by the width of the pump laser beam. Second, there is a distribution of angles ψ, ranging in our case from $\psi = 68°$ to $\psi = 90°$. This gives rise to a width in the frequency shift of approximately

$$d_\psi(\delta\nu) \cong \frac{c\Delta^2}{2\lambda a^2}(\sin^2 90° - \sin^2\overline{\psi}), \tag{5.17}$$

where $\overline{\psi}$ is the "average" angle ψ. If we take $\overline{\psi} = 79°$, this gives $d_\psi(\delta\nu) = .036 \times c\Delta^2/2\lambda a^2$. In our case the broadening is primarily from the distribution of atomic positions. For example, at $\Delta = 40$ μm, we obtain $d_\Delta(\delta\nu) = 588$ MHz and $d_\psi(\delta\nu) = 25$ MHz. Note that $\Delta = 40$ μm is the displacement at which the broadening is of the order of the cavity linewidth, which appears consistent with the data.

In addition to the broadening effect, the peaks also appear shifted to shorter cavity lengths. This can be interpreted on the basis of eqs. (5.1) and (5.2): the resonance condition is that the ray path length L_{rt} must be equal to an integer number of wavelenths λ, so in order to compensate for the additional path length introduced by the atomic displacement, the mirrors must move a little closer together. The arrows in Fig. 5.14 show the positions of the peaks predicted by eq. (5.2). Reasonable agreement is obtained with the observed shifts; the small discrepancy is presumably arises because the cavity drift was not exactly linear in time.

The data of Fig. 5.14 emphasize in a very dramatic way the importance of a well-localized, carefully positioned sample of atoms. In fact, these data are very much like what one sees during system alignment, and similar behavior is observed for displacements in the y and z directions. It should also be emphasized that the only reason that significant modulation is observed for displacements as large as 80 μm is that the atomic sample is small. If the sample size itself was as large as 80 μm, very little modulation would be observed. (This was in fact the case in preliminary experiments, in which the size of the sample was chosen too large.)

CHAPTER VI

DISCUSSION AND CONCLUSION.

In the preceding chapters, it has been demonstrated that the emission rates, linewidths, and frequencies of radiation by an atom may be modified when the atom is placed in an optical resonator. It was found that such effects may be interpreted from both classical and quantum-mechanical points of view. In this chapter we discuss a number of issues which are raised by these results, mention applications in which such effects may be important, and finally discuss several possible directions for future research.

VI.A. Classical vs. Quantum Interpretation.

We have seen that the results of our experiments may be interpreted equally well from two very different points of view: a simple classical picture, and a more detailed and rigorous quantum mechanical picture. In the classical picture, the atom is viewed as equivalent to a classical dipole oscillator. The radiation emitted by the dipole is reflected by the cavity mirrors and refocussed onto the atom; this produces an additional radiation reaction force on the dipole which accounts for its modified decay rate and for a shift in its natural frequency. On the other hand, in the quantum picture, the atom together with all modes of the radiation field must be viewed as a combined quantum-mechanical system. The atom-field coupling gives rise to a shift in the energy levels of the system, and if energy is initially stored in the atom alone, to a decay of energy from the atom to the field. An optical cavity modifies this atom-field coupling, and therefore also modifies the decay rate and level shift. This level shift appears as a shift in the resonant frequency of transitions between two levels.

In view of the fact that the result from the classical picture agrees with that of the quantum mechanical one, the question arises as to what extent the classical point of view is correct, and how necessary it is to give a quantum mechanical description. Of course, the simplest answer to this question is that the classical model fails in all of the usual ways associated with free space radiation: it cannot account for the discrete oscillation frequencies of the atom, and in general gives the wrong value of the total decay rate. Even if one somehow accounts for these discrete frequencies in a semiclassical way, it cannot explain the radiation by an atom in a pure excited state, while simultaneously accounting for the stability of the atomic ground state.

Even if these issues are swept under the rug, the classical picture fails in another way, as illustrated in Fig. 6.1. Suppose an atom has a resonance transition in the blue from level $|G\rangle$ to level $|E_1\rangle$ and a second resonance transition in the red from level $|E_1\rangle$ to level $|E_2\rangle$, and suppose this atom is placed in a cavity which reflects blue light and transmits red light. According to the quantum mechanical description, the level $|E_1\rangle$ is shifted slightly in energy due to a change in the atom-field coupling for frequencies near the blue resonance. Therefore the frequency of the red transition from $|E_1\rangle$ to $|E_2\rangle$ is also slightly shifted. It would be very difficult to account for this shift from any classical or semiclassical point of view, since the cavity doesn't even reflect the red light.

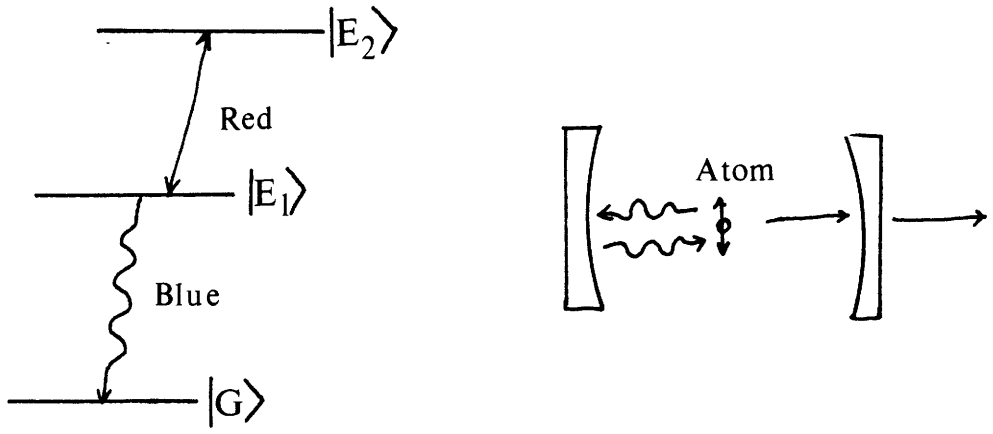

Fig. 6.1. Failure of the classical model.

Therefore, the classical model must be regarded as an incomplete picture at best. Nevertheless, it does contain an element of truth, particularly for a the case of a weakly excited two-level atom. This is because the weakly excited two level atom does behave essentially as a classical dipole oscillator, if account is taken of "oscillator strength" of the atom.[76] Further, the radiation from a two-level atom very nearly in its ground state is coherent (i.e., its phase follows from that of the expectation value of the atomic dipole moment), and has an amplitude which is correctly given by the classical dipole formula.[77] Therefore, it is not surprising that the classical picture gives the correct result for this case, whereas it fails for more general cases, such as that illustrated in Fig. 6.1.

VI.B. How Big Can the Cavity Be?

An important conclusion of this thesis is the the wavelength of the emitted radiation does not set the scale for the maximum size of a cavity that can significantly influence the total radiation rate of an atom. This naturally leads to the question of what does determine the upper limit on the size of the cavity.

The simplest case to consider is that in which some mechanism other then pure radiative broadening, such as Doppler or collision broadening, limits the linewidth of the atoms to a minimum value γ_a. Clearly in this case the cavity will have an effect only so long as the free spectral range $\Delta\omega_{fsr} = \pi c/L$ is greater than γ_a. This implies that

$$L < \pi c/\gamma_a \tag{6.1}$$

must be satisfied. If it is not, then many cavity modes lie within the atomic linewidth, effectively forming a continuum of modes whose effect is the same as free space. Mathematically, this can be included in the Wigner-Weisskopf theory by adding a factor $i\gamma_a$ to the atom field detuning $\omega_{EG} - \omega_k$.

A more fundamental limit concerns the case in which the broadening of the transition is purely radiative. In this case the question of how large the cavity can be is somewhat more subtle, so in order to simplify the following discussion we restrict our attention to the case of a complete spherical cavity. Many of the same conclusions apply to open resonators as well.

We consider that a two-level atom with excited state $|E\rangle$ and ground state $|G\rangle$ is located near the center of a complete spherical cavity of diameter L and reflectivity R. According to the theory of section III.C, provided the atom is displaced from the enter of the sphere by a distance r_a such that $\lambda << r_a << \sqrt{\lambda L}$, it interacts only with the lowest order transverse modes of the sphere, whose frequencies are degenerate, with values $\omega_n = n\pi c/L$, where n labels the value of a radial mode index. It is easy to demonstrate that, at a fixed value of cavity tuning, the combined effect of all transverse modes having resonance frequency ω_n is equivalent to that of an "effective single mode" of mode volume $V_{eff} = 3\lambda^2 L/4\pi$ at this same frequency. From here on we shall refer to these "effective single modes" simply as the "cavity modes". We suppose that the atom-cavity system is initially in the state $|E;0\rangle$; i.e. the atom is excited and the field is in the vacuum state. Its state at a later time t can be written as,

$$|\Psi(t)\rangle = a_0(t)e^{-i\omega_0 t}|E;0\rangle + \sum_{n=1}^{\infty} a_n(t)e^{-i\omega_n t}|G;n\rangle, \tag{6.2}$$

where the state $|G;n\rangle$ denotes a state in which the atom is in the ground state and one photon is in the n^{th} mode. In the same manner that was discussed in section III.A, this leads to the amplitude equations

$$\dot{a}_n = -g\, a_0\, e^{+i(\omega_n - \omega_{EG})t} \tag{6.3a}$$

$$\dot{a}_0 = \sum_n g\, a_n\, e^{-i(\omega_n - \omega_{EG})t}, \tag{6.3b}$$

where

$$g = \frac{\mu}{\hbar}\sqrt{\frac{2\pi\hbar\omega}{V_{eff}}} = \sqrt{\frac{c}{2L}\Gamma_{free}} \tag{6.4}$$

is the atom field coupling constant for each of the cavity modes and ω_{EG} is the unperturbed transition frequency between $|E\rangle$ and $|G\rangle$, and Γ_{free} the usual free space decay rate.

We focus on the solutions to eqs. (6.3) in the case where one of the cavity modes, say for n = p, is exactly resonant ($\omega_p = \omega_{EG}$), and first consider the case where all the modes with $n \neq p$ are weakly excited and may be neglected. As discussed in section I.B.4, the interaction between the atom and the p^{th} single mode will follow two types of behavior, depending on the relative values of g and the cavity linewidth $\gamma_c = c(1-R)/L$. The effect of cavity damping may be included in an approximate way in eqs. (6.3) by adding a phenomenological damping constant; doing this and neglecting all but the p^{th} mode, we find that

$$\ddot{a}_0 + \frac{\gamma_c}{2}\dot{a}_0 + g^2 a_0 = 0. \tag{6.5}$$

This equation has the solution $a_0 = e^{\alpha t}$, with

$$\alpha = -\frac{\gamma_c}{4} \pm \frac{1}{2}\sqrt{\frac{\gamma_c^2}{4} - 4g^2}\ . \tag{6.6}$$

For the low Q limit $g << \gamma_c$, this can be written as

$$|a_0(t)|^2 = e^{-\Gamma_{cav}t}, \tag{6.7}$$

where

$$\Gamma_{cav} = \frac{4g^2}{\gamma_c} = \frac{2}{1 - R}\Gamma_{free}. \tag{6.8}$$

This is just the previous result for cavity enhanced spontaneous emission. For the high Q limit, $g >> \gamma_c$, the solution becomes

$$|a_0(t)|^2 = \cos^2(gt)\ , \tag{6.9}$$

which is just the result for the vacuum Rabi oscillation referred to earlier.

Consider now what happens as the size of the cavity is varied, with its reflectivity held fixed. Since $g \propto 1/\sqrt{L}$ and $\gamma_c \propto 1/L$, it follows that $g/\gamma_c \propto \sqrt{L}$, and therefore the interaction of the atom with a single cavity mode always eventually reaches the high Q limit, for the cavity size sufficiently large. The boundary between the two regimes occurs for $g = \gamma_c$, which is equivalent to

$$\Gamma_{cav} = 4\gamma_c \,. \tag{6.10}$$

In other words, *the boundary between the high and low Q regimes occurs when the enchanced spontaneous emission rate of the atom into the cavity is of the order of the cavity linewidth.*

We next consider under what conditions the adjacent cavity modes ($n \neq p$) will be excited. According to eqs. (6.3a), the solution for early times for a_n ($n \neq p$) is given by

$$|a_n(t)|^2 = \frac{4g^2\sin^2((\omega_n - \omega_0)t/2)}{(\omega_n - \omega_0)^2} \quad , \tag{6.11}$$

where for sufficiently early times $a_0 \cong 1$. Taking the time average of the $|a_n(t)|^2$ and summing over all $n \neq p$, we find

$$\sum_{n\neq p} \overline{|a_n(t)|^2} = \frac{\pi^2}{3}\left(\frac{g}{\Delta\omega_{fsr}}\right)^2 , \tag{6.12}$$

where $\Delta\omega_{fsr} = \pi c/L$ is the spacing between adjacent cavity modes. We see that the combined effect of all the adjacent cavity modes will be small provided that $g << \Delta\omega_{fsr}$. This condition may be rewritten as

$$\frac{L}{c} << \frac{2\pi}{\Gamma_{free}} \,. \tag{6.13}$$

In other words, *the boundary between the single and multimode excitation occurs when the round trip time of light in the cavity is of the order of the free-space lifetime.* Note that, since $\Delta\omega_{fsr} > \gamma_c$, *the boundary between the high and low Q regimes always occurs in the single mode limit,* as previously assumed.

From these considerations, we see that the behavior of the radiating atom in the cavity may be divided into four distinct regimes, depending on the cavity size, as illustrated in Fig. 6.2. For very small L ($L << \lambda$), the cavity has no modes available at all near ω_{EG}, and the spontaneous emission rate is inhibited. In this case, the atom may be anywhere inside the resonator. This is the regime which has been previously studied.

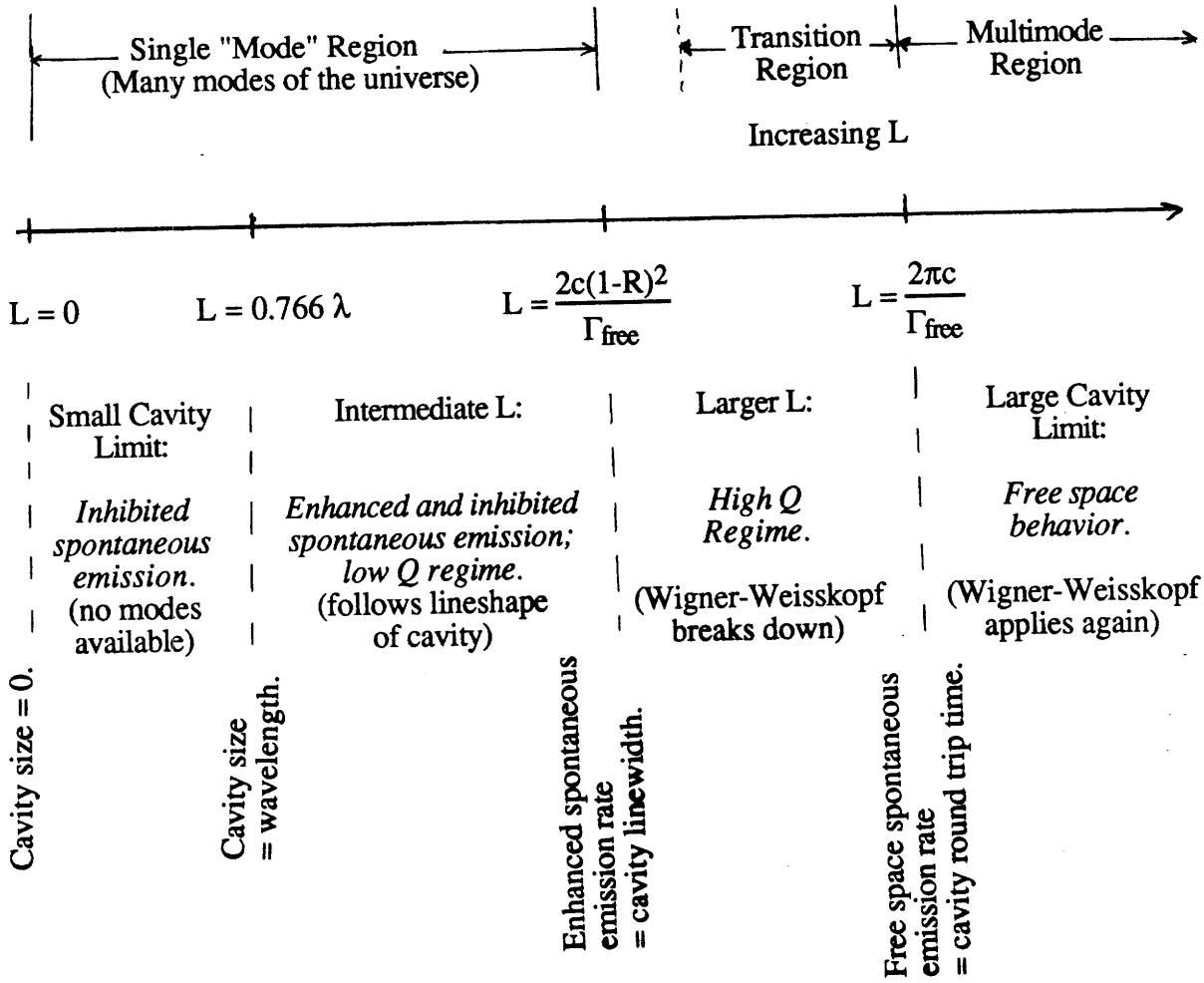

Fig. 6.2. Four regimes of spontaneous emission in a spherical cavity.

For larger size cavities ($\lambda < L < 2c(1-R)^2/\Gamma_{free}$), enhanced and inhibited spontaneous emission in the low Q limit is obtained, as has been discussed extensively in this thesis. Throughout this region, the atom interacts with one of the cavity modes at a time, and cavity damping plays an essential role. From the point of view of section III.C, the atom interacts with many "modes of the universe", and the Wigner-Weisskopf approximation holds, in the sense that these "modes of the universe" form a smooth continuum. The total spontaneous emission rate follows the lineshape of the cavity.

For still larger L satisfying $2c(1-R)^2/\Gamma_{free} < L < 2\pi c/\Gamma_{free}$, the individual cavity modes become so sharp that the Wigner-Weisskopf approximation breaks down. Again, the boundary between this region and the previous one is that the enhanced spontaneous emission rate of the atom exceeds the cavity linewidth. For cavity sizes near the lower limit

$2c(1-R)^2/\Gamma_{free}$, the interaction of the atom is still essentially with a single mode, and we have "spontaneous emission" in the high Q limit; i.e. vacuum Rabi oscillation. However, as the cavity size approaches the upper limit $2\pi c/\Gamma_{free}$, the atom begins to excite multiple modes of the cavity, resulting in a complex, high Q, multimode behavior. The extent of the high Q region depends on the reflectivity of the cavity. For very lossy cavities there is very little gap between the onset of the high Q limit and the onset of multimode behavior, whereas for very high finesse cavites, the high Q region extends very far into the single mode region. For $1/(1-R) > \sqrt{2c/L\Gamma_{free}}$, the cavity finesse is so high that the high Q region extends all the way through to the small cavity limit, and there is no low Q behavior for any cavity size.

Finally, for $L > 2\pi c/\Gamma_{free}$ (i.e., the cavity round trip time greater then the free space lifetime), the cavity modes become so closely spaced that many cavity modes are excited by the atom. In this case we are essentially back to the free space Wigner-Weisskopf limit. Whereas in the low Q limit the "modes of the universe" formed a smooth continuum, now the cavity modes themselves form a smooth continuum, and therefore the spontaneous emission rate does <u>not</u> follow the lineshape of the cavity. However, even in this regime it does not follow that the atom returns entirely to its free space behavior. This is because the equally spaced cavity modes remain coherently phased (assuming no cavity loss). This implies that at later times a rephasing of the atom-field wavefunction may occur in such a way the the excitation returns to the atom. Simply put, the wave emitted by the atom will eventually reflect off of the sphere, return back to the atom, and reexcite it. However, for times short compared to the cavity round trip time, the discrete nature of the cavity mode density is not apparent, and the behavior is essentially the same as free space.

From these considerations, we see that there are several answers to our question of "how big can the cavity be?" depending on what exactly is meant. If the question is when enhanced and inhibited spontaneous emission no longer occur in the sense discussed in this thesis, the limit is $L = 2c(1-R)^2/\Gamma_{free}$. On the other hand, if the question is when the behavior of the atom returns essentially to the free-space Wigner-Weisskopf limit, excepting the fact that in a lossless cavity the atom may eventually be reexcited, then the limit is $L = 2\pi c/\Gamma_{free}$. However, if the question is when there is *no* change from the free-space behavior, then there is no natural limit on the size of the resonator.

VI.C. Importance of Cavity-Modified Spontaneous Emission to Spectroscopy.

The most interesting potential application of cavity-modified spontaneous emission is that it might be used to reduce the natural linewidth of a transition, giving increased resolution without the loss in signal-to-noise ratio associated with other so-called "subnatural" linewidth schemes.(78) An experimental arrangement for accomplishing this is illustrated in Fig. 6.3. Atoms are placed near the center of a nearly complete spherical cavity which is detuned from the atomic resonance. The atoms are pumped by laser radiation introduced through a small hole in the resonator, and scattered fluorescence leaking through the mirrors or through another small hole in the mirrors is detected as a function of laser tuning. If desired, resonant build-up cavities could be used to enhance the interaction of the atoms with the laser or with the detector.

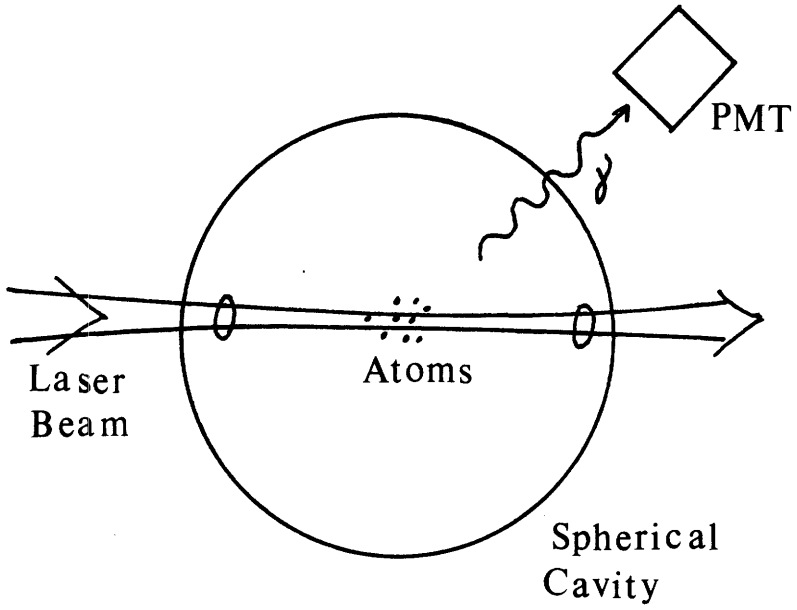

Fig. 6.3. Subnatural linewidth spectroscopy in a nearly complete spherical cavity.

Of primary importance in any such scheme are the frequency shifts introduced by the resonator. We have demonstrated in this thesis that *frequency shifts introduced by a cavity may be very nearly equal to zero if the cavity is tuned with the atomic resonance halfway between two cavity resonances.* Therefore therefore the resonator may significantly reduce the linewidth without introducing a shift. This important point has also recently been emphasized by Dehmelt.(79) Of course, the effect of any holes or gaps, as well as mirror aberrations must be carefullly understood and controlled if such a strategy is to be useful. One further point that is that the radiative shifts we have been discussing are distinct from

the shift introduced by the Van derWaals interaction of the atom with the cavity walls, which have played a role in other experiments.[19] We emphasize that in a large optical resonator, such shifts are negligible.

Even when unintended, cavity effects may arise in spectroscopic experiments and may be important. For example, build-up cavities are sometimes used to enhance the interaction of laser light with a weak atomic transition, and can in principle introduce shifts. Another example is trapped ion spectroscopy, in which the trapping electrodes may inadvertently from an optical cavity. Shifts arising from such cavity effects must be carefully evaluated if one is to have complete confidence in the result of such spectroscopic experiments. Ordinarily, the solid angle and finesse of such inadvertent cavities is likely to be small; the results of this thesis show that any shifts will be much less then the natural linewidth. Nevertheless, they may be important, since it is not uncommon to "split" a spectral line (locate its center to an accuracy much better then the linewidth). For instance, in the next generation of the Cs atomic clocks, the line will be split by six orders of magnitude.[80] Of course, radiative broadening does not play a very important role in the Cs clocks, but it has been proposed that electronic transitions of trapped ions be used as a frequency reference for an *optical* frequency standard,[81] in which case these radiative effects may be very important.

In addition to its role in determining the natural linewidth, spontaneous emission may also appear as a source of unwanted noise. For instance, the Schawlow-Townes limit on the linewidth of a laser may be interpreted as due to the phase diffusion of the laser field amplitude caused by randomly occurring spontaneous emission into the lasing mode. Spontaneous emission may also occur as a source of unwanted noise in squeezed state generation in a similar way. We do not give any detailed analysis here, but merely point out that such spontaneous emission noise is not completely unavoidable, and may be suppressed substantially if the cavity is detuned from the atomic resonance.

VI.D. Possible Directions for Future Research.

VI.D.1. Possible Discrepancy Between W_{end} and W_{side}.

In the data of Figs. 5.11-5.13, there is generally good agreement between theory and experiment, if account is taken of the effects of broadening on the cavity finesse. However, there is one experimentally measured quantity, W_{end}', which may exhibit some departure from the theoretical curve. This is particularly noticeable in the data of figure 5.12. It seems that the linewidth W_{side}' is generally in good agreement with the theoretical curve, but that the linewidth W_{end}' is slightly greater than W_{side}' when the nearest cavity mode is tuned to the red, and slightly less than W_{side}' when the nearest cavity mode is tuned to the blue. This effect is somewhat less noticeable in the data of Fig. 5.11 and Fig. 5.13, but still seems to be present to some extent.

Unfortunately, the data is not of sufficient quality to definitively state that the linewidths W_{end}' and W_{side}' differ. The error is due mostly to irregularity in the laser frequency vs. input scan voltage, and also to some extent to poor signal to noise. The error could be reduced by improving the stability of the laser and by taking several scans at each cavity tuning and averaging the result.

This effect should be investigated further to determine if it is real. If so, it is certainly in conflict with either the classical model or the simple Wigner-Weisskopf treatment given earlier. There are several possible explanations for such an effect. First, it might occur because the quantities W, $\Delta\omega$, and I are averaged over many atoms of different velocities and positions, and since these atoms are weighted differently in each measured quantity, these averaged quantities may not agree with a simple theory based on a homogeneous sample of atoms. It is also possible that this discrepancy could arise from one of two more fundamental sources (discussed further below). The first is that it may be some effect related to the onset of the high Q regime: in our cavity $g/2\pi \cong 40$ MHz, whereas $\gamma_c/2\pi \cong 500$ MHz, so the vacuum Rabi frequency is not completely negligible. The second is that it may be some effect related to stimulated absorption or emission. In our theory, this possibility was not taken into account, since the basis set did not include any states containing more than one quantum of energy. But there is no reason the cavity cannot store the spontaneously emitted photons, which could then give rise to stimulated emission or absorption.

VI.D.2. Larger Solid Angle Cavity.

It would be of great interest to see if one could achieve a truly substantial narrowing of the natural linewidth by going to a much larger solid angle cavity. In the present experiment, the observed decrease in linewidth was only about 10%, which constitutes a reasonably convincing demonstration of narrowing, but is hardly worth the trouble from a practical point of view. But there is no reason why the present cavity mirrors could not be replaced by almost hemispherical mirrors, resulting in a much larger effect. Note that, since inhibition only requires that the cavity modes be off resonance, only a modest finesse is required.

The results of section V.E are a step in this direction and indicate an important difficulty to be addressed: the lenses used to illuminate the cavity must be of imaging quality, but subtend the largest possible solid angle. Otherwise, it is impossible to know when the cavity is aligned and whether the part of the cavity outside the field of view is working properly. It is likely that the design of these lenses and the alignment of the cavity will be at least as difficult a problem as acquiring the mirrors themselves.

VI.D.3. High Q Regime.

It would be of great interest to study the behavior of a single atom interacting with a single cavity mode in the high-Q regime. For the concentric resonator, the coupling constant g between the atom and the "effective single mode" may be written as,

$$g = \frac{\mu}{\hbar}\sqrt{\frac{2\pi\hbar\omega}{V_{eff}}} = \sqrt{\frac{c}{2L}\Gamma_{free} f(\Delta\Omega_{cav})} \qquad (6.14)$$

where now $V_{eff} = 3\lambda^2 L/4\pi f(\Delta\Omega_{cav})$ is the effective mode volume. Again, the high Q regimes occurs for $g > \gamma_c$, where $\gamma_c = c(1\text{-}R)/L$ is the cavity linewidth. In our case $g/2\pi \cong 40$ MHz whereas $\gamma_c \cong 500$ MHz. Therefore, we are already approaching the high-Q limit.

It should not be too difficult to increase g/γ_c further. Note that $g/\gamma_c \propto \sqrt{L f(\Delta\Omega_{cav})} / (1\text{-}R)$, so this ratio can be increased by increasing L, increasing

$f(\Delta\Omega_{cav})$, or increasing the cavity finesse. Certainly it should not be too difficult to obtain a cavity with a linewidth of tens rather than hundreds of MHz. One difficulty with this experiment is that since we are now concerned with the *resonant* interaction of the atoms and the cavity, the effects of mirror surface aberrations, drifts in cavity tuning and alignment, transit time, Doppler broadening, and atomic displacement will begin to play a crucial role. It order to do such an experiment properly it will probably be necessary to obtain the very highest quality mirrors, and to use a slowed atomic beam to reduce transit time and Doppler effects. In spite of these difficulties, such experiments would be of great fundamental importance and are obviously worth pursuing. As one last point, we also mention that time-dependent measurements in the high-Q regime could be very interesting.

VI.D.4. Spectrum of Spontaneous Emission of a *Driven* Atom in a Cavity.

In all of the work described in this thesis, the pump laser intensity was always kept below saturation, and the total fluorescence intensity was studied. As emphasized in a recent set of papers,[43,44] it would be of great interest to spectrally resolve the fluorescence emitted by an atom in a cavity, particularly if the atom is driven by an intense laser field. In this case the usual Mollow spectrum[82] is modified, and as emphasized by Lewenstein, Mossberg, and Glauber,[43] a qualitatively differrent, "dynamical" suppression of spontaneous emission may take place.

Our system presents the ideal opportunity to study such effects. In order to carry out such experiments, it would be necessary to image the fluorescence emitted at right angles from the atomic beam through a tunable Fabry-Perot etalon before detection by the photomultiplier tube. Note that, since the the atoms constitute essentially a point sample, the light can be directed through the Fabry-Perot fairly efficiently. The signal-to-noise ratio decreases as the resolution of the Fabry-Perot is increased, but this could be compensated for by an increased atomic beam flux. One further problem which would need to be addressed carefully is the effect of spatial averaging over the Gaussian intensity profile of the pump laser beam.

IV.D.5. Effects of Stimulated Emission and Absorption , and the Single-Atom Laser.

A further interesting extension of this work is to consider under what conditions *stimulated* emission or absorption may become important to the interaction between a single driven atom and an optical cavity. Note that since the absorption cross section $\sigma = 3\lambda^2/2\pi$, the "effective gain" of a single atom in the cavity is $G_{eff} = 1 \cdot \sigma L/V_{eff} = 2f(\Delta\Omega_{cav})$, which may easily exceed the cavity loss 1-R. In the case $G_{eff} > 1\text{-R}$, the single atom is optically thick with respect to 1/(1-R) round trips of the cavity, and therefore the possibility of stimulated effects must be considered.

Note that in our case, $G_{eff} \cong 0.2$, whereas (1-R) = 0.35, so we are already near the high gain limit. However, in our experiment, the atoms are only weakly excited, so the average number of photons in the cavity is much less than one, and only spontaneous emission is important. But for conditions of strong pumping, such effects could easily become important, especially if an improved cavity is obtained.

An interesting question is under what conditions laser action by a *single* atom could be achieved. In this case it is necessary to produce a steady-state inversion in some way. One possibility is to cycle the atom around in a three-level system, as illustrated in Fig. 6.3. The pump laser continually transfers population from the ground state $|G\rangle$ to the excited state $|E_2\rangle$, and provided the decay rates of the atom are favorable, lasing could be achieved on the transition to an intermediate level $|E_1\rangle$, which then decays down to the ground state. Of course, the average inversion density of the atom will be less than 1, and the cross section on the lasing transition will be reduced from $3\lambda^2/2\pi$, so the conditions for lasing will be more stringent than simply $2f(\Delta\Omega_{cav}) > (1 - R)$.

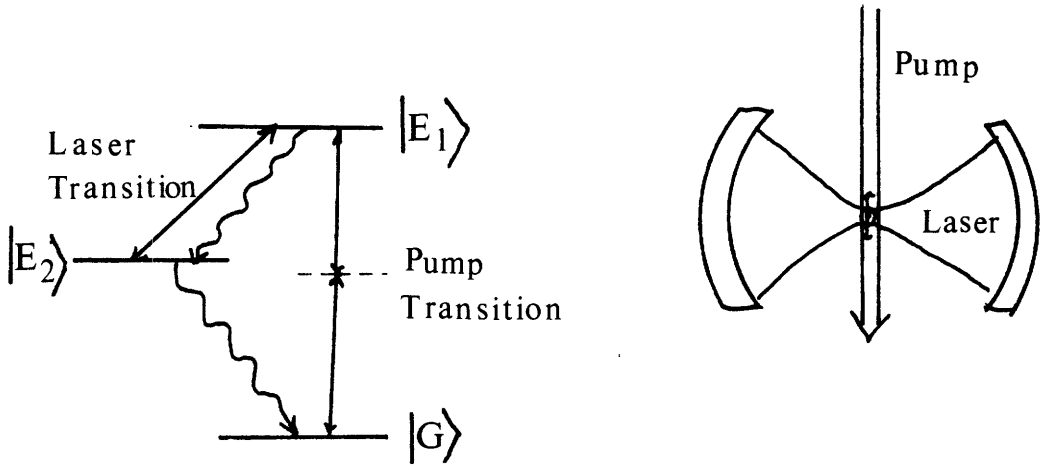

Fig. 6.3. Scheme for producing a single atom laser.

This experiment has been analyzed further; the details are extensive and will not be given here. The bottom line is that it appears to be a very difficult experiment, on the fringe of possibility. Nevertheless, it would certainly be fascinating to obtain lasing action by a single atom, and this possibility is definitely worth exploring further.

VI.D.6. Multiple Atoms Interacting with a Single Mode of an Optical Cavity.

Finally, we mention one further possibility for future research: the study of multiple atoms interacting with a single mode of an optical cavity. In this case, it would be necessary to couple the atoms to a *specific* cavity mode, such as the TEM_{00} mode of a two-mirror resonator, since there is no way to force the "effective single modes" of atoms in a degenerate cavity to overlap; i. e. the atoms would otherwise act independently.

Of course, in the case of low gain and the steady state, this is nothing more than an ordinary laser. But other interesting effects, such as cavity superfluorescence[10], and the optical analogue of the micromaser[11] could be studied if the gain is sufficiently high and the atomic linewidth sufficiently small. One interesting feature of the n-atom system is that the vacuum Rabi frequency scales as $g\sqrt{n}$. Therefore, by simply increasing the number of atoms, it would be possible to study behavior in the high Q limit in a resonator that cannot reach the high Q limit for a single atom.

VI.E. Summary.

In this thesis, the intensities, linewidths, and frequency shifts of radiation by an atom in an optical resonator were studied. A simple classical model was presented in which the atom was viewed as a classical dipole oscillator whose motion is modified when its own radiated field is reflected back onto it by the cavity mirrors. This model provided a simple and physically intuitive description of such radiative processes. We also presented a more rigorous quantum-mechanical treatment of radiation by an atom in a resonator, and found that it basically agreed with the classical treatment in its predictions for the results of the measurements carried out in this thesis. The quantum treatment was carried out in the Wigner-Weisskopf approximation, and from this point of view, the cavity enhances the interaction of the atom with certain mode frequencies, thereby modifying its spontaneous emission rate and radiative level shift.

The intensity of fluorescence emitted by ytterbium atoms in a confocal resonator was studied as a function of resonator tuning. For very small mirror spot sizes, the spontaneous emission rate into the resonator aperture was found to be enhanced and inhibited by a factor of roughly 1/(1-R), relative to the free space rate into the same aperture. For larger apertures, the radiation was enhanced by much less, due to a kind of "spherical aberration" effect. This limited limited the useful mirror aperture to a value such that the fraction of spontaneous emission intercepted by the mirrors was 0.5%, and the change in the total spontaneous emission rate was about 2%. Although the change in the total spontaneous emission rate was small, it was detected indirectly by measuring small changes in the intensity of fluorescence emitted out the sides of the resonator. It was emphasized that this change in sideways intensity is due *only* to a change in the excited state atomic population, and *not* to a "redistribution" of the spontaneous emission probability.

More extensive experiments were carried out using barium atoms in a concentric resonator. Barium was chosen for its much greater natural linewidth, and the concentric resonator allowed a much greater solid angle to be subtended, such that the cavity intercepted 11% of the free-space spontaneous emission. In this experiment, changes in the intensity of fluorescence were observed that were similar to those in the Yb experiment. In addition, changes in the natural linewidth, due to enhanced and inhibited spontaneous emission, and changes in the center frequency, due to radiative level shifts, were observed. This was the first demonstration of the importance of such effects in spectroscopic experiments. In general, good agreement between theory and experiment was obtained.

Experiments were also attempted using a significantly larger solid angle, but these produced dissapointing results, presumably because of poor surface quality of the mirrors near their edges. An experiment was also carried out which studied the spontaneous emission rate as a function of atomic position; this experiment illustrated the importance of a small, well-localized sample of atoms.

The question of interpretation was discussed, and it was found that the classical description must be regarded as incomplete, although the experiments carried out in this thesis do not genuinely distinguish between the quantum and the classical theories. We also discussed the question of how large a resonator can be, and still have an influence on spontaneous emission. It was found that, in a sense, there is no limit on the size of the resonator. Four regimes of spontaneous emission were identified. The first is the small cavity limit which has been studied in almost all previous atom-cavity experiments, the second is the large cavity, low Q limit which has been studied extensively here, and two further regimes, the high Q and multimode regimes were discussed. Both of the latter two regimes have not been studied experimentally. Finally, a number of directions for future research were identified and discussed.

Perhaps the most interesting aspect of this research is that it forces us to rethink many long-held assumptions regarding spontaneous emission and irreversible decay. Essentially, we have shown in this thesis that when an atom radiates, the influence of that radiation is not necessarily over when the wave leaves the vicinity (wavelength sized region) of the atom. Only if the wave is ultimately absorbed will it have no further influence on the atom. If it is not, it can always be reflected back onto it, and since the atom-field system is evolving as a combined quantum mechanical system, this reflected field will remain coherent with the atom and influence its radiation. This illustrates in an interesting way the importance of *dissipation* to the natural linewidth. It is hoped that this thesis has shed some new light on the problems of radiation by atoms in resonators, spontaneous emission, and radiative level shifts, and will stimulate further investigation in this area.

REFERENCES

1. A. Einstein, Phys. Z. **18**, 121 (1917).
2. V. S. Weisskopf and E. Wigner, Z. Physik **63**, 54 (1930).
3. E. M. Purcell, "Spontaneous Emission Probablities at Radio Frequencies", Phys. Rev. **69**, 681 (1946).
4. Daniel Kleppner, "Inhibited Spontaneous Emission", Phys. Rev. Lett. **47**, 233 (1981).
5. K. H. Drexhage, "Interaction of Light with Monomolecular Dye Layers", in Progress in Optics, ed. E. Wolf (North-Holland, Amsterdam, 1974), Vol 12, p. 165.
6. P. Goy, J. M. Raimond, M. Gross, and S. Haroche, "Observation of Cavity-Enhanced Single-Atom Spontaneous Emission", Phys. Rev. Lett. **50**, 1903 (1983).
7. Randall G. Hulet, Eric S. Hilfer, and Daniel Kleppner, " Inhibited Spontaneous Emission by a Rydberg Atom", Phys. Rev. Lett. **55**, 2137 (1985).
8. A. G. Vaidyanathan, W. P. Spencer, and D. Kleppner, "Inhibited Absorption of Blackbody Radiation", Phys. Rev. Lett. **47**, 1592 (1981).
9. J. M. Raimond, P. Goy, M. Gross, C. Fabre, and S. Haroche, "Collective Absorption of Blackbody Radiation by Rydberg Atoms in a Cavity: An Experiment on Bose Statistics and Brownian Motion", Phys. Rev Lett. **49**, 117 (1982)
10. Y. Kaluzny, P. Goy, M. Gross, J. M. Raimond, and S. Haroche, "Observation of Self-Induced Rabi Oscillations in Two-Level Atoms Excited inside a Resonant Cavity: The Ringing Regime of Superradiance", Phys. Rev. Lett. **51**, 1175 (1983).
11. D. Meschede, H. Walther, and G. Müller, "One-Atom Maser", Phys. Rev. Lett. **54**, 551 (1985).
12. G. Rempe, H. Walther, and N. Klein, "Observation of Quantum Collapse and Revival in a One-Atom Maser", Phys. Rev. Lett . **58**, 203 (1987).
13. S. Haroche et al, to be published.
14. P. Filipovicz, P. Meystre, G. Rempe, and H. Walther, "Rydberg Atoms: A Testing Ground for Quantum Electrodynamics", Optica Acta **32**, 1105 (1985).
15. H. A. Bethe, "The Electromagnetic Shift of Energy Levels", Phys. Rev. **72**, 339 (1947).
16. G. Barton, "Quantum Electrodynamics of Spinless Particles Between Conducting Plates", Proc. Roy. Soc. Lond. A**320**, 251 (1970).
17. P. Dobiasch and H. Walther, "Quantum Electrodynamic Effects in Finite Space", Ann. Phys. Fr. **10**, 825 (1985).
18. C. A. Lütken and F. Ravndal, "Energy-Level Shifts in Atoms between Metallic Plates", Phys. Rev. A**31**, 2082 (1985).
19. S. Haroche, "Spontaneous Emission in Confined Space", (Springer-Verlag, Berlin, 1987).
20. C. R. Stroud, Jr., and E. T. Jaynes, "Long-Term Solutions in Semiclassical Radiation Theory", Phys. Rev. A**1**, 106 (1970).
21. Jay R. Ackerhalt, Peter L. Knight, and Joseph H. Eberly, "Radiation Reaction and Radiative Frequency Shifts", Phys. Rev. Lett. **30**, 456 (1973).

22. Peter W. Milonni , Jay R. Ackerhalt, and Wallace Arden Smith, " Interpretation of Radiative Corrections in Spontaneous Emission", Phys. Rev. Lett. **31**, 958 (1973).

23. P. W. Milonni, "Semiclassical and Quantum Electrodynamical Approaches in Non-Relativistic Radiation Theory", Phys. Rep. **25**, 1 (1976).

24. J. Dalibard, J. Dupont-Roc, and C. Cohen-Tannoudji, "Vacuum Fluctuations and Radiation Reaction: Identification of their Respective Contributions", J. Phys. Fr. **43**, 1617 (1982); "Dynamics of a Small System Coupled to a Reservior: Reservior Fluctuations and Self-Reaction", J. Phys. Fr. **45**, 637 (1984)

25. P. W. Milonni and P. L. Knight, "Spontaneous Emission Between Mirrors", Opt. Comm. **9**, 119 (1973).

26. R. H. Dicke, "Coherence in Spontaneous Radiation Processes", Phys. Rev. **93**, 99 (1954).

27. E. T. Jaynes and F. W. Cummings, "Comparison of Quantum and Semiclassical Radiation Theories with Application to the Beam Maser", Proc. I.E.E.E., Jan. 1963, p. 89.

28. Rodney Loudon, The Quantum Theory of Light, 2nd Ed. (Oxford Univ. Press, Oxford, 1983), sect. 2.7.

29. *ibid*, ch. 5.

30. W. Jhe, A. Anderson, E. A. Hinds, D. Meschede, L. Moi, and S. Haroche, "Suppression of Spontaneous Decay at Optical Frequencies: Test of Vacuum-Field Anisotropy in Confined Space", Phys. Rev. Lett. **58**, 666 (1987).

31. F. DeMartini, G. Innocenti, G. R. Jacobovitz, and P. Mataloni, "Anomalous Spontaneous Emission Time an a Microscopic Optical Cavity", Phys. Rev. Lett. **59**, 2955 (1987).

32. G. Gabrielse and H. Dehmelt, "Observation of Inhibited Spontaneous Emission", Phys. Rev. Lett. **55**, 67 (1985).

33. C. H. Townes and A. L. Schawlow, Microwave Spectroscopy, (McGraw-Hill, New York, 1955) p. 336.

34. A. Kastler, "Atomes à l'Intérieur d'un Interféromètre Perot-Fabry", Appl. Opt. **1**, 17 (1962).

35. G. S. Agarwal, "Finite Boundary Effects in Quantum Electrodynamics", in Quantum Electrodynamics and Quantum Optics, ed. A. O. Barut (Plenum, New York, 1984).

36. Henk F. Arnoldus andThomas F. George, "Spontaneous Decay and Atomic Fluorescence near a Metal Surface or an Absorbing Dielectric", Phys. Rev. A**37**, 761 (1988).

37. Jonathan Parker and C. R. Stroud, Jr., "Transient Theory of Cavity-Modified Spontaneous Emission", Phys. Rev. A**35**, 4226 (1987).

38. A. O. Barut and J. P. Dowling, "Quantum Electrodynamics based on Self-Energy: Spontaneous Emission in Cavities", Phys. Rev. A**36**, 649 (1987).

39. Ephraim Fischbach and Norio Nakagawa, "Is (g_e-2) Apparatus-Dependent?", Phys. Lett. **149B**, 504 (1984).

40. Karl Svozil, "Mass and Anomalous Magnetic Moment of an Electron between Two Conducting Parallel Plates", Phys. Rev. Lett. **54**, 742 (1985).

41. Lowell S. Brown, Gerald Gabrielse, Kristian Helmerson, and Joseph Tan, "Cyclotron Motion in a Microwave Cavity: Possible Shift of the Measured Electron g Factor", Phys. Rev. Lett. **55**, 44 (1985).

42. J. J. Sanchez-Mondragen, N. B. Narozhny, and J. H. Eberly, "Theory of Spontaneous-Emission Line Shape in an Ideal Cavity", Phys. Rev. Lett. **51**, 550 (1983).

43. M. Lewenstein, T. W. Mossberg, and R. J. Glauber, "Dynamical Suppression of Spontaneous Emission", Phys. Rev. Lett. **59**, 775 (1987).

44. M. Lewenstein and T. W. Mossberg, "Spectral and Statistical Properties of Strongly Driven Atoms Coupled to Frequency Dependent Reserviors", Phys. Rev. A**37**, 2048 (1988).

45. Subir Sachdev, "Atom in a Damped Cavity", Phys. Rev. A**29**, 2627 (1984).

46. M. Lax, "Quantum Noise. IV. Quantum Theory of Noise Sources", Phys. Rev. **145**, 110 (1965).

47. H. M. Lai, P. T. Leung, and K. Young, "Electromagnetic Decay into a Narrow Resonance in an Optical Cavity", Phys. Rev. A**37**, 1597 (1988).

48. A. Heidmann, J. M. Raimond, and S. Reynaud, "Squeezing in a Rydberg Atom Maser", Phys. Rev. Lett. **54**, 326 (1985).

49. Joachim Krause, Marlan O. Scully, and Herbert Walther, "State Reduction and $|n\rangle$ - State Preparation in a High-Q Micromaser", Phys. Rev. A**36**, 4547 (1987).

50. R. R. Chance, A. Prock, and R. Silbey, "Frequency Shifts of an Electric-Dipole Transition near a Partially Reflecting Surface", Phys. Rev. A**12**, 1448 (1975).

51. W. R. Holland and D. G. Hall, "Frequency Shifts of an Electric Dipole Resonance near a Conducting Surface", Phys. Rev. Lett. **52**, 1041 (1984).

52. J. D. Jackson, Classical Electrodynamics, 2nd Ed. (Wiley, New York, 1975), p. 395.

53. *ibid*, ch. 17.

54. Amnon Yariv, Quantum Electronics, 2nd Ed. (Wiley, New York, 1975), sect. xx.

55. Max Born and Emil Wolf, Principles of Optics, 6th Ed. (Pergammon, Oxford, 1986), sect. 8.8.

56. I. S. Gradstheyn and I. M. Rhyzhik, Table of Integrals, Series, and Products, 4th ed., (Academic Press, Orlando, 1980).

57. Michael Hercher, "The Spherical Mirror Fabry-Perot Interferometer", Appl. Opt. **7**, 951 (1968).

58. J. J. Sakaurai, Advanced Quantum Mechanics (Benjamin/Cummings, Menlo Park, CA, 1967), ch. 2.

59. W. E. Lamb and R. C. Retherford, Phys Rev **72**, 241 (1947)..

60. A. E. Siegman, Lasers (University Science Books, Mill Valley,CA, 1986) ch. 14.

61. A. G. Fox and T. Li, "Resonant Modes in a Maser Interferometer", Bell System Technical Journal **40**, 453 (1961).

62. L. A. Vaynshteyn, Open Resonators and Open Waveguides (Golem Press, Boulder, CO, 1969).

63. G. D. Boyd and J. P. Gordon, "Confocal Multimode Resonator for Millimeter Through Optical Wavelength Masers", Bell System Technical Journal **40**, 489 (1961).

64. G. D. Boyd and H. Kogelnik, "Generalized Confocal Resonator Theory", Bell System Technical Journal **41**, 1347 (1962).

65. Roy Lang, Marlan O. Scully, and Willis E. Lamb, Jr., "Why is the Laser Line so Narrow? A Theory of Single Quasimode Laser Operation", Phys. Rev. A**7**, 1788 (1973).

66. Philip M. Morse and Herman Feshbach, Methods of Theoretical Physics (McGraw-Hill, New York, 1953).

67. W. C. Martin, R. Zalubas, and L. Hagen, Atomic Energy Levels -- The Rare Earth Elements, (U. S. Dept. of Commerce, NSRDS-NBS #60, 1978).

68. M. Gustavsson, H. Lundberg, L. Nilsson, and S. Svanberg, "Lifetime Measurements for Excited States of Rare-Earth Atoms Using Pulse Modulation of a CW Dye-Laser Beam", J. Opt. Soc. Am. **69**, 984 (1979).

69. J. H. Broadhurst, M. E. Cage, D. L. Clark, G. W. Greenlees, J. A. R. Griffith, and G. R. Isaak, "High Resolution Measurements of Isotope Shifts and Hyperfine Splittings for Ytterbium using a CW Tunable Laser", J. Phys. B**7**, L513 (1974).

70. AIP Handbook.

71. C. E. Moore, Atomic Energy Levels, Vol. III, (U. S. Dept. of Commerce, NSRDS-NBS35, 1971).

72. G. K. Gerke and B. A. Bushaw, "Measurement of Weak Branching out of the (near-) Two-Level System Ba 6s6p $^1P_1 \rightarrow 6s^2\ ^1S_0$", Phys. Rev. A**37**, 1502 (1988).

73. Allen Lurio, "Lifetime of the First Excited $^1P_1$ State of Mg and Ba; hfs of Ba^{137}", Phys. Rev. **136**, A376 (1964).

74. D. A. Jackson and Duon Hong Tuan, "Regularities and Anomalies in the Isotope Shifts in the Arc Sectrum of Barium", Proc. Roy. Soc. Lond. A**291**, 9 (1966).

75. W. Rasmussen, R Scheider, and H. Walther, Opt. Comm. **12**, 315 (1974).

76. M. S. Feld, "Steady Stae and Transient Behavior of Two and Three-Level Systems", in Frontiers of Laser Spectroscopy, vol I., ed. R. Balain, S. Haroche, and S. Liberman (North-Holland, Amsterdam, 1978).

77. A. V. Durrant, Am. J. Phys. **45**, 752 (1977).

78. F. Shimuzu, K Umezu, and H. Takuma, Phys. Rev Lett. **47**, 825 (1981).

79. H. Dehmelt, "Single Atomic Particle at Rest in Free Space: Shift-Free Suppression of the Natural Line Width?" in Laser Spectroscopy VIII, eds. W. Persson and S. Svandberg (Springer-Verlag, Berlin, 1987) p. 39.

80. D. J. Wineland, private communication.

81. D. J. Wineland, Wayne M. Itano, J. C. Bergquist, and Randall G. Hulet, Phys. Rev A**36**, 2220 (1987).

82. B. R. Mollow, Phys. Rev. **188**, 1969 (1969).

Appendix 1. Evaluation of Frequency Shift Integral.

In this section we evaluate the integral

$$I_1 = \int_{-\infty}^{\infty} \frac{\sqrt{1 + F}}{1 + F\sin^2(x + \phi)} \frac{x}{x^2 + \Delta^2} dx \tag{A1.1}$$

for $F \geq 0$ and in the limit as $\Delta \rightarrow 0$. The author is grateful to Eugene Gath for providing the following solution.

First, write

$$1 + F\sin^2(x + \phi) = 1 + \frac{F}{2}(1 - \cos(2x + 2\phi)) . \tag{A1.2}$$

Also, define

$$\sin\theta = \frac{F}{2 + F} ; \quad (0 < \theta < \frac{\pi}{2}) \tag{A1.3}$$

$$\xi = 2\phi \tag{A1.4}$$

$$\delta = 2\Delta \tag{A1.5}$$

$$x' = 2x . \tag{A1.6}$$

Then

$$I_1 = \frac{\sqrt{1 + F}}{1 + \frac{F}{2}} \int_{-\infty}^{\infty} \frac{1}{1 - \sin\theta\cos(x' + \phi)} \frac{x'}{x'^2 + \delta^2} dx' \; ; \; (\delta \rightarrow 0). \tag{A1.7}$$

Dropping the prime on the dummy variable x', consider now

$$I_2 = \int_{-\infty}^{\infty} \frac{1}{1 - \sin\theta\cos(x + \phi)} \frac{x}{x^2 + \delta^2} dx \; ; \; (\delta \rightarrow 0). \tag{A1.8}$$

Recalling that the Fourier series decomposition of a function f(x) on the interval [a, a+2π] may be written as

$$f(x) = \frac{a_0}{2} + \sum_{n=1}^{\infty} (a_n\cos(nx) + b_n\sin(nx)) , \tag{A1.9}$$

where

$$a_n = \frac{1}{\pi} \int_{a}^{a+2\pi} f(x)\cos(nx)dx \tag{A1.10a}$$

$$b_n = \frac{1}{\pi}\int_{a}^{a+2\pi} f(x)\sin(nx)dx \qquad \text{(A1.10b)}$$

Choosing $f(x) = \dfrac{1}{1 - \sin\theta\cos x}$ and taking $a = (2k-1)\pi$; $k \in Z$, we may easily show that

$b_n = 0$ and that

$$\frac{1}{1 - \sin\theta\cos x} = \frac{a_0}{2} + \sum_{n=1}^{\infty} a_n\cos(nx)\,, \qquad \text{(A1.11)}$$

where

$$a_n = \frac{2}{\pi}\int_{0}^{\pi} \frac{\cos(n\nu)}{1 - \sin\theta\cos\nu}d\nu\,. \qquad \text{(A1.12)}$$

Substituting $x \rightarrow x + \phi$ in eq. (A1.11) gives the desired result. Noting that[54]

$$\int_{0}^{\pi} \frac{\cos(n\nu)}{1 - \sin\theta\cos\nu}d\nu = \frac{\pi}{\cos\theta}\left(\frac{\cos\theta - 1}{\sin\theta}\right)^n \qquad \text{(A1.13)}$$

gives

$$a_n = \frac{2}{\cos\theta}\left(\frac{\cos\theta - 1}{\sin\theta}\right)^n\,. \qquad \text{(A1.14)}$$

Consider

$$I_3 = \int_{-\infty}^{\infty} \cos(n(x+\xi))\frac{x}{x^2 + \delta^2}dx$$

$$= -2\sin(n\xi)\int_{0}^{\infty} \sin(nx)\frac{x}{x^2 + \delta^2}dx\,. \qquad \text{(A1.15)}$$

Noting that[n]

$$\int_{0}^{\infty} \sin(nx)\frac{x}{x^2 + \delta^2}dx = \frac{\pi}{2}e^{-\delta n}\,, \qquad \text{(A1.16)}$$

we obtain,

$$I_3 = -\pi\sin(n\xi)e^{-\delta n}, \qquad \text{(A1.17)}$$

and therefore

$$I_2 = \int_{-\infty}^{\infty} \left(\frac{a_0}{2} + \sum_{n=1}^{\infty} a_n \cos(n(x+\xi)) \frac{x}{x^2 + \delta^2} \right) dx$$

$$= \sum_{n=1}^{\infty} a_n(-\pi \sin(n\xi) e^{-\delta n})$$

$$= \frac{i\pi}{\cos\theta} \sum_{n=0}^{\infty} \left(\left(\frac{1-\cos\theta}{\sin\theta} e^{i\xi} e^{-\delta} \right)^n - \left(\frac{1-\cos\theta}{\sin\theta} e^{-i\xi} e^{-\delta} \right)^n \right). \qquad \text{(A1.18)}$$

Letting $\delta \rightarrow 0$, the series may be summed to obtain,

$$I_2 = \frac{i\pi}{\cos\theta} \left(\frac{1}{1 - \left(\frac{1-\cos\theta}{\sin\theta} \right) e^{i\xi}} - \frac{1}{1 - \left(\frac{1-\cos\theta}{\sin\theta} \right) e^{-i\xi}} \right)$$

$$= \frac{-\pi \sin\xi \tan\theta}{1 - \cos\xi \sin\theta}. \qquad \text{(A1.19)}$$

Therefore, noting that

$$I_1 = \frac{\sqrt{1 + F}}{1 + \frac{F}{2}} I_2 ; \ (\delta \rightarrow 0), \qquad \text{(A1.20)}$$

and substituting for $\xi = 2\phi$ and $\sin\theta = \frac{F}{2 + F}$, we obtain finally,

$$I_1 = \frac{-\pi F \sin(2\phi)}{2(1 + F\sin^2\phi)}. \qquad \text{(A1.21)}$$

Appendix 2. Publication: "Coherent Ringing in Superfluorescence"

This appendix contains a reprint of the article "Coherent Ringing in Superfluorescence" (D.J. Heinzen, J. E. Thomas, and M. S. Feld, Phys. Rev. Lett. **54**, 677 (1985)). This publication summarizes work which was carried out prior to the Yb and Ba experiments described in the remainder of this thesis. In this work superfluorescence on an infrared transition of rubidium atoms in a cell was studied. The results demonstrated that coherent ringing is an intrinsic property of superfluorescence and that its absence in experiments is a spatial averaging effect.

Coherent Ringing in Superfluorescence

D. J. Heinzen, J. E. Thomas, and M. S. Feld
George R. Harrison Spectroscopy Laboratory and Department of Physics, Massachusetts Institute of Technology, Cambridge, Massachusetts 02139
(Received 12 October 1984)

Superfluorescence emitted from small regions of the output face of an initially inverted medium is found to exhibit ringing; this confirms that coherent ringing is an intrinsic property of superfluorescence. The system studied is a pure two-level Rb transition at $\lambda = 2.73$ μm, prepared in a cell by means of cw single-mode radiation. The Fresnel number of the sample is 1.7.

PACS numbers: 42.65.Gv, 32.50.+d

Superfluorescence (SF),[1] the collective radiation damping of an initially inverted assembly of two-level atoms, has been the subject of much experimental and theoretical investigation since it was first discussed by Dicke in 1954.[2] Although there is now general agreement between theory and experiment in many aspects of this phenomenon, there is debate about the conditions, if any, under which SF can exhibit oscillations or ringing, and the exact nature of this ringing. This Letter reports the results of new SF experiments which view the radiation from a small spatially resolved region of the output face of the sample. The results unambiguously demonstrate that ringing is a fundamental property of SF, and that the absence of ringing in some SF experiments is primarily a spatial averaging effect.

In the initial SF experiment, on rotational transitions in HF gas,[3] strong ringing was observed and attributed to coherent Rabi-type oscillations similar to those predicted in absorbers by Burnham and Chiao.[4] However, in a subsequent series of studies in atomic Cs,[5] a regime of "single-pulse" SF was identified in which ringing never occurred. Furthermore, the multiple pulses observed at the highest Cs densities were attributed to effects of large Fresnel number and cooperation length, and not to coherent processes.[6]

Mean-field SF theories[7] predict smooth single pulses, but these treatments assume the sample to evolve uniformly along the SF propagation axis ($\hat{z}$); this assumption is incorrect since, inherently, the high-gain medium of a superradiating sample is optically thick.[8] Ringing in SF is expected on the basis of uniform plane-wave solutions to the coupled Maxwell-Schrödinger (semiclassical) equations.[9] These results show that SF ringing is due to energy transfer among longitudinal sections of the sample, and is an essential feature of propagation in a high-gain medium. Recent quantized-field treatments confirm this expectation.[10,11]

The predictions of this plane-wave model must, however, be modified to include radial ("transverse") variations in optical polarization and inversion density.[12] These occur because the SF medium is inverted by a laser pulse with a radially varying intensity distribution. The sample may thus be considered as being divided into a number of concentric shells of decreasing density. The pulse profile and ringing period vary from one shell to another because of their different densities. In addition, the shells are coupled together by diffraction. The extent of this coupling depends on the sample's Fresnel number $F = \pi r_0^2/\lambda L$ (r_0 and L are the radius and length of the inverted medium, and λ is the SF wavelength), and is relatively small for $F \gtrsim 1$. The output of the sample as a whole is the sum of the radiation from each of the concentric shells, and this "spatial averaging" washes out the ringing.[12]

A recent theoretical analysis[13] studies the combined effects of quantum fluctuations and transverse variations in Cartesian geometry, and concludes that even for $F \sim 1$, the SF transverse intensity distribution is "completely irregular," because of "short-scale fluctuations" and "loose coupling between various portions of the beam." This gives rise to the question of whether coherent ringing can be observed at all, even within a restricted aperture.

To test this we have performed experiments examining the emission from small regions of the output face of an SF sample with $F \sim 1$. The cell contains atomic Rb vapor, and SF is produced at the $6^2P_{3/2} \rightarrow 6^2S_{1/2}$ transition, $\lambda = 2.73$ μm, inverted by a pump pulse from a dye laser tuned to the $5^2S_{1/2} \rightarrow 6^2P_{3/2}$ transition of ^{87}Rb ($I = \frac{3}{2}$), $\lambda_p = 420$ nm [Fig. 1(a)]. In order to obtain a pure two-level system, required for unambiguous interpretation of the results, the cell is placed in a 5000-G magnetic field, uniform to better than 1 G. The magnetic field, SF propagation direction ($\hat{z}$), and linearly polarized laser field are all mutually perpendicular. The laser is tuned to the

$$5^2S_{1/2}[M_J, M_I = -\tfrac{1}{2}, +\tfrac{3}{2}] \rightarrow 6^2P_{3/2}[-\tfrac{3}{2}, +\tfrac{3}{2}]$$

transition, which is resolved from the nearest-neighboring Zeeman component by 1300 MHz. This level can decay only to the $6^2S_{1/2}[-\frac{1}{2}, +\frac{3}{2}]$ level, resulting in pure two-level SF.[14]

Controllable, reproducible conditions are achieved by use of stabilized cw single-mode dye-laser radiation at $\lambda_p = 420$ nm to invert the sample [Fig. 1(b)]. An

electro-optic shutter switches out a pump pulse of duration τ from this beam. The pulse height is adjusted to provide π-pulse inversion of the (optically thin) pump transition for atoms along $\hat{z}$ (i.e., radial coordinate $r=0$) with axial velocity component $v=0$.[15] The inversion density per unit velocity interval is then given by

$$\mathcal{N}(r,v)=\mathcal{N}_0\frac{\sin^2(\frac{1}{2}\pi\exp[-(r/r_p)^2/2]\{1+(k_pv\tau/\pi)^2\exp[(r/r_p)^2]\}^{1/2})}{1+(k_pv\tau/\pi)^2\exp[(r/r_p)^2]}, \quad (1)$$

with $\mathcal{N}_0$ the density of atoms in the ground state per unit velocity interval, r_p the $1/e$ half-width of the pump laser intensity, and $k_p=2\pi/\lambda_p$.[16] The $1/e$ radius of $n(r)=\int_{-\infty}^{\infty}\mathcal{N}(r,v)dv$ is then $r_0=1.31r_p$. Both velocity and spatial distributions of the inverted atoms are thus well defined. In addition, only a narrow velocity group of atoms is excited, resulting in long dephasing times, T_2^*, without the need for an atomic beam: Equation (1) gives $T_2^*=0.38(\lambda/\lambda_p)\tau$. From Eq. (1), the total number of inverted atoms is

$$N=\int n(r)d^3r=3.34\mathcal{N}_0\pi r_p^2L(\pi/k_p\tau).$$

This is the first time that single-mode cw radiation has been used to produce SF. The reproducibility of our results is largely due to the precision of this method of preparation.

In the experiments a 60-mW, $\tau=8$ ns pump pulse is focused to a waist of $r_p=188$ μm in an $L=4$ cm cell, giving $r_0=245$ μm, $F=1.7$, and $T_2^*=20$ ns. The SF emission in the forward direction is collected by an $f/10$ lens system and imaged onto an InAs photodiode (Judson J12-LD, 250-μm diam, 5-mA bias current). Only a 50-μm region near the lead wire of the detector exhibits fast response, so that great care is taken to ensure that all light is focused onto this area. This signal is amplified and fed into a transient digitizer. The overall response time of the system is 1.6 ns.

The optics are carefully designed to eliminate spherical aberration in order to provide adequate spatial resolution at the pinhole and adequate focusing on the detector. A two-element CaF_2 lens images the output face of the cell with a magnification of 1.0 onto a plane in which a pinhole is inserted. The SF signal then passes through a Ge filter which blocks the pump light, and then through a three-element CaF_2 lens which focuses the light onto the detector with a magnification of $\frac{1}{10}$.

The left and right columns of Fig. 2 show data taken for $N=5\times10^8$ and 2.4×10^8, estimated with 10% accuracy from depletion of the pump pulse. In each column the top trace shows the pump pulse. The second trace shows, on the same time scale, the SF signal when all light in the forward direction is collected. In this case no ringing is observed, and the signals appear very similar to those of the Cs experiment.[5] Finally, in the lowest traces the pinhole has been inserted into the beam. In this case the tail of the pulse is

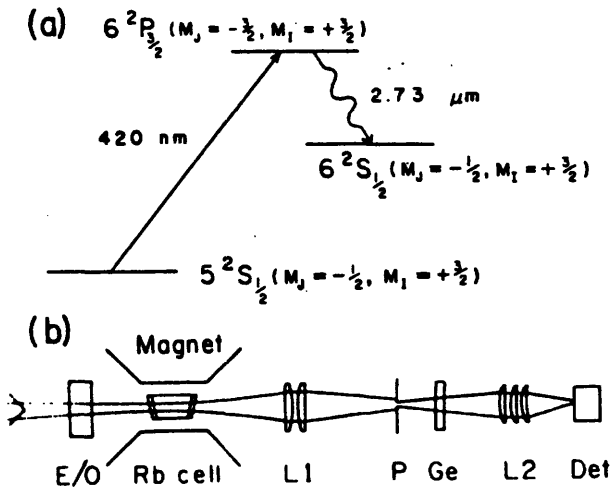

FIG. 1. (a) Rubidium energy-level diagram, showing relevant Zeeman sublevels. (b) Experimental arrangement. SF emitted from the cell is collected by lens L1, which images the output face of the sample onto plane P. A pinhole may be placed at P if desired. The light then passes through a Ge filter, and is refocused by L2 onto the detector.

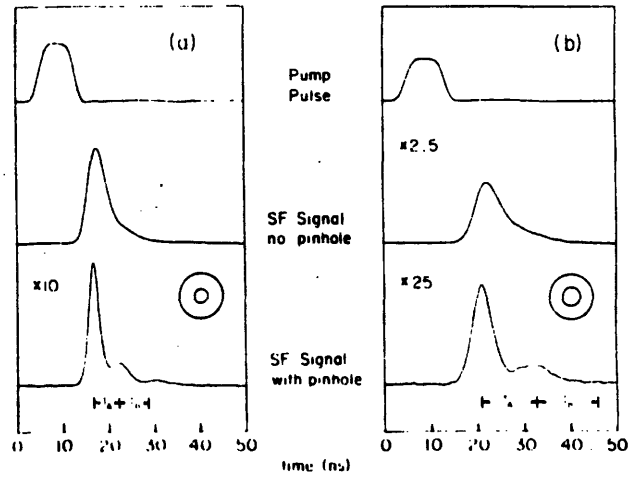

FIG. 2. Pinhole experiment results. The inset circles, drawn to scale, represent the relative diameters of pinhole and sample. For three of the traces the vertical sensitivity was increased by the factor shown to the left. Also shown in the figure are the times T_A and T_B derived from theory. Sample diameter $d=2r_0=490$ μm. (a) $N=5.0\times10^8$, pinhole diameter 150 μm; (b) $N=2.4\times10^8$, pinhole diameter 200 μm.

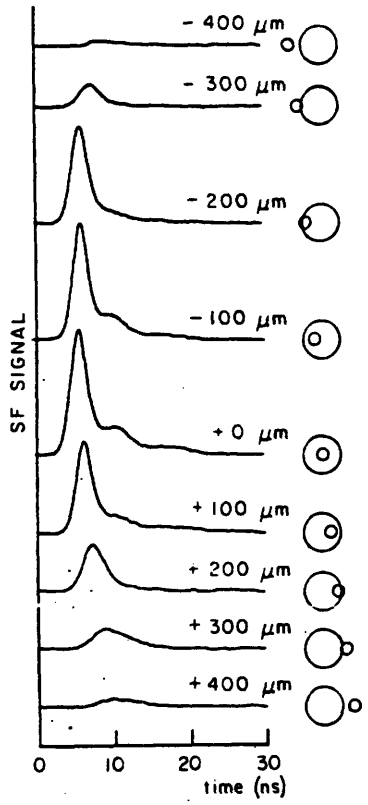

FIG. 3. Results of experiment in which a 150-μm pinhole is translated in 100-μm steps across the image of the output face of the sample. The inset circles show the relative size and position of the sample and pinhole.

reduced dramatically and ringing is clearly observed.

Each trace records a single SF pulse. Shot-to-shot fluctuations are small: Delay-time variations are $\sim 8\%$ and pulse-height variations are $\sim 17\%$. The fluctuations may be partly due to pump-intensity variations. The ringing shown in Fig. 2 was the strongest observed. The ratio of the height of the second lobe (above the tail) to the height of the first lobe varied up to 0.13, with the average being about 0.06; nearly every pulse showed some ringing.

Figure 3 presents a series of SF pulses in which a 150-μm pinhole is scanned across the laser beam in 100-μm steps. The experimental conditions are identical to those in Fig. 2(a). These data make it clear that the pulse shape is a strong function of position. Toward the edges of the beam the pulses are smooth with relatively long delays, whereas toward the center of the beam the pulses become larger, are delayed less, and exhibit ringing similar to that in Fig. 2. Figure 3 makes it clear how, by summing together of the pulse shapes from all parts of the output face, a smooth total SF signal is obtained.

Because of the prediction of Ref. 13 that the SF transverse intensity distribution should be spatially irregular, one may question whether the ringing observed, rather than being true coherent ringing, is instead some kind of multiple pulsing or spiking. The data clearly show that this is not the case. Examination of many single-shot traces shows that the ringing period is very regular and not randomly fluctuating. Further, this period is nearly exactly that predicted by plane-wave theory: Using $\theta_0 = 2/\sqrt{N} \approx 1\times10^{-4}$, we calculate[9] separations of $T_A = 32T_R$ and $T_B = 36T_R$ between the first and second pairs of SF lobes, respectively, with $T_R = \hbar/2\pi k\mu^2 nL$.[15] Using for n the value $n(0)$ estimated from Eq. (1) gives, for the experimental conditions of Fig. 2(a), $T_A = 5.6$ ns and $T_B = 6.3$ ns, and for those of Fig. 2(b), $T_A = 11.7$ ns and $T_B = 13.2$ ns, in excellent agreement with the data.

We conclude that coherent ringing is an intrinsic property of SF, and that its absence in experiments is primarily a spatial averaging effect. The Cs experiment[5] showed no ringing because the entire SF output was observed, whereas it is likely that the HF experiment[3] showed ringing because the detector viewed only a small region in the near field of the beam.

Contributions of Dave Anderson, Burt Bernstein, Igor Shumay, Carter Kittrell, Judson Infrared, and Coherent, Inc. are gratefully acknowledged. This work was supported by the MIT Laser Research Center and the U.S. National Science Foundation under Grant No. 8313248-PHY. One of us (D.J.H.) is a Lester Wolfe Predoctoral Fellow.

[1]We adopt here the definitions of superradiance as the general term for collective radiative damping, and SF as superradiance from an initially inverted sample.

[2]R. H. Dicke, Phys. Rev. 93, 99 (1954).

[3]N. Skribanowitz, I. P. Herman, J. C. MacGillivray, and M. S. Feld, Phys. Rev. Lett. 30, 309 (1973).

[4]D. C. Burnham and R. Y. Chiao, Phys. Rev. 188, 667 (1969).

[5]H. M. Gibbs, Q. H. F. Vrehen, and H. M. J. Hikspoors, Phys. Rev. Lett. 39, 547 (1977).

[6]Q. H. F. Vrehen and H. M. Gibbs, in *Dissipative Systems in Quantum Optics*, edited by R. Bonifacio (Springer, Berlin, 1982), p. 111.

[7]R. Bonifacio and L. A. Lugiato, Phys. Rev. A 11, 1507 (1975), and references therein.

[8]R. Friedberg and S. R. Hartmann, Phys. Lett. 37A, 285 (1971).

[9]J. C. MacGillivray and M. S. Feld, Phys. Rev. A 14, 1169 (1976).

[10]D. Polder, M. F. H. Schuurmans, and Q. H. F. Vrehen, Phys. Rev. A 19, 1192 (1979).

[11]F. Haake, H. King, G. Schröder, J. Haus, and R. Glauber, Phys. Rev. A 20, 2047 (1979).

[12]F. P. Mattar, H. M. Gibbs, S. L. McCall, and M. S. Feld,

Phys. Rev. Lett. 46, 1123 (1981).

[13]E. A. Watson, H. M. Gibbs, F. P. Mattar, M. Cormier, Y. Claude, S. L. McCall, and M. S. Feld, Phys. Rev. A 27, 1427 (1983).

[14]The relevant dipole matrix elements indicate that $4D$ and $5S$ branching is unimportant.

[15]Dipole matrix elements of pump and SF transitions are $\mu_p = 0.63$ D and $\mu = 12.1$ D, respectively [A. Lindgard and S. E. Nielsen, At. Data Nucl. Data Tables 19, 533 (1977)].

[16]Equation (1) assumes negligible pump depletion. In the experiment in Fig. 2(a), the pump beam was depleted by 46%, and in Fig. 2(b) by 29%.

Appendix 3. Publication: "Enhanced and Inhibited Visible Spontaneous Emission by Atoms in a Confocal Resonator"

This appendix contains a reprint of an article which summarizes the ytterbium atom-confocal resonator experiments (D. J. Heinzen, J. J. Childs, J. E. Thomas, and M. S. Feld, Phys. Rev. Lett. **58**, 1320 (1987)).

Enhanced and Inhibited Visible Spontaneous Emission by Atoms in a Confocal Resonator

D. J. Heinzen, J. J. Childs, J. E. Thomas,[a] and M. S. Feld

George R. Harrison Spectroscopy Laboratory and Department of Physics, Massachusetts Institute of Technology, Cambridge, Massachusetts 02139

(Received 5 December 1986)

We report the alteration of visible spontaneous emission by atoms coupled to the degenerate modes of a confocal resonator. The partial emission rate into the resonator modes is enhanced by a factor of 19 when the resonator is tuned to the atomic transition frequency and inhibited by a factor of 42 when it is detuned. This results in a fractional increase of 1.6% and decrease of 0.5%, respectively, in the total spontaneous emission rate, which we verify by monitoring changes in the intensity of light emitted out the sides of the resonator as it is tuned.

PACS numbers: 32.80.−t, 42.50.−p

It has long been recognized that the spontaneous-emission rate of an atom in a resonator may be altered from the free-space value, because of a change in the density of modes.[1-3] Changes in spontaneous-emission rates due to cavity-like effects were first observed in the fluorescence of dye molecules deposited on a thin dielectric layer over a metal substrate.[4] Recently, several experiments have demonstrated such effects in a true resonator structure at long wavelengths: enhanced spontaneous emission of Rydberg atoms in a millimeter-wave cavity,[5] and inhibited spontaneous emission of cyclotron radiation by an electron in a Penning trap[6] and of a Rydberg atom in a waveguide below cutoff.[7] This Letter reports the first observation of enhanced and inhibited spontaneous emission by atoms in a resonator at visible wavelengths.

The ratio of the spontaneous-emission rate into a single resonant cavity mode of quality factor Q and volume V to the total rate in free space is given by[5] $\eta=(3Q/4\pi^2)(\lambda^3/V)$, where λ is the emission wavelength. A recent discussion[8] that considers only a single nondegenerate mode points out that one cannot hope to observe cavity-enhanced spontaneous emission at visible wavelengths because $\lambda^3 \ll V$. However, in certain resonator geometries a large number of modes have the same resonant frequency. In this case the enhancement—or inhibition—may be significant. In our experiment, atoms are excited near the center of a confocal optical resonator. As is well known,[9] the transverse modes of this resonator are degenerate, so that many modes are simultaneously brought into and out of resonance as the resonator is tuned.

In our experiment, the resonator linewidth is greater than the linewidth of the atomic transition, and in addition, the atomic sample is of negligible optical thickness. Under these conditions, the changes in spontaneous emission may easily be understood as an interference effect. Consider an atom near the center of a confocal resonator of length L composed of mirrors $M1$ and $M2$ of reflectivities R_1 and R_2, both with aperture diameter $2b$. The atom illuminates the cavity with dipole radiation, producing a series of reflected and transmitted waves. The radiated power is obtained by adding together the multiple contributions of these transmitted waves. The ratio of γ, the spontaneous-emission rate into the cavity, to γ_{sp}, the free-space rate into the same solid angle, is then given by

$$\frac{\gamma}{\gamma_{sp}}=\frac{1}{1-R}\frac{1}{1+[1/(1-R)]^2\sin^2 kL}, \tag{1}$$

where $R=(R_1R_2)^{1/2}$, $k=2\pi/\lambda$, and it is assumed that $(1-R)\ll 1$. From Eq. (1), the maximum rate is $\gamma_{enh}=\gamma_{sp}/(1-R)$ and the minimum rate $\gamma_{inh}=(1-R)\gamma_{sp}$. For a $\Delta M=0$ transition with polarization perpendicular to the cavity axis, $\gamma_{sp}=(3/8\pi)\Gamma_{sp}\Delta\Omega$, where Γ_{sp} is the total free-space spontaneous-emission rate and $\Delta\Omega=8\pi b^2/L^2$ the solid angle subtended by both cavity mirrors. Therefore, the total spontaneous-emission rate is given by

$$\Gamma=\Gamma_{sp}\left[1+\left[\frac{\gamma}{\gamma_{sp}}-1\right]\frac{3}{8\pi}\Delta\Omega\right]. \tag{2}$$

This gives [if we assume $(1-R)\ll 1$]

$$\Gamma_{enh}=\Gamma_{sp}\left[1+\frac{1}{1-R}\frac{3}{8\pi}\Delta\Omega\right] \tag{3a}$$

and

$$\Gamma_{inh}=\Gamma_{sp}\left[1-\frac{3}{8\pi}\Delta\Omega\right]. \tag{3b}$$

The field in the resonator consists of a pair of plane waves and a pair of tightly focused spherical waves, with the atom situated at one focus. The field distribution at the atom is then just the diffraction-limited focal spot of the circular mirror aperture and has a radius $\sim\lambda L/2\pi b$. Thus the effective mode volume of the total resonator field is $V=2\pi a^2L=4L\lambda^2/\Delta\Omega$, and using $Q=2\pi L/\lambda(1-R)$, we find $\eta=(3/8\pi)[1/(1-R)]\Delta\Omega$, exactly as in Eq. (3a). From this point of view we see that [illegible] is in-

dependent of λ/L and depends only on R and the solid angle $\Delta\Omega$. Note that, in contrast, for the case of a single nondegenerate resonator mode $a \sim \sqrt{\lambda L}$, and $\Delta\Omega \sim \lambda/L$, which is small, whereas in our case $\Delta\Omega$ can be very large.

The experimental arrangement is shown in Fig. 1. An atomic beam of Yb is intercepted by a beam from a cw dye laser (Coherent model 699-21) tuned to the $^1S_0$-$^3P_1$ transition of Yb ($\Gamma_{sp} = 1.1 \times 10^6$ s^{-1}) at 556 nm [Fig. 1(a)]. The excited atoms are positioned at the center of a confocal mirror resonator, and are confined to a region of size approximately 1.5 mm (along the resonator axis) $\times$ 0.4 mm $\times$ 0.4 mm. The laser is linearly polarized perpendicular to the resonator axis and is tuned to the ^{174}Yb isotopic component of the line. Since this isotope has zero nuclear spin and is well resolved from the other components, only a single $\Delta M = 0$ transition is excited. The Doppler width of the atomic beam along the resonator axis is 12 MHz. The laser linewidth of 1 MHz is narrower than the Doppler width of the atomic beam as seen by the laser, and the laser frequency is locked to the center of the atomic resonance line in order to prevent it from drifting during a scan. The density of the ^{174}Yb is $\lesssim 2 \times 10^8$ cm^{-3}; only a small fraction of the atoms are excited by the laser.

The confocal mirrors have a separation of $L = 5.00$ cm, corresponding to a free spectral range $c/4L = 1500$ MHz. Each mirror has a clear aperture of $2b = 4$ mm. The measured transmissions of the mirrors are $T_1 = 2.8 \pm 0.1\%$ and $T_2 = 1.8 \pm 0.1\%$. The observed cavity linewidth for small (0.2–0.3 mm) spot sizes is limited by mirror transmission; from this we can determine

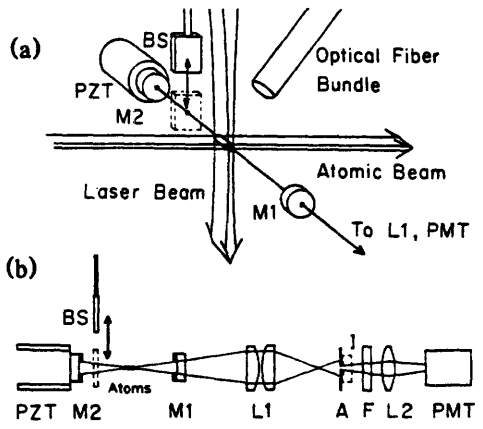

FIG. 1. Experimental apparatus. (a) Atomic-beam excitation geometry, showing the relative orientation of the atomic and laser beams, confocal resonator mirrors $M1$ and $M2$, the moveable beam stop BS, and the optical fiber bundle. (b) On-axis optical configuration, showing the positions of the imaging lens ($L1$), adjustable aperture (a), image of $M1$ by $L1$ (I), interference filter (F), lens ($L2$), and photomultiplier tuber (PMT).

that cavity losses are small (<0.2%/surface). Thus $1/(1-R) \cong 2/(T_1+T_2) = 43.5 \pm 2$. For larger spot sizes (>1 mm), the peaks are broadened by aberrations in the mirror surface, the most serious being spherical aberration. For the cavity on resonance, this limits the spot size for constructive interference to a radius[10] $(\lambda L^3/F)^{1/4} = 1$ mm, with $F = \pi/[2(1-R)]$ the resonator finesse. For the cavity off resonance, the spot radius for destructive interference, $(\lambda L^3/2)^{1/4} = 2.4$ mm, is larger because the resonance condition is less critical.

The fluorescence signal emerging through one of the mirrors is collected by a lens and passed through an aperture of variable size located at the image of $M1$ [Fig. 1(b)]. The lens collects all the light emerging from the cavity with a magnification of 1.0, so that the aperture effectively behaves as if it were located at the output mirror. The light then passes through an interference filter, and is refocused by a lens onto a photomultiplier tube (Hamamatsu R1635-02). The cavity is scanned by applying a voltage ramp to the piezoelectric transducer (PZT) on which $M2$ is mounted, and the resulting signal is processed by photon counting electronics and stored by computer.

In order to compare the cavity-modified spontaneous-emission rate to the free-space rate, a movable beam stop is inserted between the atoms and the mirror opposite the detector, thus removing the effect of the cavity. Then, by multiplying the counting rate with the cavity blocked by $2/(T_1+T_2)$, the data are normalized correctly so that the ratio of the signal with the cavity open to that with the cavity blocked equals γ/γ_{sp}. We estimate the relative accuracy of this calibration to be $\pm 20\%$.

The experimental results are plotted in Fig. 2. Traces a–c show the data for an aperture diameter of 1 mm and laser power of 60 μW. Trace a shows the signal with the cavity open, and trace b shows the signal with the cavity blocked, multiplied by $2/(T_1+T_2)$, thus showing the free-space counting rate into the same solid angle as a. Trace c shows the counting rate with the resonator unblocked, but the laser detuned from the atomic resonance; these data are just the background counting rate, and demonstrates the absence of scattered laser light in the system. In the plotting of a and b, the background counting rate of 30 counts/sec was subtracted from each trace, and a small correction was made for a known error in the focus of $L1$.

As expected, the spontaneous-emission rate into the resonator modes is dramatically changed by tuning of the resonator. The maximum enhancement factor is $\gamma_{enh}/\gamma_{sp} = 19$ and the maximum inhibition factor $\gamma_{sp}/\gamma_{inh} = 42$. The enhancement is smaller than the expected value of $1/(1-R)$ because of broadening of the resonance due to Doppler shifts and mirror surface aberrations. Off resonance the radiation is inhibited by a factor of $1/(1-R)$, as expected. Trace d (dotted line) shows the Airy function of Eq. (1), convolved with a nor-

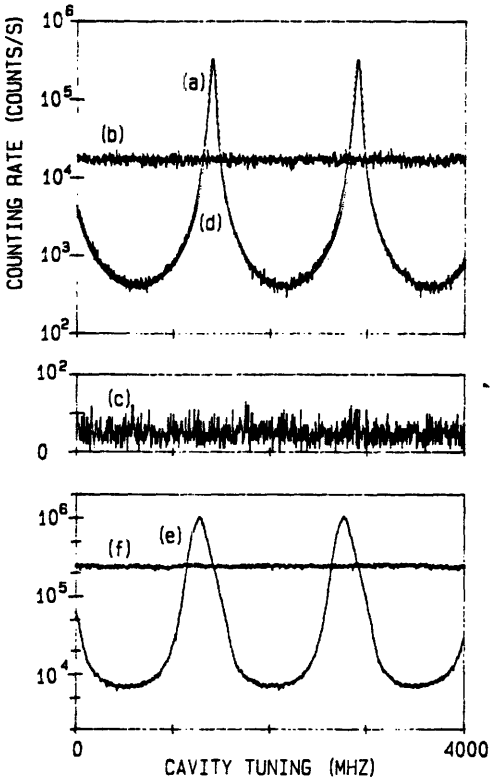

FIG. 2. Photon counting rate for light transmitted through the cavity mirror, as a function of cavity tuning. Curves *a*–*c*, light emitted through the center of the mirror. Curves *e* and *f*, light emitted through the full mirror aperture. Curves *a* and *e*, counting rate with the cavity open. Curves *b* and *f*, normalized counting rate with the cavity blocked, showing the free-space rate into the same aperture. Curve *c*, cavity open but laser detuned from the atomic resonance. Curve *d*, theoretical fit (dotted line).

malized Gaussian distribution of resonance frequencies to take into account the broadening. The measured values of $\gamma_{sp}=1.73\times10^4$ counts/sec [from trace *b*] and $1/(1-R)=43.5$ were used, and the width of the Gaussian (half width at $1/e$ point) was chosen as 32 MHz to fit the data.

The data for the full mirror aperture are shown in traces *e* and *f* of Fig. 2. Trace *e* shows the signal with the cavity open and *f* with the cavity blocked, multiplied by $2/(T_1+T_2)$. In this case, the enhancement factor is 4.3, which is much less than $1/(1-R)$ because of the spherical aberration. However, the inhibition factor is 35, which is still nearly equal to $1/(1-R)$. These data may be used to estimate the changes in the total spontaneous-emission rate. Noting that $\Delta\Omega=4.0\times10^{-2}$ sr, we expect that $\Delta\Gamma_{enh}/\Gamma=+1.6\%$ and $\Delta\Gamma_{inh}/\Gamma=-0.5\%$, where $\Delta\Gamma=\Gamma-\Gamma_{sp}$. [Equation (2) rather than Eqs. (3) must be used for these estimates.]

This change in total spontaneous-emission rate is observable as a change in the intensity of the light emitted out the side of the cavity. This intensity, I_{side}, is simply proportional to the population of excited atoms $n_e=R_{12}n_0/\Gamma$, where R_{12} is the average rate of induced transitions by the laser, n_0 is the total atomic population, and we have assumed that $R_{12}\ll\Gamma$. Therefore, $\Delta I_{side}/I_{side}=\Delta n_e/n_e=-\Delta\Gamma/\Gamma$.

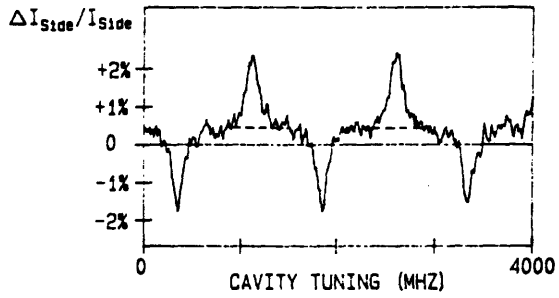

FIG. 3. Fractional change in the intensity of light emitted out the sides of the cavity, as a function of cavity tuning. The alternate peaks of opposite sign (above dashed line) are an artifact of the modulation technique used to record the data. The position $\Delta I_{side}=0$ is determined from the on-axis data.

In order to observe this effect we applied a square-wave modulation of one-half free spectral range amplitude (750 MHz peak to peak) at 35 Hz to the cavity resonance frequency as it is tuned, and monitored the side-light signal collected by the optical fiber bundle with a lock-in amplifier. The pump power, 10 μW, was well below saturation. The resulting change signal occurs every one-half free spectral range and its maximum value is the difference between I_{side} with the cavity on resonance and I_{side} with the cavity off resonance.

The result is shown in Fig. 3. As expected, the fluorescence intensity decreases on resonance, corresponding to an increase in the total spontaneous emission rate. (The correct sign of the change was determined in a separate experiment by our applying a small sinusoidal modulation to the cavity resonant frequency and observing the sign of the resulting modulation in the side-light signal.) The total magnitude of the change is $2.2\pm0.2\%$. This is in good agreement with the value 2.1% predicted from the on-axis data, consisting of an on-resonance decrease of 1.6% and an off-resonance increase of 0.5%.

In our experiment the magnitude of the total change in the spontaneous-emission rate is limited by spherical aberration of the mirror surface. However, this limitation is not fundamental. By use of parabolic confocal mirrors or spherical concentric mirrors, a much larger effect could be observed.

It should be emphasized that these changes in the spontaneous-emission rate into the cavity modes are not merely a redistribution of the intensity, as in a two-slit experiment. The reason is that, at any one resonator tuning, the phase of the interference in all directions is

the same. However, if a plane-parallel[11,12] or other resonator with a nondegenerate mode spectrum had been used, the phase of the interference would vary with angle, resulting only in a spatial modulation in the intensity which would have little effect on the total rate. Also, it should be emphasized that this is not a stimulated-emission effect. Not only is the sample extremely optically thin (Doppler broadened absorption coefficient $\lesssim 10^{-3}$), but the inversion density is negative, so that the system exhibits loss rather than gain.

In conclusion, we have demonstrated that visible spontaneous emission can be modified in a resonator with degenerate modes. Our system has several advantages over long-wavelength atom-cavity experiments.[5,7] The Yb atoms may be excited with a single cw dye laser, resulting in stable, reproducible conditions and large S/N. Also, in the visible, blackbody photons play a negligible role, even at room temperature. Further, one may measure the state of both the atoms (from the side light) and the field (from the axial light). Finally, the statistical properties of the emitted visible radiation are much easier to study than those of microwaves, because single photons can easily be detected. The ability to suppress spontaneous emission noise along a resonator axis may prove useful in applications such as squeezed-state generation. By use of a much larger solid angle, it should be possible to significantly reduce or broaden the natural linewidth of an optical transition.

We would like to acknowledge the valuable assistance of George R. Welch and Carter Kittrell, and a useful discussion with Daniel Kleppner. D. J. Heinzen is a Lester Wolfe Predoctoral Fellow, and J. J. Childs is supported by the Long Term Training Program of the Naval Surface Weapons Center, Dahlgren, VA. This work was performed at the Massachusetts Institute of Technology Laser Research Center, a National Science Foundation Regional Instrumentation Facility. It was supported by th National Science Foundation under Grant No. PHY-8313248.

---

[a]Present address: Department of Physics, Duke University, Durham, NC 27706.

[1]E. M. Purcell, Phys. Rev. **69**, 681 (1946).

[2]C. H. Townes and A. L. Schawlow, *Microwave Spectroscopy* (McGraw-Hill, New York, 1955), p. 336.

[3]D. Kleppner, Phys. Rev. Lett. **47**, 233 (1981).

[4]K. H. Drexhage, *Progress in Optics*, edited by E. Wolf (North-Holland, Amsterdam, 1974), Vol. 12, p. 165.

[5]P. Goy, J. M. Raimond, M. Gross, and S. Haroche, Phys. Rev. Lett. **50**, 1903 (1983).

[6]G. Gabrielse and H. Dehmelt, Phys. Rev. Lett. **55**, 67 (1985).

[7]R. G. Hulet, E. S. Hilfer, and D. Kleppner, Phys. Rev. Lett. **55**, 2137 (1985).

[8]P. Filipovicz, P. Meystre, G. Rempe, and H. Walther, Optica Acta **32**, 1105 (1985).

[9]See, for example, Amnon Yariv, *Quantum Electronics*, (Wiley, New York, 1975), 2nd ed., p. 140.

[10]M. Hercher, Appl. Opt. **7**, 951 (1968).

[11]A. Kastler, Appl. Opt. **1**, 17 (1962).

[12]P. W. Milonni and P. L. Knight, Opt. Commun. **9**, 119 (1973).

Appendix 4. Publication: "Vacuum Radiative Level Shift and Spontaneous-Emission Linewidth of an Atom in an Optical Resonator"

This appendix contains a reprint of an article which summarizes the barium atom-concentric resonator experiments (D. J. Heinzen and M. S. Feld, Phys. Rev. Lett. **59**, 2623 (1987)).

Vacuum Radiative Level Shift and Spontaneous-Emission Linewidth of an Atom in an Optical Resonator

D. J. Heinzen and M. S. Feld

G.R. Harrison Spectroscopy Laboratory and Department of Physics, Massachusetts Institute of Technology, Cambridge, Massachusetts 02139

(Received 24 August 1987)

The center frequency and linewidth of the $^1S_0$-$^1P_1$ resonance line of barium atoms placed near the center of a concentric optical resonator are studied as functions of cavity tuning. Shifts in the transition center frequency, due to radiative level shifts, and changes in linewidth, due to enhanced and suppressed spontaneous emission, are observed. A QED calculation which explicitly includes the resonator mode density gives good agreement with the data.

PACS numbers: 31.30.Jv, 32.70.Jz, 32.80.−t, 42.50.−p

The radiative decay and level shifts of atomic states are well understood when the atom is in free space, beginning with the work of Weisskopf and Wigner[1] for the description of spontaneous emission and with Bethe's calculation[2] of the Lamb shift for radiative level shifts. Recently, much attention has focused on the changes in spontaneous-emission rates which occur for an atom in a cavity, and this has now been demonstrated experimentally.[3-7] In addition to changes in spontaneous-emission rates, it may be expected that radiative level shifts will also be modified when an atom is placed in a cavity.[8] This paper presents the first observation of changes in the radiative level shift of an atom in a resonator. We also directly observe, for the first time, changes in the natural linewidth of a transition. A QED calculation, which explicitly includes the resonator density of modes, is presented and gives good agreement with the results.

The changes in radiative processes which occur in a resonator may be attributed to a change in mode density. In particular, the spontaneous-emission rate Γ and level shift $\delta\omega$ of an atom in the excited state $|E\rangle$ are given by[9]

$$\Gamma = 2\pi \int\int \frac{|\mu_{EG}\cdot\epsilon_k|^2}{\hbar^2}\frac{2\pi\hbar\omega_k}{V}\delta(\omega_{EG}-\omega_k)\rho(\omega_k,\mathbf{k})d\Omega_k d\omega_k, \tag{1}$$

$$\delta\omega = \sum_I \int\int \frac{|\mu_{EI}\cdot\epsilon_k|^2}{\hbar^2}\frac{2\pi\hbar\omega_k}{V}\frac{1}{\omega_{EI}-\omega_k}\rho(\omega_k,\mathbf{k})d\Omega_k d\omega_k, \tag{2}$$

where it is assumed that $|E\rangle$ only decays to a single lower state $|G\rangle$, and the sum is over all states of the atom $|I\rangle$; $\hbar\omega_{EI} = E_E + \hbar\delta\omega - E_I$ is the perturbed energy difference between $|E\rangle$ and $|I\rangle$, μ_{EI} the dipole matrix element between those states, V the quantization volume, and $\rho(\omega_k,\mathbf{k})$ the number of modes per unit frequency interval per unit solid angle, and the integral includes a sum over the two possible polarizations ϵ_k for each $\mathbf{k}$. Ordinarily free space is considered, for which $\rho_{\text{free}}(\omega) = V\omega^2/(2\pi)^3c^3$; the insertion of this into Eq. (1) gives the familiar result $\Gamma_{\text{free}} = 4\mu_{EG}^2\omega_{EG}^3/3\hbar c^3$. The corresponding result for $\delta\omega_{\text{free}}$ diverges because the mass renormalization term has been neglected.[9] However, in our experiment we will only be concerned with the difference $\Delta\omega_{\text{cav}} = \delta\omega_{\text{cav}} - \delta\omega_{\text{free}}$ between the shift with the atom in the cavity and that with the atom in free space. For this difference it may easily be seen that mass renormalization is unimportant.

It has recently been demonstrated that changes in spontaneous emission can occur when an atom is placed in an open optical resonator with degenerate modes.[7] In the present experiment, atoms are placed near the center of a concentric resonator of mirror separation L and reflectivity R. Provided the atoms are displaced by a distance from the center less than $r_0 = [\lambda L(1-R)]^{1/2}$, where λ is the emission wavelength, the eigenfrequencies of the resonator modes which interact with the atom are completely degenerate. This means that the line-shape function of the cavity as seen by the atoms is given by the Airy function,

$$\mathcal{L}(\omega) = \frac{(1+F)^{1/2}}{1+F\sin^2(\omega L/c)}, \tag{3}$$

irrespective of the propagation direction of the mode $\mathbf{k}$ in the resonator, where the parameter $F = 4R/(1-R)^2$ is related to the finesse $\mathcal{F}$ by $F = (2\mathcal{F}/\pi)^2$. From a ray-optics point of view, this may be seen by our noting that every ray emitted by the atom will return to it after one round trip, and that the round trip phase of all such rays is identical.

The effect of the resonator is to modify the mode density over that part of the solid angle $\Delta\Omega_{\text{cav}}$ controlled by the resonator, with the mode density over the remaining

solid angle $\Delta\Omega_{side}$ unchanged. This may be accounted for in Eqs. (1) and (2) by our making the replacement

$$\rho_{cav}(\omega,\mathbf{k}) = \begin{cases} \rho_{free}(\omega)\mathcal{L}(\omega), & \mathbf{k} \text{ in } \Delta\Omega_{cav}, \\ \rho_{free}(\omega), & \mathbf{k} \text{ in } \Delta\Omega_{side}, \end{cases} \quad (4)$$

where the normalization of $\mathcal{L}(\omega)$ is chosen such that the average mode density over one free spectral range is the same as for free space. Substituting $\rho_{cav}(\omega,\mathbf{k})$ in Eq. (1) gives

$$\Gamma_{cav} = \Gamma_{free}\{1 + [\mathcal{L}(\omega_{EG}) - 1] f(\Delta\Omega_{cav})\}, \quad (5)$$

where $f(\Delta\Omega_{cav})$ is the fraction of the total free-space spontaneous emission ordinarily emitted into the solid angle $\Delta\Omega_{cav}$. For the case of circular mirrors of half-angle θ and a $\Delta m = 0$ transition with polarization perpendicular to the cavity axis,

$$f(\Delta\Omega_{cav}) = 1 - \tfrac{3}{4}\cos\theta - \tfrac{1}{4}\cos^3\theta.$$

If also $\theta \ll 1$, $f(\Delta\Omega_{cav}) = (3/8\pi)\Delta\Omega_{cav}$. This result [Eq. (5)] was derived from a different point of view in Ref. 7.

Referring now to Eq. (2), it is easy to see that the only contribution to the difference in frequency shifts $\Delta\omega_{cav}$ occurs near a resonance, $\omega_k \simeq \omega_{EG}$. Therefore, substituting in Eq. (2) for $\rho_{cav}(\omega,\mathbf{k})$ and $\rho_{free}(\omega,\mathbf{k})$, we find

$$\Delta\omega_{cav} = \Gamma_{free}\frac{f(\Delta\Omega_{cav})}{4}\frac{F\sin(2\omega_{EG}L/c)}{1 + F\sin^2(\omega_{EG}L/c)}. \quad (6)$$

Also, if $|G\rangle$ is the ground state, the shift in transition frequency is entirely due to the level shift $\Delta\omega_{cav}$.

Physically, the level shifts are due to contributions from the emission and reabsorption of virtual photons at all possible frequencies. In free space, virtual photons are emitted with essentially equal probability at frequencies slightly above and below resonance, resulting in no net contribution to the frequency shift from a small region of frequency near the atomic resonance. However, in a cavity, the virtual photon emission may be enhanced by a cavity resonance on one side of the atomic resonance relative to the other, resulting in a net contribution to the shift.

In the above it was assumed that the mirrors have perfectly shaped surfaces, that the atoms are located at distances $r \ll r_0$ from the center of the cavity, and that Doppler shifts are negligible. If these conditions are not satisfied, they may be accounted for by modification of the line-shape function $\mathcal{L}(\omega)$. In general, these effects will broaden the peaks in $\mathcal{L}(\omega)$ and reduce the amplitude of its modulation.

The experimental apparatus is illustrated in Fig. 1. A beam of barium atoms is collimated by aperture A1 (1 mm diam) and intercepted by a beam from a cw dye laser, and then recollimated by a second aperture A2 (25 μm diam) and intercepted by a second beam from the same laser. The mean thermal speed of the atoms is 2.4×10^4 cm/s. The laser is tuned near the $^1S_0$-$^1P_1$ transition of ^{138}Ba at $\lambda = 553$ nm. The $^1P_1$ state has a free-space radiative linewidth of 19 MHz.[10] Two regions of excited atoms are thus created, one ("region 1") outside the cavity, and a second ("region 2") inside the cavity. The excited atoms inside the cavity are confined to a region extending $\simeq 30$ μm in each dimension, and are carefully positioned at the center of the cavity. The laser is linearly polarized perpendicular to the resonator axis, and since the ^{138}Ba isotope has zero nuclear spin and is reasonably well resolved from other isotopic components, only a single $\Delta m = 0$ transition is excited. The laser power in both beams is kept well below saturation; the beam in region 2 is focused to a diameter of 30 μm and has a power of 0.02 μW. The sideways fluorescence is collected by optical fiber bundles OFB1 and OFB2 and detected by photomultiplier tubes PMT1 and PMT2.

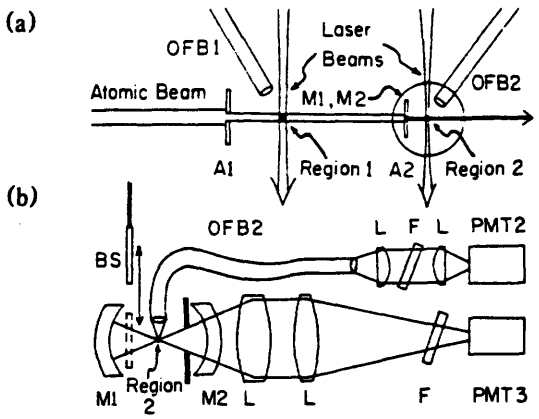

FIG. 1. Experimental apparatus. (a) Atomic-beam excitation geometry. (b) View from side of cavity. PMT1, not shown, detects light from optical fiber bundle OFB1. L, lens; F, interference filter.

The concentric cavity mirrors M1 and M2 have a radius of curvature of 2.50 cm, corresponding to $L = 5.00$ cm and a free spectral range (FSR) $\Delta\nu_{FSR} = c/2L = 3000$ MHz. Their clear diameter is 1.88 cm, so that $\theta = 22°$. The mirrors are coated with a thin bare aluminum film of reflectivity $R = 0.65$, corresponding to $F = 21.2$. The fluorescence emerging through one of the mirrors is collected by an $f/1.2$ camera lens and focused onto a third photomultiplier tube PMT3. The cavity is carefully aligned to concentricity with three independent piezoelectric transducers attached to cavity mirror M1. A small ($\lesssim 1$ free spectral range) linear displacement of M1 from this position tunes the cavity. In order to compare the cavity-modified quantities to those in free space, a movable beam stop BS may be inserted between the atoms and the mirror M1, thus removing the effect of the cavity.

In the experiment, the cavity tuning is held fixed and the fluorescence intensity from all three channels is simultaneously recorded as a function of laser frequency. A typical scan for the fluorescence out the end of the

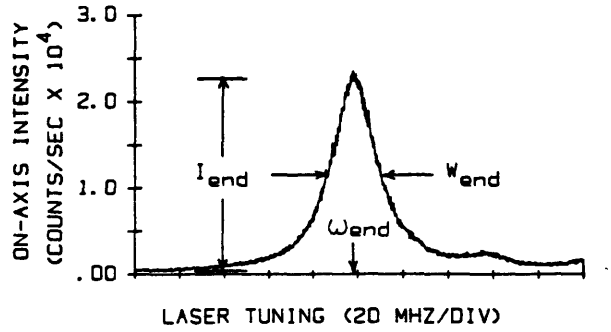

FIG. 2. Spontaneous-emission intensity out the end of the cavity vs laser tuning. The feature on the high-frequency side of the transition is the next isotopic component.

cavity versus laser tuning is shown in Fig. 2. For each such scan, the peak intensity I, width W (full width at half maximum), and frequency shift $\Delta\omega'$ are measured for the fluorescence out of both the ends of the cavity (I_{end}, W_{end}, and $\Delta\omega'_{end}$) and the sides of the cavity (I_{side}, W_{side}, and $\Delta\omega'_{side}$). Here $\Delta\omega' = \Delta\omega - \Delta\omega_0$, where $\Delta\omega = \omega - \omega_{free}$ is the difference between the center frequency ω for the atoms inside the cavity (region 2) and the center frequency ω_{free} for the atoms outside the cavity (region 1); $\Delta\omega_0$ is the same quantity with the cavity blocked.[11] The main purpose of region 1 is to provide an accurate frequency reference for the measurement of $\Delta\omega'$. The experiment is then repeated at a succession of different cavity tunings.

The results are summarized in Fig. 3. The top set of data (a) shows the peak height I_{end}, the second set (b) shows the peak height I_{side}, the third set (c) shows the widths W_{end} and W_{side}, and the last set (d) shows the observed frequency shifts $\Delta\omega'_{end}$ and $\Delta\omega'_{side}$, all as functions of cavity tuning. In each case the straight line shows the same quantities I^0_{side}, I^0_{end}, and W_0 observed with the cavity blocked, thus giving the free-space values of these quantities. (Here I^0_{end} was corrected for the attenuation of the remaining mirror.) The width $W_0 = \Gamma_{free} + \Gamma_0$ contains a contribution Γ_0 from a combination of transit-time broadening, laser frequency jitter, and Doppler broadening.

The curves for each set of data show a theoretical fit by the functions,

$$I_{end} = I^0_{end} \frac{\Gamma_{free}(\Gamma_{free}+\Gamma_0)}{\Gamma_{cav}(\Gamma_{cav}+\Gamma_0)} \mathcal{L}(\omega_{EG}), \tag{7}$$

$$I_{side} = I^0_{side} \frac{\Gamma_{free}(\Gamma_{free}+\Gamma_0)}{\Gamma_{cav}(\Gamma_{cav}+\Gamma_0)}, \tag{8}$$

$$W = \Gamma_{cav} + \Gamma_0, \tag{9}$$

$$\Delta\omega' = \Delta\omega_{cav}, \tag{10}$$

where Γ_{cav} and $\Delta\omega_{cav}$ are given by Eqs. (5) and (6), $\Gamma_{free} = 19$ MHz, and the measured values of $f(\Delta\Omega_{cav})$ $= 0.106$, $\Gamma_0 = 5.0$ MHz, and I^0_{end} and I^0_{side} are used.[12] The parameter F was adjusted, to produce the best fit to the data, at $F = 8.0$. This is somewhat less than the ideal value; the reduced value takes into account the various broadening mechanisms, as discussed earlier. Good agreement with the theory is obtained.

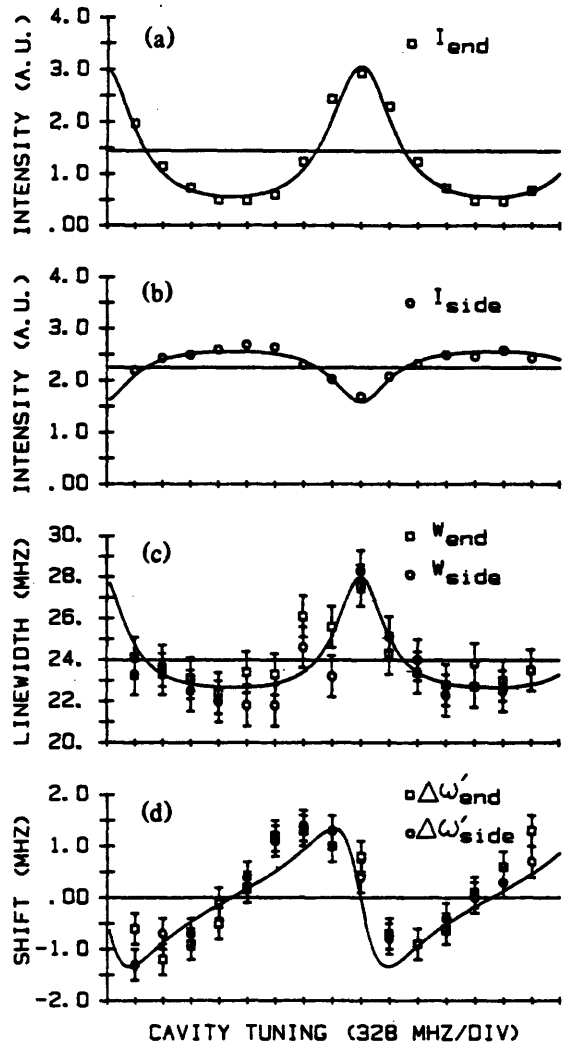

FIG. 3. Observed intensities, linewidths, and frequency shifts as functions of cavity tuning. The cavity length decreases from left to right.

There are a number of important features to notice about the data. First, the intensity out of the sides of the cavity decreases when the intensity out the ends of the cavity increases. This decrease is *not* a "spatial redistribution" of the spontaneous-emission probability. It arises only because of a decrease in the excited-state atomic population, caused by an increase in the total decay rate Γ.[12] Second, the linewidth of the transition increases or decreases in direct proportion to the total spontaneous-emission rate. This confirms that the en-

hanced and inhibited decay of the atoms is spontaneous rather than stimulated. Finally, the radiative shift vanishes when the atomic resonance either coincides with a cavity resonance, or is exactly between two cavity resonances, and the transition shifts to the blue when the nearest cavity mode is tuned to the red, and vice versa. This may be understood by our viewing the atom as interacting primarily with the nearest cavity mode; the atom-cavity mode coupling pushes their eigenfrequencies apart.

Several points should be emphasized. First, the laser is not directly coupled into the cavity; the cavity perturbs the atom, and the laser is only used to probe the atom. Second, the experiment is carried out under true single-atom conditions: The density of the beam is $\simeq 10^8$–10^9 atoms/cm^3, resulting in $\simeq 1$–10 atoms in the resonator at any given time. Further, even if several atoms are present, they will not interact appreciably since the focused beam waists of the generated fields do not coincide. As emphasized above, the *net* radiative lifetime has changed, as the changes in linewidth confirm. Finally, we note that the radiative level shifts of an atom may be important in precision spectroscopy, if one hopes to use suppressed spontaneous emission to narrow a spectral line. Our experiment shows that, in the case of an open degenerate optical resonator, the radiative level shift vanishes when the greatest suppression occurs: when the atomic frequency is between two cavity modes.

In conclusion, we have demonstrated that the energy levels of an atom may be radiatively shifted by a change in the density of vacuum modes of the field when the atom is placed in a resonator. We have also directly shown that, when the atom's spontaneous-emission rate is enhanced or suppressed, the natural linewidth of the transition increases or decreases in direct proportion. We find that these effects are well described by a QED calculation in which the mode density of free space is replaced by that of the resonator.

We would also like to acknowledge the valuable contributions of J. J. Childs, Eugene Gath, and C. R. Monroe. This work was performed at the Massachusetts Institute of Technology Laser Research Center, a National Science Foundation Regional Instrumentation Facility. This work was supported by the National Science Foundation under Grant No. PHY-8313248.

---

[1]V. F. Weisskopf and E. Wigner, Z. Phys. **63**, 54 (1930).

[2]H. A. Bethe, Phys. Rev. **72**, 339 (1947).

[3]P. Goy, J. M. Raimond, M. Gross, and S. Haroche, Phys. Rev. Lett. **50**, 1903 (1983).

[4]G. Gabrielse and H. Dehmelt, Phys. Rev. Lett. **55**, 67 (1985).

[5]R. G. Hulet, E. S. Hilfer, and D. Kleppner, Phys. Rev. Lett. **55**, 2137 (1985).

[6]W. Jhe, A. Anderson, E. A. Hinds, D. Meschede, L. Moi, and S. Haroche, Phys. Rev. Lett. **58**, 666 (1987).

[7]D. J. Heinzen, J. J. Childs, J. E. Thomas, and M. S. Feld, Phys. Rev. Lett. **58**, 1320 (1987).

[8]Dobiasch and Walther have proposed a related experiment to observe a modified radiative level shift using Rydberg atoms between two parallel plates: P. Dobiasch and H. Walther, Ann. Phys. (Paris) **10**, 825 (1985).

[9]See, for example, J. J. Sakurai, *Advanced Quantum Mechanics* (Benjamin/Cummings, Menlo Park, CA, 1967), pp. 65–72.

[10]A. Lurio, Phys. Rev. **136**, A376 (1964).

[11]The frequency shift $\Delta\omega_0 = +1.8$ MHz is due to a difference in the slight residual first-order Doppler shift between region 1 and region 2. This shift occurs because the laser beams in the two regions are not exactly perpendicular to the atomic beam, so that a small component of the atomic velocity appears along the propagation direction of the laser beam.

[12]The expressions for $I_{\rm end}$ and $I_{\rm side}$ are derived by our noting that $I_{\rm side} \propto n_e$, whereas $I_{\rm end} \propto n_e \gamma_{\rm cav} \propto n_e \mathcal{L}(\omega_{EG})$, where n_e is the excited-state population and $\gamma_{\rm cav}$ the partial spontaneous-emission rate of the atom into the cavity. The assumption of unsaturated excitation of a homogeneously broadened transition gives $n_e \propto \sigma/\Gamma \propto [(\Gamma+\Gamma_0)\Gamma]^{-1}$, where σ is the absorption cross section. Note that this effect may be viewed as a variation of the transition saturation intensity as a function of cavity tuning.